

DOCTOR OF PHILOSOPHY

Grating Devices in polymer optical fibre

Ian Johnson

2012

Aston University

GRATING DEVICES IN POLYMER OPTICAL FIBRE

IAN PAUL JOHNSON

Doctor of Philosophy

ASTON UNIVERSITY

August 2011

©Ian Paul Johnson, 2011

This copy of the thesis has been supplied on condition that anyone who consults it is understood to recognise that its copyright rests with its author and that no quotation from the thesis and no information derived from it may be published without proper acknowledgement.

ASTON UNIVERSITY

GRATING DEVICES IN POLYMER OPTICAL FIBRE

IAN PAUL JOHNSON

Doctor of Philosophy

August 2011

This thesis presents the fabrication of fibre Bragg gratings (FBGs) and long period gratings (LPGs) in polymer optical fibre (POF). Possible fabrication techniques were discussed to fabricate FBGs in polymer optical fibre including a detailed description of the phase mask inscription technique used to fabricate FBGs in both single and multi mode microstructured polymer optical fibre (mPOF). Complementing the fabrication of polymer optical fibre Bragg gratings (POFBGs), a technique has been developed to permanently splice POF to silica optical fibre with the use of an optical adhesive. This allowed for the fabricated POFBGs to be characterised away from the optical table, allowing for application specific characterisation. Furthermore Bragg gratings have been fabricated in polymer POF with a Bragg response within the 800nm spectral region. Within this spectral region, POF predominantly manufactured from PMMA experiences considerably smaller attenuation losses when compared to the attenuation losses within the 1550nm spectral region.

The effect of thermally annealing fabricated POFBGs has been studied. This included demonstrating the ability to tune the Bragg wavelength of a POFBG sensor to a desired wavelength. Thermal annealing has also been used to manufacture wavelength division multiplexed sensors with the use of a single phase mask.

Finally POFBGs have been fabricated in Topas Cyclic Olefin Copolymer. Fabrication of Bragg gratings within this copolymer allowed for the first demonstration of near immunity to relative humidity whilst monitoring changes in temperature of the environment the POFBG sensor was in. Bragg gratings fabricated in the Topas copolymer demonstrated sensitivity to relative humidity which was 65 times less than that of a PMMA based POFBG sensor. This decrease in sensitivity has the potential to significantly reduce the potential of cross sensitivity to relative humidity whilst being employed to monitor measurands such as temperature and axial strain.

Keywords:

Wavelength division multiplexing, photonic crystal fibre, PMMA, Topas Cyclic Olefin Copolymer, Fibre Bragg Gratings

Firstly my gratitude goes to Dr. David Webb for giving me the opportunity to be part of the Photonics Research Group at Aston University and for the guidance, advice, patience and never ending enthusiasm which has been greatly appreciated.

My appreciation also goes to Prof. Kyriacos Kalli, who has provided endless enthusiasm about my work whilst giving the guidance and advice needed, and also for offering me the time in Cyprus to investigate femtosecond laser inscription of polymer optical fibre.

I would like to acknowledge the Engineering and Physical Sciences Research Council (EPSRC) and the European Commission via the Framework 7 project PHOtonic Skins For Optical Sensing (PHOSFOS) for funding during this PhD.

I would like to thank: Bert Biggs and Andrew Abbot for their excellent technical support in all areas of the Photonics Research Group at Aston University. Karen Carroll and Chi Zhang for sharing their knowledge and tips of fabricating fibre Bragg gratings in polymer optical fibre and finally David Sáez-Rodríguez, Dr Xianfeng Chen and Lutful Khan for their characterisation of fabricated devices.

I would like to show my appreciation to Kiriama Pty Ltd and the Optical Fibre Technology Centre (OFTC) of the University of Sydney, in particular Dr M.C.J. Large and Dr A. Argyros, Dr O. Bang at the Technical University of Denmark and finally Dr G.D.Peng. All of which provided the polymer optical fibre which made this thesis possible.

I would like to thank my parents for their endless support throughout all my studies.

Finally, my heart warmed thanks go to Rebecca Johnson, who has showed extraordinary patience, whilst encouraging and offering the support needed to get to this point.

TABLE OF CONTENTS

1	Thesis Motivation and Outline.....	16
1.1	Status of Technology Prior to Thesis	16
1.1.1	Photosensitivity	16
1.1.2	Advantages of Polymer Optical Fibre	18
1.1.3	Fabrication of FBGs in POF	19
1.2	Chapter Outline.....	20
2	Grating Theory	22
2.1	Optical Fibres.....	22
2.2	Gratings in Optical Fibres	23
2.2.1	Long Period Gratings	25
2.3	Sensing Characteristics	25
2.3.1	Temperature Sensitivity.....	26
2.3.2	Axial Strain Sensitivity	26
2.4	Fabrication of Fibre Bragg Gratings	26
2.4.1	Internally Written Fibre Bragg Gratings.....	27
2.4.2	Externally Written Fibre Bragg Gratings	27
2.5	Summary	34
3	Polymer Optical Fibre Bragg Gratings (POFBG).....	35
3.1	Chemistry of Polymer Optical Fibre.....	36
3.1.1	Poly (methyl methacrylate) (PMMA)	37
3.1.2	Polystyrene (PS)	37
3.1.3	Free Radical Vinyl Polymerisation	37
3.2	Optical Properties of Polymer Optical Fibre	39
3.2.1	Loss Mechanisms.....	40
3.2.2	Intrinsic Absorption Losses.....	41
3.2.3	Intrinsic Scattering Losses.....	42
3.2.4	Perfluorination and Deuteration	42
3.3	Photosensitivity.....	43

3.3.1	Mechanism of Increased refractive Index	43
3.3.2	Photosensitivity to lower UV wavelengths	44
3.4	Temperature Sensitivity	45
3.5	Summary	50
4	Grating Fabrication in POF	51
4.1	Fibre Bragg Grating Fabrication in Polymer Optical Fibre	51
4.1.1	Phase Mask Inscription of FBGs in POF	52
4.1.2	Fibre Bragg Grating Interrogation	57
4.1.3	Fabrication of FBGs in few-mode mPOF	59
4.1.4	Fabrication of FBGs in Multimode mPOF	62
4.2	Summary of All FBG Fabrication in POF.....	66
4.3	Long Period Grating Fabrication in Polymer Optical Fibre.....	66
4.3.1	Experimental Investigation of Mechanically Induced LPGs.....	67
4.3.2	UV Inscribed LPG in mPOF.....	69
4.4	Other Grating Structures.....	72
4.5	Summary	73
4.5.1	Future Work	73
5	Splicing.....	74
5.1	Comparison of Optically Transparent Adhesives.....	75
5.2	Optical Adhesive Splicing Technique	77
5.3	Optical Adhesive Splicing for mPOF	80
5.4	Optical Adhesive Protection.....	84
5.5	Summary	85
5.5.1	Future Work	85
6	Fabrication of POFBGs in the Low Attenuation Band	87
6.1	Groundwork for fabrication of shorter Bragg wavelength POFBGs.....	90
6.1.1	1300nm FBG Fabricated in MMmPOF	90
6.1.2	Resolution of Refractive Index Change in PMMA Planar Sample	93
6.1.3	Lloyd's Mirror Interferometer Fabrication of FBGs within the 800nm Spectral Region95	
6.2	FBG Fabrication within the 800nm Spectral Region in MMmPOF	96

6.2.1	Fabrication of FBGs with a 860nm Bragg Wavelength Response.....	96
6.2.2	Fabrication of FBGs with a 827nm Bragg Wavelength Response.....	97
6.2.3	Optimisation of FBGs with a 800-900nm Bragg Response, Fabricated in MMmPOF	99
6.3	Attempted FBG Fabrication in Perfluorinated POF.....	101
6.3.1	FBG Fabrication Attempts in CYTOP PF GI POF.....	101
6.3.2	FBG Fabrication Attempts in Chromis PF GI POF	102
6.4	Summary	106
6.5	Future Work.....	107
7	Applications.....	109
7.1	Axial Strain Sensitivity.....	109
7.1.1	Axial Strain Sensitivity of 1500nm POFBGs	109
7.1.2	Axial Strain Sensitivity of 800nm POFBGs	113
7.2	Summary	115
7.3	Future Work.....	115
8	Thermal Annealing & WDM Sensor Fabrication.....	123
8.1	Thermal Annealing & WDM Sensors within the 1550nm Spectral Region	123
8.1.1	Two FBG WDM Sensors Fabricated in MMmPOF	123
8.1.2	Thermal Annealing of POFBGs	127
8.1.3	Thermal Annealing of Multimode mPOF.....	129
8.1.4	Characterisation of Thermal Annealing Against Time	133
8.1.5	WDM of Three FBGs Fabricated From a Single Phase Mask	137
8.2	Thermal Annealing & WDM Sensors within the 800nm Spectral Region.....	143
8.2.1	Two FBG WDM Sensor Fabricated in the 800nm Spectral Region.....	143
8.2.2	Characterisation of Thermal Annealing of FBG Responses within the 800nm Spectral Region.....	144
8.2.3	Continuous Monitoring of the Bragg Wavelength Shift Due to Thermal Annealing	147
8.2.4	24 Hour Thermal Annealing of a FBG Fabricated in the MMmPOF	151
8.3	WDM Sensors Manufactured in the 800nm Spectral Region.....	154
8.3.1	Second Attempt at the Manufacture of a WDM Sensor Using a Single Phase Mask	158

8.4	Fabrication of a WDM Sensor Using Two Phase Masks	160
8.5	Summary	163
8.5.1	Future Work	164
9	TOPAS Cyclic Olefin Copolymer	166
9.1	Cross-Sensitivity to Relative Humidity in PMMA based POF.....	166
9.2	TOPAS COC POF	169
9.3	Fabrication of FBG sensors in TOPAS POF	169
9.4	Temperature Characteristics of Fabricated FBG sensor in TOPAS mPOF.....	172
9.5	Fabrication of TOPAS POFBGs in the 800nm Spectral Region	173
9.5.1	Fabrication of a WDM Sensor in TOPAS POF.....	177
9.6	Humidity Sensitivity.....	178
9.7	Summary	179
9.7.1	Future Work	179
10	Discussion.....	181
10.1	Fabrication of Polymer Optical Fibre Bragg Gratings	181
10.1.1	Interrogation of Polymer Optical Fibre Bragg Gratings	184
10.2	Adhesive Splicing	185
10.3	POFBGS with Bragg Responses in Lower Attenuation Wavelengths.....	186
10.4	Applications and WDM sensors	188
10.5	Future Work with Femtosecond Point-by-Point Inscription	190
11	Authors Publications.....	191
12	References.....	192

LIST OF FIGURES

Figure 2-1 Illustration of the end face of a mPOF	23
Figure 2-2 Illustration of uniform Bragg grating in a optical fibre waveguide	24
Figure 2-3 A typical amplitude splitting interferometer used to fabricated FBGs	28
Figure 2-4 (a) Structural Diagram of a Lloyd's Mirror Wavefront Splitting Interferometer. (b) Structural Diagram of a Prism Interferometer.	29
Figure 2-5 Incident UV beam passing through a phase mask, demonstrating beam splitting into different orders	31
Figure 2-6 UV interference pattern generated from -1 and +1 diffraction orders of the phase mask	32
Figure 3-1 Chemical Structure of Ethylene and Polyethylene	36
Figure 3-2 MMA and PMMA Chemical Structure	37
Figure 3-3 Styrene and Polystyrene Chemical Structures	37
Figure 3-4 Chemical Structure of 2-2'azo-bis-isobutyrylnitrile (AIBN)	38
Figure 3-5 Thermal Breakdown of AIBN	38
Figure 3-6 Initiator Fragment attaching to the MMA vinyl monomer, thus starting a chain reaction and creating a polymer chain	39
Figure 3-7 Attenuation losses of optical fibres at various wavelengths, from [41]	40
Figure 3-8 Harmonics of C-H bond in the PMMA core of a POF	41
Figure 3-9(a) Attenuation due to Rayleigh scattering in PFCB (TVE), PMMA, Cytop, Teflon and Silica. (b) Attenuation due to Rayleigh scattering, linearised to $(1/\lambda^4)$ abscissa [42]	42
Figure 3-10 Chemical Structure of PF GI POF (CYTOP)[39]	42
Figure 3-11 UV absorption of PMMA. Noted wavelengths correspond with the emission wavelengths of an excimer laser.	45
Figure 3-12 Thermal sensitivity of a PMMA based POFBG, results taken with a constant relative humidity of 45%	47
Figure 3-13 Bragg wavelength shift due to three heating cycles of a FBG fabricated in pure PMMA mPOF, insert illustrates the offset of the linear fit	48
Figure 4-1 Optical setup for the fabrication of POFBGs	52
Figure 4-2 V-groove plates which the POF is mounted onto, which in turn is fixed to a translation stage	53
Figure 4-3 Position of screen and aperture in fabrication setup to aid in the alignment to the fibre core	55
Figure 4-4 Second aperture used to align interference pattern to the core of the POF. (a) demonstration position of white screen in optical system (whilst laser is turned off)(b) reflected fringe pattern off the surface of POF observed on the underside of the screen	56
Figure 4-5 Examples of observed scatter patterns for the fibre surface when aligning to the core	57

Figure 4-6 Reflection POFBG Interrogation Setup	58
Figure 4-7 Example of guidance of the red laser diode in the core of POF.....	59
Figure 4-8 Microscope image of end face of FMmPOF	59
Figure 4-9 Reflection spectrum of a FBG fabricated in FWmPOF, resolution bandwidth = 0.5nm.....	60
Figure 4-10 Growth characteristics of FBG fabricated in FMmPOF, with a Bragg wavelength of 1562nm.....	61
Figure 4-11 Positive Bragg wavelength shift due to axial strain. — no strain, — arbitrary amount of axial strain applied by hand	62
Figure 4-12 Microscope image of end face of MMmPOF	63
Figure 4-13 Optical interrogation setup to monitor FBG fabricated in MMmPOF	63
Figure 4-14 Reflected Bragg response of a FBG fabricated in MMmPOF with a phase mask with a period of 1057.20nm.....	65
Figure 4-15 The growth curve of a FBG fabricated in MMmPOF using a phase mask with a period of 1057.20nm.....	65
Figure 4-16 Fabrication setup for mechanically induced LPGs.....	67
Figure 4-17 Mechanically induced LPGs in Corning SMF28 whilst varying the tilt of the v-groove plate. Key: — spectrum before & after induced LPG.  v-groove placed square on fibre.  v-groove slightly tilted -- v-groove angle increased further	68
Figure 4-18 Microscope image of end face of elliptical core of mPOF used for LPF fabrication	70
Figure 4-19 Optical setup for the UV laser fabrication of LPGs in mPOF.	71
Figure 4-20 Transmission Spectrum of a LPG Fabricated in mPOF	72
Figure 5-1 Reflection POFBG interrogation setup with additional silica pigtail.....	77
Figure 5-2 Physical setup of Melles Griot XYZ translation stage, including v-groove plates and fibre positions.....	78
Figure 5-3 Comparing reflection spectra of a FBG fabricated in Peng D2 POF before and after adhesive is cured.....	79
Figure 5-4 Peng D2 POF permanently butt coupled to a SMF28 pigtail using Loctite 3525. 80	
Figure 5-5 Resolution of 300pm, due to loss of index guiding within the MMmPOF because of adhesive travelling along the hole structure of the mPOF	81
Figure 5-6 Optical adhesive Loctite 3525, which is UV cured inside the holes of the MMmPOF	82
Figure 5-7 Comparing reflection spectra of a FBG fabricated in MMmPOF before and after adhesive is UV cured	84
Figure 5-8 Metallic sleeve used protect adhesive splice.....	84
Figure 6-1 Absorption Loss PS (solid line) and PMMA (dotted line) core POFs when measured in transmission, from[77]	88
Figure 6-2 Experiment setup for attenuation measurements	89

Figure 6-3 Optical power during cutback measurements at: (a) 830nm (b) 1550nm.....	89
Figure 6-4(a) Captured reflection before and after fabrication (b) FBG response growth at 1290nm.....	91
Figure 6-5 Bragg response of a FBG fabricated in MMmPOF which was fabricated for 90 minutes.....	92
Figure 6-6 Change in wavelength of Bragg response of a FBG fabricated in MMmPOF due to the application of heat from a desk lamp.....	93
Figure 6-7 Refractive index change in PMMA planar sample using a phase mask with a period of 580nm.....	94
Figure 6-8 Reflected Bragg response of FBGs fabricated in hydrogen loaded B/Ge doped silica optical fibre, using a Lloyd's mirror interferometer inscription technique.....	95
Figure 6-9 (a) Growth curve of a typical FBG fabricated in MMmPOF at 860.5nm (b) Typical Bragg response of a FBG with a Bragg wavelength of 860.5nm.....	96
Figure 6-10(a) Typical growth curve of a FBG fabricated in MMmPOF with a Bragg wavelength of 828.50nm (b) Typical Bragg response of a FBG fabricated with a phase mask with a period of 557.50nm.....	97
Figure 6-11 Comparison of Bragg response of one FBG through different lengths of MMmPOF.....	98
Figure 6-12 Demonstration of the interrogation of a reflected 828nm Bragg response along 23cm length of MMmPOF.....	99
Figure 6-13(a) growth curve of FBG fabricated in MMmPOF at 861nm (b) reflected Bragg response of fabricated FBG at 861nm.....	100
Figure 6-14(a) growth curve of peak reflected Bragg signal of a FBG fabricated in MMmPOF at 828nm (b) reflected Bragg response of a fabricated FBG, with a Bragg wavelength of 828nm.....	100
Figure 6-15 Stretching and thermally annealing CYTOP POF at 100°C.....	102
Figure 6-16 Visual inspection of attempted fabrication of FBG in PF Chromis POF focussed on fibre surface.....	103
Figure 6-17 Evidence of scorching of the PF Chromis POF during FBG fabrication, focussed on fibre surface.....	104
Figure 6-18 40x Microscope image of the air(top)/cladding(bottom) interface of PF Chromis POF after FBG fabrication.....	104
Figure 6-19 40x Microscope image of the air(top)/cladding(bottom) interface of PF Chromis POF after FBG fabrication demonstrating scorching at the surface of the POF.....	105
Figure 6-20 40x microscope images, comparing PF Chromis POF surface quality, when submerged in DCM for: (a) 0 minutes (b)1 minute (c) 5 minutes (d) 10 minutes.....	106
Figure 6-21 Spectral attenuation of PF GI POF.....	108
Figure 7-1 Experimental setup for axial strain characterisation.....	109
Figure 7-2 Bragg response of a FBG fabricated in MMmPOF before axial strain sensing.	110

Figure 7-3 Strain response of a FBG fabricated at 1529nm in MMmPOF (a) up to 20 mε (b) up to 48 mε	112
Figure 7-4 Bragg response at 825.5nm of a FBG fabricated in MMmPOF prior to strain characterisation	113
Figure 7-5 Strain response of a FBG fabricated at 825.5nm in MMmPOF up to 10mε	115
Figure 7-6 Experimental setup for pressure sensing	117
Figure 7-7 Reflected Bragg response of a FBG fabricated in singlemode silica optical fibre	117
Figure 7-8 Pressure response of SOF FBG	118
Figure 7-9 Bragg response of FBG fabricated in MMmPOF prior to pressure sensing	119
Figure 7-10 Pressure response of a multimode microstructured POFBG	119
Figure 7-11 Pressure response of a FBG fabricated in MMmPOF, with the free end sealed with adhesive	120
Figure 7-12 Bragg response of FBG fabricated in few mode step index POF prior to pressure sensing	121
Figure 7-13 Pressure response of a FBG fabricated in few-mode step index POF; (a) tracking 1st peak, (b) tracking 3 rd peak.....	122
Figure 8-1 First Fabricated FBG of a two FBG WDM sensor, Bragg wavelength 1563.25nm	124
Figure 8-2 Growth Curve of a FBG Fabricated in MMmPOF, with a Bragg wavelength at 1530nm.....	125
Figure 8-3 Reflected FBG response in MMmPOF with a Bragg wavelength of 1528.8nm .	126
Figure 8-4 Reflected spectrum of two fabricated FBGs fabricated in MMmPOF with the use of two separate phase masks.....	127
Figure 8-5 Bragg wavelength shift of three different FBGs fabricated in pure PMMA mPOF, from [24]	128
Figure 8-6 Reflected Bragg response of a FBG fabricated in MMmPOF, prior to thermal annealing	130
Figure 8-7 Reflected Bragg response after thermally annealing the MMmPOF at 71°C for 8 hours.....	131
Figure 8-8 Two FBG WDM sensor fabricated in MMmPOF using a single phase mask and thermal annealing	132
Figure 8-9 Three FBG WDM sensor fabricated in MMmPOF. OSA Bandwidth resolution of 0.5nm.....	133
Figure 8-10 Three FBG responses fabricated in separate lengths of MMmPOF prior to thermal annealing characterisation	134
Figure 8-11 Reflected Bragg wavelength observed during thermal annealing cycles. ▪ FBG1 thermally annealed in 10 minute cycles • FBG2 thermally annealed in 20 minute cycles ▲FBG3 thermally annealed in 30 minute cycles.....	136

Figure 8-12 Thermally induced permanent blue Bragg wavelength shifts depending on length of time of anneal	136
Figure 8-13 a: Growth of first FBG of a WDM sensor. b: Bragg response of first FBG of WDM sensor in the 1550nm spectral region	138
Figure 8-14 Permanent wavelength shift of the first FBG of a WDM sensor fabricated in MMmPOF due to a thermal anneal of 30 minutes at 71°C	139
Figure 8-15 (a) the growth curve of FBG2 fabricated for 63 minutes in the MMmPOF (b) the resultant 2 FBG response fabricated in MMmPOF with a spectral response in the 1500nm wavelength range.....	140
Figure 8-16 Bragg wavelength shift of 2 FBGs, due to thermally annealing the MMmPOF at 71°C for 6 hours.....	141
Figure 8-17 (a) The growth curve of the third fabricated FBG of the WDM sensor (b) Spectral response from the first demonstrated WDM sensor fabricated in POF using a single phase mask	142
Figure 8-18 A WDM sensor made of 2 FBGs fabricated in MMmPOF using individual phase masks	144
Figure 8-19 Three reflected responses within the 800nm spectral region of FBGs used in thermal annealing characterisation	145
Figure 8-20 The Bragg wavelength shift of each FBG at the different intervals of thermal annealing ▪ 10 minutes, • 20 minutes, ▲ 30 minutes	146
Figure 8-21 Experimental setup to monitor the real time Bragg wavelength shift due to thermal annealing	147
Figure 8-22 Reflected Bragg response of FBG to be used in real time monitoring of thermal annealing at 80°C	148
Figure 8-23 Real time monitoring of the Bragg wavelength of a FBG fabricated in MMmPOF which was thermally annealed at 80°C for 7.5 hours.....	148
Figure 8-24 Bragg wavelength against time on a log scale monitoring of the Bragg wavelength of a FBG fabricated in MMmPOF which was thermally annealed at 80°C for 7.5 hours.....	149
Figure 8-25 Immediate effect on Bragg wavelength after thermal annealing, whilst returning to room temperature	150
Figure 8-26 Change in Bragg wavelength following thermal annealing, once at room temperature	151
Figure 8-27 Reflected Bragg response of a FBG fabricated in MMmPOF prior to 70°C thermal annealing for 24 hours.....	152
Figure 8-28 Real time monitoring of the Bragg wavelength of a FBG fabricated in MMmPOF which was thermally annealed at 70°C for 24 hours.....	153
Figure 8-29 (a) Reflected Bragg response of the first fabricated FBG (FBG1) (b) Bragg response of FBG1 after thermally annealed at 80°C for 10 minutes.....	155

Figure 8-30(a) Bragg response of the WDM sensor after fabrication of the second FBG (FBG2) (b) Bragg response after the second thermal anneal at 80°C for 30 minutes	156
Figure 8-31(a) Reflected Bragg responses of the WDM sensor after the fabrication of the third FBG (FBG3) (b) Reflected response after the third thermal anneal at 80°C for 2 hours	157
Figure 8-32 First demonstration of a MMmPOF WDM sensor manufactured in the 800nm spectral region, consisting of 3 FBGs fabricated from a single phase mask	157
Figure 8-33 Second manufactured WDM sensor, consisting of 3 FBGs fabricated from a single phase mask	159
Figure 8-34 Normalised Reflected Power WDM sensor around 820nm.....	160
Figure 8-35 Reflected Bragg response of the first fabricated FBG of a 3 device WDM sensors prior to thermal annealing (b) Bragg response of same FBG after thermal annealing at 70°C for 24 hours.....	161
Figure 8-36 (a) growth curve of FBG2 of the WDM sensor fabricated at 861nm (b) reflected Bragg responses of FBG1 and FBG2 of the WDM sensor	163
Figure 8-37 (a) growth curve of FBG3 of the WDM sensor fabricated at 828nm (b) reflected Bragg response of all three FBGs of a WDM sensor manufactured with two phase masks and the aid of thermal annealing	163
Figure 8-38 Reflected Bragg response of a 3 FBG WDM sensor fabricated in MMmPOF which has been embedded in a PDMS tube, Figure supplied by Bram Van Hoe, Ghent University.....	165
Figure 9-1 Relative humidity sensitivity of a FBG sensor fabricated in step index PMMA based POF at 22°C [89].....	167
Figure 9-2 Time response of the diffusion of water into a 200µm diameter POF [89]	167
Figure 9-3 LPG attenuation resonance wavelength shift due to water diffusion into PMMA mPOF	168
Figure 9-4 Cleaved end face of TOPAS COC mPOF	170
Figure 9-5 Reflection spectrum from a FBG fabricated in TOPAS mPOF, with a Bragg wavelength of 1568nm.....	171
Figure 9-6 Growth of a FBG reflection against time during fabrication in TOPAS mPOF, with a Bragg wavelength of 1567.9nm.....	172
Figure 9-7 Thermal response of a FBG fabricated in TOPAS mPOF.....	173
Figure 9-8 Reflection spectrum from a FBG fabricated in TOPAS mPOF, with a Bragg wavelength of 849nm.....	175
Figure 9-9 Growth of the reflected power against time during fabrication of a TOPAS POFBG, with a Bragg wavelength of 849nm	175
Figure 9-10 Reflection spectrum from a FBG fabricated in TOPAS mPOF, with a Bragg wavelength of 882nm.....	176

Figure 9-11 Growth of the reflected power against time during fabrication of a TOPAS POFBG, with a Bragg wavelength of 882nm	177
Figure 9-12 WDM sensor response within the 800nm spectral region, fabricated in TOPAS mPOF	177
Figure 9-13 Relative humidity sensitivity of a FBG fabricated in TOPAS mPOF with a Bragg wavelength of 1568nm.....	179
Figure 10-1 The growth characteristics of a FBG fabricated in FMmPOF with a Bragg length of 1562nm.....	184
Figure 10-2 Demonstration of POF spliced to silica optical fibre using optical adhesive	186
Figure 10-3 POFBG fabricated in MMmPOF with a Bragg wavelength of 860.5nm.....	187
Figure 10-4 Bragg wavelength shift of a FBG fabricated in step index POF whilst monitoring an increase in hydrostatic pressure.....	189
Figure 10-5 Oesophageal Sensor [92]	189

LIST OF TABLES

Table 1 Summary of loss mechanisms in POF.....	40
Table 2 Summary of Silica and PMMA thermal expansion and thermo-optic coefficients....	47
Table 3 Summary of FBG Fabrication in Various POFs	66
Table 4 Review of available optical adhesives	76
Table 5 Optical power measurements of each light source, taken at exit of a silica multimode (50/125 μ m) pigtail	90
Table 6 Summary of applied axial strain to 1529nm FBG fabricated in MMmPOF	111
Table 7 Summary of applied axial strain to FBG fabricated in MMmPOF with a Bragg response at 825.5nm	114
Table 8 Comparison of reflected Bragg response of a FBG fabricated in MMmPOF before and after thermal annealing at 71°C for 8 hours.....	131
Table 9 Summary of the three Bragg responses shown in Figure 8-10	134
Table 10 Summary of Bragg responses of FBG 1 & 2 after second thermal anneal at 71°C for 6 hours, whilst manufacturing a WDM sensor	141
Table 11 Summary of the Bragg responses of the seen in Figure 8-19.....	145
Table 12 Review of POF which were used for FBGs fabrication using the Phase Mask Inscription Technique.....	182

1

THESIS MOTIVATION AND OUTLINE

Fibre reflection filters fabricated in germanium (Ge) doped silica core optical fibre were first observed by Hill *et al* in 1978[1-2]. At this early stage sensitivity of the filters to environmental measurands were noted, particularly sensitivity to temperature and mechanical stress which were applied to the fibre considerably affected the response of the filter[1]. In the time following this, Lam *et al* determined that the photo-induced refractive index change upon which the in-fibre filters where based upon were induced as a result of a two-photon process[3]. Furthermore in 1989, Meltz *et al* documented a technique of fabricating fibre Bragg gratings (FBG) via side inscription where the core of the optical fibre was exposed to a two beam ultraviolet (UV) interference pattern[4]. Photo-induced periodic refractivity in optical fibres transformed the field from a scientific curiosity to the basis of a technology that has a broad and important role in optical communications and sensory systems[5].

In more recent years, the interest in polymer optical fibres (POFs) has increased due to the potential advantages they have in telecommunication and sensor applications. As a consequence, the motivation of this thesis is to discover and detail FBGs fabricated in POF, whilst demonstrating their optical and mechanical performance, and detailing application specific characterisation. Documented in this thesis is the development of the FBGs fabricated in POF.

1.1 Status of Technology Prior to Thesis

To appreciate the technological advancement partaken in this thesis the current position of the technology prior to this thesis must be conveyed.

1.1.1 Photosensitivity

The photosensitivity of reportedly pure Polymethyl Methacrylate (PMMA) was first demonstrated at the start of the 1970s. An increase in the density and the refractive index of PMMA planar samples was observed when exposed to a ~6mW ultra violet light at 325nm. It was concluded that this was the result of polymerisation of remaining monomer which was not polymerised during the synthesis of the material. The reports documented that the increase in refractive index only reached equilibrium several hours after ultra violet exposure had ceased[6-8].

The photosensitivity of POF was only investigated at the end of the 1990s; because of this the technology is still in its infancy when compared to its silica counterparts. Predominantly

PMMA is used for POF, this is usually impure as it is required to dope the core of the fibre to increase the refractive index and thus create waveguiding conditions. The increase in refractive index is often achieved by adding a copolymer such as polystyrene and poly (ethyl methacrylate). A more recent alternative to this is to use microstructured polymer optical fibre (mPOF) which is more commonly known as photonic crystal fibre when employed in silica optical fibre (SOF). Unlike the early forms of POF where waveguiding was created by doping the core with a copolymer, waveguiding in mPOF is provided by a matrix of air holes, creating a lower refractive region around a solid homogeneous higher refractive index core[9]. This allows for hypothetically pure PMMA polymer to be used for POF and thus comparable to the early work of Tomlinson *et al.* Fibre Bragg gratings are predominantly fabricated in PMMA mPOF during the work documented in this thesis.

FBG fabrication in POF was first demonstrated by Xiong *et al*[10] in 1999. The fibre used by Xiong was a step index (SI) polymer fibre whose base material was PMMA, with a core that contained polymerised ethyl benzyl methacrylate. The synthesis of the polymer was enabled with a low level of lauryl peroxide initiator at a temperature below the glass transition (T_g) of the polymer, which followed the method previously used by Tomlinson *et al*[6]. It was noted in the report by Xiong *et al* that when fabricating the Bragg gratings in the POF using a 325nm UV laser that a response of the grating was observed during the fabrication and the growth ceased as the fabrication was completed. This was the opposite to what Tomlinson *et al* previously documented with the growth of gratings hours after the exposure of a UV laser had ended. Xiong *et al* hypothesized that the exposure to the UV laser initiated either cross linking or polymerisation within the doped core of the step index POF, however did not provide any evidence of either suggested UV sensitivity.

Following the first report by Xiong *et al* of the first FBG fabricated in POF, further work by the same group in Sydney, Australia concentrated on the growth of FBGs in POF[11-12]. Experiments were completed using a pulsed 325nm laser on fibre with a pure PMMA cladding and a doped PMMA core using benzyl methacrylate. The research group noted two inscription regimes, the first saw a linear increase in refractive index of the core of the POF for the first 60 minutes. After 60 minutes, a second regime was seen with a rapid increase of the refractive index. After inspection of the POF using a microscope it was noted that the second regime resulted in damage at the core/cladding interface of the POF. As a result the first regime and second regimes were noted as Type I and Type II respectively.

A later paper reports the research into the growth of FBGs in POF[13], whilst using a UV laser at a lower intensity. Here, growth of the Bragg grating was observed for the first 28 minutes at which point there was a constant reflected power until 48 minutes at which point the reflection from the FBG decreased until there was minimal reflection at 88 minutes when the UV laser inscription was stopped. It was reported that the reflected Bragg response grew

back over the course of the next 8 hours and then remained at a constant reflected power. It was speculated that the re-growth of the Bragg response coincided with the relaxation of the thermal stresses applied to the fibre during the UV fabrication.

It is understood the only FBGs fabricated in commercially available POF is reported by Harbach[14]. The fibre was a single mode step index fibre from Paradigm Optics in the United States of America. The POF consisted of a core doped with a polystyrene copolymer to increase the refractive index of the core and enable waveguiding conditions. FBGs were fabricated in this POF using a 308nm pulsed UV laser. An increase in the refractive index of core was reported to decrease by up to 50% over a 100 hour period after the UV inscription; and it was noted on several occasions that the FBG response diminished completely.

As previously mentioned mPOF gives rise to POF made from a single material typically PMMA without the need of a dopant. Previous work by the group at Aston University has demonstrated the successful inscription of FBGs in pure PMMA mPOF[15]. FBGs were fabricated using a 30mW continuous wave UV laser at 325nm. Typically inscription times of around 30-60 minutes were reported with no noteworthy change in the Bragg response after the fabrication had ceased. Research in this thesis aims to build upon the inscription of FBGs in mPOF using the UV 325nm laser system within the Aston University group and characterise the Bragg gratings in application specific environments. It should be highlighted that the long term growth of the Bragg gratings observed in bulk PMMA by Tomlinson *et al* has not been seen in the research carried out by the Aston University group. Rather the Bragg response was observed during the UV inscription reaching a maximum at which point the UV inscription was stopped. It would be desirable to understand these differences in the Bragg growth behaviour between the bulk and mPOF PMMA and will be monitored during the experimental work of this thesis.

1.1.2 Advantages of Polymer Optical Fibre

The advantages that POF holds over their silica counterparts include their organic biocompatibility, which enables sensing of 'in-vivo' biomedical applications[16]. This application also takes advantage of the enhanced temperature sensitivity which is supplied by FBGs fabricated in POF[17]. Furthermore polymers can have a Young's modulus which is 25 times smaller than that of silica [18], which has enabled SI POF to be used in the demonstration of monitoring of recoverable strains as large as 13%[17]. Applications which require immunity to electromagnetic interference (EMI) are a large area of employment for FBGs fabricated in optical fibres due to their dielectric nature[19]. One specific application which requires EMI immunity is in-vehicle local area networks (LANs) which require shielding from the interferences of the vehicle's engine[20]. POFs are now becoming a popular choice for vehicle manufacturers as it is deemed a cost effective material to use in LANs, as material costs are cheaper and the larger core diameters of POF enable easy

connecterisation to and from hubs, also simple light sources and detectors are only required. It is also possible to fabricate multiple FBGs within the same length of fibre unlike comparable electronic counterparts in a technique called wavelength division multiplexing (WDM)[19]. It is desirable to highlight the advantages of POF in application specific characterisation within this thesis whilst demonstrating the ability to employ polymer FBG sensors away from the laboratory utilising connecterisation already seen with POF in LANs.

1.1.3 Fabrication of FBGs in POF

Research before this thesis documented FBGs which have been fabricated in POF using both the phase mask technique[15] which is described in Chapter 2 and also a ring interferometer arrangement[21], whilst using either a continuous wave or pulsed UV laser source operating at 325nm[15] or 355nm[21]. Polymer FBGs with a 28dB transmission rejection band and a bandwidth of less than 0.5nm have been observed by the Australian group[12]. Previous work by the Aston University group has seen successful fabrication of FBGs in an array of POFs including single and multi-mode fibre in both step index and mPOF. All of which were fabricated by a 30mW, 325nm UV laser (Kimmon IK series HeCd), whilst employing a phase mask fabrication technique. This technique and other possibilities for FBG fabrication are summarised in Chapter 2. Based on the previous success of FBG fabrication within the Aston group, Chapter 4 includes a more detailed description of the technique used to fabricate FBGs in POF throughout the research of this thesis.

Prior to the work completed in this thesis all FBGs fabricated in POF had a Bragg response within the 1550nm spectral region. This is a popular region for telecommunications using silica as the transmission medium for optical fibre due to the low losses experienced. It is felt that the readily available light sources and fabrication methods for FBGs in silica optical fibre influenced the choice of 1550nm as the spectral window for POFBGs. However the attenuation losses of POF are very high at these wavelengths: in the order of 1dB/cm for PMMA at 1550nm. This therefore limits the length of POF to around 5-10cm when used as a FBG sensor. Furthermore connecterisation has been limited to butt coupling between polymer and silica optical fibre to achieve longer lengths of fibre required for interrogation of the Bragg response. As a result no polymer FBGs have been used or characterised away from the optical bench. This has resulted in only a single application of polymer FBGs has been demonstrated which was a tunable mirror in a fibre laser system on an optical bench[22].

The sensitivity of the Bragg wavelength of a FBG fabricated in PMMA POF has been characterised against strain and temperature[17, 23-24]. However the latter characterisation highlighted the limitations of working within the laboratory environment on the optical bench. Temperature measurements were mostly complicated by the sensitivity of PMMA to relative humidity at different temperatures, something which was not considered at the time of the

experiment[24]. Therefore, to allow for characterisation of polymer FBGs to application specific measurands a technique needs to be developed where the FBGs can be placed within a controlled environment away from the optical bench, something which is investigated within this thesis.

1.2 Chapter Outline

The forthcoming chapters of this thesis concern the fabrication and characterisation of Bragg grating devices fabricated in polymer optical fibre and includes the following:

Chapter 2: Grating Theory

The theory of fibre Bragg gratings (FBGs) and long period gratings (LPGs) are introduced. The optical characteristics of both of these grating structures are detailed together with their sensing applications. Furthermore the fabrication techniques available to fabricate FBGs in optical fibre are described.

Chapter 3: Polymer Optical Fibre Bragg Gratings (POFBG)

Polymer optical fibre is introduced, detailing polymer materials commonly used for POF fabrication. Several aspects such as optical properties, mechanical properties and photosensitivity to UV wavelengths are also given. Furthermore handling and fibre preparation descriptions are discussed.

Chapter 4: Grating Fabrication in POF

The techniques which have been used to successfully fabricate both FBGs and LPGs in various POFs; including multimode (MM), microstructure POF (mPOF) and single mode (SM) mPOF are discussed in this chapter. Also included is the method of interrogating FBGs by monitoring their Bragg responses in reflection, which is essential when characterising the sensitivity of application specific measurands.

Chapter 5: Splicing

Detailed in this chapter is the successful technique of splicing POF to silica optical fibres (SOF) with the use of an optical adhesive. A review of available adhesives is given, including a discussion of which adhesive was chosen as the most appropriate for the splicing. Permanent adhesive splices were developed to enable connecterisation between SOF and both step index and microstructured POFs. Splicing gave the ability to move POFBGs away from the optical bench upon which it was fabricated on and into application specific characterisation environments, which was essential for the remainder of the thesis.

Chapter 6: Fabrication of POFBGs in the Low Attenuation Band

Here a significant enhancement for the POFB technology is detailed. The first reported fabrication of the FBGs with a Bragg response within the 800nm wavelength region. Fabricating POFBGs with a Bragg response within this spectral region takes advantage of the lower attenuation losses of PMMA based POF and also where suitable broadband interrogating light sources are readily available.

Chapter 7: Applications

Application specific characterisation of FBGs fabricated in POF is completed in this chapter. Specifically the sensitivity of FBG sensors fabricated in MM POF to axial strain is detailed up to 50mε. Furthermore the first documented sensitivity to hydrostatic pressure is detailed including the unexpected positive wavelength shift response to an increase in pressure of up to 10MPa.

Chapter 8: Thermal Annealing & WDM Sensor Fabrication

This chapter demonstrates the ability to permanently tune a Bragg response over a minimum -16nm wavelength range as a result of thermally annealing the POF for up to 24 hours at temperatures between 70-80°C. Thermally annealing the POF gave the possibility to tune a Bragg response to a specific wavelength required without the need to purchase relatively expensive additional phase masks. What's more thermal annealing gave the opportunity to fabricate up to three FBGs within one POF length with responses at different wavelengths, thus demonstrating the first wavelength division multiplexed devices in POF.

Chapter 9: TOPAS Cyclic Olefin Copolymer

Topas cyclic olefin copolymer POF is introduced in this chapter as a solution to eliminate cross sensitivity to relative humidity, as is often observed with FBG sensors fabricated in PMMA based POF when monitoring changes in temperature of the environment the sensor is in. Details of the fabrication of FBGs in the Topas POF are given which gave Bragg responses in both the 1550nm and 800nm wavelength regions. Furthermore the initial sensitivity to temperature is detailed including the substantially lower sensitivity to changes in relative humidity.

Chapter 10: Discussion

This chapter discusses how the technology of polymer optical fibre has advanced with the research completed in this thesis. Technology breakthroughs are highlighted and their impact discussed. Future research based on the work completed in this thesis is also considered. The thesis is ended with a list of published work which was a consequence of the research completed in this thesis.

2

GRATING THEORY

This chapter details the operation of gratings fabricated in optical fibre. Both fibre Bragg gratings (FBGs) and long period gratings (LPGs) are described. Additionally the sensing of these gratings is described together with the fabrication techniques for both types of gratings.

2.1 Optical Fibres

Optical fibre is essentially a length of cylindrical dielectric waveguide. Optical fibre consists of a central cylindrical core region with a given refractive index (n_{co}), which is surrounded by an outer ring of material known as the cladding, this has a lower refractive index (n_{cl}) when compared to the core. In the case of multimode fibre, light guiding within the core of the fibre takes place from the phenomenon of total internal reflection; here light strikes the boundary interface between the core and cladding at an angle larger than the critical angle with respect to the normal to the boundary. When n_{co} is greater than n_{cl} and the incident angle is greater than the critical angle then the light is reflected and remains within the core of the optical fibre. The two indices also define the numerical aperture (NA) which defines the range of angles at which light can be accepted into or emitted out of the waveguide and is given by[25]:

Equation 1

$$NA = (n_{co}^2 - n_{cl}^2)^{\frac{1}{2}}$$

Light is coupled into the core of the optical fibre and guided within the waveguide provided the angle of incidence ($\sin\theta$) is within the NA of the optical fibre. Where the angle is larger the light will escape across the core/cladding interface and will be lost. The NA of the optical fibre can also be determined by the refractive index of the core (n_{co}) and the angle of incidence ($\sin\theta$) as shown in Equation 2.

Equation 2

$$NA = n_{co} \sin\theta$$

Optical fibre waveguides can support many light propagation paths also known as transverse modes which are referred to as multimode (MM) fibres and as little as a single mode which are referred to as single mode (SM) fibres. The number of modes supported in a step index (SI) optical fibre waveguide is related to the v-parameter (V), this is a measure

to determine if the optical fibre is SM or MM. If the v-parameter is less than or equal to 2.405 ($V \leq 2.405$) then the optical fibre is termed as SM. The v-parameter is calculated by:

Equation 3

$$V = \frac{2\pi a}{\lambda_c} (n_{co}^2 - n_{cl}^2)^{\frac{1}{2}} = \frac{2\pi a}{\lambda_c} (NA)$$

Other variants of optical fibre also exist. One is known as microstructured polymer optical fibre (mPOF) or more commonly referred to as photonic crystal fibre (PCF) when manufactured in silica. Light guidance within mPOF is provided by an array of holes acting as a cladding which encompasses a solid core. The holes run the length of the fibre as would the core of a step index optical fibre. An illustration of the end face of an mPOF is shown in Figure 2-1. When the holes are made small enough then the cladding of the mPOF can be considered homogeneous. The holes will simply contain air unless filled with another material. When the holes are filled with air the average refractive index of the cladding is decreased compared to the solid polymer core. Therefore allowing for the conditions of total internal reflection to be met and providing light guidance.

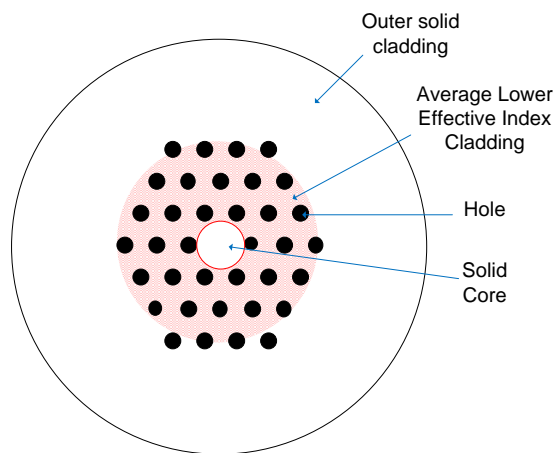


Figure 2-1 Illustration of the end face of a mPOF

Microstructured POF provides the advantage of not needing to add a copolymer to the core of the POF to increase the refractive index to provide light guidance. However this results in the whole of the POF being made from the same material and hence sensitive to UV inscription at the same rate throughout the fibre. This together with the matrix of holes potentially hinders the external UV inscription of FBG.

2.2 Gratings in Optical Fibres

Gratings in optical fibre are the result of the fabrication of periodic perturbations within the core of the waveguide. The perturbations are usually created by exposing the core of the fibre to a UV interference pattern, which increases the refractive index of the core (n_{co}) at the points of exposure, known as grating planes. In the simplest form the assumption is made

that the grating planes are perpendicular to the length of the optical fibre axis and have a constant period as is shown in Figure 2-2.

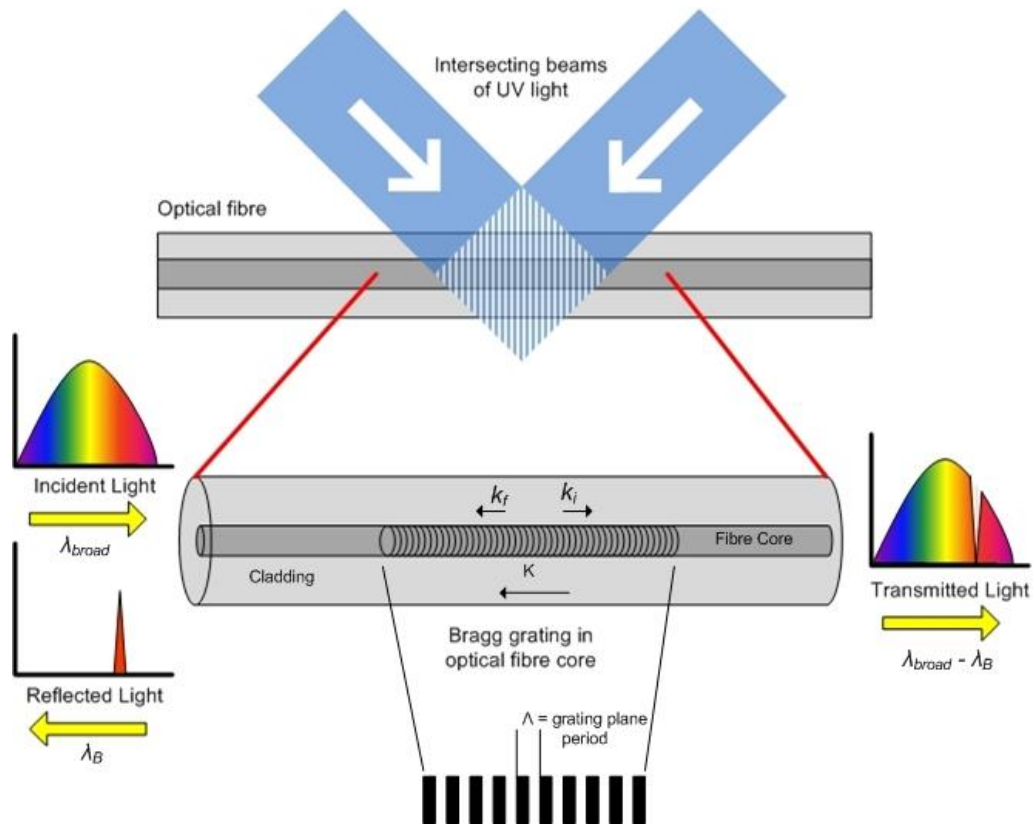


Figure 2-2 Illustration of uniform Bragg grating in a optical fibre waveguide

The incident light which is guided along the waveguide must phase match the periodic grating planes to be reflected back along counter propagating modes within the core of the waveguide to meet the Bragg condition. If the incident light is out of phase with the grating planes then no reflection is observed from the Bragg grating because the Bragg condition is not met. However where the Bragg condition is satisfied the reflected light from each grating plane is in phase and constructively interferes, thus adding together in an opposing backwards direction to the incident light producing a back reflected signal known as the reflected Bragg response, this reflected response will have a centre wavelength known as the Bragg wavelength (λ_B) which is defined by the parameters of the Bragg grating. In the illustration of Figure 2-2, the grating planes are shown as a stepped index change, however a true representation would resemble nearer to a sinusoidal index change along the core of the waveguide.

The Bragg grating condition is met when both the energy and momentum is conserved, energy conservation ($\hbar\omega_f = \hbar\omega_i$) requires that the frequency of the reflected radiation is equal to the incident radiation[26]. Momentum conservation requires that the addition of the incident wave vector (k_i) and the grating wave vector (K) is equal to the wave vector of the scattered radiation (k_f) as summarised in[26]:

Equation 4

$$k_i + K = k_f$$

When the grating wave vector (K) has a direction which is normal to the grating planes it is equal to $2\pi/\Lambda$ (Λ = grating plane period). The diffracted wave vector and the incident wave vector are equal in magnitude but opposite in direction, therefore the momentum conservation condition becomes[26]:

Equation 5

$$2 \left(\frac{2\pi n_{eff}}{\lambda_B} \right) = \frac{2\pi}{\Lambda}$$

This now simplifies to give a first order Bragg condition:

Equation 6

$$\lambda_B = 2n_{eff}\Lambda$$

Where λ_B is the Bragg wavelength which is the centre wavelength of the reflected signal and n_{eff} is the effective refractive index of the core along the Bragg grating length.

2.2.1 Long Period Gratings

Long period gratings (LPGs) typically have grating planes with periods ranging in hundreds of micrometers compared to FBGs that have periodicities typically in the order of $1\mu\text{m}$ [27]. LPGs instigate coupling between the core mode and the co-propagating cladding modes. These cladding modes are attenuated along the cladding due to out-coupling at the cladding/air interface, further attenuation of the cladding modes is seen when bending the waveguide. As a result attenuation bands can be seen in the transmission spectrum, where each band corresponds to coupling to a cladding mode[26].

Phase coupling between the core propagating mode and a forward propagating cladding mode occurs at the wavelength (λ_{res}), given by[28]:

Equation 7

$$\lambda_{res} = (n_{co}^{eff} - n_{clad}^i)\Lambda$$

Where $n_{co}^{eff}(\lambda)$ is the effective refractive index of the propagating core mode at wavelength (λ), $n_{clad}^i(\lambda)$ is the effective refractive index of the i th cladding mode and Λ is the period of the grating planes of the LPG.

2.3 Sensing Characteristics

As was previously demonstrated by Equation 6, the Bragg wavelength which is the centre wavelength of the back reflected signal depends on either or both the period of the grating planes (Λ) and the effective refractive index (n_{eff}) of the optical fibre waveguide. Both of

these parameters can be influenced by external measurands such as temperature and axial strain. Therefore Bragg gratings fabricated in optical fibre can be used to directly monitor a change in these measurands by monitoring the Bragg wavelength (λ_B) of the reflected Bragg response from the grating planes.

2.3.1 Temperature Sensitivity

The Bragg wavelength shift ($\Delta\lambda_{B, temp}$) due to a change in temperature (ΔT) is given by:

Equation 8

$$\Delta\lambda_{B, temp} = \lambda_B(\alpha_\lambda + \alpha_n)\Delta T$$

Where α_λ is thermal expansion coefficient for the fibre given by $(1/\lambda)(\partial\lambda/\partial T)$, and α_n is the thermo-optic coefficient given by $(1/n_{eff})(\partial n_{eff}/\partial T)$ [29].

2.3.2 Axial Strain Sensitivity

The Bragg wavelength shift ($\Delta\lambda_{B, strain}$) due to the change in axial strain ($\Delta\varepsilon_z$), which is applied along the axis of the length of fibre is given by:

Equation 9

$$\Delta\lambda_{B, strain} = \lambda_B(1 - \rho_\alpha)\Delta\varepsilon_z$$

Where ρ_α is the photoelastic coefficient of the optical fibre, and is defined as:

Equation 10

$$\rho_\alpha = \frac{n^2}{2}[\rho_{12} - \nu(\rho_{11} - \rho_{12})]$$

Where ρ_{11} and ρ_{12} are the components of the fibre optic strain tensor and ν is Poisson's ratio.

2.4 Fabrication of Fibre Bragg Gratings

This section describes various techniques of fabricating fibre Bragg gratings in optical fibre, all of which were originally implemented in silica optical fibre. The developed technique of phase mask inscription which has been used to fabricate POFBGs throughout the research of this thesis will be described in more detail in Chapter 4. The fabrication techniques can be separated into two categories, internally and externally written. Although the internal writing technique is not commonly employed because of its impracticalities it is first described due to its importance in the history of fibre Bragg gratings. After this, externally written fabrication techniques will be detailed, describing methods such as amplitude-division interferometry, wavefront-division interferometry, phase mask and point-by-point inscription. Externally written fabrication techniques are considered a much more practical method to manufacture fibre Bragg gratings, the practicality of each technique are discussed for fabricating POFBGs.

2.4.1 Internally Written Fibre Bragg Gratings

As previously noted, Hill *et al* first demonstrated the fabrication of internally written FBGs in 1978[1-2]. The periodic perturbations were formed by launching a single mode argon ion laser operating at either 488nm or 514.5nm into germanium doped silica core optical fibre. The laser beam launched into the core interfered with 4% of light reflected back from the cleaved end of the fibre, opposite to the end at which the laser beam was launched into the fibre. The interference resulted in a standing wave pattern within the core of the fibre. At the high intensity points of the pattern the refractive index of the fibre was permanently changed and therefore generated a periodic perturbation of the refractive index along the length of the fibre core.

Internally written FBG inscription is not considered a practical solution, particularly in POF. The Bragg wavelength will be limited to the inscription wavelength only, therefore in the case of FBG inscription in POF the Bragg wavelength will be around 325nm. At this wavelength the absorption of the polymer will limit the propagation of light into the fibre to only a few centimetres and thus preventing any practical FBG inscription in POF using this technique.

2.4.2 Externally Written Fibre Bragg Gratings

In order to fabricate a FBG in either silica or polymer optical fibre a periodic perturbation of the refractive index is required along the fibre core, usually created by an optical interference pattern. Although recently the periodic refractive index change has also been achieved using a pulsed laser which inscribes each grating plane individually. Therefore four different techniques of externally inscribing FBGs in optical fibre are discussed; these are amplitude splitting interferometry, wavefront splitting interferometry, phase mask inscription and point-by-point inscription.

2.4.2.1 Amplitude Splitting Interferometry

Amplitude splitting interferometry was first used by Meltz *et al* who demonstrated the first results of fabricating a FBG when exposing the fibre perpendicular to the fibre axis with a two beam UV interference pattern[4]. The fabrication was achieved by splitting the inscription UV laser beam into two separate beams of equal intensity, which was then recombined, producing an intensity pattern. This pattern was then focussed into the core of the fibre by using a cylindrical lens for each of the separated UV beams; this also had the effect of increasing the intensity of the pattern and therefore improving the FBG fabrication.

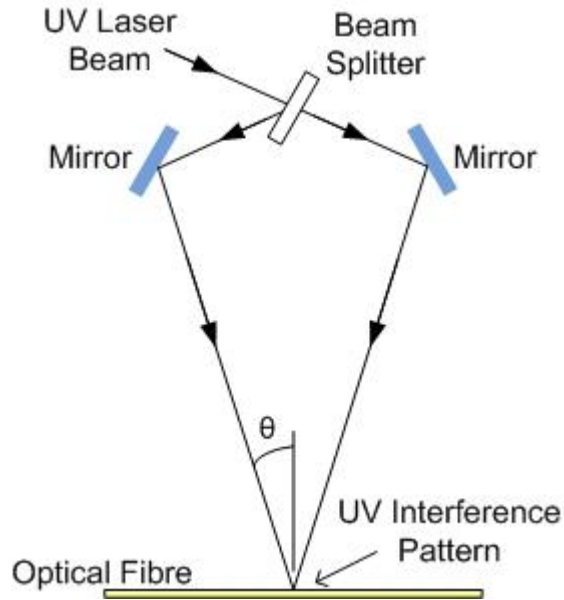


Figure 2-3 A typical amplitude splitting interferometer used to fabricate FBGs

An example of a traditional amplitude splitting interferometer can be seen in Figure 2-3. Here the UV laser beam is directed towards a beam splitter which splits the beam into two separate beams of equal intensity. The two beams are reflected off the appropriate mirror and directed towards the optical fibre at which point the two beams are recombined. This results in a two beam UV interference pattern in the optical fibre and consequently at the high intensity points of the pattern the refractive index of the core is permanently changed, hence creating Bragg grating planes. The period (Λ) of the grating planes is defined by both the UV laser beam wavelength (λ_{UV}) and the angle separation (θ) between the two beams when recombining as shown by the following equation:

Equation 11

$$\Lambda = \frac{\lambda_{UV}}{2 \sin(\theta)}$$

Combining Equation 11 and Equation 6 the Bragg wavelength (λ_B) of the FBG response can therefore be defined by the inscription UV laser beam wavelength (λ_{UV}) and the angle separation (θ) between the two separated beams when recombining as follows:

Equation 12

$$\lambda_B = \frac{n_{eff} \lambda_{UV}}{\sin \theta}$$

where n_{eff} is the effective index of the core along the length of the Bragg grating. The choice of the wavelength (λ_{UV}) of the inscription UV laser beam is defined by the photosensitivity of the optical fibre being used, whether it is silica or polymer optical fibre this wavelength is limited to a relatively small UV wavelength region, which ultimately provides no scope to control the Bragg wavelength (λ_B). This leaves the angle between the recombining beams

(θ) as a controlling feature, this has no restriction and can be used to determine the Bragg wavelength (λ_B) and is therefore a particular advantage when using the amplitude splitting interferometry technique. A distinct disadvantage with this fabrication technique is the vulnerability of the mirrors, beam splitter or other optical components included in the setup to mechanical vibrations. The slightest of movements of any of the optical components could result in the deformation of the desired interference pattern of the recombining UV beams, resulting in a poor quality FBG response.

2.4.2.2 Wavefront Splitting Interferometry

As with amplitude splitting interferometry, wavefront splitting interferometry is used to fabricate FBGs by exposing the fibre side-on to a UV interference pattern. With this technique half of the UV inscription beam is reflected back across the path of the remainder of the beam which has not been reflected. This technique is best described with two examples, these are the Lloyd's mirror interferometer and the prism interferometer both of which are shown in Figure 2-4[26].

The Lloyd's mirror interferometer shown in Figure 2-4(a) is constructed using a single dielectric mirror which is positioned perpendicular to the fibre axis. The UV inscription beam is directed and centred at the point where the mirror's reflecting surface meets the surface of the optical fibre. Consequently the mirror reflects half of the UV beam back towards the fibre; this in turn creates an interference pattern between the non-reflected and reflected halves of the UV inscription beam. The interference pattern overlaps the optical fibre and the refractive index is changed at the high intensity points of the pattern. As is seen in Figure 2-4(a) a cylindrical lens is often used to focus the interference pattern along the length of the core within the optical fibre.

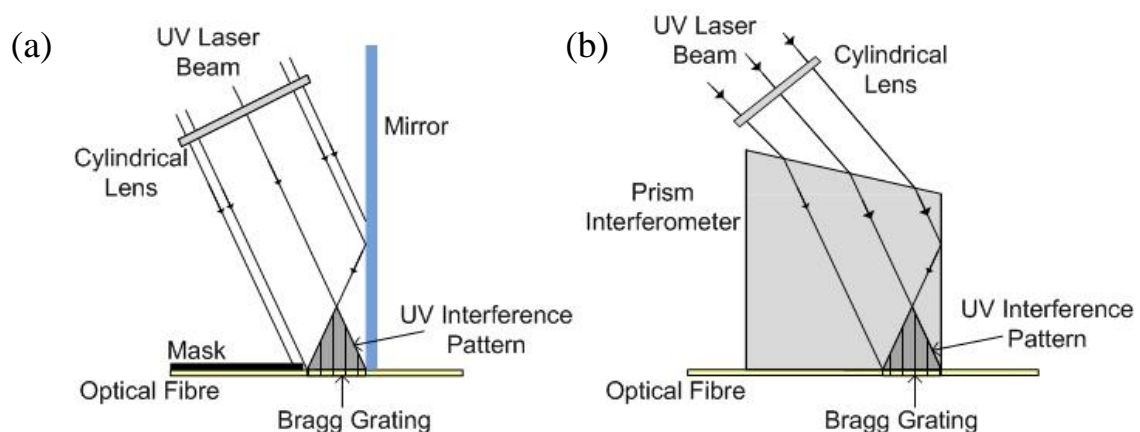


Figure 2-4 (a) Structural Diagram of a Lloyd's Mirror Wavefront Splitting Interferometer. (b) Structural Diagram of a Prism Interferometer.

The prism interferometer shown in Figure 2-4(b) uses a prism made from UV-grade fused silica, allowing for good UV transmission when the inscription laser beam is launched into it.

The UV beam is directed towards the meeting point between the surfaces of the prism which are parallel and perpendicular to the fibre axis. Similar to the Lloyd's mirror technique half of the UV beam is reflected off the surface of the perpendicular surface towards the fibre by total internal reflection. The reflected half of the UV beam is then recombined with the non-reflected half at the output surface of the prism, which is parallel to the fibre length. This results in an interference pattern which overlaps the optical fibre. At the high intensity points of the pattern the refractive index of the fibre is changed. Additionally like the Lloyd's mirror setup a cylindrical lens is included in the setup before the prism which focuses the UV beam along the length of the optical fibre core.

Both the wavefront splitting interferometer techniques hold a distinct advantage over the amplitude splitting interferometer in that they only have one optical component, significantly reducing the effects of mechanical vibrations. Additionally the separated UV beams travel a much shorter distance than the amplitude splitting interferometer reducing the potential risk of air current disturbances. The disadvantage of using this technique for fabricating FBGs is the setup only provides FBG lengths of up to half the width of the UV inscription laser beam. The Bragg wavelength (λ_B) can be defined by controlling the angle between the recombining UV beams, this can be adjusted by rotating the setup so to change the angle at which the UV laser beam is originally directed towards the reflecting surface.

2.4.2.3 Phase Mask Inscription

The phase mask inscription is a popular technique due to the high reliability and relative ease of fabricating FBGs. The phase mask technique was first seen in 1993[30-31] and has since surpassed both the amplitude and wavefront splitting interferometry techniques. The phase mask technique consists of passing a UV inscription laser beam through a single diffracting optical element (phase mask), which results in the production of an interference pattern similar to the previous two interferometry techniques.

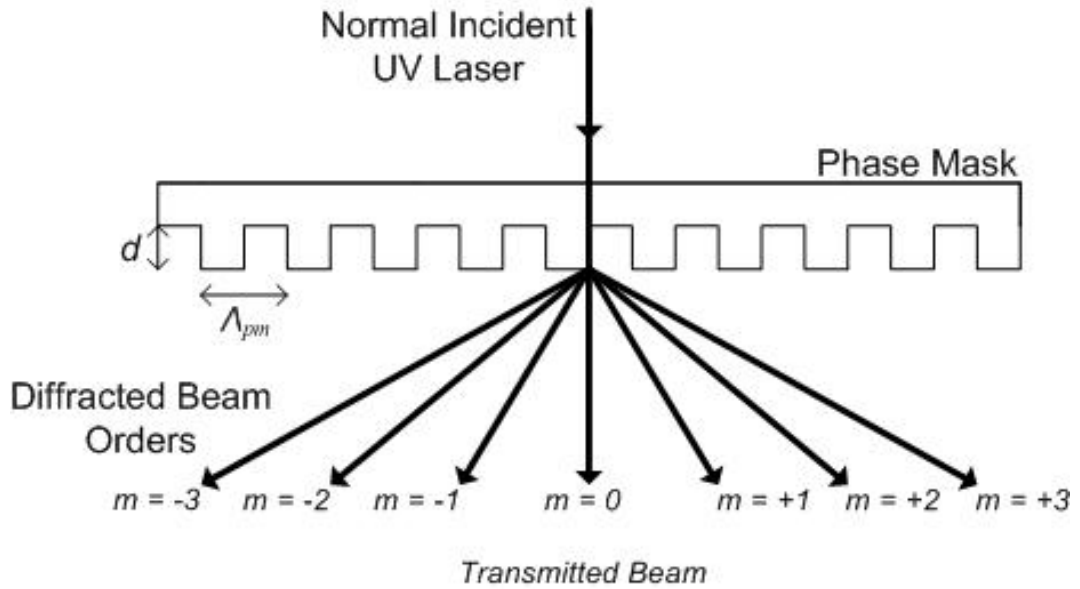


Figure 2-5 Incident UV beam passing through a phase mask, demonstrating beam splitting into different orders

The phase mask itself is a plate of fused silica which is transparent to the UV laser beam. On one side of the mask is a surface relief pattern with a square wave profile which has been etched into the surface using electron beam lithography or holographically. When the UV laser beam passes through the mask from the top surface the light is diffracted by the periodic relief pattern on the bottom surface of the mask. The UV laser beam is diffracted and split into different beams which travel in different directions, known as orders, specifically $m = 0, \pm 1, \pm 2, \pm 3$ and so on as demonstrated in Figure 2-5. The angle of diffraction (θ_m) can be calculated for each order in the following diffraction equation:

Equation 13

$$m\lambda_{UV} = \Lambda_{PM}(\sin\theta_m + \sin\theta_i)$$

Where (λ_{UV}) is the wavelength of the inscription UV laser beam, (Λ_{pm}) is the period of the relief pattern and (θ_i) is the angle of incidence of the UV inscription beam to the top surface of the phase mask. When the angle of incidence (θ_i) of the UV laser beam is normal to the top surface of the phase mask as shown in Figure 2-5, Equation 13 simplifies as shown:

Equation 14

$$m\lambda_{UV} = \Lambda_{pm}\sin\theta_m$$

$$\therefore \Lambda_{pm} = \frac{m\lambda_{UV}}{\sin\theta_m}$$

Whilst the angle of incidence (θ_i) is normal to the phase mask the angle of diffraction (θ_m) for both the positive and negative orders ($\pm m$) are equal. For the majority of FBG fabrications the diffracted light is limited to the orders $m = 0$ and ± 1 . For FBG fabrication the intensity pattern is generated from the diffracted ± 1 orders, therefore to maximise the intensity pattern

the zeroth order needs to be suppressed. This is achieved by careful design of the periodic profile of the surface relief pattern of the mask[32].

The generated interference pattern from the diffracted ± 1 orders can be considered the same as the one generated from the two separated beams in the amplitude splitting interferometry technique. Thus using Equation 11 and Equation 14, the period of the interference pattern (Λ) is one half of the period of the surface relief pattern of the mask (Λ_{pm}) as follows:

Equation 15

$$\lambda_{UV} = \Lambda 2 \sin\theta_m = \Lambda_{pm} \sin\theta_m$$

$$\therefore \Lambda = \frac{\Lambda_{pm}}{2}$$

As demonstrated in Figure 2-6, the phase mask is positioned parallel to the fibre surface as close as possible without actually touching so to protect the surface relief pattern of the mask from damage. The intensity pattern is typically focused along the length of the core of the optical fibre using a cylindrical lens prior to the phase mask. As with the previous fabrication techniques the high intensity points of the pattern result in a permanent refractive index change within the fibre core.

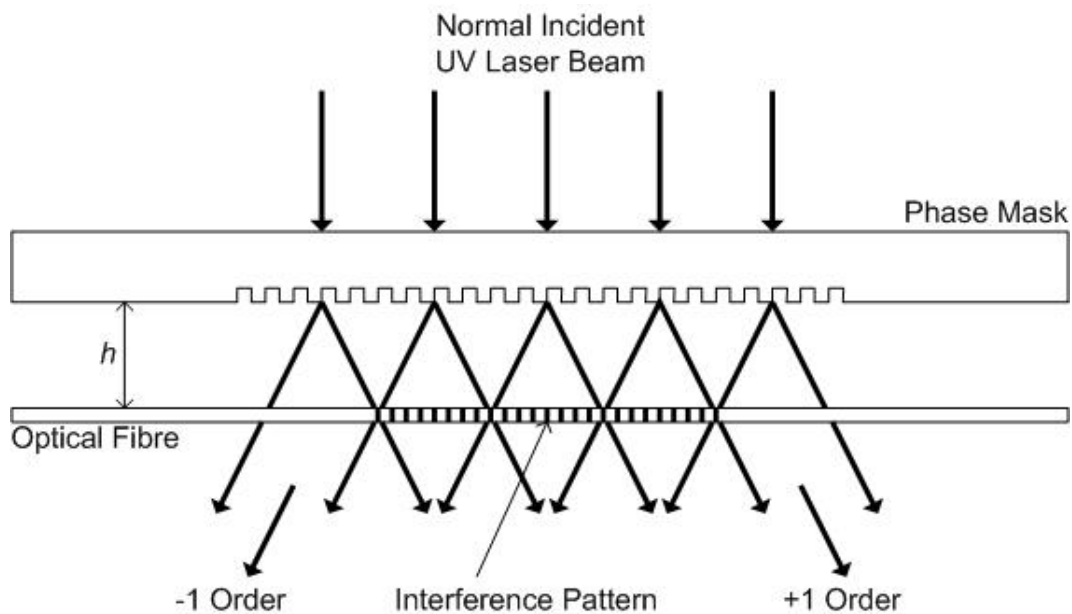


Figure 2-6 UV interference pattern generated from -1 and $+1$ diffraction orders of the phase mask

The clear advantage of the phase mask inscription technique over the two previous interferometry techniques is the high mechanical stability. The diffracted beams only have to travel a small distance from the relief pattern of the mask to the optical fibre. The ease of only using one optical component also adds to this stable setup, and at the same time allows

for a simpler and reliable fabrication technique. Nevertheless the phase mask technique has a significant disadvantage in that a new phase mask is required for each FBG designed with a different Bragg wavelength as can be seen when combining Equation 6 and Equation 15, where the Bragg wavelength (λ_B) is dependent on the period of the phase mask (Λ_{pm}):

Equation 16

$$\lambda_B = n_{eff} \Lambda_{pm}$$

This may lead to costly tooling especially if WDM sensors are required where a new phase mask would be needed for each FBG with a different Bragg wavelength. There is the possibility to slightly tune the Bragg wavelength by applying axial strain to the fibre during fabrication, and then once fabrication is complete the strain is released. An approximate 2nm Bragg wavelength shift was observed when this technique was employed in silica optical fibre[33].

2.4.2.4 Point-by-point inscription

This fabrication technique uses pulsed laser systems to directly fabricate each grating plane individually[34]. Malo *et al*[34], demonstrated the fabrication of a FBG with a krypton fluorine (KrF) excimer laser, emitting at 248nm. The UV laser beam was passed through a slit approximately 15 μ m wide and a lens with a focal length of 15mm was used to image the slit onto the core of the optical fibre. Gratings were fabricated in silica D-type polarisation maintaining D-shaped fibre. The point laser source exposure was through the flat side of the cladding of the D-shaped fibre. One pulse of the laser was used to fabricate a point change in refractive index of the core and hence a single grating plane. The optical fibre was then translated along its fibre axis a distance equal to the desired grating plane period (Λ). Here the next refractive index change would be induced from a single pulse of the laser, and so on until the fabrication of a FBG was complete. This same technique has also been demonstrated with a femtosecond pulse laser[35].

This technique is highly flexible with a wide range of grating periods, lengths and designs such as chirped Bragg gratings are possible, and is only limited by the resolution of the translation stage used to position the optical fibre.

2.4.2.5 LPG Fabrication

The fabrication of LPGs have been demonstrated using a point-by-point technique using UV radiation where each grating plane of the LPG was fabricated individually[36]. LPG fabrication has also been demonstrated with UV radiation with the use of an amplitude mask[37].

Furthermore femtosecond pulsed lasers have been used to fabricated LPGs as was demonstrated by Kondo *et al*[38]. Who first demonstrated the use of a 120 femtosecond

pulse width laser emitting at 800nm, with a repetition rate of 200kHz to fabricate LPGs in optical fibre.

2.5 Summary

In this chapter optical fibre has been introduced and the possible light propagation paths within the high refractive index core of the fibre waveguides. Additionally, microstructured polymer optical fibre (mPOF) was presented. Detailing how an array of air holes around a solid higher refractive index core enabled waveguiding conditions by reducing the average refractive index of the cladding region. As discussed mPOF allows for essentially pure polymer fibre to be used, this type of fibre has been used in the research of this thesis to fabricate POFBGs and their sensing capabilities to be characterised. Both FBGs and LPGs were explained in this chapter together with FBG sensing mechanisms to temperature and axial strain measurands.

Furthermore examples of internally and externally written FBG inscription techniques are reviewed. Particular focus was given to the phase mask technique as this has proven to be the most successful method by various research groups across the globe including Aston University. The phase mask technique provides the advantage of being the most stable inscription setup over long periods of time. This is vital for POFBGs with inscription times of at least 40 minutes reported[15, 24].

The research documented in this thesis is based on POFBGs which have been fabricated using the phase mask inscription technique. A detailed description of the inscription setup is described in Chapter 4 together with the optical interrogation method used to observe the Bragg response from the fabricated POFBGs.

3

POLYMER OPTICAL FIBRE BRAGG GRATINGS (POFBG)

Traditionally POF has been fabricated with a PMMA core and a fluorinated cladding, however in more recent years an increase in performance has been achieved where perfluorinated polymers for POF. Within the telecommunications industry perfluorinated POF has become a noteworthy component of transmission networks. For the last mile or local area networks (LANs) copper cabling is nearing an end due to the increasing demands on larger bandwidths needed to accommodate internet and other cable services. Therefore this final non-optical section of transmission networks needs to be replaced. However due to the large amount of cabling used in this section an economical solution was needed to complete a total optical transmission network. The cost-effective solution to this was and still is to use POF as the transmitting medium. Multimode POF (MM POF) with a typical diameter of 1mm offers desirable features to network installers; albeit at these large diameters POF is flexible and survives placement around sharp bends, ideal for LANs. However, it should be noted that large core step index POFs (SI POF) have limited bandwidth but this can be improved by employing graded index POF (GI POF). In addition, POF can be easily connected as the large diameter permits low alignment and positioning tolerances, termination is possible by cleaving the fibre ends simply by using a knife. Finally POF can be used in combination with low cost, broad emission area light sources such as light emitting diodes (LEDs) to provide the transmitting optical signal. Because of these features POF is often portrayed being low cost. However this is an advantage which really only applies to the telecommunication applications and does not truly apply to the POF itself but the cheaper installation costs and accompanying components needed when compared to silica based optical fibre networks.

The aforementioned advantages and thus the low cost classification however do not lend themselves to FBGs fabricated in POF. Mainly single mode POF (SM POF) is required for polymer optical fibre Bragg gratings (POFBG). Furthermore single transverse mode light sources are usually required to interrogate any FBG response, which are relative expensive components to purchase. As a result the motivation for fabricating FBGs in POF needs to be obtained from other properties of POF, which are somewhat different to silica. Therefore the optical and mechanical properties of POF will be discussed in the following sections.

FBGs have been mostly fabricated in poly (methyl methacrylate) (PMMA) based POFs. Therefore when reviewing the different properties of POF and characteristics of FBGs fabricated in POF they are given from a PMMA perspective unless stated. Other polymers

may be in existence which may possibly have more desirable properties compared to PMMA and attempts will be made to highlight these when they are significant to certain applications.

3.1 Chemistry of Polymer Optical Fibre

The chemical structure and properties of PMMA and polystyrene (PS) which is another common polymer used in POF are reviewed before the optical and mechanical properties of POF are discussed. These two polymers are also known as vinyl polymers and are made from vinyl monomers. Vinyl monomers are small molecules which contain a carbon-carbon double bond and make up the largest family of polymers which is the vinyl group, which is a group of organic compounds with a double bond. An example of a vinyl polymer is polyethylene, which is made from the vinyl monomer ethylene. The chemical structure of ethylene is shown in Figure 3-1 together with polyethylene, the product of polymerising ethylene. Once the vinyl monomers are polymerised they join together along the axis of their double bonds to form a long chain of carbon atoms and thus a polymer molecule chain is formed. Upon polymerising the carbon atoms only contain single bonds to other atoms and thus no vinyl groups exist in vinyl polymers. Vinyl polymers are a name given to polymers which are created from vinyl monomers.

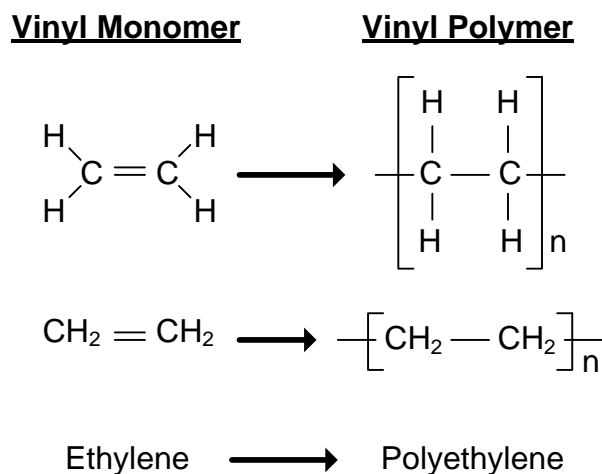


Figure 3-1 Chemical Structure of Ethylene and Polyethylene

Vinyl polymers are made from the polymerisation of the vinyl monomer through a chemical procedure known as free radical vinyl polymerisation. This will be discussed in more detail in Section 3.1.3. Before then, two more complex vinyl polymers will be introduced in the following sections, namely PMMA and PS. These are made from vinyl monomers where one or more of the hydrogen atoms of ethylene have been replaced with other atoms.

3.1.1 Poly (methyl methacrylate) (PMMA)

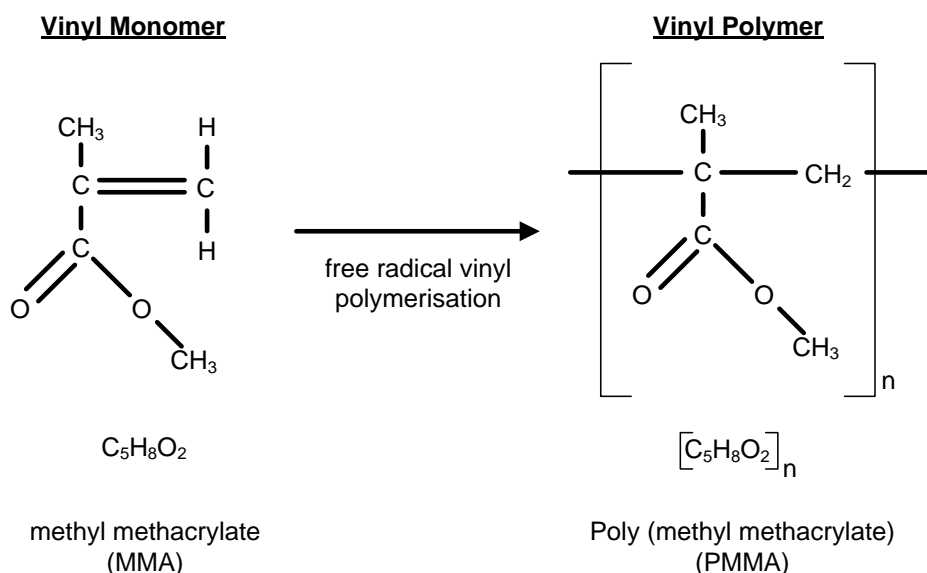


Figure 3-2 MMA and PMMA Chemical Structure

The majority of POFs are based on the vinyl polymer Poly (methyl methacrylate) which is normally abbreviated to PMMA, is also known as acrylic glass and also various trade names such as Perspex Plexiglas and Lucite. This vinyl polymer is manufactured from the vinyl monomer MMA as shown in Figure 3-2. PMMA has a glass transition temperature 103°C and a refractive index of 1.49[39].

3.1.2 Polystyrene (PS)

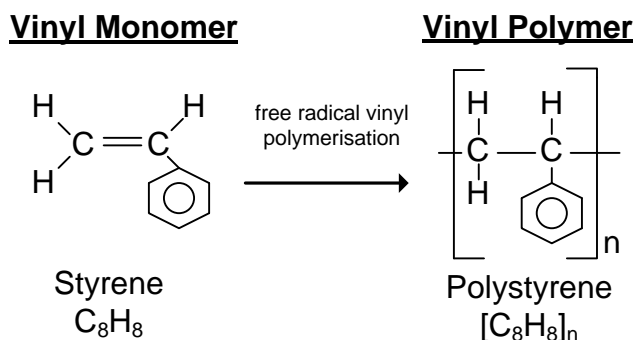


Figure 3-3 Styrene and Polystyrene Chemical Structures

Another vinyl polymer often used in the fabrication of POFs is polystyrene (PS), which is manufactured from the vinyl monomer styrene with a benzene ring, as shown in Figure 3-3. Polystyrene has a glass transition temperature of 100°C and a refractive index of 1.59[39].

3.1.3 Free Radical Vinyl Polymerisation

Free radical polymerisation is one of the most common reactions for making polymers and is used to produce polymers from vinyl monomers such as MMA. These monomers are exposed with another molecule known as a polymerisation initiator. One typical initiator which is often used is 2,2'-azo-bis-isobutyronitrile (AIBN), the chemical structures of this

molecule is shown below in Figure 3-4. Another polymerisation initiator often used is benzoyl peroxide.

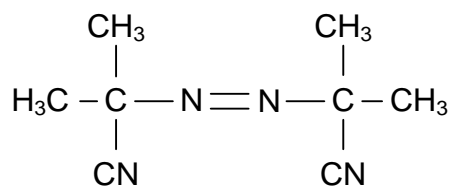


Figure 3-4 Chemical Structure of 2-2'azo-bis-isobutyronitrile (AIBN)

The AIBN molecule can easily be split by heating, once split the pair of electrons between the broken bond will separate. The molecule is split into two pieces known as initiator fragments of the molecule. These fragments will each have an unstable unpaired electron, and thus are known as free radicals, hence the name free radical vinyl polymerisation. AIBN can be broken down by heating the molecule to around 60-80°C, the thermal break down of AIBN is shown in Figure 3-5, where • represents a single unstable electron. Also shown is the escape of nitrogen (N) forming a triple covalent bond, thus very stable and prevents any reversing of the thermal breakdown.

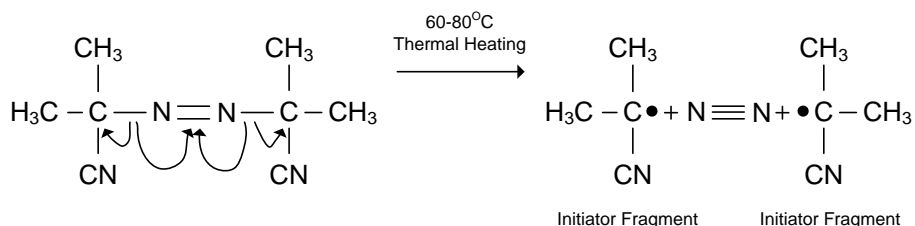


Figure 3-5 Thermal Breakdown of AIBN

The unstable free electrons look to become stable by bonding to other electrons to gain stability. The double C-C bond of a vinyl monomer is easily broken by the free radical and a new electron pairing forms a new chemical bond between the initiator fragment and one of the double carbon bonds of the monomer molecules, as is shown in Figure 3-6. This new pairing now leaves a remaining electron from the double carbon bond of the vinyl monomer and is thus a free radical. This new free radical is now looking to become stable by breaking the double carbon bond of another vinyl monomer and thus a chain reaction is begun and long polymer chains are created.

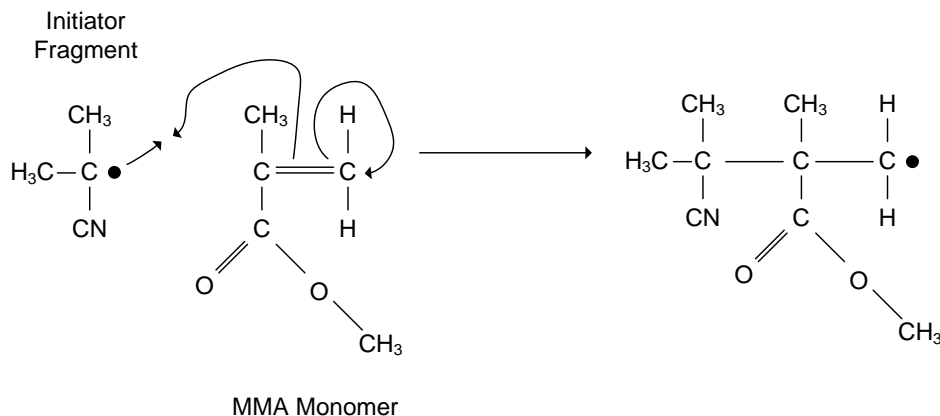


Figure 3-6 Initiator Fragment attaching to the MMA vinyl monomer, thus starting a chain reaction and creating a polymer chain

The polymer chain growth is stopped in a number of ways; one way is when two free radicals meet from separate polymer chains and form one longer chain, this is known as coupling. Another way to stop the chain reaction is when two growth polymer chains become in close proximity it is possible for a free radical of one of the chains to bond with an electron in the carbon-hydrogen bond of the carbon atom which is next to the other free radical of the second polymer chain. This results in the first polymer chain to have no free radicals and is thus stable, this is known as disproportionation.

It should be noted that a chain transfer agent is added to the chemical reaction, this is used to control the length of the resulting polymer chains. Controlling the length of the polymer chains allow for definition of different physical properties of the polymer[40]. Therefore using a suitable initiator and chain transfer agent polymerisation occurs and the polymer chain length or weight can be defined. Additionally the remaining amount of monomer after polymerisation can be controlled thus producing POF with an increased amount of monomer residue[10].

3.2 Optical Properties of Polymer Optical Fibre

Considered by many as a major disadvantage of POF are the wavelength dependent losses. The attenuation losses of a number of polymers are considerably larger than that seen in silica optical fibre. Across all wavelengths POFs have larger losses when compared to SOF, SOFs have their lowest losses in the 1300nm and 1500nm spectral regions whereas POF experience their lowest losses in the visible spectral region (550 – 750nm), and above this range the losses in POF significantly increase. Thus, silica optical fibre telecommunications systems are operated at either 1300nm or 1500nm and POF based transmission systems tend to be in the visible wavelength range. However POF is still impractical for long or medium haul telecommunication transmission links because of the relatively high losses even within the visible spectral range. The loss spectrum of PMMA based POF is

demonstrated in Figure 3-7, which also compares deuterated and fluorinated POF and additionally SOF for comparison.



Figure 3-7 Attenuation losses of optical fibres at various wavelengths, from [41]

3.2.1 Loss Mechanisms

The origins of loss in POF can be split into two categories, these are: intrinsic losses and extrinsic losses. Intrinsic losses are associated with both the material absorption and Rayleigh scattering; both of these are dependent upon the structure of the material of the POF and are therefore impossible to totally eliminate. Extrinsic losses are concerned with the imperfections within the POF normally created during the fabrication of the POF. But can also be created through bad examples of handling, for example inappropriate winding around sharp bends resulting in kinks along the POF length. During attempts to manufacture SM POF the polymer is often heated to a higher temperature during the drawing process which often leads to increased imperfections. Extrinsic losses can be minimised though by carefully optimising the POF manufacturing conditions and careful handling of the manufactured POF. Because of this intrinsic losses will be reviewed in more detail in the following sections, both types of losses are summarised in

Table 1[41].

Table 1 Summary of loss mechanisms in POF

Intrinsic Losses	
Loss Mechanism	Cause of Loss
Absorption	Vibration between carbon-hydrogen bonds Electronic Transition

Scattering	Rayleigh Scattering
Extrinsic Losses	
Loss Mechanism	Cause of Loss
Absorption	Contamination of POF by organic pollutants Dust
Scattering	Bubbles within the POF Micro-fractures along fibre length Core-cladding interface imperfections
Out coupling	Micro bending losses, resulting in permanent kinks along length of fibre

3.2.2 Intrinsic Absorption Losses

As was seen in Figure 3-7 PMMA based POFs demonstrate high attenuation particularly in the near infrared (NIR) wavelength region. The reason for these high attenuation losses are predominantly associated with the non-metal carbon-hydrogen (C-H), nitrogen-hydrogen (N-H) and oxygen-hydrogen (O-H) bonds of the polymer material with a particular high absorption band seen between the C-H bonds. This absorption band is directly related to the harmonics of the vibrations of the C-H bonds. Figure 3-8 demonstrates with increasing wavelength the attenuation of a PMMA core of a POF increases due to the harmonics of the C-H bond. Losses of around 10dB/km are seen in the visible spectral region, whereas losses of up to 10^6 dB/km are seen at 1300nm or 1500nm, regions which are commonly used for silica optical fibre transmission networks.

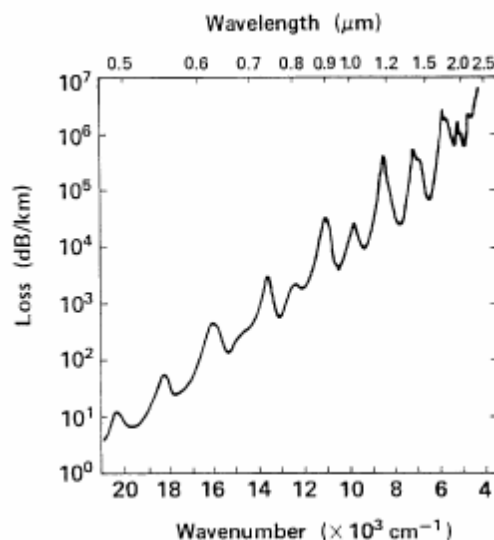


Figure 3-8 Harmonics of C-H bond in the PMMA core of a POF

Another type of absorption is electronic transition absorption. This is the UV absorption in solid materials and in the case of POF concerns the transitions between the electronic energy levels within the polymer molecule chain bonds.

3.2.3 Intrinsic Scattering Losses

Rayleigh scattering is a result of irregularities of the chemical structure of the polymer core within the POF. These irregularities are a result of fluctuations in the core material density, together with changes in the composition and orientation of the polymer molecules. Thus if the core of a POF is fully polymerised Rayleigh scattering is a result of fluctuations in the material density whereas if the core is only partially polymerised then Rayleigh scattering tends to be a result of the varying composition of the material. As the wavelength of the light which is being guided within the core of a POF increases the Rayleigh scattering decreases. Ballato *et al* calculated the Rayleigh scattering of a number of polymers and compared them to that of SOF[42]. It can be seen in Figure 3-9 that these polymers have a lower Rayleigh scattering than that of silica.



Figure 3-9(a) Attenuation due to Rayleigh scattering in PFCB (TVE), PMMA, Cytop, Teflon and Silica. (b) Attenuation due to Rayleigh scattering, linearised to $(1/\lambda^4)$ abscissa [42]

3.2.4 Perfluorination and Deuteration

Another type of POF which should be introduced is perfluorinated (PF) graded index (GI) polymer optical fibre (PF GI POF). Manufacturers of this PF GI POF are Chromis Fiber Optics[43] and also Asashi Glass Co. Ltd produced a PF GI POF with a trade name of CYTOP (Cyclic Transparent Optical Polymer) but is also known as LUCINA[44]. This later CYTOP POF has demonstrated the potential to replace the copper cabling in the last mile of LAN networks for telecommunications, when in the year 2000 a 1Gbit/s LAN was installed at Keio University which was made from this POF and has since progressed into other LANs across Tokyo[44].



Figure 3-10 Chemical Structure of PF GI POF (CYTOP)[39]

As can be seen in Figure 3-7 PF GI POF has significantly lower attenuation losses across the 700-1500nm wavelength range and was also discussed in ref[45]. CYTOP has a refractive index of 1.34 and a glass transition temperature (T_g) of 108°C[39]. As can be seen in Figure 3-10, there are no C-H bonds, which are a main source of absorption due to their harmonic vibrations as discussed in section 3.2.2. Instead C-F bonds instead exist; this is a much stiffer bond and thus reduces the vibration absorption of the material when compared to PMMA.

Deuterium also known as heavy hydrogen can also be added to PMMA and made into the deuterated PMMA POF. This is likely to give lower attenuation when compared to standard PMMA POF as was shown in Figure 3-7. The lower attenuation is the result of the heavier hydrogen used which harmonic vibrations between the C-H bonds, this in turn increase the absorption wavelength to much higher in the spectrum. However deuteration is not a simple process which is reflected in the cost of deuterated PMMA POF which has lead to limited research using this type of POF.

3.3 Photosensitivity

As was discussed in Chapter 1, research into the photosensitivity of PMMA began in the early seventies. Both Tomlinson[6], Moran[46] and Bowden[8] focused in inscribing grating structures into planar waveguides of polymer. It was first reported by Tomlinson *et al*[6] that an increase in the refractive index in a specifically prepared PMMA sample when exposing the point in the sample of increased refractive index to UV irradiation from a 325nm HeCd laser. However Tomlinson reported that the PMMA sample required pre-conditioning prior to the UV exposure to enable the increase in refractive index by up to 3×10^{-3} . This involved exposing the MMA to oxygen and UV light from a 5W mercury lamp for 48hours. The exposure resulted in peroxidation of the monomer, oxygen atoms are formed leading to the production of peroxides. It was also noted that when exposing a PMMA sample which had not gone through the additional peroxidation stage did not exhibit any photosensitivity to the UV exposure from the HeCd laser.

3.3.1 Mechanism of Increased refractive Index

Two mechanisms have been suggested for the origin of the increase refractive index when exposed to UV irradiation. Either or possibly both the density of the polymer at the point of exposure increases in density or the molecular polarisability, hence changing the molecule electron distribution at the point of UV exposure. In the first report by Tomlinson *et al*[6], the increase in refractive index is attributed to increase in density of the peroxidised polymer sample. It has also been demonstrated that the density of a PMMA sample increases when exposed to 325nm UV irradiation by Bowden *et al*[8]. The demonstration consisted on optimising the concentration of a calcium nitrate ($\text{Ca}(\text{NO}_3)_2$) bath so to balance an unexposed polymer sample on its surface, the sample was then irradiated by a UV light

source and was placed back into the bath. The sample then floated to the bottom of the bath suggesting the density of the irradiated sample had indeed increased.

3.3.2 Photosensitivity to lower UV wavelengths

Characterisation of the photosensitivity of PMMA to lower wavelengths, namely 193nm and 248nm has also been conducted by Wochnowski *et al*[47]. Both X-ray photoelectron spectroscopy (XPS) and fourier transform infrared (FTIR) spectroscopy were used to compared samples of PMMA which had been UV irradiated. Using an irradiating wavelength of 248nm and a fluence of less than 15mJ/cm² it was noted that complete scission of the side chains was caused by the exposure. Whereas when the fluence was increased to 30mJ/cm² can keeping the same wavelength of 248nm fragmentation of the polymer side chain was noted. It was also noted when the sample was exposed to these conditions for a prolonged period of time to resulted in the scission of the polymer backbone. When the effect of the 193nm UV light source was investigated it was noted that partial side chain separation was caused, however no backbone scission was observed.

In the research of Wochnowski *et al*[47], an increase in refractive index was also noted at both wavelengths as a result of densification. It was speculated that the most probable cause of the increase in density was Van der Waals forces pulling neighbouring molecules closer together as a result of the removal of the polymer side chains from the UV irradiation. It was noted that the greatest densification resulted from the 248nm irradiation, hence where the greatest side chain removal was observed.

Although refractive index changes have been demonstrated in PMMA samples using either 248nm or 193nm irradiation wavelengths these are impractical for POFBG inscription due to the absorption spectrum of PMMA. The penetration depth of either 248nm or 193nm into PMMA is less 10µm. If this is compared to the standard geometry of optical fibre then the distance to the core through the cladding is 62.5µm, thus highlighting the impractical task of inscribing a grating within the core of the fibre. Figure 3-11 shows the results gathered by Srinivasan *et al*[48] which demonstrate the UV absorption of PMMA. The results show the increased UV absorption for both the 248nm and 193nm emission wavelengths of an excimer laser when compared to the 325nm emission wavelength of a HeCd laser.

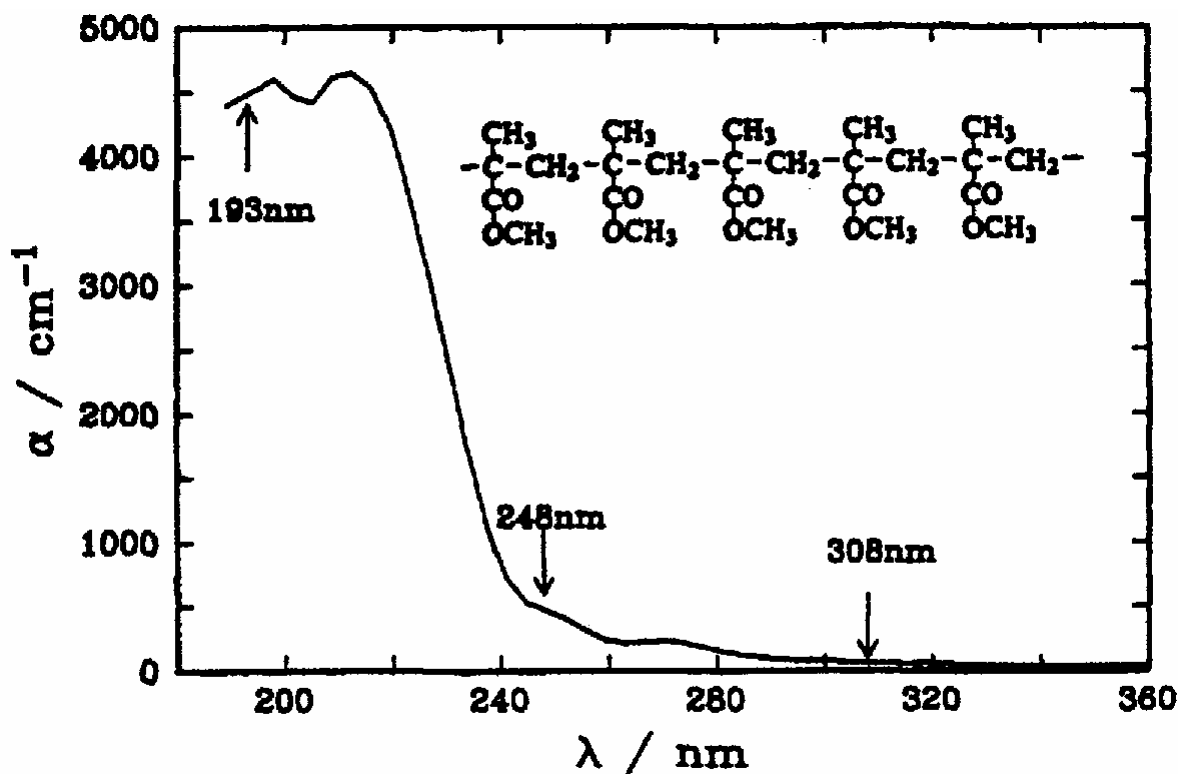


Figure 3-11 UV absorption of PMMA. Noted wavelengths correspond with the emission wavelengths of an excimer laser.

It should also be noted POFBGs have also been fabricated in fibre where the core has been doped to increase the photosensitivity when compared to the cladding and thus controlling the location of the Bragg grating and increasing fabrication times. In 1971 Laming[49] demonstrated photosensitivity to 488nm by adding p-benzoquinone to PMMA. Ultra violet exposure was then used to fix gratings in the PMMA, where a decrease in the refractive index was observed. Research into adding dopants to POF based on PMMA to provide photosensitivity at other inscription wavelengths includes work from Peng *et al*[50], who added fluorescein which increased the photosensitivity at both 488nm and 524nm. Also, Yu *et al*[51] used trans-4-stilbenemethanol to demonstrate trans-cis photoisomerisation when using a light source within the 250-350nm spectral region.

3.4 Temperature Sensitivity

When considering the thermal response of PMMA, the most common choice of material for POF, the humidity sensitivity of this material also has to be considered. Sensitivity to humidity and the effects of cross-sensitivity of relative humidity (RH) when measuring temperature sensitivity is discussed further in Chapter 9. Previously the temperature sensitivity of PMMA based POFBGs have been characterised within the laboratory environment, which has the possibility to be influenced by any change in relative humidity of this given environment. As a result it is felt this may be a contributing factor to temperature sensitivities quoted in previous work[21]. Liu demonstrated a temperature sensitivity of around 300pm/°C, although varying sensitivities may also be a result of different materials used in the manufacturing of the POF

and hence different temperature sensitivities or also different drawing parameters used during fibre manufacturing can change the temperature sensitivities of POF.

However, more recently the temperature response of a PMMA based POFBG has been captured where the relative humidity was kept at a constant 45 %, by placing the POF sensor in an environmental chamber. Figure 3-12 demonstrates a temperature sensitivity of -43pm/°C; this was calculated whilst monitoring the Bragg wavelength shift across a temperature range of 18-39°C and keeping the relative humidity constant at 45%. The negative temperature sensitivity of the PMMA based POFBG can be explained when reviewing Equation 17[26]:

Equation 17

$$\Delta\lambda_B = \lambda_B(\alpha_\lambda + \alpha_n) \Delta T$$

Where $\Delta\lambda_B$ is the change in Bragg length, λ_B is the original Bragg wavelength, ΔT is the change in temperature, α_λ is the thermal expansion coefficient and α_n is the thermo-optic coefficient. First, if silica fibre is investigated both α_λ (0.55×10^{-6} cm/cm/°C) and α_n (8.6×10^{-6} /°C) are positive and the resultant index change is the dominating factor. Therefore, when reviewing Equation 17, a positive temperature sensitivity of approximately 14pm/°C is observed for a silica optical fibre FBG fabricated with a 1550nm Bragg response[26, 52].

When considering POF based on PMMA, the material thermal expansion coefficient (α_λ) is 8.0×10^{-5} cm/cm/°C and the thermo-coefficient (α_n) is -1×10^{-4} /°C[52]. Again, when considering Equation 17, it can be seen how the negative sign of the thermo-optic coefficient and the relative magnitudes of both coefficients generates a negative temperature sensitivity for POFBGs based on PMMA. Table 2 summarises the thermal expansion and thermo-optic coefficients for both silica and PMMA. It can be seen in Table 2 that the change in refractive index has a much larger effect on the Bragg wavelength compared to the change in period of the UV inscribed fringes of the interference pattern within the POF core.

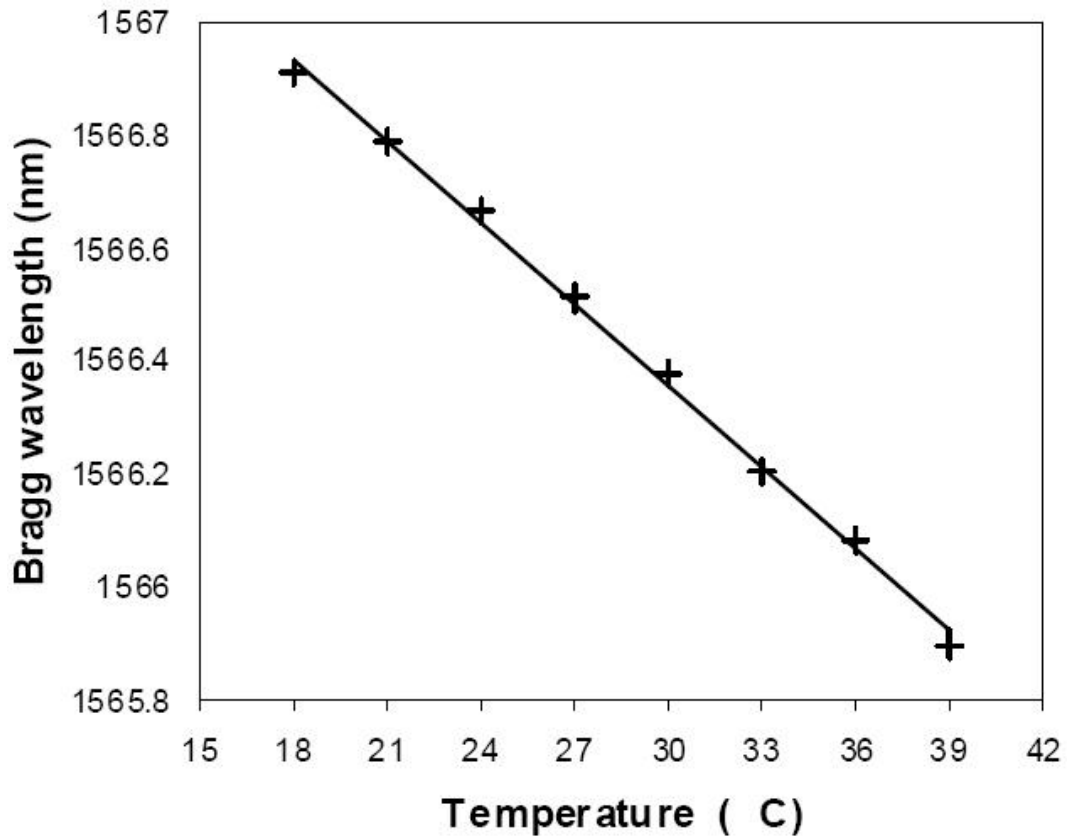


Figure 3-12 Thermal sensitivity of a PMMA based POFBG, results taken with a constant relative humidity of 45%

Table 2 Summary of Silica and PMMA thermal expansion and thermo-optic coefficients

Fibre Material	α_{λ} (cm/cm/°C)	α_n (/°C)
Silica	0.55×10^{-6}	8.6×10^{-6}
PMMA	8.0×10^{-5}	-1×10^{-4}

Using Equation 17 and the data given in Table 2, the temperature sensitivity can be predicted for the POFBG used to measure the temperature sensitivity from Figure 3-12. The expected temperature sensitivity for the POFBG with a Bragg wavelength at 1566.9nm is -31pm/°C. When comparing the predicted sensitivity to the measured sensitivity in Figure 3-12, it is important to note the varying coefficient values quoted in literature. For example the refractive index changes as the water content increases within the fibre and will inevitably cause a variety of stated thermo-optic coefficients depending on the relative humidity the measurements were made in and hence the water absorption of the polymer[53]. Furthermore, differences of the relative humidity when thermo-optic coefficient measurements were made of bulk polymer and when temperature sensitivity characteristics of POFBG were taken are also likely to induce slight discrepancies in measured and predicted temperature sensitivities in POFBG sensors.

The glass transition temperature (T_g) of PMMA which is 105°C[39], limits the temperature operating range of POFBG sensors. PMMA is an organic glass at room temperature or at any temperature below the T_g , above this temperature PMMA is in a rubbery state, where it is soft and flexible. PMMA is an amorphous polymer, when above the T_g the polymer molecule chains move freely around and slide over each other, therefore when PMMA is bent for example above 105°C the molecules, already in motion, hold no resistance to move into new positions and relieve any stress that has been placed on them. On the other hand when PMMA is below the T_g the polymer chains are unable to move, therefore when stress is applied to the material the chains are unable to dissipate the stress and the chains will either resist the stress if they are strong enough or the stress will be too large for the chains to resist and the polymer will break or shatter.

As the temperature of the POFBG nears the T_g a significant amount of hysteresis is seen when returning to the original Bragg wavelength as the POFBG sensor is cooled down. Work completed by Carroll found that annealing the POFBG increased the operating temperature range of a PMMA based POFBG[24]. Here a FBG fabricated in pure PMMA mPOF was heated in three consecutive cycles using a 25W power resistor, after each cycle the temperature was returned to room temperature. Once room temperature had been reached the following heat cycle was then applied, ten minutes was allowed for each new temperature to stabilize before a Bragg response was captured on an OSA. The first heating cycle took the temperature to 77°C, the second increased the temperature range to 86°C and the third cycle increased the temperature range further to 92°C. Shown in Figure 3-13 is the resultant Bragg wavelength shift of the POFBG against temperature during each heating cycle.

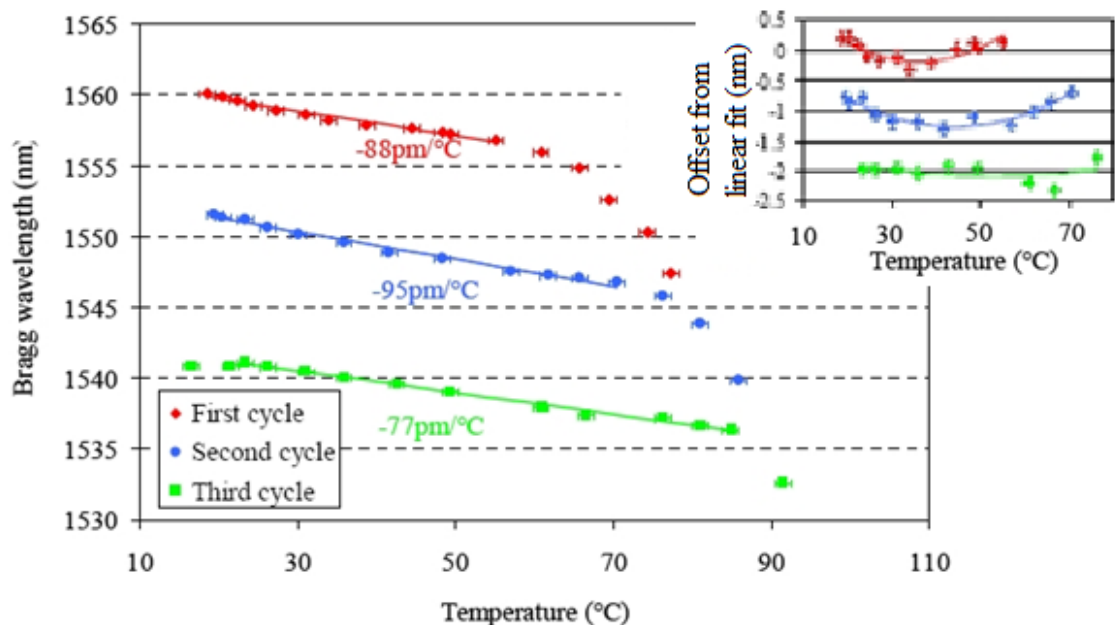


Figure 3-13 Bragg wavelength shift due to three heating cycles of a FBG fabricated in pure PMMA mPOF, insert illustrates the offset of the linear fit.

As is seen in Figure 3-13, during the first heating cycle the Bragg wavelength is seen to decrease considerably after 60°C, the temperature is increased further to 75°C. At this point the heat was removed and the POFBG is returned to room temperature (23°C) where a shift in the Bragg wavelength was observed of -8.4nm when compared to the starting Bragg wavelength at room temperature. During the second heating cycle a dramatic decrease in the Bragg wavelength is now seen after 76°C, close to the temperature where the first cycle was stopped. The second cycle was stopped at 85°C, once the grating had returned to 23°C a difference of -10.1nm was measured between the start of the second and third heating cycles. The same trend was seen during the third heating cycle, where a linear temperature sensitivity response was seen up to 85°C, again a similar temperature to the maximum temperature of the previous heating cycle, the third heating cycle was stopped at around 90°C. After the three heating cycles a Bragg wavelength shift of -18.5nm was measured.

It should be highlighted that although Figure 3-13 shows a linear trend during the three cycles at low temperatures, this is actually a nonlinear region. The deviation from the linear fit as demonstrated in the inset of Figure 3-13 and is attributed to the sensitivity to relative humidity of the POF, as there was no control of the humidity during the investigations.

It was concluded that the observed negative Bragg wavelength shift monitored at room temperature of the POFBG and the rapid decrease in Bragg wavelength against increased temperature once a certain temperature had been reached was a result of the POF shrinking. Hence the linear temperature sensitivity range was increased for each cycle as the fibre was shrinking further the temperature was increased in each heating cycle[24].

POF is manufactured by pulling a polymer in fibre under tension at a temperature above its T_g of around 200°C, resulting in the alignment of the molecular chains of the PMMA along the fibre axis, hence in the axis it was pulled in and left over stress remains within the fibre. As the POF is heated towards the T_g the molecular chains are thought to begin to relax causing the fibre to shrink and near a rubbery state which is fully achieved once the temperature is increased above the T_g . In the work by Carroll, shown in Figure 3-13 this transition and hence shrinkage appears to begin at 60°C[24]. Previously this shrinking effect has been reported as a function of the drawing tension when manufacturing the fibre[54]. The temperature at which the shrinkage begins has previously been shown to be influenced by the fibre drawing parameters[54] and also the exposure to UV[55].

Furthermore Carroll also investigated if the pure PMMA mPOF could be thermally annealed prior to FBG fabrication[24]. A length of the mPOF was heated in an oven at 80°C for 7 hours, resulting in the fibre length decreasing by $(98.7 \pm 0.5)\%$ and the fibre diameter increased by $(105.6 \pm 0.5)\%$. A FBG sensor was successfully then fabricated into the thermally annealed mPOF and when the temperature sensitivity of the sensor was found to be linear up to 89°C with a sensitivity of -52pm/°C. This therefore demonstrates an extended

operating temperature range up to 90°C whilst experiencing no change in the Bragg wavelength when returning to room temperature. Furthermore there has been no permanent negative Bragg wavelength shift as a result of heating the mPOF post FBG fabrication.

The permanent negative Bragg wavelength shifts documented by Carroll[24] can however be used as a tool to tune a Bragg response to a desired wavelength to coincide with an interrogating light source for example or be used as part of a fabrication technique to manufacture wavelength division multiplexed (WDM) sensors in POF, both of which are demonstrated within this Thesis. Thermal annealing of mPOF and fabrication of WDM sensors is discussed further in Chapter 8.

Temperature sensitivities of POFBG sensors, whether stated by Liu, Carroll or Harbach[14, 21, 24] compare favourably with the typical temperature sensitivity of +10pm/°C for FBG sensors fabricated silica optical fibre[5, 29]. A clear disadvantage of using POFBGs as temperature sensors is their limited temperature range of up to 100°C.

3.5 Summary

This chapter has seen PMMA introduced as the most common polymer choice for POF to fabricate FBGs in. As part of the introduction the chemical structure of PMMA was given together with the explanation of how PMMA is produced from a MMA vinyl monomer using free radical vinyl polymerisation. Based on PMMA the optical properties POF were also discussed. The optical losses of POF were presented and the mechanisms behind those losses detailed.

The photosensitivity of PMMA to UV irradiation has been discussed together with the possible mechanism of densification resulting in the increase in refractive index of the polymer after being exposed to a UV source.

Finally the sensitivity of PMMA POFBGs to temperature was reviewed and the cross-sensitivity to relative humidity debated. It should be highlighted that POF does not necessary need to be fabricated from PMMA. Bragg gratings has also been demonstrated mPOF has been fabricated from TOPAS[56] a cyclic olefin copolymer[57]. TOPAS POF offers the potential resistance to relative cross humidity when monitoring changes in temperature, and is investigated further in Chapter 9.

4

GRATING FABRICATION IN POF

In this chapter the techniques for fabricating FBGs in POF are reviewed. Building on the previous work of Dobb *et al*[15], the phase mask fabrication technique is employed to manufacture FBGs in POF in this thesis and is thus detailed. Also in this chapter, the interrogation procedure is documented allowing for the optical response of the FBGs to be characterised and additionally the growth of the Bragg response of the gratings to be monitored. Furthermore the fabrication of LPGs in POF is demonstrated. Finally the fabrication of more complex interferometric grating structures is discussed.

4.1 Fibre Bragg Grating Fabrication in Polymer Optical Fibre

Previously FBG sensors have been fabricated in POF using a ring interferometer setup[21] and the phase mask technique[15] using an inscription UV laser with a wavelength of 355nm or 325nm respectively. The fabrication technique chosen for FBGs in POF in this thesis is developed from the phase mask technique demonstrated in[15]. This technique is chosen because of the potential inscription times of at least 40 minutes in PMMA based POF, requiring the optical setup to be extremely stable. As discussed in Chapter 2 the phase mask technique has the best immunity to mechanical vibrations due to the small optical path the diffracted beams travel before recombining and producing an interference pattern within the fibre.

Dobb investigated the possibility of applying an amplitude splitting interferometry technique to fabricate gratings in POF[58]. This was explored because of the potential to define the Bragg wavelength and hence investigate the fabrication of Bragg gratings at lower wavelengths where the attenuation of POF is significantly lower[59]. Using a Mach-Zehnder Interferometer, Dobb demonstrated the continuous movement of the interference pattern generated from the two recombining beams. The pattern randomly moved in excess of the width of one fringe of the intensity pattern and therefore demonstrated the instabilities of the optical setup. Possible reasons for this arose from the inscription UV laser being positioned on the same optical bench as the interferometer resulting in vibrations being transferred to the optical bench and therefore the optical setup. Additionally the cooling fan of the laser pushed air across the un-shielded optical setup, resulting in inevitable air current disturbances. Furthermore the random movement of the interference pattern may have been a result of instabilities of the optical components and their mounts themselves. Because of these instabilities, Dobb ruled out amplitude splitting interferometry as a technique to fabricate POFBGs especially when considering the long exposure times required for POFBG

fabrication. The same potential instabilities were likely during fabrication of POFBGs in the work reported in this thesis and therefore the decision was made to continue with the phase mask technique of fabricating POFBGs used by Dobb[15].

4.1.1 Phase Mask Inscription of FBGs in POF

The phase mask technique used to fabricate POFBGs in this thesis is shown in Figure 4-1. Although the range of Bragg wavelengths possible is limited by the amount of phase masks available it was felt the phase mask technique would produce the most consistent and reproducible inscriptions.

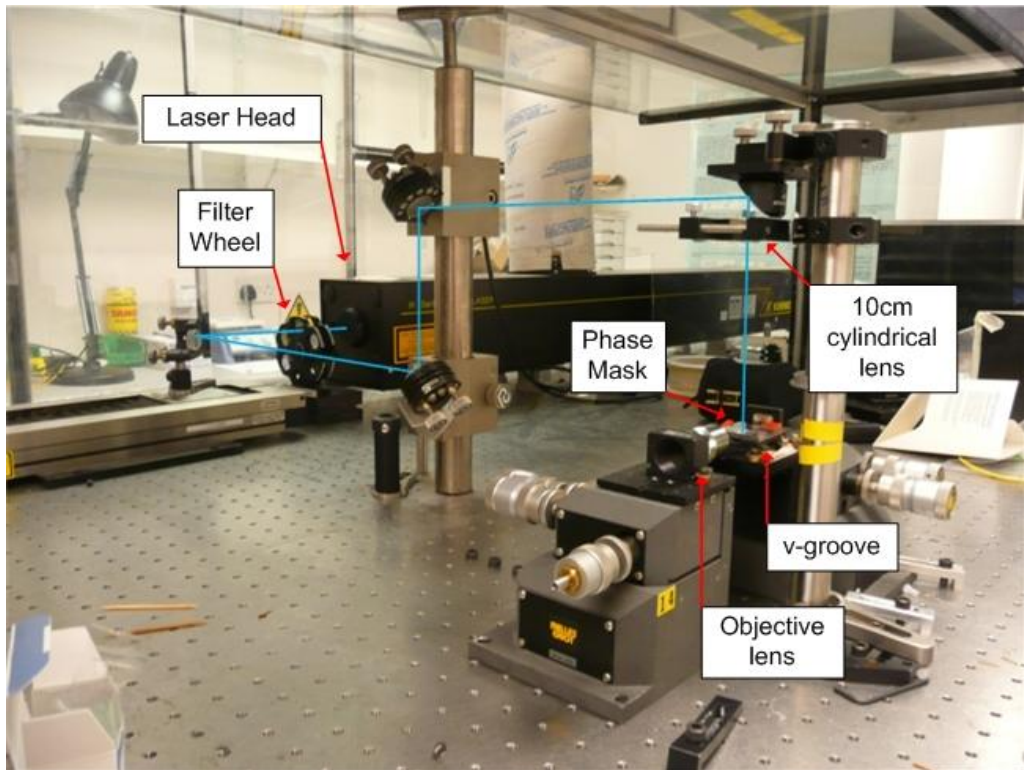


Figure 4-1 Optical setup for the fabrication of POFBGs

A continuous wave, 30mW Kimmon Koha Co, Ltd, IK3301R-G helium cadmium (HeCd) laser was used as the UV inscription light source with a wavelength of 325nm. This particular choice of wavelength is discussed in Chapter 3. The laser was placed directly onto the optical bench and the emitted laser beam was directed towards a periscope at its original height from the laser head using a single mirror. The height of the beam was increased to approximately 40cm above the optical bench and directed across towards the second stanchion. The mirror on the second stanchion then directed the UV beam vertically down, perpendicular to the optical bench. The vertical beam was passed through a plano-convex cylindrical lens which had a focal length of 10cm. This lens focused the UV light down to the POF, which was mounted upon a v-groove plate. Suspended above the POF was the phase mask. The focussed UV laser beam passed through the mask and the intensity pattern of the diffracted orders was projected into the POF core, resulting in a periodic refractive index change.

4.1.1.1 Fibre and Phase Mask Mounting

Due to the POFBG fabrication times, not only does the stability of the optical components need to be maximised but also the POF itself. When fabricating FBGs in silica optical fibre inscription times are typically between 90-120 seconds, therefore the stability of the fibre is less crucial than with POF. The POF is susceptible to drooping if mounted in a similar way to silica optical fibre over long time periods, where the fibre is suspending between two spring clamps. The drooping of the fibre will also be exaggerated by the heating of the POF due to the UV exposure. This together with further displacement of the POF because of any air currents across the optical bench has the potential of misaligning the focussed UV intensity pattern away from the POF core, resulting in no fabrication of a POFBG.

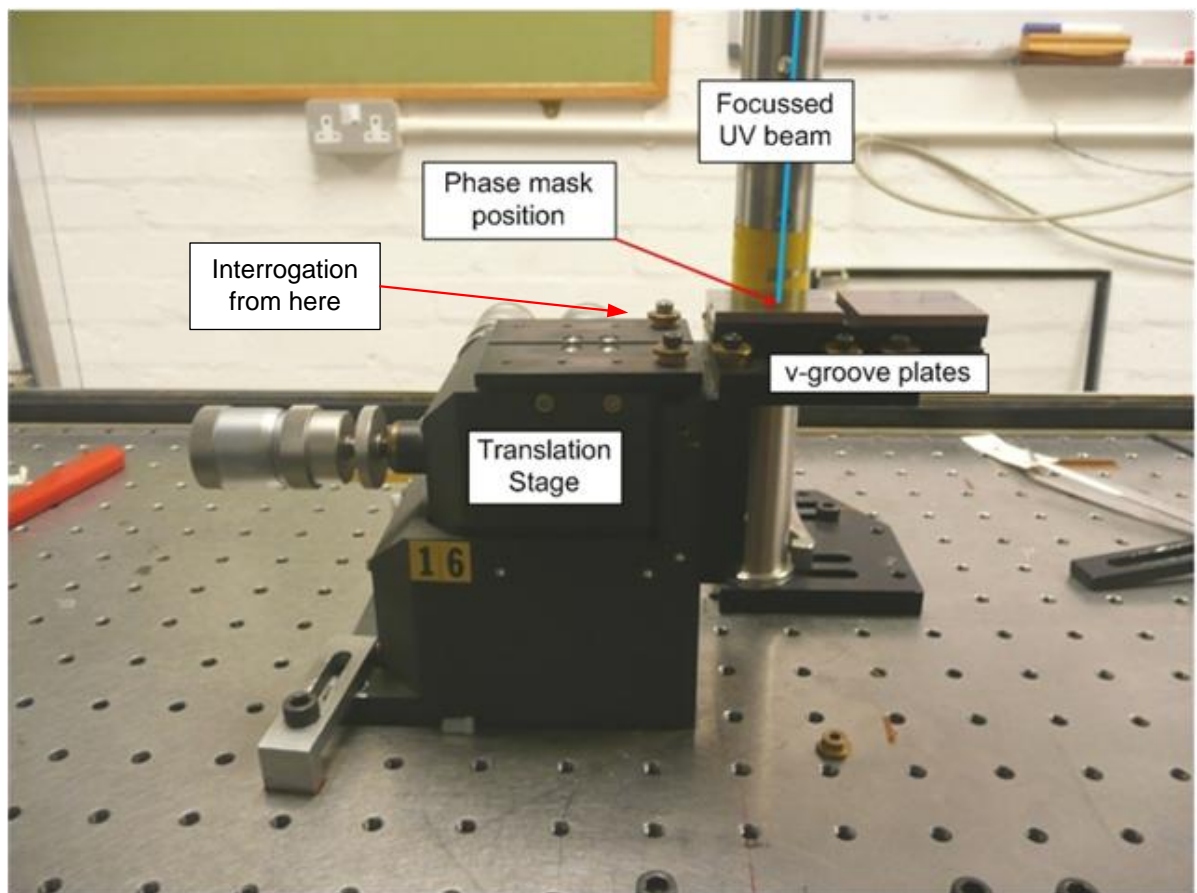


Figure 4-2 V-groove plates which the POF is mounted onto, which in turn is fixed to a translation stage.

Additionally the spring loaded clamps used to suspend silica optical fibre are likely to crush the POF, resulting in permanent damage to the fibre. This would possibly prevent guidance in the core of the POF at either end of the fibre; consequently the monitoring of the growth of the Bragg response from the grating would not be possible. Conceivably the damaged ends of the POF could be removed after inscription, however POF is not currently readily available and it would not be cost effective to sacrifice approximately 5cm of POF for each fabrication. Furthermore fibre clamp holders do not lend themselves well to POFBG interrogation as

discussed later in this chapter where butt coupling is used to launch the interrogate light into the POF and monitoring any possible reflected Bragg response.

A preferred, more practical way for POFBG fabrication is to mount the POF onto v-groove plates along the entire length of fibre where the FBG is being inscribed, thus preventing the POF from any sagging during grating fabrication. The v-groove plates in-turn are permanently mounted onto the stationary part of a Melles Griot XYZ translation stage as shown in Figure 4-2.

To mount the POF it was first placed onto the permanently fixed v-groove at the interrogation end of the plate with a 1mm overhang clear of the edge. The small overhang enables interrogation via butt coupling to silica optical fibre yet small enough to minimise displacement due to air currents across the optical bench or curling of the POF. The fibre was then taped down at this end using polyimide tape and pulled taut along the v-groove. The fibre was then taped down in two intermediate positions along the fibre length, ensuring the fibre was taut with no slack or curvature along the fibre length. The two intermediate sections of tape are positioned both sides of the focus point of the UV laser beam into the POF and consists of three layers of polyimide tape. This was essentially to rest the phase mask upon either side of the surface relief pattern, suspending the silica mask a measured distance of 200 μ m above the fibre surface. The distance of 200 μ m was achieved by using three layers of polyimide tape, which was measured using a set of callipers. The remaining end of the fibre was then taped down along the remainder of the v-groove, again ensuring the fibre is taut in the groove and there was sufficient overhang off the plate to allowing monitoring of light guidance within the core when interrogating the Bragg grating, as explained later.

4.1.1.2 UV Laser Beam Alignment

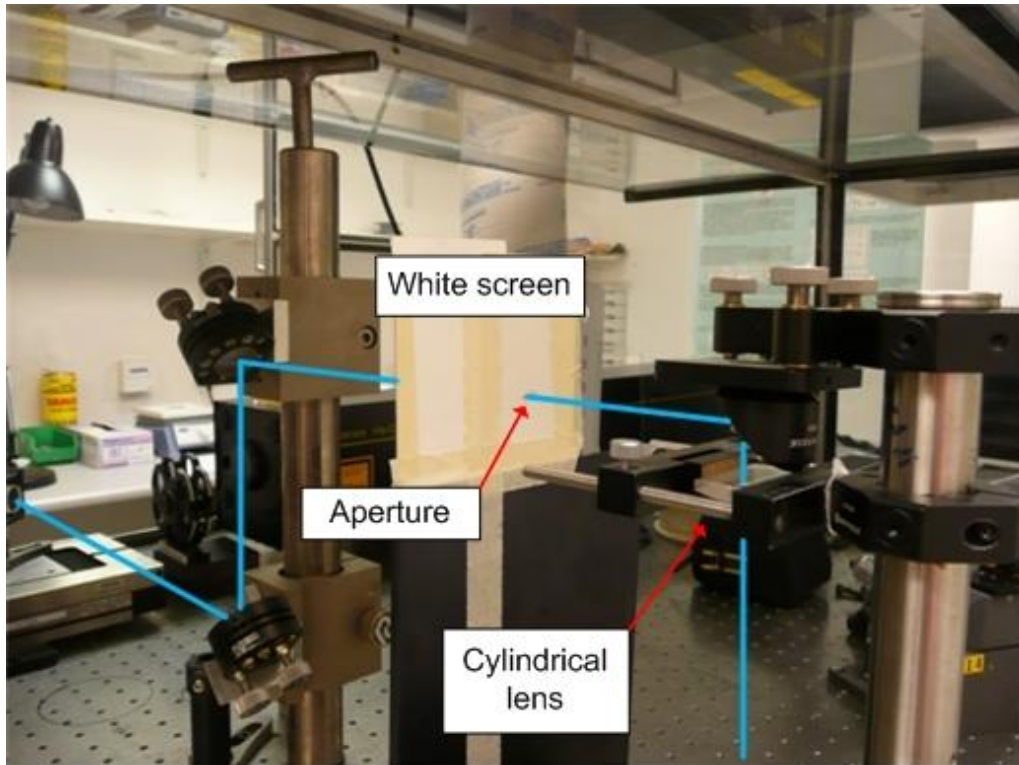


Figure 4-3 Position of screen and aperture in fabrication setup to aid in the alignment to the fibre core.

The alignment of the UV beam and ultimately the fringe pattern to the core of the fibre was inspected at different stages of the POF and phase mask mounting onto the v-groove. The alignment was reviewed by observing the fluorescence of the back reflections from the cylindrical lens, top outer surface of the POF and the phase mask on a white screen which has an aperture to allow the laser beam to pass. The screen was positioned between the two raised mirrors as shown in Figure 4-3. The aperture was also used to confirm normal alignment of the first mirror and periscope up to this point. Firstly the back reflection from the cylindrical lens should overlap the aperture, confirming the lens was perpendicular to the UV beam. Secondly, once the fibre had been laid onto the v-groove plates and taped down, it was established if the fibre had been laid taut along the groove by verifying the back reflection from the top surface of the fibre overlaps the aperture and was also vertical to the optical bench. The phase mask was then positioned upon the intermediate three layered pieces of polyimide tape; making sure to rest the mask on the non-patterned areas of the bottom surface. Much like the cylindrical lens, the back reflection off the top surface of the phase mask should also align with the aperture to verify the UV inscription beam is normal to the phase mask and thus the angle of diffraction for both the positive and negative orders ($\pm m$) are equal as discussed in Chapter 2. If this was not the case the intermediate layers of tape are adjusted until alignment was seen. Care should also be taken to ensure that the periodic relief pattern of the phase mask is perpendicular to the fibre axis.

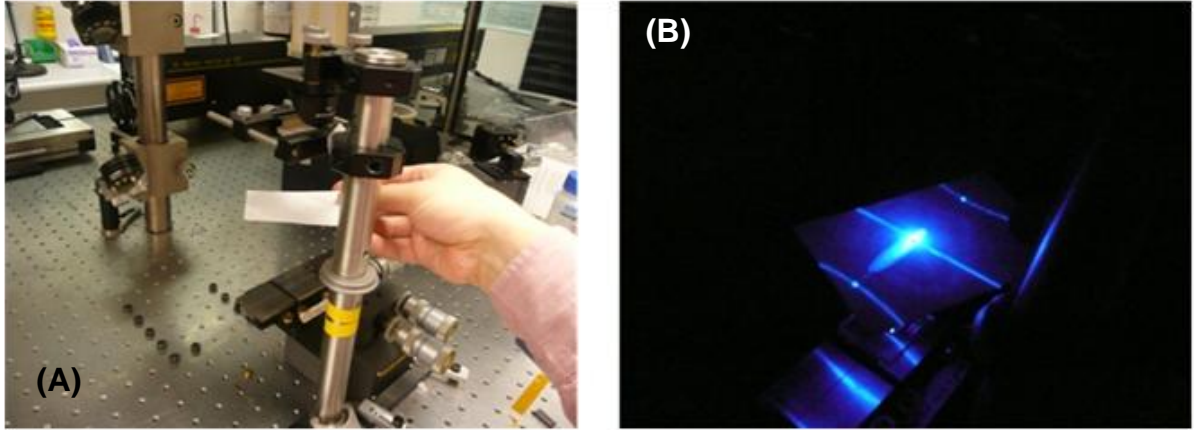


Figure 4-4 Second aperture used to align interference pattern to the core of the POF. (a) demonstration position of white screen in optical system (whilst laser is turned off)(b) reflected fringe pattern off the surface of POF observed on the underside of the screen.

Finally the back reflection was again reviewed to align the interference pattern to the core of the POF. Here a second screen with an aperture was used, which was held over the fibre between the lens and phase mask as seen in Figure 4-4. The assumption was made that the core lies at the centre axis of the fibre and therefore alignment to the core was achieved by aligning to the centre of the outer fibre diameter, hence the highest point of the fibre curvature. A particular scatter pattern was observed once alignment to the centre of the fibre is reached; the pattern resembles a sharp intermittent line as seen in Figure 4-5.

It is felt a vision system which was focussed into the POF would have aided with the alignment of the UV inscription beam to the core of the POF. Another technique which may have aided the alignment of the UV beam to the core of the fibre is to monitor the end face of POF. This would have allowed monitoring of any UV light being guiding within the core of the POF, something which was observed when the UV inscription beam was aligned to the core of the fibre. However neither of these two techniques was available during the work completed in this thesis.

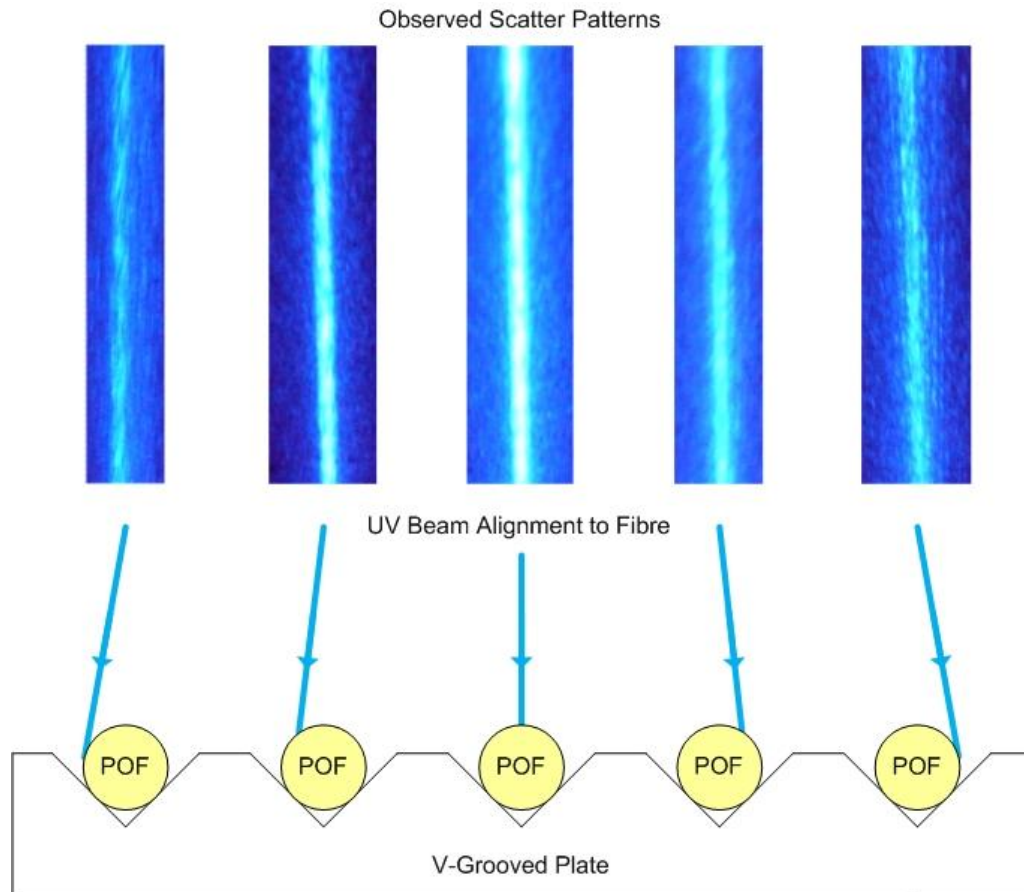


Figure 4-5 Examples of observed scatter patterns for the fibre surface when aligning to the core.

4.1.2 Fibre Bragg Grating Interrogation

When interrogating gratings with a Bragg wavelength within the 1550nm spectral region the attenuation of the POF becomes a determining factor. With attenuation losses of 1dB/cm at 1550nm[59] it was essential that PMMA POF lengths are kept to a minimum. However POF lengths of at least 8cm are needed for the fibre to overhang each end of the v-groove plate during fabrication, which was essential for butt coupling to the POF and monitoring any Bragg response.

The focal point of the vertical UV laser beam upon the v-groove plate was offset towards one end of the plate. With a length of only 2cm from the UV focus point to the end of the fibre, it was possible to interrogate Bragg gratings in reflection. Therefore a 2x2 silica, single mode (9/125 μ m) 50:50 at 1550nm coupler was used in the optical interrogation setup, which can be seen in Figure 4-6. A broadband ASE light source was used with an operating spectral range of 1.53-1.61 μ m (Thorlabs ASE-FL7002-C4 5mW. Erbium white light source, typical spectral power density of -11dB/nm @ 1540-1600nm) to interrogate the fabricated FBG, together with a HP 70951B optical spectrum analyser (OSA) to monitor any reflected Bragg response. The spare arm of the coupler was terminated with a FC/APC pigtail which had been fusion spliced to the coupler and index matching gel (RI = 1.4587) was applied to the

tip of the connector to reduce any Fresnel reflections from disturbing the monitoring of the reflected Bragg response from the terminated end.

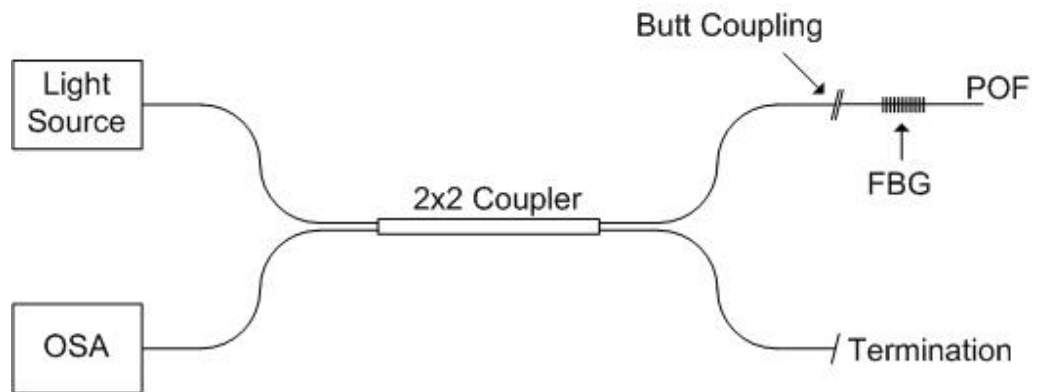


Figure 4-6 Reflection POFBG Interrogation Setup

The interrogation light source and the reflected Bragg response were launched into and out of the POF via butt coupling to the arm of the coupler to the POF. First, a FC/APC pigtail was spliced to the arm of the coupler which was going to be coupled to the POF; this was to reduce the reflections which would inevitably have been observed from a FC/PC connector and resulted in an increase in the noise of the reflected spectrum and hence a decrease of the signal-to-noise ratio of any Bragg response. Polymer index matching gel (RI = 1.4917) was applied to the tip of the FC/APC to further reduce Fresnel reflections from both the ferrule connector and the end face of the POF. The ferrule connector was fixed to the travelling part of the translation stage shown in Figure 4-2 and brought to within 0.5mm of the POF which was already overhanging the v-grooved plate. The cores of the silica coupler arm and the POF were now ready to be aligned. Fibre core alignment was achieved by temporarily changing the ASE broadband light source for a 635nm visible laser diode (Oz Optics FODL-23S-635-1, fibre optic fault locator); this in turn was launched into the POF via free space coupling. The guidance within the POF was inspected by projecting the output at the far end of the POF onto a white screen using an x10 objective lens. Using the micrometers of the translation stage the ferrule connector was adjusted perpendicular to the fibre length axis until guidance was seen within the core of the POF only, as demonstrated in Figure 4-7. The ferrule connector was then brought into contact with the end face of the POF and guidance within the core was checked again with any realignment taking place as needed. Changing back to ASE light source allowed for the growth of any FBG to be monitored using the OSA.

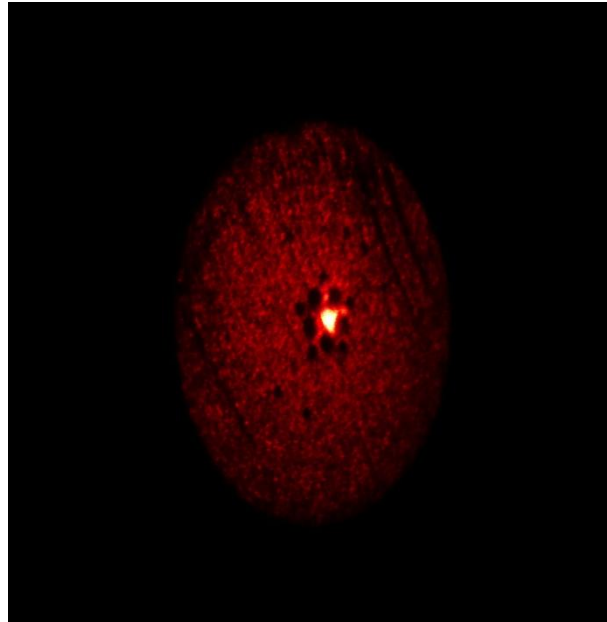


Figure 4-7 Example of guidance of the red laser diode in the core of POF

4.1.3 Fabrication of FBGs in few-mode mPOF

Part of the research in this thesis has involved fabricating POFBGs in pure PMMA few-mode microstructured POF (FMmPOF) provided by The Optical Fibre Technology Centre, University of Sydney. This fibre has previously been used to examine the thermal behaviour of a FBG which was fabricated in the fibre using a method similar to the technique described in this thesis[24]. The fibre has two flat sides as can be seen in Figure 4-8. The reasoning for the flat sides was to assist with alignment to the fibre core and additionally to ensure the UV interference pattern was perpendicular to a flat edge of the hexagonal hole structure of the mPOF. However no improvement had been observed of the alignment to fibre core when compared to fully cylindrical fibre.

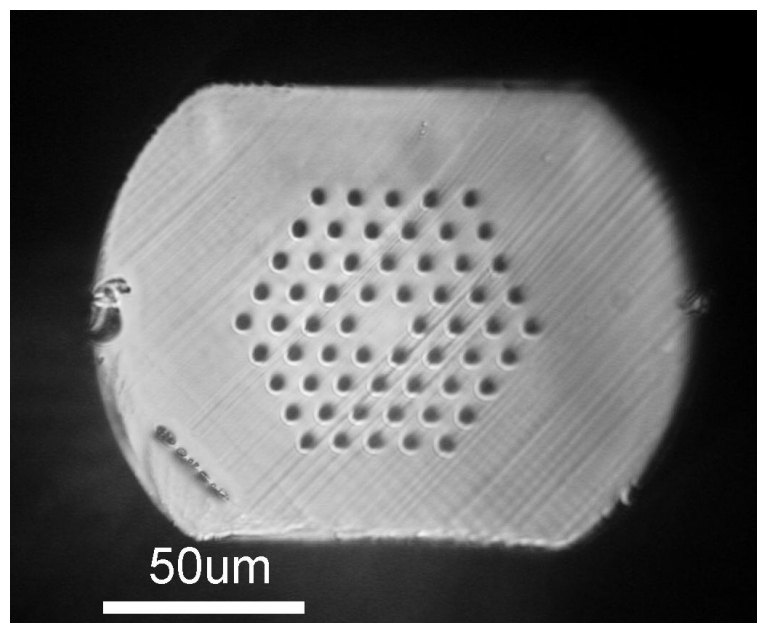


Figure 4-8 Microscope image of end face of FMmPOF

Before the mPOF was drawn into fibre from its preform the holes were drilled and the edges were milled off to create the desired geometry. The outer diameter of the fibre consisted of two measurements; 150 μm between the round edges and 115 μm between the flat edges. The core of diameter 14.6 μm was surrounded by four rings of holes, a total of 60 holes were employed each with a diameter (d) of 2.6 μm and a separation between each other (Λ_{hs}) of 8.6 μm , resulting in a ratio of $d/\Lambda_{hs} = 0.3$.

A grating was fabricated in the FWmPOF using a phase mask with a period (Λ_{pm}) of 1057.2nm; the resultant reflected spectra can be seen in Figure 4-9 captured on an OSA with a bandwidth resolution of 0.5nm. After a 45 minute exposure the reflected Bragg response had a peak signal at 1562nm which had a signal-to-noise ratio of around 20dBm. A bandwidth, full wave half maximum (FWHM) of 1.5nm was measured. The FBG length was determined by the UV laser beam diameter which was 1.8mm; hence as the UV beam was static the FBG length was 1.8mm in length. Using the period of the phase mask and the Bragg wavelength of the reflected Bragg response the corresponding effective refractive index was calculated to be 1.477.

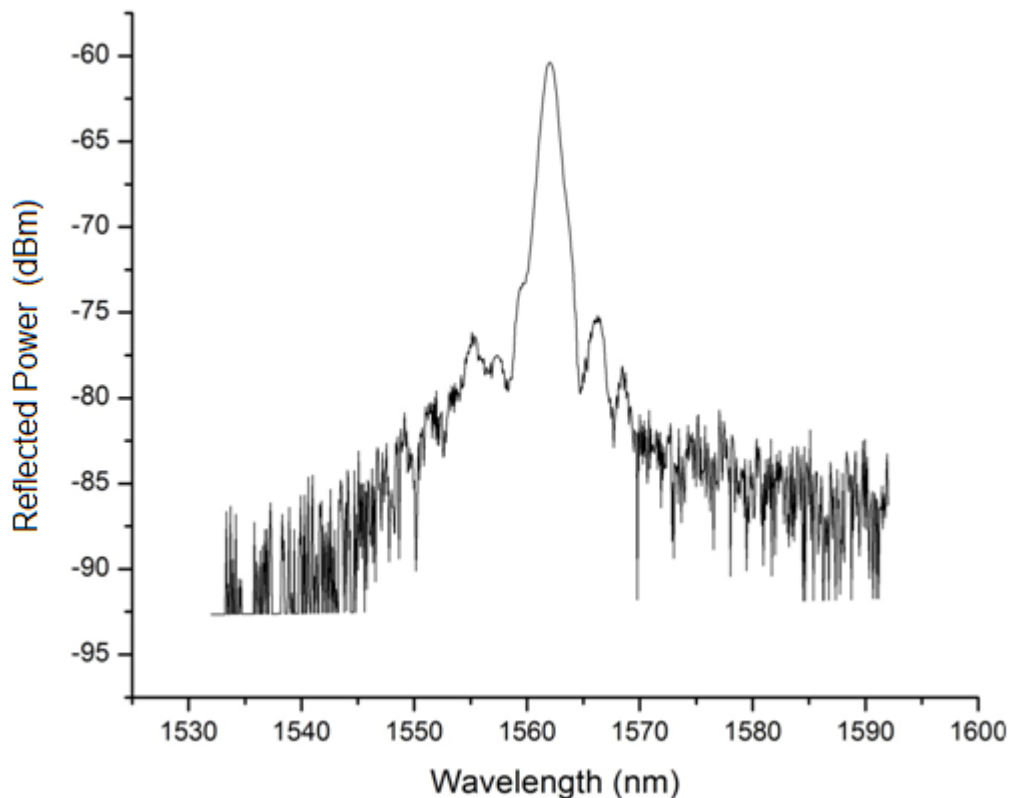


Figure 4-9 Reflection spectrum of a FBG fabricated in FWmPOF, resolution bandwidth = 0.5nm

The Bragg wavelength (λ_B) was calculated using the centroid calculation shown in Equation 18 of all data points from the captured reflected spectrum which was within -3dBm of the peak value. Where λ_i is the wavelength of the data point and P_i is the optical power in dBm.

$$\lambda_B = \frac{\sum \lambda_i P_i}{\sum P_i}$$

The growth characteristics of the FBG fabricated in the FMmPOF is shown in Figure 4-10, demonstrating the peak reflected signal every minute. It can be seen that no visible Bragg response was seen until 13 minutes into the fabrication. It is undetermined whether this delay in growth is due to a minimum amount of refractive index change needed to observe a Bragg response or the sensitivity of the interrogation system. It is felt it is likely to be a combination of both; however future work should investigate the origin of this delay by first using an interrogation system with increased sensitivity. After the delay in growth of the Bragg response there was rapid growth for ten minutes, after which the rate of growth slows down and a saturation level was reached after 45 minutes.

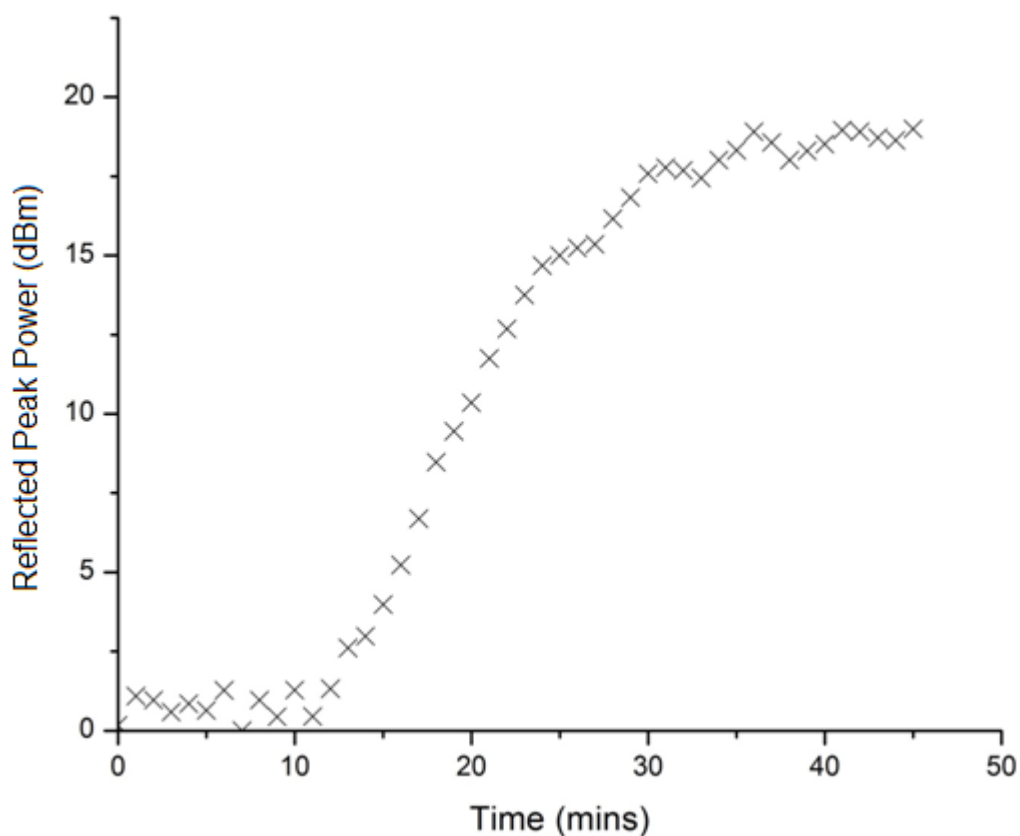


Figure 4-10 Growth characteristics of FBG fabricated in FMmPOF, with a Bragg wavelength of 1562nm

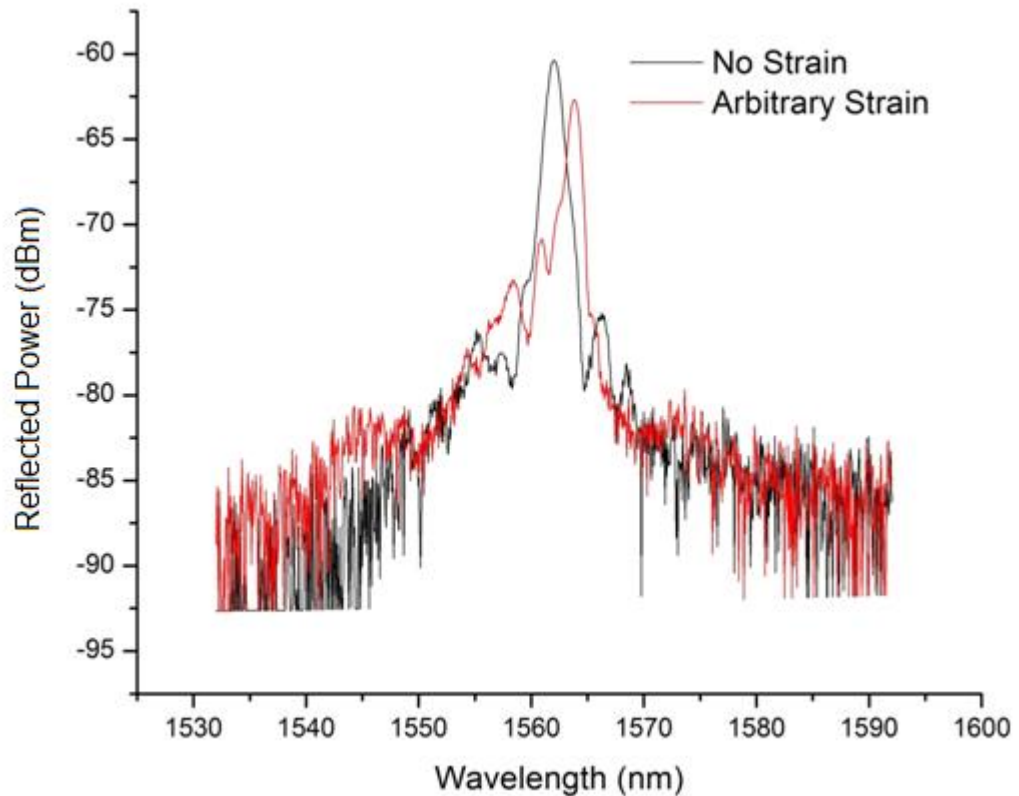


Figure 4-11 Positive Bragg wavelength shift due to axial strain. — no strain, — arbitrary amount of axial strain applied by hand

To confirm the peak signal of the reflection spectrum was indeed induced from a FBG fabricated in the FMmPOF, a small amount of axial strain was applied to the fibre. Lightly running a finger along the v-groove at the far end of the POF to the butt coupling and away from the FBG fabrication point a red wavelength shift was observed of 1.8nm, as is shown in Figure 4-11. Which demonstrates the POFBG response to an increase in axial strain and suggests a FBG sensor was present within the POF.

4.1.4 Fabrication of FBGs in Multimode mPOF

The fabrication of FBGs in multimode (MM) POF has also been investigated during this thesis. The appeal of using MM POF is that it offers the potential of a relatively low cost sensing system compared to the interrogation system described previously in this chapter. MM fibre allows for coupling between the POF and other components such as couplers, light sources and OSAs to be less critical. As the coupling or splicing between POF to other optical components is not as conventional as their silica counterparts, more effort is required to make an efficient link to the POF, in particular for single or few mode fibres. Possibilities arise from fabricating FBGs in MM POF where the POF can be embedded into ferrule connectors and the tips of the connectors polished down to allow for quick and easy demountable connection into an optical system[60]. Here any slight misalignment of the embedded POF in the ferrule with another multimode fibre connector would be insignificant compared to the impracticalities of attempting such a thing with SM fibres. Additionally

employing multimode POF lends itself to the requirement of cheaper light sources when comparing the costs of broad area emitters to a single transverse mode light source.

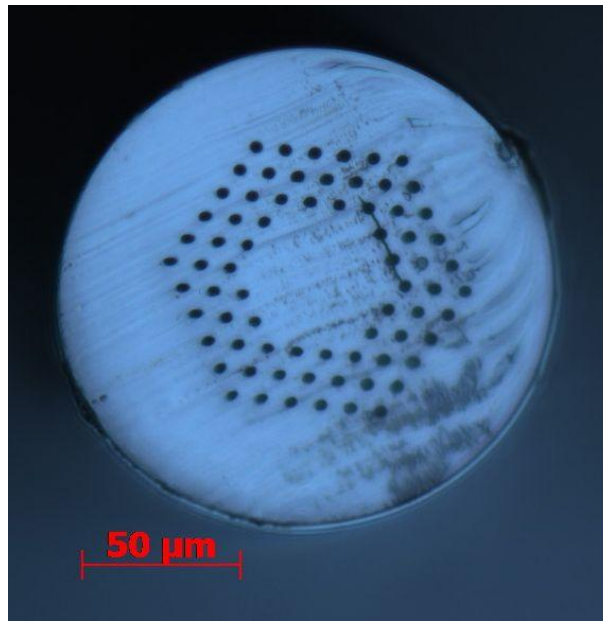


Figure 4-12 Microscope image of end face of MMmPOF

Multimode microstructured POF (MMmPOF) had been made available originally from Optical Fibre Technology Centre (OFTC), University of Sydney, and currently from Kiriama Pty Ltd. This MMmPOF is made purely from PMMA and contains a total of 72 holes within a three ring structure as shown in Figure 4-12. The fibre had an outer measured diameter of 150 μm and a core diameter of 50 μm , the higher refractive index of the core was contained by the lower effective refractive index of the cladding provided by the hole structure, presenting index guiding within the solid core region.

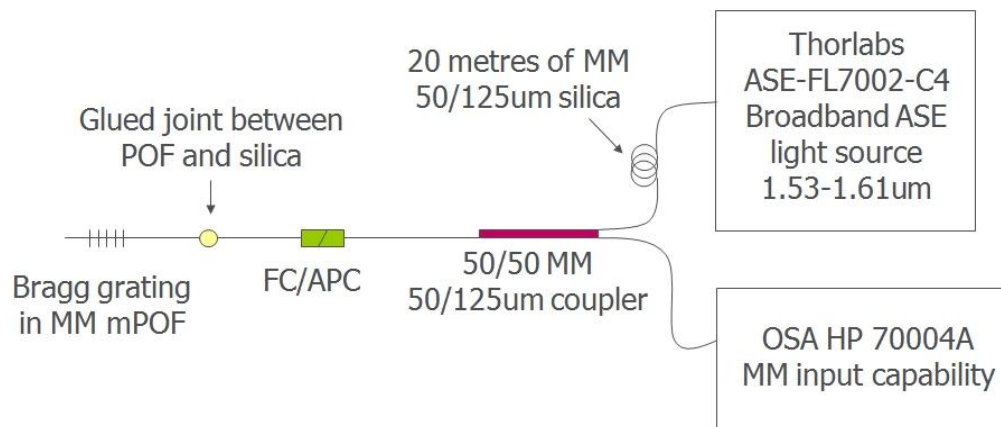


Figure 4-13 Optical interrogation setup to monitor FBG fabricated in MMmPOF

Bragg gratings were fabricated in the MMmPOF using the phase mask technique described earlier in this chapter; the surface relief pattern of the mask had a period (Λ_{pm}) of 1057.2nm. However the use of polyimide tape to suspend the phase mask above the POF was not used. Attempted fabrications using three (200 μm), two (133 μm) and one (67 μm) layer of

tape all proved unsuccessful, however resting the phase mask directly on top of the POF successfully worked.

At least fifty attempts were made to fabricate FBGs in the MMmPOF when suspending the phase mask over the fibre using the polyimide tape. An approximate inscription success rate as low as 10% was noted when two or three layers of tape were used to suspend the phase mask. The success rate increased to around 50% when the phase mask was suspended 67µm above the mPOF surface. Whereas, when the phase mask was rested directly upon the mPOF, FBGs were inscribed within the mPOF with at least a 90% success rate. It is felt that minimising the distance between the fibre and phase mask allowed for a deeper penetration of the UV fringe pattern acquired from the phase mask into the fibre. This therefore accommodates for the large cladding of the mPOF as shown in Figure 4-12. To ensure the preservation of the phase mask it was regularly cleaned in a sulphuric acid bath to prevent the surface relief pattern becoming too dirty. It was also felt that the phase mask was no more likely to get damaged from being rested upon the POF directly as it was being suspended by polyimide tape over the POF.

Assuming the effective refractive index of the MMmPOF within the core is 1.477 (as calculated from the Bragg response in the FWmPOF previously), a Bragg wavelength of 1562nm is expected. During the fabrication the reflection spectra was monitored and the resulting FBG response was captured again in reflection as described previously. Since gratings are being fabricated in a large 50µm core, action was taken to ensure an even modal distribution within the core of the MMmPOF. As demonstrated in Figure 4-13, a spool of 20m of silica multimode optical fibre (50/125µm) is spliced into the arm of the coupler connected to the light source, a tight enough coil of fibre should result in an even power distribution of the modes within the multimode fibre in the system. In an attempt to maintain this even modal distribution across the optical system silica multimode (50/125µm) pigtails were spliced to each arm of the coupler and also a silica multimode (50/125µm) 2x2 coupler was employed with a 50:50 splitting ratio at 1550nm. Again a broadband light source was used which operated in the 1.53-1.61µm spectral region (Thorlabs ASE-FL7002-C4) and a HP 70951B OSA was used which supports fibre types up to 62.5/125µm with a bandwidth resolution of 0.5nm. Figure 4-14 shows a typical FBG response in the MMmPOF after being exposed to the UV interference pattern for 52 minutes. The reflected Bragg response had a Bragg wavelength of 1564nm and a bandwidth (FWHM) of 2nm. Again the FBG length was determined by the diameter of the laser beam which in this case was 1.8mm. The corresponding effective refractive index (n_{eff}) was calculated to be 1.479. Figure 4-15 illustrates a reflected 20dBm Bragg signal-to-noise ratio was achieved after the 52 minute fabrication. A break in the growth data can be seen after 33 minutes where the butt coupling conditions between the silica and polymer optical fibres were optimised. The fabrication was

stopped after 52 minutes to prevent over exposure as a decrease in the rate of growth was observed.

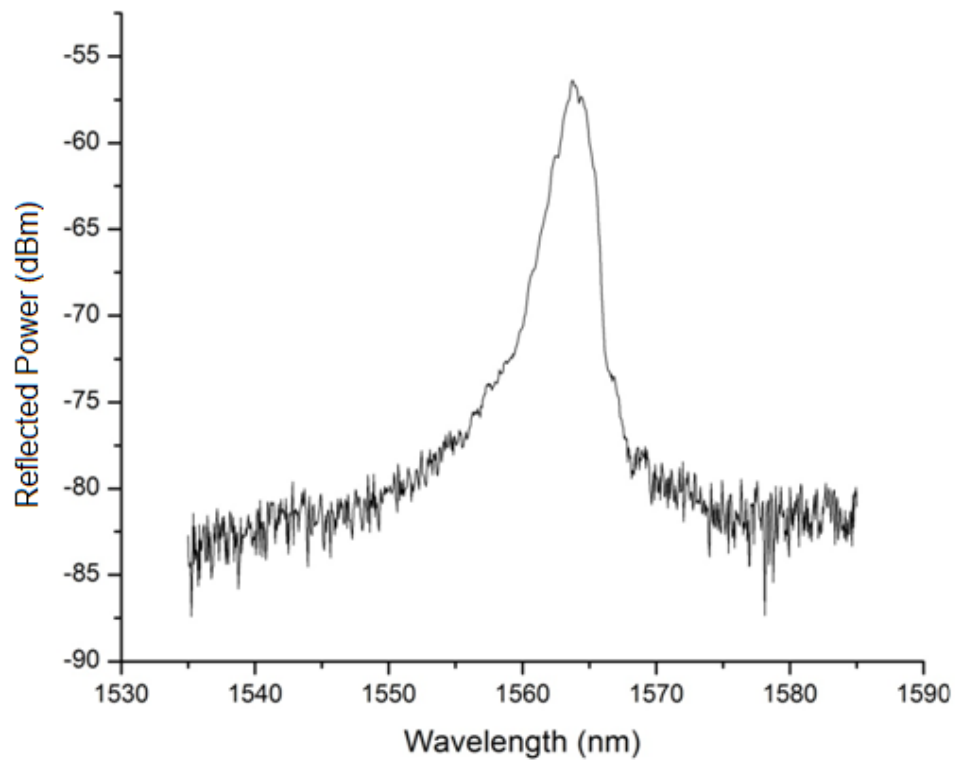


Figure 4-14 Reflected Bragg response of a FBG fabricated in MMmPOF with a phase mask with a period of 1057.20nm

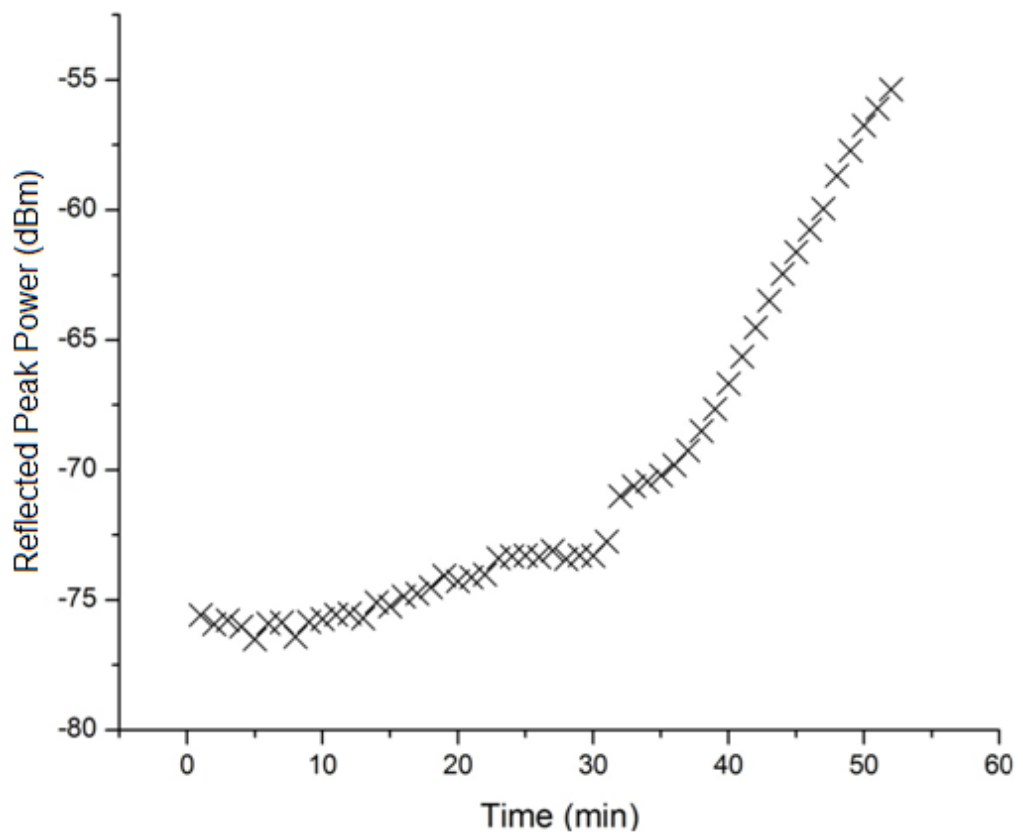


Figure 4-15 The growth curve of a FBG fabricated in MMmPOF using a phase mask with a period of 1057.20nm

4.2 Summary of All FBG Fabrication in POF

Below, Table 3 summarises the POFs in which FBGs have been fabricated in for the work in this thesis. All the gratings were fabricated using the HeCd laser, optical components and techniques described in this Chapter. Resultant Bragg responses are demonstrated throughout this thesis.

Table 3 Summary of FBG Fabrication in Various POFs

Fibre Type	Acronym	Source	Comments	Discussed
Few moded, microstructured	FMmPOF	A	Pure PMMA	Chapter 4
Multimode, microstructured	MMmPOF	A	Pure PMMA	Chapters 3.5, 5, 6, 7, 8
Single Mode, microstructured	TOPAS	B	TOPAS cyclic olefin copolymer	Chapter 9
Single Mode, Step index	SM SI POF	C	Doped fibre, fabrication time decreased to 7.5 minutes with 30mW HeCd laser power	Chapters 5 & 7

A = Institute of Photonics and Optical Science, University of Sydney

B = Department of Photonics Engineering, Technical University of Denmark

C = University of New South Wales

4.3 Long Period Grating Fabrication in Polymer Optical Fibre

Research into Long Period Gratings (LPG) fabricated in POF have not had the same amount of interest as LPGs fabricated in silica optical fibre mainly because of the high attenuation of POF and the lack of availability of single-mode POF. Because of this, very little research into POF LPGs has been conducted. However, the fabrication of LPGs was first seen in step-index single-mode POF with a highly photosensitive poly(methyl methacrylate-co-methyl vinyl ketone-co-benzyl methacrylate) core using $0.3\text{mW}/\text{cm}^2$ of UV irradiation from a high-pressure mercury lamp[61]. A 1.5mm thick piece of Pyrex glass was used as a filter, affectively blocking the wavelength range 200-300nm so not to inscribe the periodic structure into the cladding of the POF and only in the higher wavelength photosensitive doped core. The remaining UV light from the lamp irradiates the POF through an amplitude mask of length 3cm, with a pitch of $275\mu\text{m}$ and a duty cycle of 50%. The POF was exposed in 30s periods for a total of 200s to prevent any heating of the POF from the exposure of the mercury lamp. The transmission spectrum of the LPG observed a maximum loss resonance of 3dB at a wavelength at 1568nm and a FWHM of the resonance of 3nm.

LPGs were first seen mechanically induced in single mode (SM) mPOF (SMmPOF) in[62], where the SMmPOF had an outer diameter of $270\mu\text{m}$ and was found to be single mode at a wavelength of 633nm. An LPG response was seen when a triangular grooved PMMA template was pressed upon the SMmPOF because of the stress induced periodic refractive index changes experienced within the fibre at the tips of the triangular pattern. The triangular

grooved template consisted of 150 grooves over a length of 15cm; each groove had a depth of 0.2mm and a period (Λ_{LPG}) of 1mm. Attenuation resonances of up to 34dB were seen at 530, 577, 811 and 884nm. Additionally increasing the amount of applied pressure on the grooved template saw an increase in the depth of the attenuation resonances with an average increase in strength of 4.8dB/kg up to 12kg. Furthermore when the grooved template was removed the transmission spectra returned to its original form. Therefore demonstrating LPGs fabricated in SMmPOF which were tuneable and erasable.

Fabrication via mechanical imprinting was later developed to produce a permanent LPG response through a thermal mechanical fabrication technique[63]. The same experimental setup was used as above with the inclusion of a heated plate, which the SMmPOF was laid upon. Two 15cm long individual grooved templates were used during this experiment, the first with grooves with a depth of 0.29mm and a period of 1mm and the second with a depth of 0.125mm and a period of 0.5mm. Weight was added to either template evenly across the grooved pattern onto the SMmPOF and a LPG is fabricated in the POF by heating the plate the fibre is laid on; the growth of the LPG was monitored by observing the transmission spectrum. Permanent LPGs remained once the weight and grooved templates were removed, strong attenuation resonances were observed at 510 and 651nm when using the 1mm grooved template, additionally attenuation resonances were observed at 510nm and 683nm when using the second grooved template with a period of 0.5mm. This method of fabrication demonstrated a distinct advantage of not relying on relatively expensive high power lasers and amplitude masks to manufacture LPGs in POF. This type of mechanical LPG can be fabricated quickly without the need of alignment of a UV laser inscription beam. Additionally, no dopants are required within the core to enable higher photosensitivity compared to the cladding of the mPOF, however long term repeatability of similar LPG responses issues may arise.

4.3.1 Experimental Investigation of Mechanically Induced LPGs

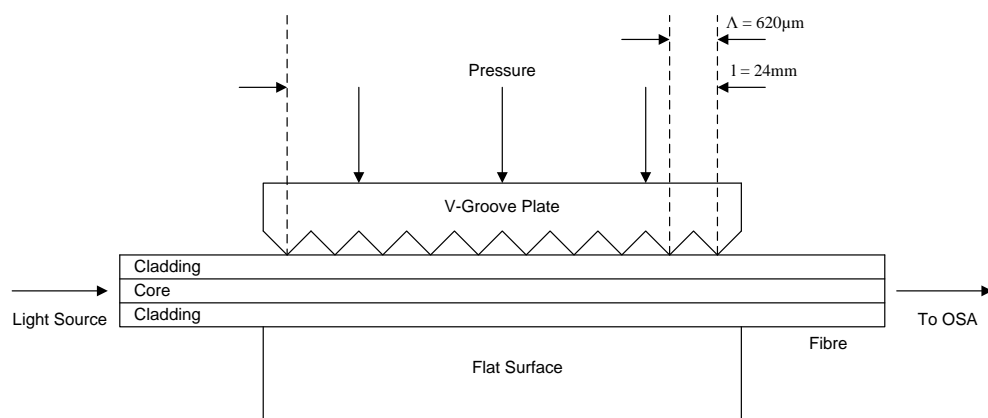


Figure 4-16 Fabrication setup for mechanically induced LPGs

Work was completed to duplicate the mechanical induced LPGs by Eijkelenborg[62] firstly on un-sleeved Corning SMF-28 silica optical fibre[64]. A small metal triangular grooved template was applied to the stripped fibre with hand pressure to the plate as shown in Figure 4-16. The length of the plate was 2.4cm, consisting of 38 grooves with a period of 620 μ m. This initial experiment was intended for familiarity with the experiment, allowing for progression onto mechanically induced LPGs fabricated within POF. This can thus be used as an aid when calculating a required period for either UV or femtosecond laser point-by-point fabrication of LPGs in POF.

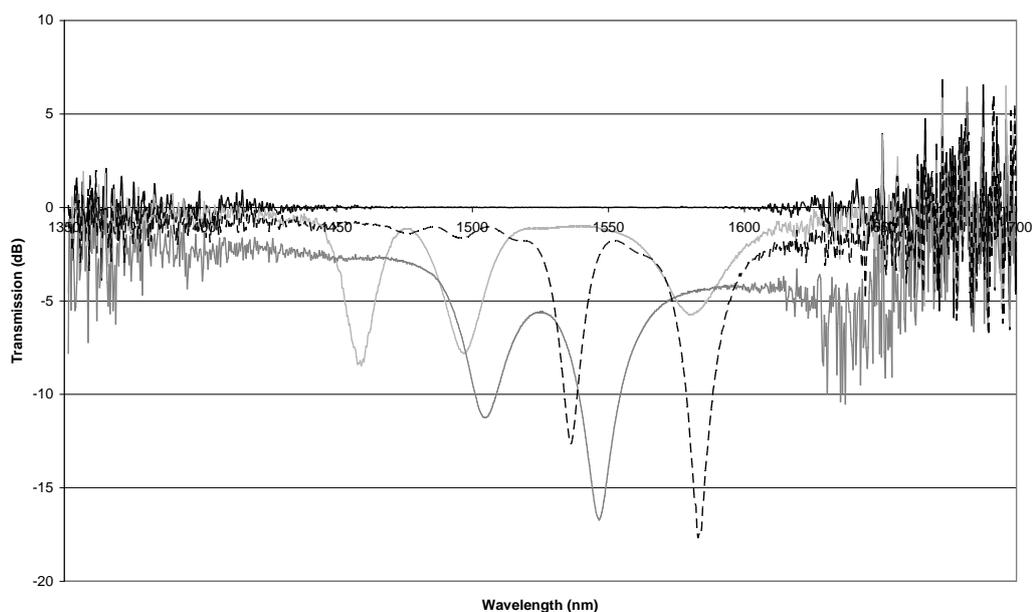


Figure 4-17 Mechanically induced LPGs in Corning SMF28 whilst varying the tilt of the v-groove plate.
Key: — spectrum before & after induced LPG. . . . v-groove placed square on fibre. ▨ v-groove slightly tilted -- v-groove angle increased further

Figure 4-17 illustrates the captured transmission spectra of a mechanically induced LPG in SMF-28 silica fibre with pressure applied by hand. Figure 4-17 demonstrates the effect of increasing the 90° angle of the triangular grooved pattern of the template to the fibre axis, thus increasing the period of the imprinted LPG. As expected, increasing the angle between the grooved template and the fibre axis resulted in a positive wavelength shift. Also observed, the attenuation resonances became stronger and their bandwidths became smaller, this was possibly an effect of more pressure being applied and the grating length increasing as the angle between the grooved pattern and fibre axis was increased. Attempts were made to increase the length of the grating further by imprinting the metal grooved template into an acrylic plate when heated to 150°C, thus stitching a number of imprints together. However alignment of a number of heated imprints proved challenging with stitching errors resulting in no fabrication of an LPG.

Attempts were made to fabricate mechanically induced LPGs in SM SI POF using an acrylic version of the same template used in Figure 4-16. An acrylic template was manufactured by heating the metal plate to 150°C and imprinting it into the acrylic, so to reduce the risk of damaging the POF. The intention was to prove LPGs could be mechanically fabricated in the available POF and then for longer specific triangular grooved templates to be manufactured which would be designed to give a specific spectral response.

Fabrication of mechanically induced LPGs were attempted in SM SI POF, however no LPG response was seen during optical interrogation. This could have been for a number of reasons; firstly the transmission of the supercontinuum source was not strong enough, due to the high attenuation of the POF and the butt coupling losses at either end of the fibre. Additionally each time pressure was applied to the grooved template resulted in movement of the fibre and thus weakening the butt coupling at either end of the fibre. Attempts were made to lay the fibre on a similar v-groove to the one used to support POF during FBG fabrication, however due to the small outer diameter of the fibre the v-groove template essentially stopped the full impression onto the fibre. The small diameter also proved troublesome when increasing the pressure applied to the grooved template, which resulted in breakage of the POF. When comparing the diameter of SM SI POF with the mPOF used by Eijkelenborg *et al*[62] it is clear to see the outer cladding of the mPOF used by Eijkelenborg with an approximate thickness of 115µm acts as a buffer, allowing for light guidance within the core of the fibre. As no appropriate POF was available to withstand the pressures needed to fabricate mechanical LPGs this area of work was suspended.

4.3.2 UV Inscribed LPG in mPOF

Collaboration work¹ with David Sáez-Rodríguez of the University of Valencia saw the first UV inscribed LPG in mPOF including the study of sensitivity to water absorption[65]. As can be seen in Figure 4-18, the microstructured fibre had an elliptical core with a largest diameter of 7.6µm and a shortest diameter of 4.2µm measured. The core was surrounded by 56 holes each with a 0.72µm diameter and spaced 2.59µm apart. The fibre had an outer diameter of 250µm and had a birefringent response due to the elliptical core. There was no intention for the core to be elliptical and it is believed one of the holes around the core of the mPOF structure may have collapsed during the fabrication of the fibre.

¹ LPG fabrication was undertaken by both parties at Aston University; LPG response analysis and application characterisation was solely completed by David Sáez-Rodríguez.

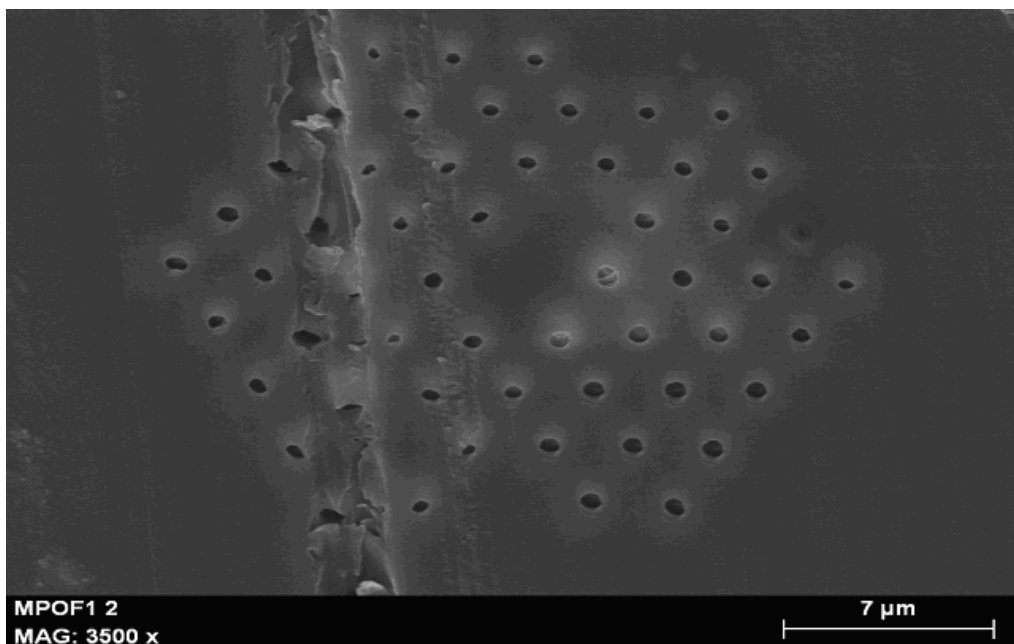


Figure 4-18 Microscope image of end face of elliptical core of mPOF used for LPF fabrication

Before the UV inscription of the grating, the two ends of the mPOF were each spliced to silica 50/125 μm pigtails using optical adhesive as described in Chapter 5. The permanent splicing allowed for continuous interrogation of the transmission spectrum whilst not disrupting the coupling between the polymer and silica fibres. The same UV 325nm CW 30mW output HeCd laser was used which fabricated FBGs. The 1.8mm diameter beam was focussed onto the mPOF using a spherical lens with a focal length of 20cm. The fibre was mounted on two XYZ translation stages either side of the adhesive splicing joint, using spring clamps only on the silica fibre so to protect the POF. The translation stages were adjusted until the focussed beam was aligned to the core along the length of the mPOF. The photo inscribed fabrication was completed using a point-by-point technique. The UV laser beam was scanned along the fibre length by relocating the mirror and lens on a translation stage, which had a micrometer resolution of 10 μm ; whilst the mirror and lens was relocated the laser beam was shut off. The experimental setup is shown in Figure 4-19.

It was found that focussing the maximum 30mW of optical power from the laser onto the POF ultimately melted the fibre. After numerous attempts of reducing the laser power using neutral density filters, as shown in Figure 4-19, the optimal laser power after the filter was 1mW. Using 1mW prevented the holes of the mPOF from collapsing yet an optimum refractive index was achieved when the fibre was exposed for 6s at each point, so not to overheat the fibre, resulting in damage of the polymer and thus the guidance characteristics.

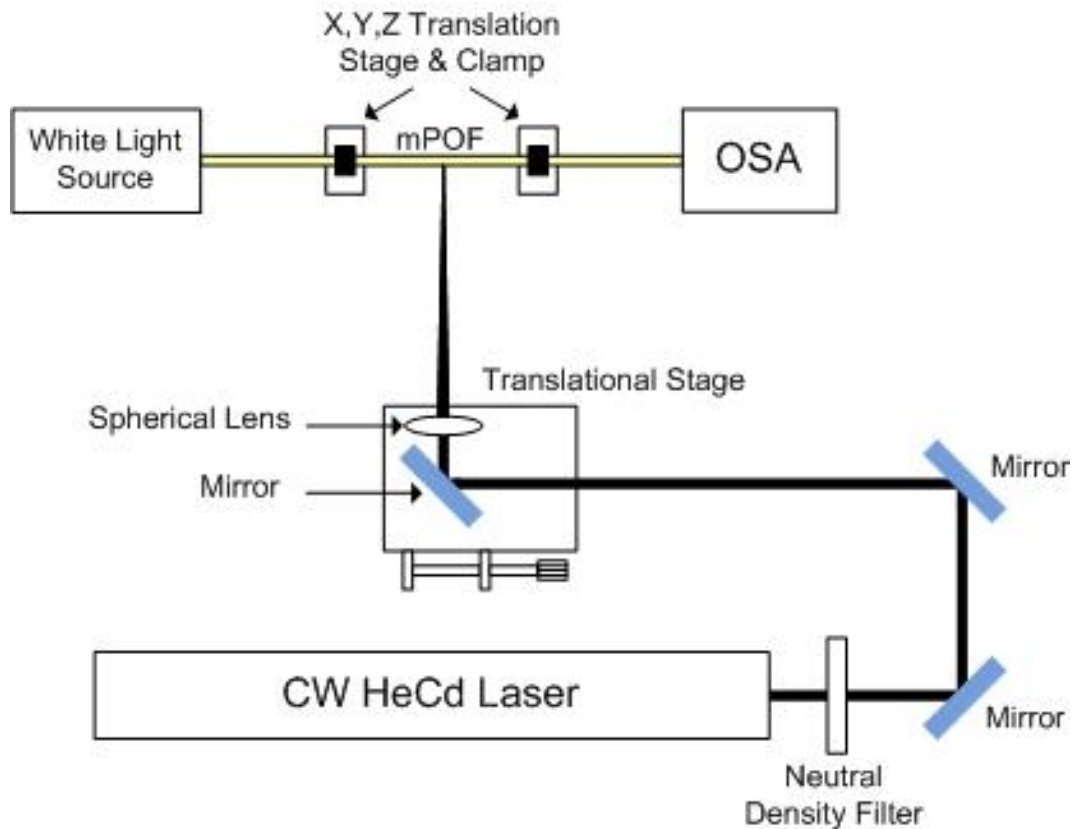


Figure 4-19 Optical setup for the UV laser fabrication of LPGs in mPOF.

A LPG was fabricated in the mPOF with a length of 2cm and a point-to-point period of 1mm. A 150W halogen white light source was used to interrogate the LPG, with the transmission spectra monitored on an OSA. Figure 4-20 shows the obtained transmission spectrum with a bandwidth resolution of 5nm in the spectral range of 600-1100nm. Six attenuation resonances can be seen in the transmission spectrum, each of which demonstrates the coupling from the guided core mode to different cladding modes. Sáez-Rodríguez then went on to demonstrate the attenuation resonances of the LPG were sensitive to water diffusion in the mPOF[65]. Sáez-Rodríguez concluded that the LPG had a response which saw wavelength shifts as large as 50nm in the first 30 seconds whether soaking or drying the mPOF. This fast response makes LPGs fabricated in mPOF an ideal candidate for a water level sensor compared to FBGs fabricated in mPOF which experiences around an 8 minute delay before a change in the Bragg wavelength is observed due to the water taking this amount of time to diffuse into the core of the fibre.

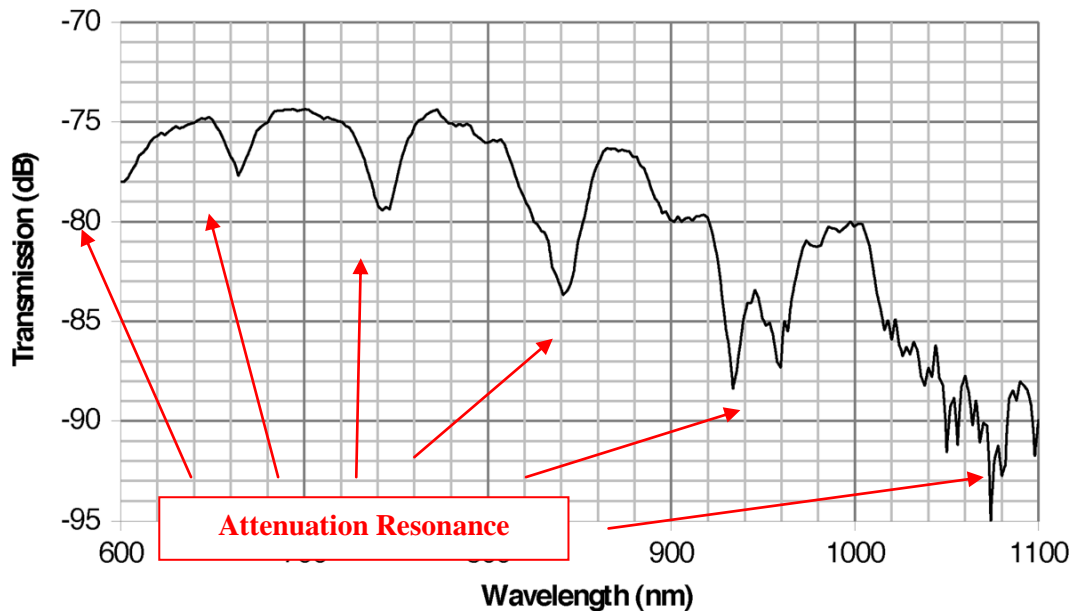


Figure 4-20 Transmission Spectrum of a LPG Fabricated in mPOF

4.4 Other Grating Structures

It is also possible to manufacture interferometric devices using the fabrication of Bragg gratings in optical fibre. These more complex structures have made the transition from silica fibres to step index PMMA based POF. Dobb has presented reflected responses from a Fabry Perot cavity and a phase shifted grating in POF[66]. The Fabry Perot cavity was manufactured by fabricating two FBGs using an expanded UV beam, creating gratings with lengths of 1cm, the two gratings were separated by around 3cm along the fibre length.

The second device, a phase shifted grating is an alternative approach of manufacturing an interferometric cavity. Here, the central grating planes of a uniform FBG are phase shifted, which in effect creates two gratings which are out of phase from each other. This in turn forms a wavelength selective Fabry Perot resonance which allows a narrow band of light to pass through the stop-band reflector of the initial uniform FBG. The phase shift can be created by several techniques, these include: using a phase mask which has a phase shift within the surface relief pattern[67], exposing a region of an initial FBG to further UV radiation[68] or thermally exposing a region of a fabricated FBG[69]. The phase shift grating manufactured in POF was completed by first fabricating a 1cm long uniform grating using an expanded UV beam. Then the unexpanded 1mm wide laser beam was used to expose the centre of the grating which resulted in a phase shifted grating response.

Both the Fabry Perot and phase shifted devices were fabricated within the 1550-1600nm spectral range and therefore experienced the high attenuation of POF as other Bragg gratings do in this spectral range. Partially because of this, a low finesse response was seen from the Fabry Perot cavity and a lack of sharpness was seen on the central reflection notch of the phase shifted device. It is felt that developing the POFBG technology to fabricate Bragg gratings within the visible spectral region where the attenuation is relatively smaller

will lead to improved Fabry Perot cavity responses and sharper reflection notches from phase shifted gratings.

4.5 Summary

The phase mask fabrication technique was successfully demonstrated by fabricating FBGs in few mode mPOF and multi mode mPOF. FBGs have been fabricated in both types of fibre frequently with fabrication times under one hour. Specific detail was made to the long term stability needed to fabricate FBGs in POF due to the long UV exposure times needed to fabricate the FBGs. Also included in this chapter were the details of interrogation of FBG responses fabricated in POF.

The fabrications of LPGs were also attempted in this chapter. Mechanical induced LPGs were demonstrated in single mode silica optical fibre (SMF28) however no successful LPG responses were monitored in POF. Nevertheless LPGs were successfully UV photo-inscribed in a single mode mPOF using a point-by-point fabrication technique. The laser used was an UV 325nm CW HeCd laser whose optical power could be reduced from 30mW to 1mW with the use of neutral density filters. The LPG was 2cm in length and had a 1mm period, where the mPOF was exposed to the UV laser beam for 6 seconds; resulting six attenuation resonances within the 600-110nm wavelength range, and as a consequence resulted in a publication in 2010[65].

4.6 Future Work

Future work in the fabrication of FBGs in POF should be focussed on fabricating FBGs with Bragg responses in the lower wavelengths where attenuation losses are much lower, 2dB/m at 800nm compared to 1dB/cm at 1550nm[59]. Work completed in Chapter 6 investigates the fabrication of FBGs in the 800nm wavelength region.

Advances to the fabrication setup should be made; these should include the ability to translate the platform the v-grooves and POF are mounted on. This will provide more control over the location of FBGs along the length of the POF which may suit application specific FBG sensors. Furthermore the POF could be translated during UV exposure thus scanning along the fibre core. This would essentially create longer FBGs in POF, with expected stronger Bragg responses and narrower bandwidths. It is also felt the technique of suspending the phase mask should be improved upon to give more accuracy and alignment of the phase mask to the focussed UV beam. What is more, the scenario of butt coupling silica fibre to POF during fabrication is not ideal. Preferably the coupling between the silica and polymer fibres would be permanent, and developments in this are made in Chapter 5. Another possible solution is to embed POF into a ferrule connected as suggested by Lwin [60], thus providing a detachable connector solution.

5

SPLICING

There are several factors which influence the length of POF when used as a Bragg sensor, these may include the attenuation of PMMA based POF which is in the order of 1dB/cm within the 1550nm spectral region[59]. The POF length is therefore limited to a few centimetres as reducing the amount of fibre the interrogation light source experiences in turn reduces the experienced attenuation. It also follows, as the FBG is offset to one side of the POF due to the inscription setup by detecting a Bragg response in reflection the relative length of the fibre is shorter compared to interrogation in transmission. Nevertheless a reflected response of a POFBG with a 20dBm signal-to-noise ratio would have a limited length of a few centimetres. An additional impact of the POF length is the current fabrication setup, the v-groove plate upon which the POF is rested on is 7cm in length. It is essential that the POF over hangs both ends of the v-groove plate to aid with the alignment of the POF core to the core of the silica arm of the coupler as discussed in Chapter 4. Therefore in an attempt to conserve relatively expensive POF, the length of fibre is kept to a minimum length of 8cm. In the current setup FBG fabrication is located 2cm along the length of the fibre from the cleaved end face which is butt coupled to the silica optical fibre arm of the coupler.

Limiting the POF to this length clearly restricts the range of applications for FBG sensors fabricated in POF which operate within the 1550nm spectral region. To employ these short sensors in any application a method of splicing POF to SOF is needed. Silica fibre has a much smaller attenuation of 0.17-0.18dB/km at 1550nm[64], thus enabling a FBG sensor fabricated in POF to be utilized in a number of applications via longer silica optical fibre leads connected to the optical interrogation system.

Arguably the immediate objective is to obtain the ability to interrogate a POFBG in reflection away from the XYZ translation stage it was fabricated on. Primarily a POFBG would be interrogated in reflection, by butt coupling a FC/APC of a silica arm from a coupler to the POF end face as described in Chapter 4. As this was the only current interrogation setup, characterisation of FBGs fabricated in POF was limited due to the butt coupling being temporary. As the POF is only taped to a v-groove plate using polyimide tape there is a distinct possibility the fibre may move whilst interrogating a measurand thus changing the coupling conditions and therefore any captured Bragg response may be affected.

However, although butt coupling between polymer and silica optical fibre was not ideal, it should be highlighted that the temperature behaviour of FBGs fabricated in the few-moded microstructured POF (FMmPOF) was studied by interrogating the Bragg response in reflection using the butt coupling technique previously described[24]. Nevertheless it is felt that to realise the full potential of FBG sensors fabricated in POF they need to be characterised and usable in real applications out of the laboratory. When characterising axial strain sensitivity for example a big burden is put on the butt coupling, likewise to study the response to relative humidity or pressure would require the inconvenience of constructing a translation stage for butt coupling within an oven or environmental chamber.

Therefore a technique of splicing polymer and silica optical fibre together is needed so the POF can be taken off the v-groove plates with the same coupling conditions intact. Clearly a fusion splicer would not be appropriate as an electric arc would melt the POF. Harbach has previously employed an optical transparent adhesive to fix the butt-coupling between POF and silica optical fibre[14]. Norland optical adhesive NOA 78 was used to enable stable coupling during FBG fabrication and thereafter during any characterisation of the Bragg response to a measurand.

5.1 Comparison of Optically Transparent Adhesives

In this thesis, research and experimental work has been concluded to develop a technique of splicing POF to silica optical fibre similar to Harbach using an optically transparent adhesive. A specification review of possible optically transparent adhesives is given in Table 4.

The decision was made to use Loctite 3525 to splice the polymer and silica optical fibres together. It was felt that the Loctite adhesive had the best combination of qualities. The most important being Loctite 3525 has a much higher tensile strength of 3500psi compared to the other adhesives. Both Norland 81 and Dymax OP-4-20632 have larger tensile strengths of 4,000 and 8,900psi respectively however both of these adhesives demonstrate poor optical transmission with refractive indices above 1.55. Additionally a high viscosity is desirable; if the viscosity is too low the potential of the adhesive running away from the butt coupling joint is likely before it is permanently fixed. Additionally if the viscosity is too low there is the possibility of the adhesive flowing along the hole structure of a mPOF, preventing the index guiding within the core of the mPOF. Taking this into account, Loctite 3525 also has the advantage of a high viscosity of 15000 centipoise (cP), Dymax OP-4-20641 does have a higher viscosity of 21000cP however it has a smaller tensile strength of 1500psi less than half of that of Loctite 3525.

Table 4 Review of available optical adhesives

Manufacturer & Code	Refractive Index (Cured)	Viscosity	Tensile Strength	Shrinkage	Comments
Dymax OP-4-20632	1.554	500 cP	8900 psi	< 0.2%	Rigid
Dymax OP-4-20639	1.470	200 cP	400 psi	2.4%	Elastic. Good optical transmission but poor tensile strength when compared to NOA 81
Dymax OP-4-20641	1.505	21000 cP	1500 psi	< 0.5%	Rigid
Dymax OP-4-20647	1.470	120 cP	120 psi	1.6%	Elastic
Dymax OP-4-20655	1.480	800 cP	100 psi	1.9%	Soft
ResinTech RT153FC	1.55	Mixed. 1000- 3000 cP	-	-	Glass Transition >100°C
Loctite 358	1.51	1750- 3500	≥1450 psi steel pin to glass	-	Recommended by Prof Peng, Univ New South Wales
Loctite 3525	1.51 1.48 (<i>uncured</i>)	15000c P	3500 psi (<i>at break</i>)	-	Recommended by Henkel UK Acrylic
Norland 76	1.51	3500- 5500 cP	450psi	-	Designed to give best possible optical bond when using plastic to glass substrates
Norland 78	1.50	8000- 11000 cP	649 psi	<i>low</i>	Used by Harbach[14]. Liquid photopolymer
Norland 81	1.56	300 cP	4,000 psi	-	Good Tensile Strength / poor optical transmission compared to Dymax.

The Loctite adhesive is a light curing adhesive, which provides a number of advantages; this allows the polymer and silica fibre cores to be accurately aligned before a permanent splice is created. Additionally a two-part mix is not needed eliminating repeatability errors when measuring different ingredients of an adhesive. The following section describes the process of splicing POF to silica optical fibre, allowing for POFBGs to be interrogated in reflection using stable and constant butt coupling between the two types of fibres.

5.2 Optical Adhesive Splicing Technique

As a permanent splice is to be made between the polymer and silica optical fibres, a temporary connection is also required between the polymer splice and coupler to allow different POFBGs to be interrogated in reflection using the same interrogation optical setup. Therefore the POF will be spliced to a silica pigtail which can be connected and disconnected easily to a FC/APC connector which is fusion spliced to the silica arm of the coupler, as shown in Figure 5-1.

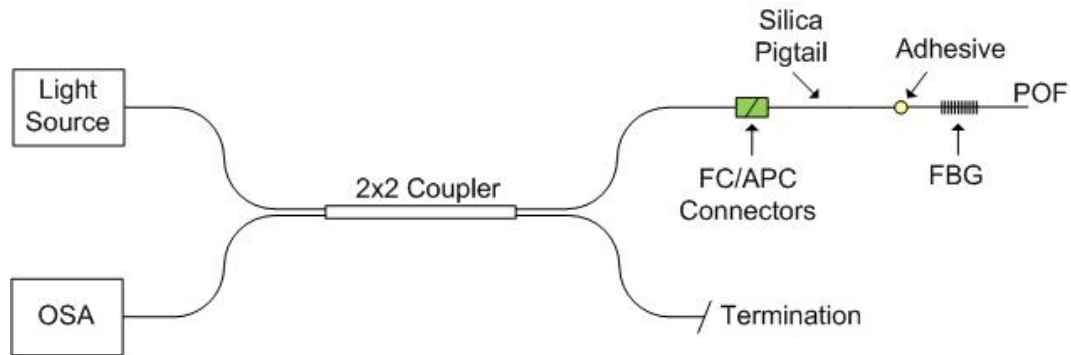


Figure 5-1 Reflection POFBG interrogation setup with additional silica pigtail

The procedure for splicing is as follows: first, preparation of the silica and polymer fibres was needed. The end face of the POF was prepared in the same way as discussed in chapter 4, using a feather razor blade which is heated to 80°C together with the end of the POF which was to be cleaved. The fibre end of the silica pigtail is stripped and cleaved using an 8° angle cleaver (Oxford Fiber Ltd HSAFC-2008) so to reduce the Fresnel reflections from the silica fibre end face. All adhesive splicing is completed after the fabrication of a FBG in POF, allowing for optimisation of the Bragg response before the butt coupling is permanently fixed. The physical layout of v-grooves, translation stage and optical fibres is shown in Figure 5-2. Once the fibre ends were prepared the pre-fabricated POFBG was laid onto the v-groove plate in a similar manner as when laying the POF ready for inscription, although no alignment of the UV inscription laser was needed. The v-groove was tied down to the stationary part of the Melles Griot XYZ translation stage shown in Figure 5-2. The POF was taped down onto the v-groove using polyimide tape leaving an approximate overhang of 2mm of POF over the edge of the plate towards the travelling part of the translation stage. Both ends of the POF were taped down to keep the fibre taut and axis straight, it was also ensured that the opposite end of the POF to the butt coupling overhung the far end of the v-groove plate as this will assist in monitoring the core guidance within the POF and thus help when aligning the two fibre cores together. The stripped end of the silica pigtail was fixed to a second v-groove plate, again with the cleaved angled end overhanging the plate by around 2mm towards the POF. The silica fibre was secured along the v-groove using magnets. The Loctite 3525 was now applied to the tip of the silica fibre; using a short cylindrical stick enough adhesive was applied to the fibre to resemble a pin head with a diameter of around

1mm. The second v-groove plate was then tied down to the travelling part of the translation stage, leaving around a 3mm gap between the polymer and silica fibres. The silica fibre was then brought to within 0.5mm of the POF using the micrometers of the translation stage and adjusted in the x and y axis, perpendicular to the fibre axis until guidance of a 635nm laser diode (Oz optics FODL-235-635-1) was seen in the core of the POF, which was launched into the input arm of the 2x2 coupler. Still ensuring guidance within the core of the POF, the silica fibre was brought towards the POF end face until the adhesive was spread across both the polymer and silica fibres. After a final check of the guidance of the red laser diode in the core of the POF, the appropriate interrogating light source and OSA was used to monitor the Bragg response. Finally, slight adjustment was made to the position of the silica fibre along the x and y axis perpendicular to the fibres lengths to optimise the Bragg response.

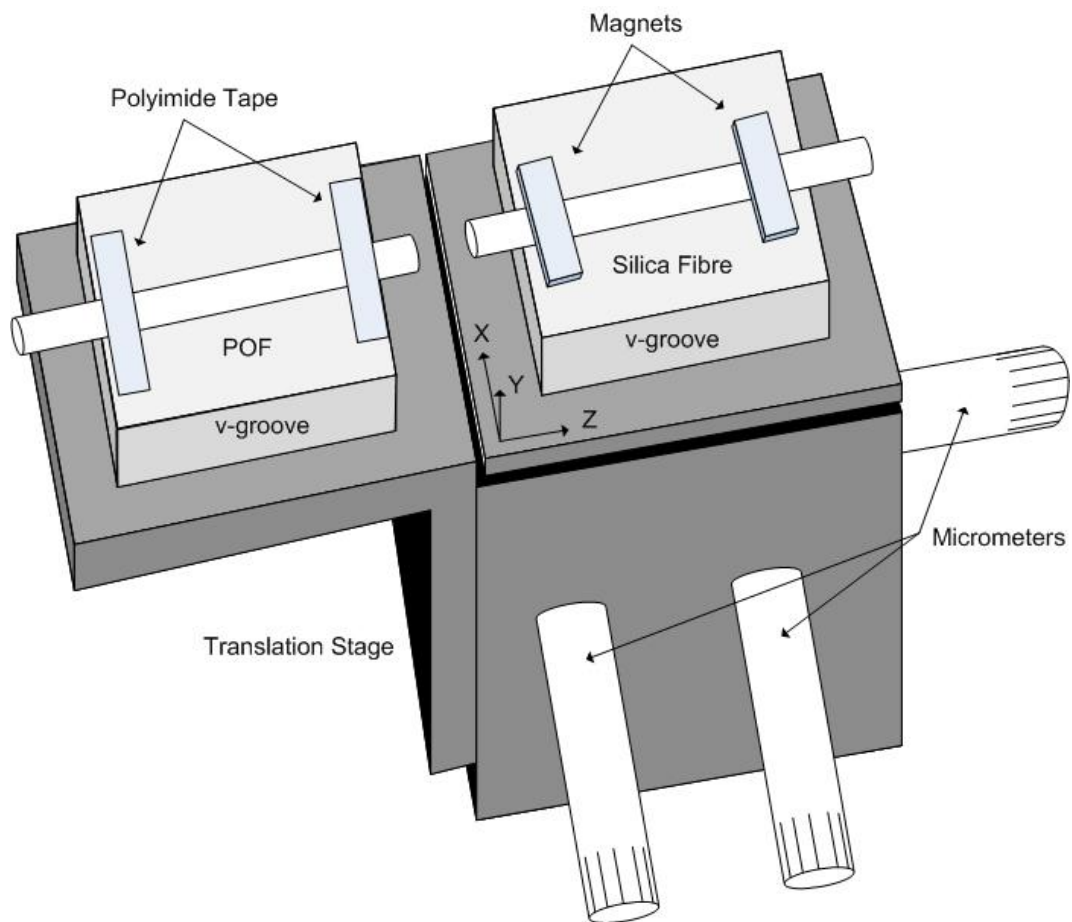


Figure 5-2 Physical setup of Melles Griot XYZ translation stage, including v-groove plates and fibre positions

Once the coupling was optimised with the largest signal-to-noise ratio of the Bragg reflection, a UV curing light was used to cure the adhesive and permanently fix the butt coupling. An OmniCure Series 1000 UV light source was used to solidify the adhesive, the iris of the light source was set to a 2% opening which was measured to pass 60mW of light using an optical power meter. The UV curing light source was suspended 1cm above the butt coupling joint and exposed the adhesive for 20 minutes to ensure the adhesive was entirely set.

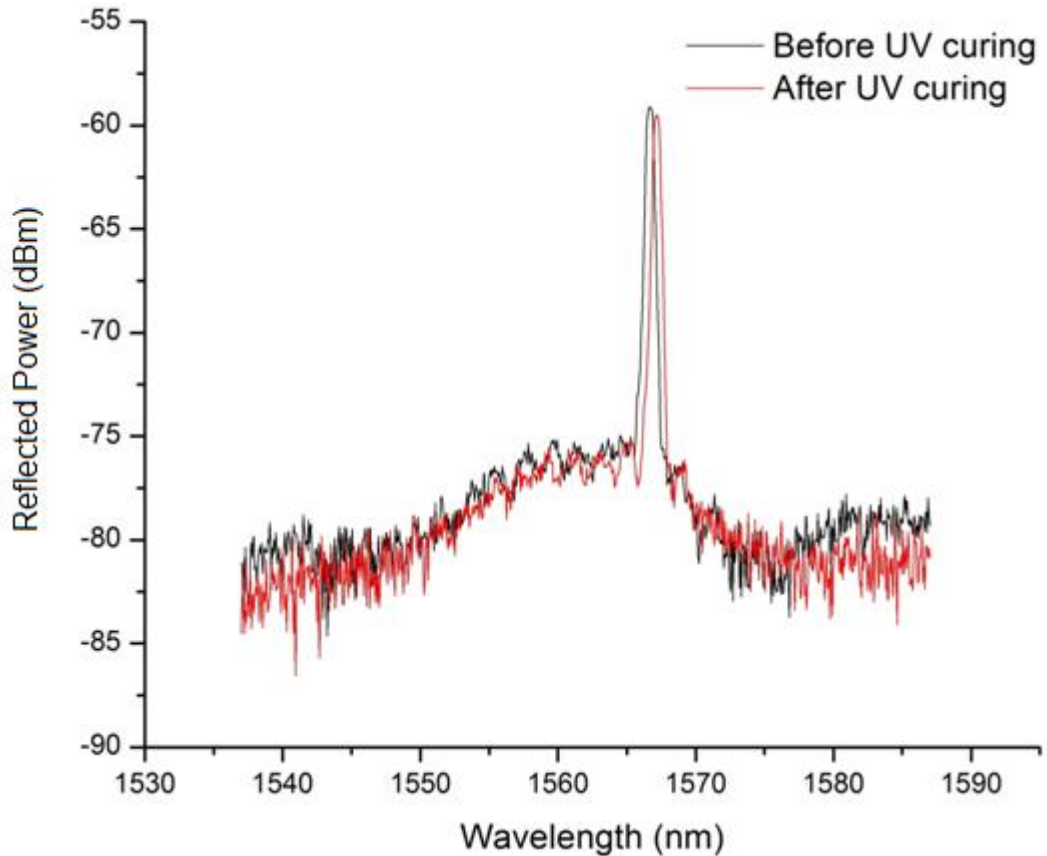


Figure 5-3 Comparing reflection spectra of a FBG fabricated in Peng D2 POF before and after adhesive is cured.

This splicing technique was first successfully attempted with G. D. Peng D2 step index POF. A FBG was first fabricated in the doped PMMA based single mode POF. Captured with a bandwidth resolution of 0.5nm on a HP 70951B OSA, a single peak response was observed with a central wavelength at 1566.5nm and a bandwidth (FWHM) of 0.5nm, the signal-to-noise ratio was in the order of 17dBm. This reflected Bragg response was captured as described in Chapter 4; however instead of using a refractive index matching gel the uncured liquid form of the Loctite adhesive was used with a refractive index of 1.48. Once the Bragg response was optimised as shown with the black spectrum in Figure 5-3 the adhesive was UV cured for 20 minutes. The resultant Bragg response is shown with the red spectrum in Figure 5-3. The Bragg response was observed with a central wavelength of 1567nm and a bandwidth (FWHM) of 0.5nm. A positive wavelength shift of 0.5nm had been observed, this was because the POF was slightly curved during the second interrogation resulting in a small amount of strain being applied to the POFBG sensor once the adhesive was cured, as can be seen in Figure 5-4. Additionally a decrease of around 0.5dBm was seen in the signal-to-noise ratio after the adhesive had been cured this could possibly be a result of the refractive index of the adhesive changing from 1.48 to 1.51 when UV cured.

Figure 5-4 demonstrates the physical permanent splice between polymer and silica fibres whilst interrogating a FBG which was fabricated in POF, this now enables the potential of characterisation of the Bragg response to numerous measurands away from the translation stage it was fabricated on, which previously was needed for temporary butt coupling.

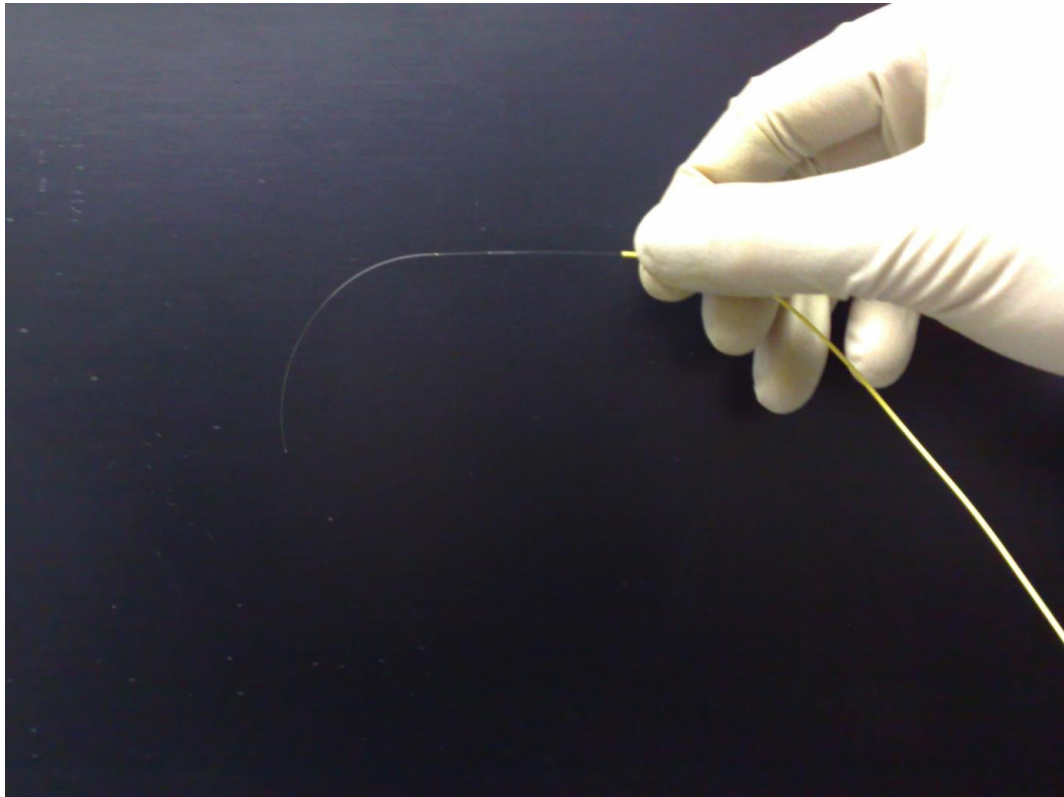


Figure 5-4 Peng D2 POF permanently butt coupled to a SMF28 pigtail using Loctite 3525

5.3 Optical Adhesive Splicing for mPOF

The same technique described above in section 5.2 was attempted to splice MMmPOF with a silica multimode (50/125 μm) pigtail. However this technique proved troublesome, initial results saw significant change in the modal distribution when bending the MMmPOF and the adhesive splice. The calculated reflected Bragg wavelength of the grating response varied as much as 300pm whilst handling the POF and curving the splice between the polymer and silica fibres as demonstrated in Figure 5-5. Here reflected modal redistribution was seen, including loss of optical power. The reason for the changing modal distribution and power loss may possibly be due to the adhesive travelling along the holes of the MMmPOF resulting in a non index guiding section of fibre where modes may have been lost as shown in Figure 5-6. Whilst following the adhesive technique, once the adhesive was spread across the two fibres it had enough time to travel 180 μm along the holes of the mPOF as is shown. Once the adhesive was cured the refractive index within these lengths of holes increased to 1.51, an increase above the refractive index of the POF's PMMA base material which resulted in a higher effective refractive cladding when compared to the refractive index

of the core and hence there was no internal reflection. As the MMmPOF was bent or curved there was a modal redistribution because of the resulting non-guidance along the 180 μ m length of mPOF at the adhesive joint and thus light was coupled out of the fibre rather than guided, as the fibre was curved in a different position loss within different modes was observed.

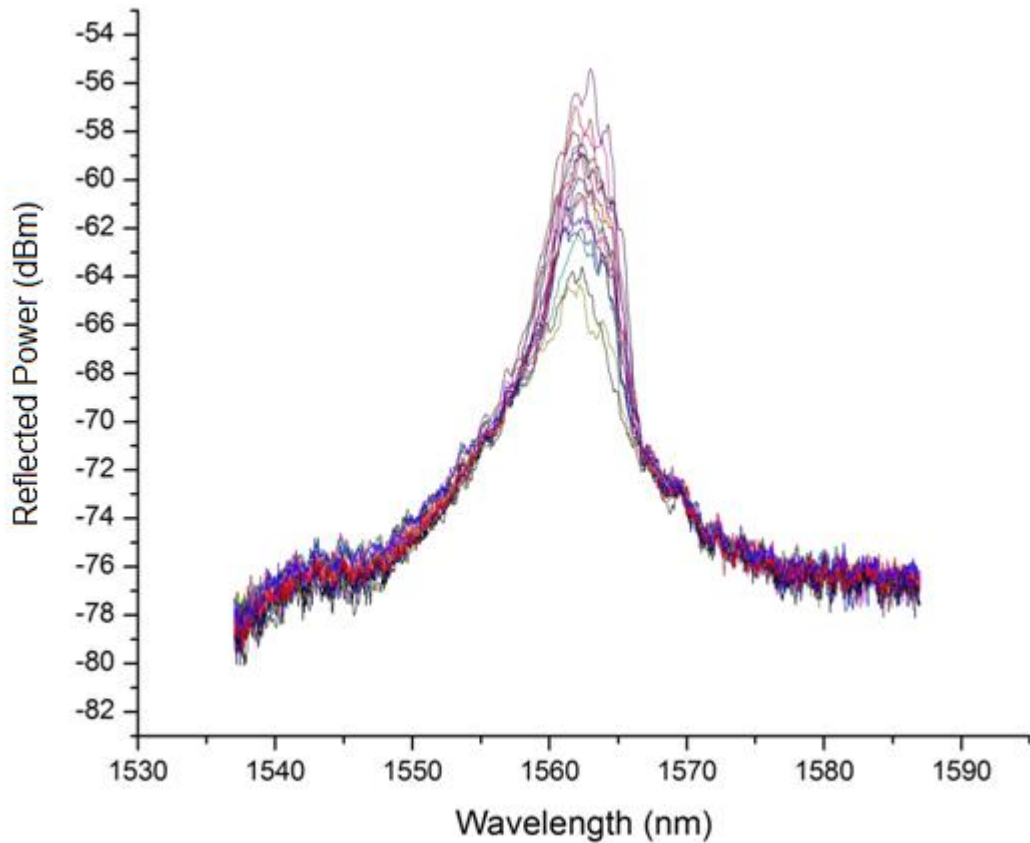


Figure 5-5 Resolution of 300pm, due to loss of index guiding within the MMmPOF because of adhesive travelling along the hole structure of the mPOF

In an attempt to reduce the amount of, or prevent the travel of the adhesive along the holes of the MMmPOF the application technique of the Loctite 3525 was modified. Both the polymer and silica fibre ends were prepared the same way as previously detailed and both were mounted onto their respective v-groove plates as per the previous method. However no adhesive was applied to the end of the cleaved silica pigtail, this was applied later. Both v-grooves were tied to the XYZ translation stage as before with around 3mm between the two fibre ends. The silica pigtail was then repositioned to within 0.5mm of the POF and alignment of the two fibres cores was completed using the red laser diode launched into the input arm of the coupler, whilst adjusting the position of the silica fibre along the x and y axis using the micrometers of the translation stage. The silica fibre was then brought closer to the POF by adjusting the z axis micrometer of the translation stage. Using a magnifying glass to observe the two fibre ends the silica fibre was brought close enough until no visible opening between the two fibres could be seen. This was then followed by fine adjustment of the silica fibre position along the x and y axis, confirming the guidance of the red laser diode in the core of

the MMmPOF. Once the index guidance was confirmed, the normal interrogation setup was implemented, the broadband ASE light source (1.53 – 1.61 μm) was launched into the MMmPOF and an OSA (HP 70951B) was used to observe the reflected Bragg response. Initially, interrogation of the butt coupling setup saw a high background noise level as the broadband light source was reflected off the MMmPOF end face due to no index matching gel or adhesive being applied.

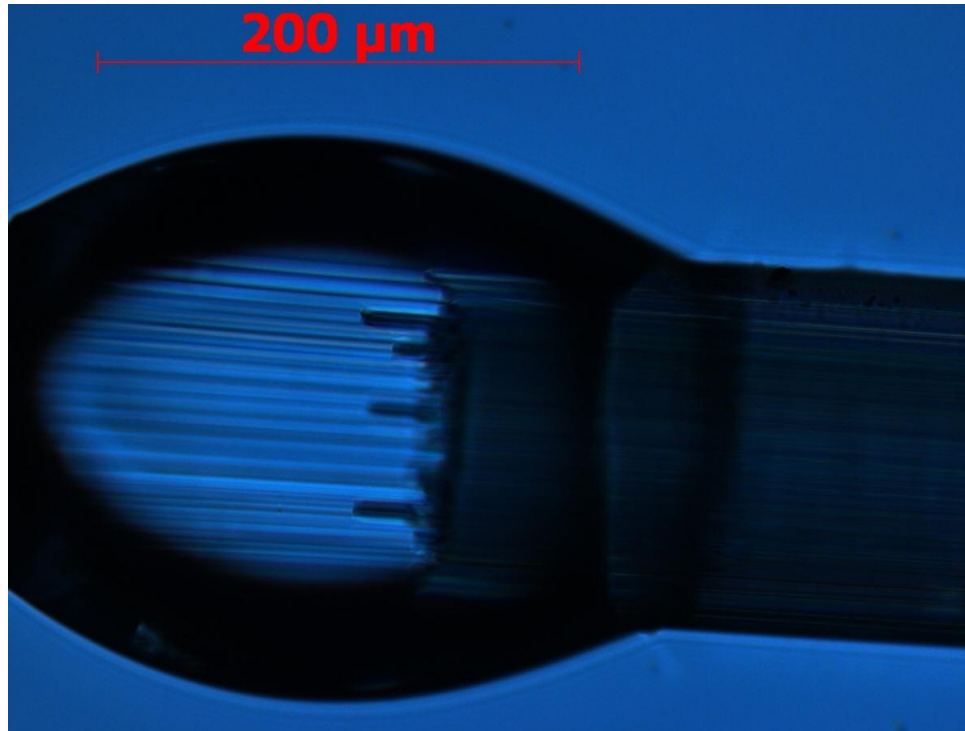


Figure 5-6 Optical adhesive Loctite 3525, which is UV cured inside the holes of the MMmPOF

The objective of this amended procedure was to set a small amount of adhesive as quickly as possible before travelling any distance along the holes of the MMmPOF. Therefore the UV curing light source was setup in advance to enable a quick curing time when required. A small bead of Loctite 3525 adhesive with an approximate diameter of 0.5mm was applied to the joint of the two fibres. This reduced the background noise level by reducing the Fresnel reflections and allowed the reflected Bragg response to be observed during interrogation, immediate adjustment of the silica fibre position in the x and y axis was made to optimise the Bragg response. The adhesive was then set using the UV curing light positioned 5mm above the butt coupling and exposed the adhesive for 10 minutes. This first stage of the modified technique was designed to grip the two fibres together and seal the holes of the MMmPOF at the same time; from the application of the adhesive to exposure of the UV light was no more than 30 seconds. A second coating of adhesive was then applied to the butt coupling joint; a bead of adhesive was left around the joint of diameter 1mm and was UV exposed for 10 minutes. Finally a third application of adhesive was applied around the joint, ensuring the adhesive is spread evenly over both the silica and polymer fibres, resulting in a final diameter of around 2mm which again was UV exposed of 10 minutes. The final two layers of

adhesive were applied to support the joint further compared to the previous method, it was felt that by keeping the joint more rigid the splice would be less susceptible to bending losses.

The enhanced technique of splicing polymer and silica fibre together proved a success. With less time and less adhesive present at the joint during the initial application no significant amount of adhesive travelled along the hole structure and therefore index guiding along the core of the MMmPOF was no longer interrupted. This resulted in no variation of the Bragg response as was previously witnessed in Figure 5-5.

Shown in Figure 5-7, is the reflected Bragg response of a FBG fabricated in MMmPOF whilst interrogated by butt coupling to the MMmPOF using a FC/APC and index matching oil as described in Chapter 4 prior to UV curing. The reflected response had a Bragg wavelength of 1562.5nm and a bandwidth of 2.5nm (FWHM), the reflected Bragg response had an apparent signal-to-noise ratio of 16dBm. The same MMmPOF sensor was then re-cleaved and adhesive spliced to a multimode pigtail again presented in Figure 5-7. This second capture of the same grating had a Bragg wavelength of 1562nm and a bandwidth of 3nm (FWHM), the Bragg response had a signal-to-noise ratio of 20dBm. An increase of 4dBm was seen in the reflected signal-to-noise ratio once the MMmPOF was permanently butt coupled to the silica pigtail; it is felt this is may be due to a better cleave using the heated razor blade for the adhesive splice. Additionally a negative Bragg wavelength shift of 0.5nm was observed after the adhesive splice; again this may be due to a re-cleaved MMmPOF end face, with an improved quality of end face the optimisation of the reflected Bragg response has redistributed modal coupling between the two fibres.

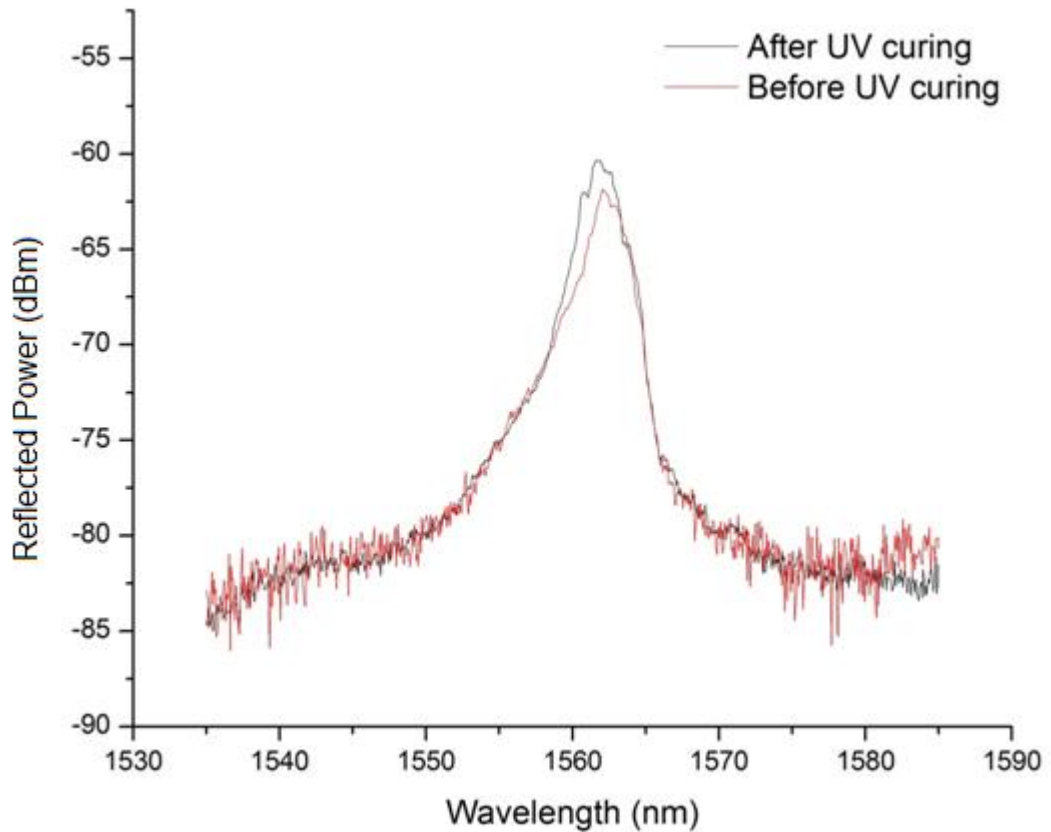


Figure 5-7 Comparing reflection spectra of a FBG fabricated in MMmPOF before and after adhesive is UV cured

5.4 Optical Adhesive Protection

In further work, metallic sleeves were placed over the adhesive splice between the polymer and silica fibres. The sleeve was 15mm long and had an AWG12 diameter which equates to 2.05mm; each end of the sleeve was then bunged with silicone sealant. This added extra impact protection to the splice, including protection against bend breakage of the stripped length of SOF. Furthermore the sleeve prevented any bending of the adhesive splice.

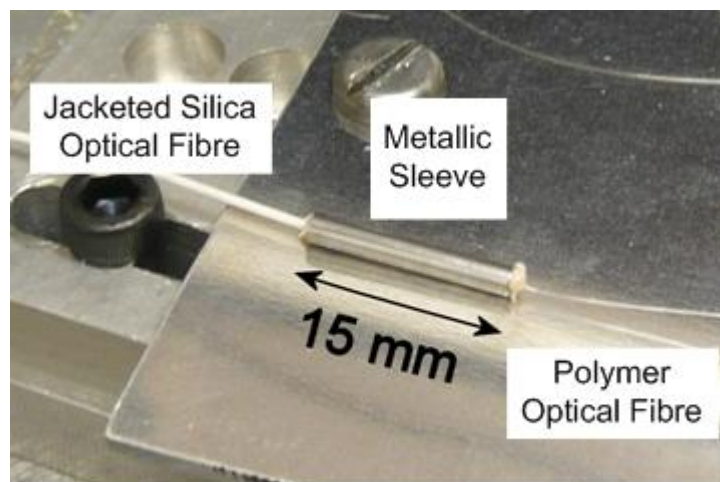


Figure 5-8 Metallic sleeve used protect adhesive splice

5.5 Summary

Documented in this chapter is the technique which was developed to splice both step index and microstructured POF and silica optical fibres together. With a product summary, it was decided Loctite 3525[70] had the optimum combination of properties best suited for this optical fibre splice. The adhesive splice has enabled POFBG devices to move away from the translation stage they were fabricated on and into application specific characterisation environments. This technique has permitted the first publications which have taken advantage of the adhesive splice[71-75], furthermore the adhesive splice has enabled the completed work in thesis including; axial strain and hydrostatic pressure characterisation (Chapter 7), thermal annealing characterisation and wavelength division multiplexed (WDM) sensor fabrication (Chapter 8) and characterisation of FBGs fabricated in TOPAS Cyclic Olefin Copolymer POF (Chapter 9).

5.6 Future Work

Although no apparent optical loss was seen from the adhesive splice between MMmPOF and multimode silica optical fibre and only 0.5dBm loss seen from the adhesive splice between step index single mode polymer and step index single mode silica optical fibres it is felt full characterisation of the adhesive splice is needed. This characterisation would include both optical and mechanical tests, including optical transmission across a wide spectral range (500nm-1600nm) and mechanical strength testing, investigating the point where optical transmission is lost.

Although this technique was developed to allow movement of the POFBGs away from the optical bench whilst still interrogating the Bragg response in application specific environments a full understanding of the splice is needed if this was to be a solution for commercially available POF devices. Furthermore these adhesive splices are relatively bulky, fragile and time consuming to implement, all factors which do not lend this technique to applications out of the laboratory. Additionally the Loctite 3525 adhesive has a glass transition temperature of 43°C[70], which clearly limits POFBG sensors above this temperature.

One possible future solution is embedding the POF end into a ferrule connector, which was suggested by Lwin[76], here microstructured POF would be permanently fixed within a ferrule connector with the use of an epoxy and the POF end polished down to the end surface of the connector enabling connection to another ferrule connector. Some restraints would come with this concept however, as the manufacturing of POF is still often varied the location of the core may not always be within the centre of the cross sectional area of the fibre, what is more diameters of core and outer surface not only vary between fibres but also along the length of the same fibre. This restricts the alignment capabilities of this ferrule

technique when using single mode POF, however with large multimode cores ($+50\mu\text{m}$) more tolerance to misalignments are possible.

Finally, it is felt that the quality of the cleaved end face of the POF has a big influence on the quality of the adhesive splice. Thus a more reproducible method of cleaving the polymer fibre end face that results in consistent low losses may need to be found which is also quick and simple to complete from a manufacturing point of view. One step towards this may be to use TOPAS Cyclic Olefin Copolymer POF (Chapter 9), which is not required to be heated. A cleave of this type of POF can be carried out at room temperature including the temperature of the razor blade, thus eliminating one variable aspect of the cleaving process.

6

FABRICATION OF POFBGS IN THE LOW ATTENUATION BAND

So far all the fabricated POFBGS described have been manufactured using a single phase mask with a surface relief pattern that has a period of 1057.2nm as described in Chapter 4. It was demonstrated that using this phase mask resulted in the fabrication of Bragg grating sensors with a Bragg wavelength of around 1562nm when interrogating the FBG in reflection. The drawback of fabricating devices which operate in and around this wavelength region is the high attenuation of POF, which is mainly due to the harmonic vibration absorption of the C-H chemical bond as discussed in Chapter 3.

A large number of Bragg gratings fabricated in PMMA based POF have a Bragg wavelength within the 1500nm spectral range[10, 15, 24, 66, 72] and hence experience attenuation losses which are typically around 1dB/cm[59]. As was discussed in Chapter 5, the breakthrough of developing permanent adhesive splices between POF and SOF did however allow POFBGS to leave the optical bench and into a wider range of applications such as monitoring the condition of textile tapestries described by Ye *et al*[75].

However, although the splicing technique was a breakthrough for the POFBG technology the close proximity between the adhesive splice and the FBG fabrication point is far from ideal. The relatively fragile and bulky adhesive splice left the POFBG sensors susceptible to mechanical failure of the splice, even with the addition of the metal sleeves to increase the protection of the splice this ultimately added to the bulkiness of the device. Difficulties were encountered when mounting the POF into or onto application specific experimental equipment for POFBG sensor characterisation, such as humidity sensing, pressure sensing and thermal tuning characterisation all of which are discussed in later chapters. The necessity to increase the distance between the fabricated POFBG and the adhesive splice to silica optical fibre was apparent. This would enable increased protection of the adhesive splice by applying the metal sleeve over the splice and would still be far enough away so not to hinder the response of any POFBG sensor.

Kaino presented results shown in Figure 6-1, demonstrating that the lowest loss seen in both PS and PMMA core POFs is within the 500-700nm spectral range, with losses as small as 100dB/km for the PMMA core POF[77]. It would therefore be desirable to fabricate POFBGS with a Bragg response within the 500-600nm spectral region, which gives the possibility of longer POF lengths.



Figure 6-1 Absorption Loss PS (solid line) and PMMA (dotted line) core POFs when measured in transmission, from[77]

Additionally Boom *et al* quoted losses of 2dB/m within the 800nm spectral region[59]. In this area of work the aim is to fabricate POFBGs in the PMMA MMmPOF with a Bragg response in the 800nm spectral region. As discussed this will allow POF devices up to tens of centimetres in length and will also allow for the use of cheaper broadband semiconductor light sources to be used in the Bragg response interrogation. The choice of attempting to fabricate POFBGs in the 800nm rather than within the 500-600nm spectral region was determined by available phase masks. The purchase of phase masks which produced Bragg gratings in the 800nm region was influenced by the availability of an interrogating light source around 830nm being readily available. Furthermore the decision to take a cautious approach when investigating the possible index change feature size needed in PMMA to fabricate FBGs with a lower wavelength Bragg response influenced the choice.

Transmission attenuation measurements were taken of the PMMA based MMmPOF at both 1550nm and 830nm. Two light sources were used; these were a Thorlabs (ASE-FL7002-C4) broadband light source with an operating range of 1530–1610nm and second a superluminescent diode (SLD) (Superlum SLD-361) operating at 830nm.

Light was launched into the POF using a silica multimode (50/125 μ m) pigtail which was permanently spliced to the POF using the Loctite 3525 optical adhesive. The cores of the two fibres were aligned slightly differently to the technique described in Chapter 5 as there was no reflected Bragg response to optimise, however the 635nm laser diode (Oz Optics 23S-635-1) was launched into the POF via the silica pigtail and the coupling was optimised by observing the projected guidance of the red light using a 10x microscope objective lens onto a white card. Once optimised the adhesive was added to the polymer and silica fibre joint and was UV cured for 30 minutes as described in Chapter 5. The optical power exiting

the far cleaved end of the MMmPOF was measured using a Gentec PH series Photo Detector, the head of the detector was positioned within 1mm of the POF end. Index matching oil (RI = 1.4917) was placed over and around the surface of the MMmPOF 1cm from each end of the POF so to strip out any cladding modes from the fibre, as is shown in the setup diagram of Figure 6-2.

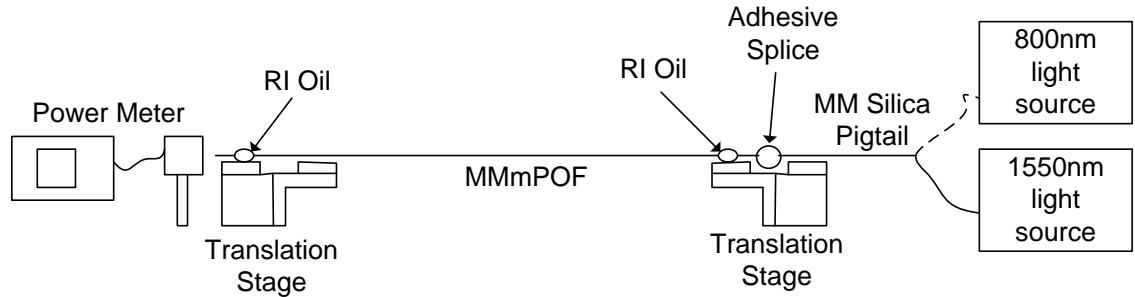


Figure 6-2 Experiment setup for attenuation measurements

The attenuation of the MMmPOF was calculated using the cut back method. Originally 264cm in length, the POF was cleaved back in sections, using the hot razor blade method described in Chapter 3 and detailed by Law *et al*[78]. After each cleave the transmitted power was measured using the Gentec power meter. The splice between the polymer and silica fibres was permanently taped to the translation stage in an attempt to gain consistent conditions throughout the experiment. The FC/PC connector of the silica pigtail was swapped between the two light sources depending on which measurement was being taken.

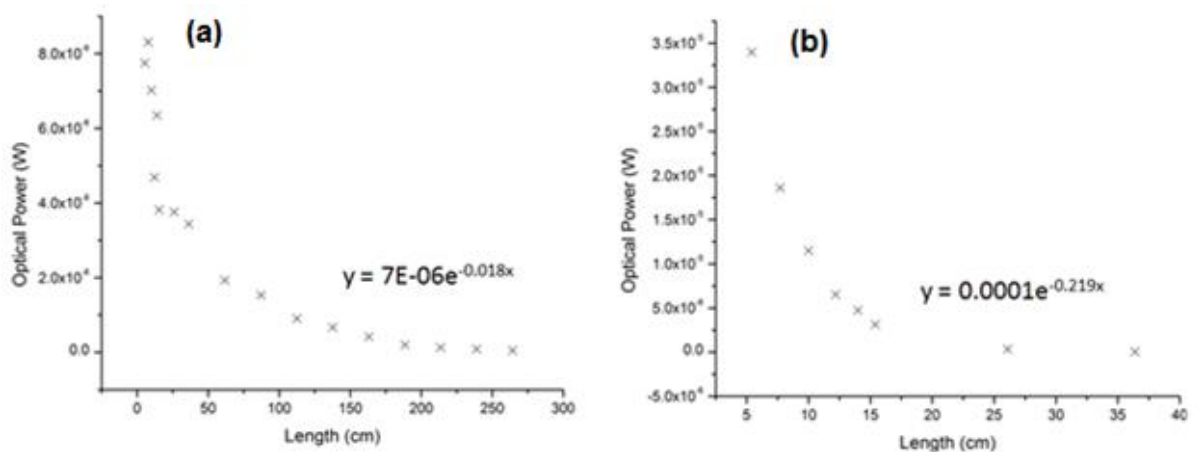


Figure 6-3 Optical power during cutback measurements at: (a) 830nm (b) 1550nm

The optical power measurements at both wavelengths are presented in Figure 6-3. Although it was possible to take power measurements along the whole length of the POF (264cm) at 830nm, it was not possible to take optical power measurements at 1550nm until the POF length was reduced to 36cm because of the high attenuation. Once the cut back measurements had been taken the silica pigtail was re-cleaved and the optical power of

either light source was measured exiting the silica fibre, again the power meter head was positioned within 1mm of the end of the SOF. The optical powers are presented in Table 5.

Table 5 Optical power measurements of each light source, taken at exit of a silica multimode (50/125 μ m) pigtail

Wavelength	Optical Power
1550nm	492 μ W
830nm	188 μ W

Using the data presented in Figure 6-3, the transmission attenuation losses of the PMMA based MMmPOF was calculated to be 95dB/m at 1550nm and 8dB/m at 830nm. Therefore demonstrating the significantly better attenuation losses at 830nm compared to at 1550nm. The measured attenuation of 0.95dB/cm at 1550nm is comparable to that by Boom *et al*[59] of 1dB/m. However the measured attenuation loss of 8dB/m at 830nm is 4x larger than that given by Boom *et al*[59] (2dB/m), this is likely to be due to the difference in composition of the PMMA materials used in either of the experiments, additionally imperfections induced during the drawing manufacture of the MMmPOF would also add to the increased attenuation loss.

6.1 Groundwork for fabrication of shorter Bragg wavelength POFBGs

Described in this section is the preliminary work completed whilst working towards the aim of fabricating FBGs in POF with a Bragg response within the 800nm spectral region. Demonstrations have already been presented of Bragg gratings being fabricated in POF with a Bragg wavelength of 980nm[79]. Here, the phase mask technique was used with a mask period of 658nm which was illuminated with a XeCl excimer laser at 308nm, the FBGs were written with a laser repetition rate of 8Hz and had a length of 15mm. Two types of POF were used, both of which were based on PMMA[79].

6.1.1 1300nm FBG Fabricated in MMmPOF

In a step towards fabricating POFBGs with a Bragg response in the 800nm spectral region, attempts were first made to fabricate FBGs with a response in the 1300nm spectral region using an available phase mask. The phase mask was optimised for use with the 325nm UV HeCd laser (Kimmon Koha Co, Ltd, 1K3301R-G) and had a surface relief pattern with a period (Λ_{pm}) of 873.10nm.

The same technique described in Chapter 4 to fabricate FBGs in the MMmPOF was used here to fabricate a FBG in the MMmPOF with a Bragg response around 1300nm. Again the phase mask was positioned directly on top of the POF and the FBG fabrication was positioned 2cm along the fibre length from the cleaved POF end. The only available light source which operated within the 1300nm spectral region was a small bandwidth tuneable

laser, which was scanned across a wavelength range of 1279.5-1310nm in 0.5nm steps. A Bragg response was expected at around 1290nm assuming an effective refractive index (n_{eff}) of 1.48 of the PMMA MMmPOF core and using Equation 19, previously given in Chapter 2. The refractive index of 1.48 was obtained by back calculation from FBG responses at 1562nm which were fabricated using a phase mask with a period of 1057.2nm, rather than the refractive index given by Brandrup[39].

Equation 19

$$\lambda_B = n_{eff} \Lambda_{pm}$$

Therefore the tuneable 1300nm laser was tuned to 1290nm in an attempt to monitor the growth of the FBG. Shown in Figure 6-4(a) is the reflected response of the light source prior to fabrication. The red trace (before fabrication) shows the background reflected signal of the tunable laser when no FBG had been fabricated. Whereas the black trace (after fabrication) demonstrates an increase in the reflected signal of the laser after a FBG had been fabricated hence the increase in reflected signal is possibly from the Bragg grating. Therefore shown in Figure 6-4(a) is the reflected response after the fabrication of the FBG at the same wavelength. Figure 6-4(b) demonstrates the growth of the Bragg response at 1290nm when the core of the MMmPOF was exposed to the UV interference pattern for 90 minutes. It would appear from Figure 6-4(b) that the Bragg response has a signal-to-noise ratio of at least 15dBm. As stated all the Bragg responses were captured in reflection, this was achieved using a silica multimode (50/125 μ m) 2x1 coupler with a coupling ratio of 50:50 at 1550nm. The reflected signal was captured on an OSA (HP 70951B) with a bandwidth resolution of 0.5nm. For these experiments the silica arm of the coupler was butt coupled to the end face of the MMmPOF with the aid of a translation stage and index matching oil to reduce Fresnel reflections, this is described in more detail in Chapter 4.

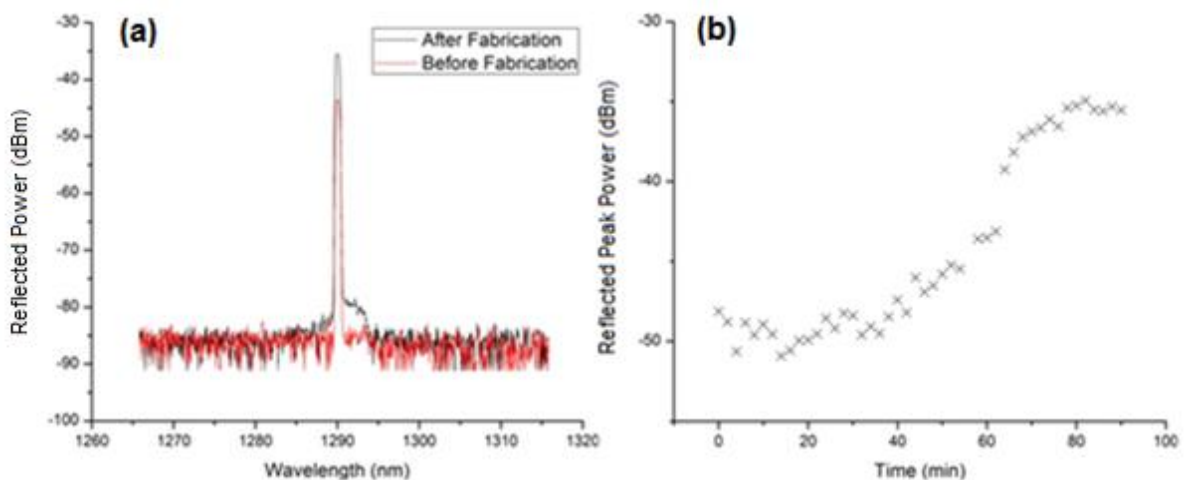


Figure 6-4(a) Captured reflection before and after fabrication (b) FBG response growth at 1290nm

The Bragg response of the fabricated FBG is shown in Figure 6-5. Here the background reflection noise level was determined prior to fabrication by taking the peak reflection point of each reflected signal whilst scanning the tuneable laser across a wavelength range of 1280-1310nm, the laser was scanned in 0.5nm steps. Once the fabrication had finished after 90 minutes, the tuneable laser was again scanned across the same wavelength range of 1280-1310nm, the peak data point was recorded every 0.5nm. The resultant Bragg response is shown in Figure 6-5, with a peak reflection seen at 1292nm.

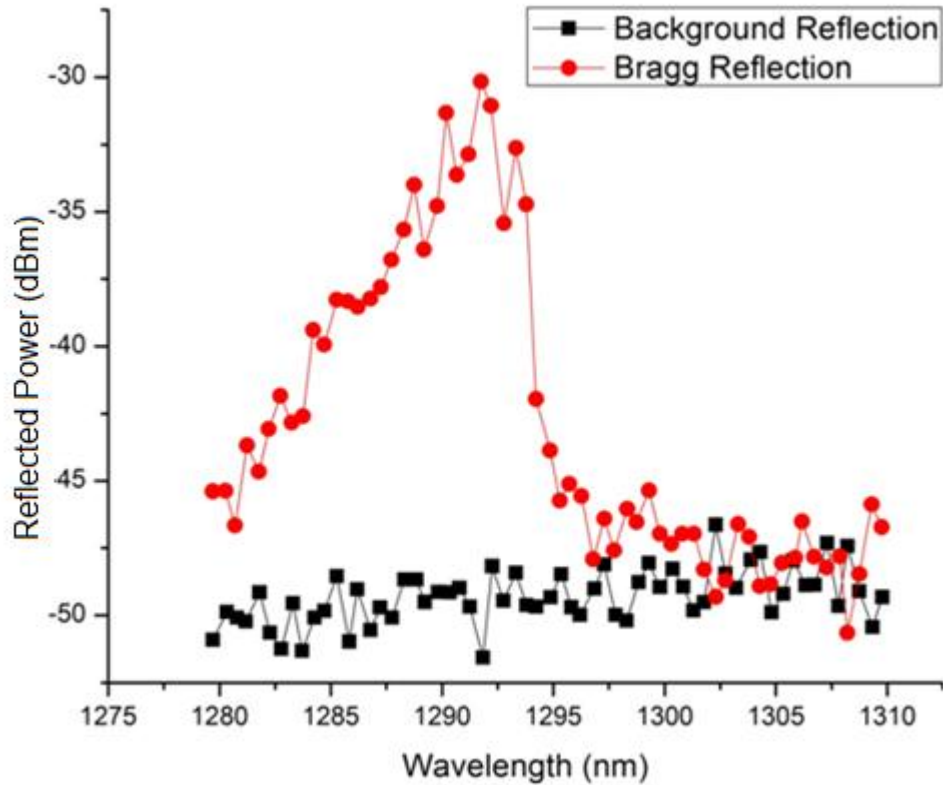


Figure 6-5 Bragg response of a FBG fabricated in MMmPOF which was fabricated for 90 minutes

In an attempt to verify the Bragg response shown in Figure 6-5 was due to the fabrication of a FBG in the core of the MMmPOF a desk lamp with a 60W bulb was held above the POF at a distance of around 10cm. The arbitrary heat from the bulb induced a negative Bragg wavelength shift of the Bragg response as can be seen in Figure 6-6. The shifted Bragg response had a peak at 1290.5nm, suggesting the heat from the bulb induced a negative wavelength shift of 1.5nm. If the two falling edges of the two Bragg responses are compared in Figure 6-6, then this would suggest the heating of the MMmPOF induced a negative wavelength shift of 1nm. Once the heat was removed the Bragg response returned to the original position in the spectral region, and the device therefore responded how a POFBG sensor would have been expected to.

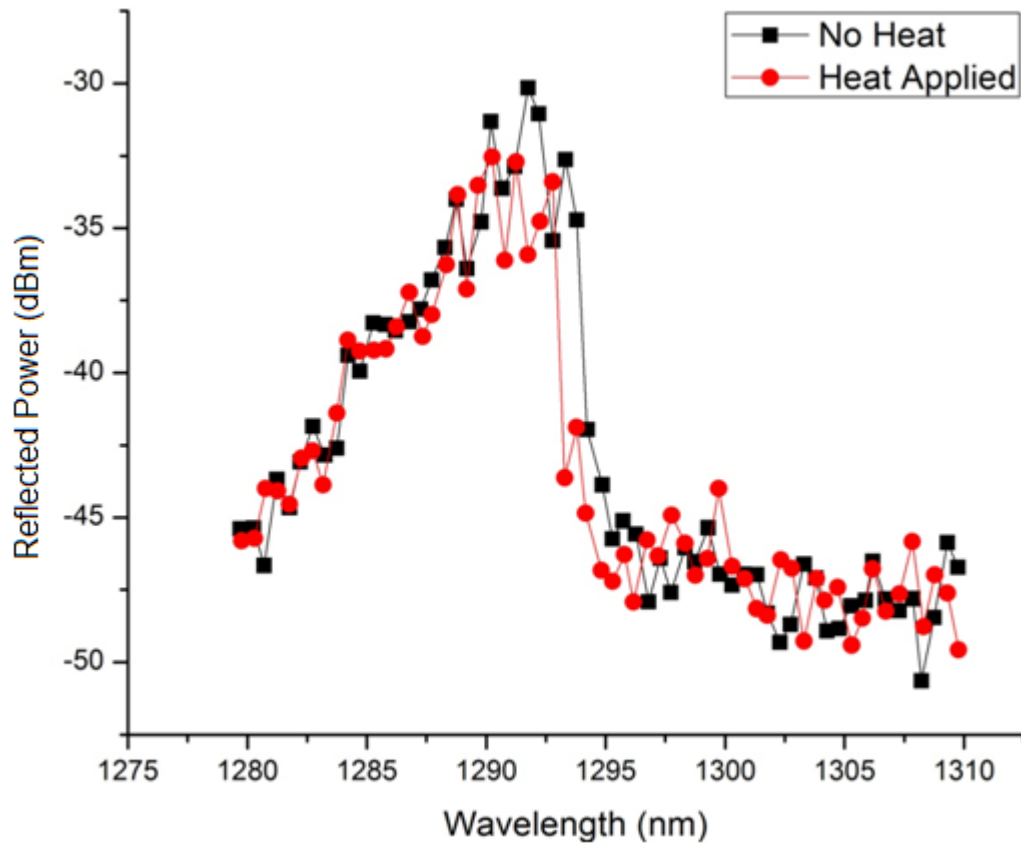


Figure 6-6 Change in wavelength of Bragg response of a FBG fabricated in MMmPOF due to the application of heat from a desk lamp

6.1.2 Resolution of Refractive Index Change in PMMA Planar Sample

In the early 1970's work that was carried out by Tomlinson, Kaminow *et al* demonstrated the fabrication of gratings in planar PMMA samples where the pitch of the grating planes exceeded those needed to fabricate Bragg gratings with a Bragg response at 800nm. Tomlinson *et al* found that PMMA displays a significant increase in refractive index when irradiated with UV light at 325nm. Using a HeCd laser, index changes as large 3×10^{-3} and a resolution of ~ 5000 lines/mm were seen[6]. Kaminow *et al* followed this by fabricating two gratings in PMMA doped with rhodamine 6G to produce a PMMA red dye laser with an internal diffraction grating resonator[7]. Kaminow *et al* measured a grating reflectivity of 20% at a wavelength of 559.1nm[7]. Therefore using Equation 20, which is the combination of Equation 15 and Equation 16 from Chapter 2, a line resolution better than 200nm was achieved.

To obtain a desired Bragg response within the 800nm spectral region a periodic increase in the refractive index with a grating period (Λ) of 268.46nm is needed within the core of the PMMA based MMmPOF, which was calculated using Equation 20 and assuming an effective index (n_{eff}) of 1.49 and a Bragg wavelength (λ_B) of 800nm.

$$\Lambda = \frac{\lambda_B}{2n_{eff}}$$

Figure 6-7 demonstrates the resultant index change in a planar sample of PMMA, taken with a 63x objective lens microscope. The sample was provided by Kiriama Pty Ltd and was polished down from a similar perform from which the PMMA based mPOF was drawn from. An optimised phase mask for use with a 325nm UV HeCd laser with a 580nm periodic surface pattern was suspended 67nm above the surface of the sample; this was the thickness of one layer of polyimide tape. It was found that using a multiple of two layers of tape resulted in the fringes of the grating structure to be on the top surface of the sample and hence any larger multiple layers of tape resulted in no observed index fringes within the material. The sample was exposed to the UV interference pattern for 2 hours.

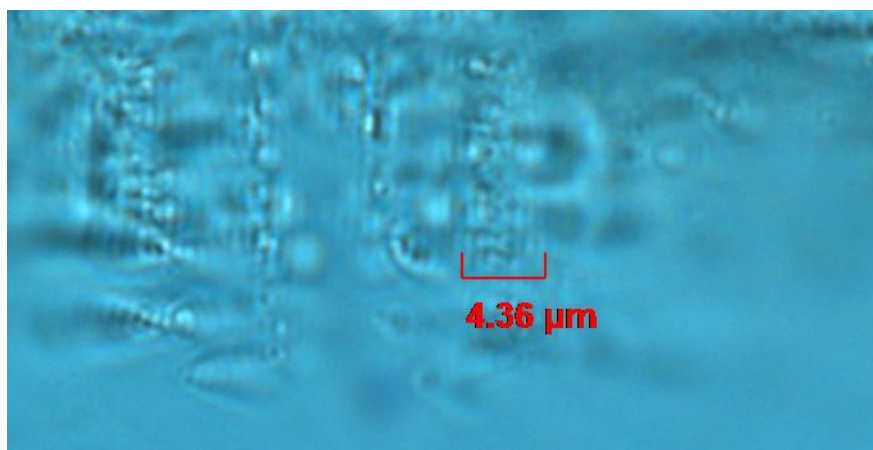


Figure 6-7 Refractive index change in PMMA planar sample using a phase mask with a period of 580nm

A distance of 4.36μm across 8 fringes was measured in Figure 6-7, resulting in an apparent fabricated grating period of 545nm. This is twice as large as what was expected, however this phenomenon has been witnessed before in Chapter 4 and also documented by Webb and Kalli, who suggested that this may be a result of insufficient suppression of the phase mask zeroth order[41]. Thus following this tendency the grating period within the PMMA planar sample is as expected at around 272.5nm. This therefore suggests that the line resolutions of refractive index changes are possible in the PMMA based material of the MMmPOF which would produce a FBG with a Bragg response at 864nm using Equation 19, and assuming an effective index (n_{eff}) of 1.48 within the core of the MMmPOF and a phase mask period (Λ_{pm}) of 580nm. There is the possibility that the drawing process of the PMMA material into fibre may affect the possible index change feature size, however this would be determined visually using a microscope to inspect the index change fringes within the POF core if no Bragg response was observed.

6.1.3 Lloyd's Mirror Interferometer Fabrication of FBGs within the 800nm Spectral Region

Here, work was completed as part of a collaboration by Dr Xianfeng Chen as part of a collaboration at Aston University. A Lloyd's mirror interferometer inscription setup was constructed similar to that described in Chapter 2 and was optimised for use with a UV 325nm HeCd CW laser (Kimmon Koha Co Ltd, 1K3301R-G). To verify the optical setup Chen completed 3 fabrications of FBGs in hydrogen loaded, boron/germanium (B/Ge) codoped photosensitive single mode silica fibre. Figure 6-8 presents the fabricated reflected Bragg responses; Chen illustrates how the Bragg response is optimised with a reflected 12dBm signal-to-noise ratio of the response by exposing the silica optical fibre to the UV interference pattern for 5 minutes, resulting in a Bragg wavelength of around 1533nm.

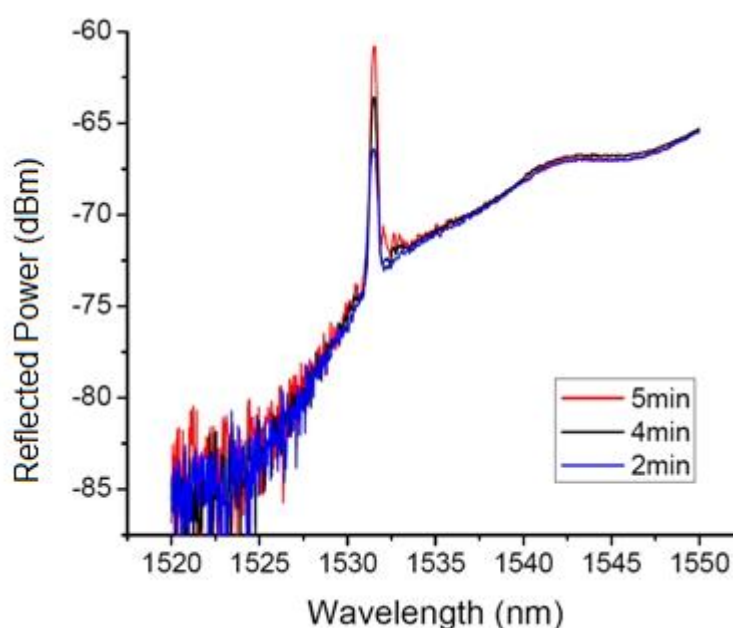


Figure 6-8 Reflected Bragg response of FBGs fabricated in hydrogen loaded B/Ge doped silica optical fibre, using a Lloyd's mirror interferometer inscription technique

The same interferometer setup was then used with the PMMA based MMmPOF, due to the resultant Bragg wavelength (1533nm) in the SOF it was expected that a Bragg response of around 1565nm would be possible in the PMMA MMmPOF. However after inscription times of up to 30 minutes Chen observed no possible Bragg reflections across a 1530-1610nm spectral range using a broadband ASE light source (Thorlabs ASE-FL7002-C4).

It is felt Chen may have possibly needed to expose the MMmPOF to the UV interference pattern for longer irradiation times of at least 2 hours. Additionally, intermediate development steps may have been taken where possible index fringes were inspected using a microscope in both fibre and planar PMMA samples.

6.2 FBG Fabrication within the 800nm Spectral Region in MMmPOF

Two phase masks were purchased to enable fabrication of FBGs in PMMA based POF with Bragg responses in the 800-900nm wavelength range. Both phase masks were optimised for operation with the 325nm UV HeCd laser and had surface relief patterns with periods of 557.50nm and 580nm.

6.2.1 Fabrication of FBGs with a 860nm Bragg Wavelength Response

First, the phase mask with the larger period (580nm) was used. The fabrication setup was the same as that described in Chapter 4 for MMmPOF, where the phase mask was mounted directly on top of the fibre. The interrogation of any potential FBG was by an Amonics benchtop superwide band short wavelength source (ASLD-CWDM-3-B-FA) with a wavelength range of 730-900nm and a typical output power of 1.5mW. Any Bragg responses were captured in reflection using a 2x1 silica multimode (50/125 μ m) coupler with a 50:50 splitting ratio at 800nm, the reflections were captured on an OSA (HP 70951B) with a bandwidth resolution of 0.5nm. Initial interrogations were completed by butt coupling the FC/APC silica optical fibre arm of the coupler to the cleaved end of the POF with the aid of index matching oil and a translation stage, which is described further in Chapter 4.

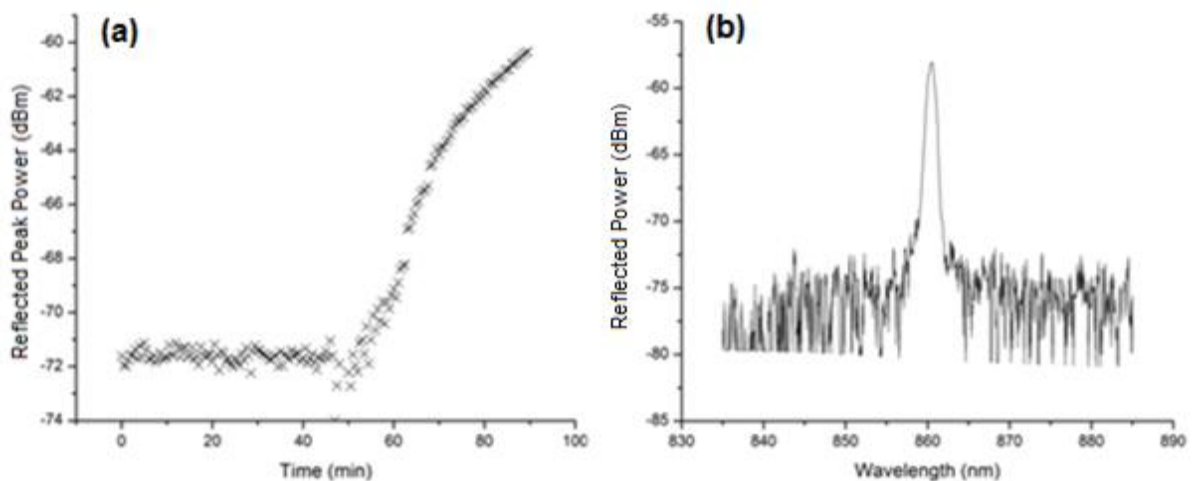


Figure 6-9 (a) Growth curve of a typical FBG fabricated in MMmPOF at 860.5nm (b) Typical Bragg response of a FBG with a Bragg wavelength of 860.5nm

Figure 6-9(a) illustrates a typical growth curve of a Bragg response from a FBG fabricated in the MMmPOF. The MMmPOF was exposed to the UV interference pattern for 90 minutes, this proved to be the optimum time for exposure before the bandwidth of the Bragg signal started to expand, a characteristic seen from over exposure. Whilst at the same time the gradient of the lower wavelength edge of the Bragg signal started to decrease, which is an indication of cladding modes being reflected. As can be seen in Figure 6-9(a) a 12dBm signal-to-noise ratio of the Bragg response was achieved after the 90 minute UV exposure. A small amount of optimisation of the butt coupling between the polymer and silica fibres took place after 45 minutes, resulting in the irregular data points in Figure 6-9(a). Figure

6-9(b) illustrates a typical reflected Bragg response after the 90 minute fabrication when using the 580nm period phase mask, the reflected Bragg response shown has a Bragg wavelength of 860.5nm and a bandwidth (FWHM) of 1.00nm.

6.2.2 Fabrication of FBGs with a 827nm Bragg Wavelength Response

FBGs were also fabricated in the MMmPOF using the second phase mask with the smaller period of 557.50nm. Again the phase mask was placed directly on top of the POF and hence there was no separation between the two. Once more, typical UV exposure times were 90 minutes, Figure 6-10(a) illustrates a typical growth curve of the peak reflected power from the Bragg response. Optimisation of the butt coupling between the silica and polymer optical fibres can be seen around 45 minutes by the irregular results. After a 90 minute UV exposure a Bragg signal-to-noise ratio of around 12dBm is seen. The reflected Bragg response after fabrication is seen in Figure 6-10(b), after further optimisation of the butt coupling a signal-to-noise ratio of 18dBm was measured. The Bragg wavelength of the response was 828.50nm and the bandwidth (FWHM) of the signal was 1nm. The reflected signal was captured on an OSA (HP 7091B) with a bandwidth resolution of 0.5nm.

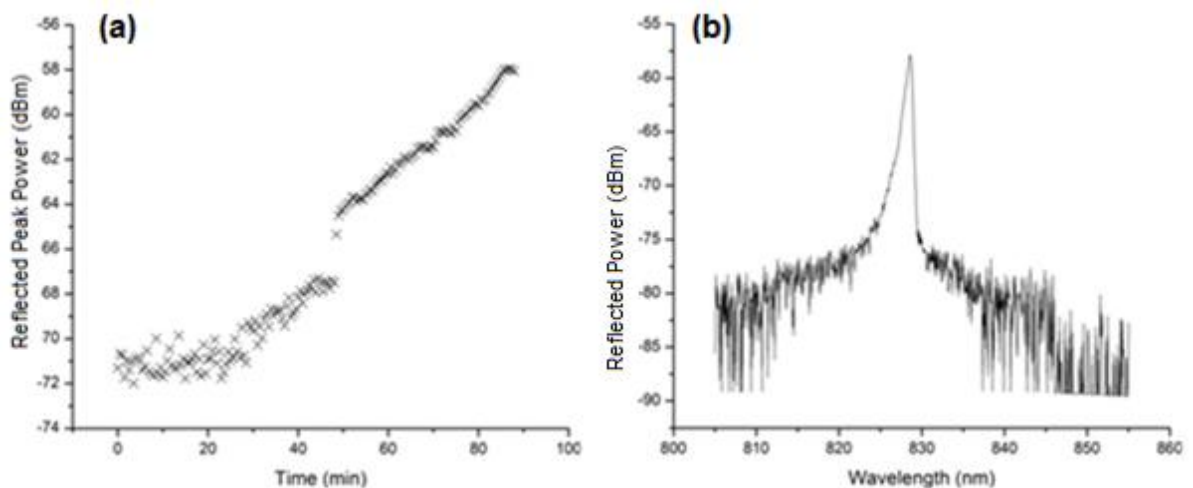


Figure 6-10(a) Typical growth curve of a FBG fabricated in MMmPOF with a Bragg wavelength of 828.50nm (b) Typical Bragg response of a FBG fabricated with a phase mask with a period of 557.50nm

FBGs could be regularly fabricated with Bragg wavelengths within the 800nm spectral region with typical Bragg responses like those shown in Figure 6-9 and Figure 6-10. And therefore these FBGs take advantage of the lower attenuation losses of 8dB/m which was measured at 830nm. Fabrication success rates at this wavelength are estimated around 50%. In particular fabricating Bragg gratings at 828nm gave a poor yield. The phase mask was cleaned in a sulphuric acid bath on numerous occasions; however this did not appear to improve the fabrication yield.

The FBG whose Bragg response was shown in Figure 6-10 was fabricated in a 25cm length of the MMmPOF. The FBG was fabricated 2cm from one end of the fibre to allow interrogation of the response during fabrication, which was dictated by the fabrication setup and position of the v-grooves with respect to the focussed UV laser beam. However after the completed FBG fabrication the Bragg response was again interrogated but from the far end of the POF thus along 23cm. Figure 6-11 demonstrates the difference in Bragg responses of the same FBG along the two different lengths of the MMmPOF. It would appear that interrogating the Bragg response over an additional 21cm resulted in a reduction of the Bragg signal-to-noise ratio by nearly 9dBm. This would suggest a loss of 0.2dB/cm which is comparable to the 0.08dB/m losses expected in 830nm the spectral region.

A further observation is the reduction of the bandwidth (FWHM) of the reflected signal which travels through the longer length of fibre. The bandwidth (FWHM) is reduced in half from 1nm to 0.5nm. This may be a result of higher order core modes getting lost through the longer length of fibre; this is also suggested by the increased gradient of the lower wavelength edge of the Bragg signal.

Figure 6-12 illustrates the length of POF of the FBG device which has a reflected Bragg response shown in Figure 6-11.

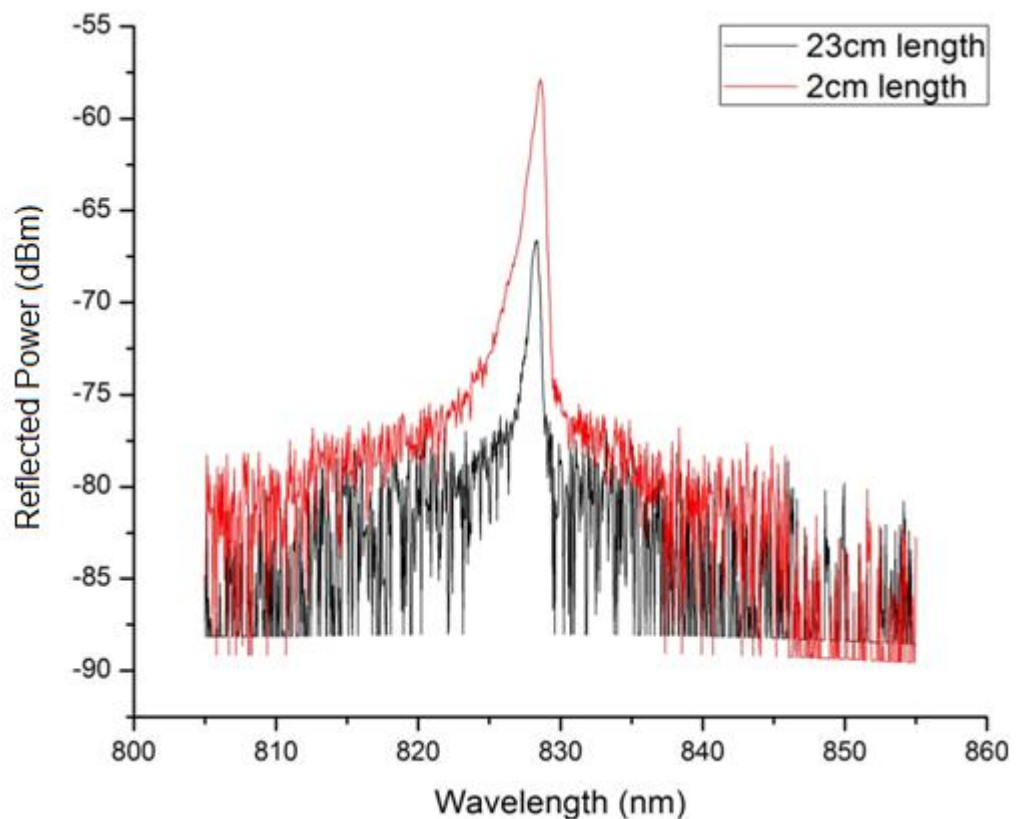


Figure 6-11 Comparison of Bragg response of one FBG through different lengths of MMmPOF

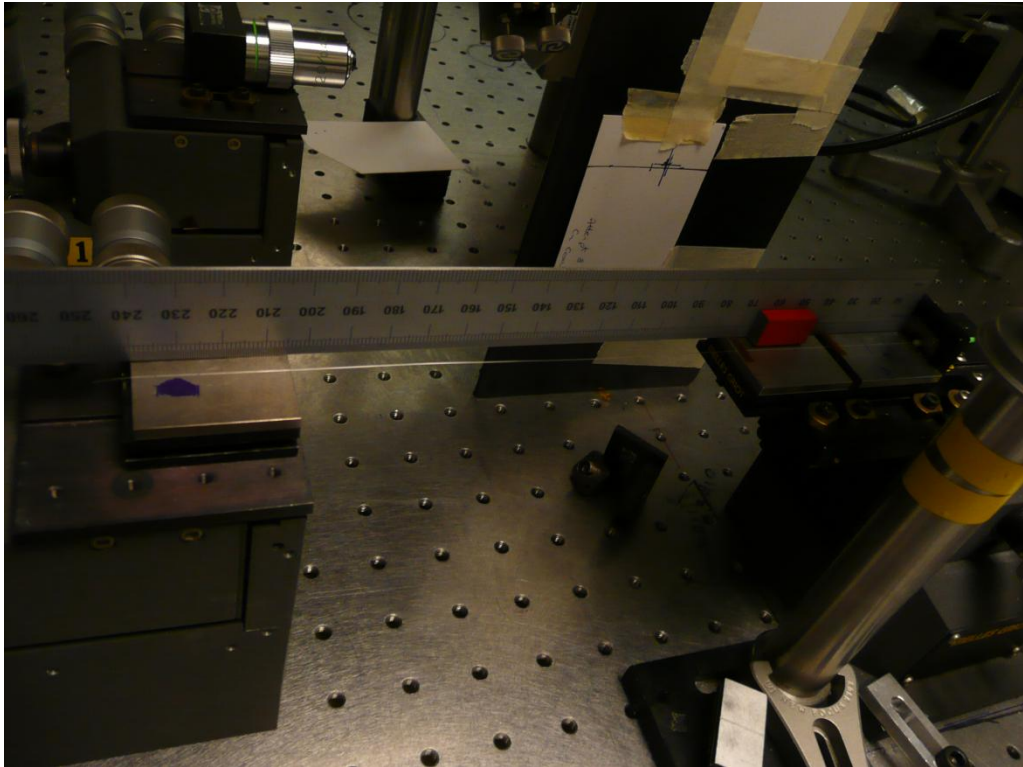


Figure 6-12 Demonstration of the interrogation of a reflected 828nm Bragg response along 23cm length of MMmPOF

6.2.3 Optimisation of FBGs with a 800-900nm Bragg Response, Fabricated in MMmPOF

During the manufacture of wavelength division multiplexed (WDM) sensors with responses in the same 800nm spectral region it became apparent FBGs fabricated within this wavelength range were being UV exposed for too long. During the WDM study POF was spliced to silica optical fibre pigtailed prior to FBG inscription. This allowed for improved monitoring of the grating growth as the coupling conditions were now constant provided by the optical adhesive. The construction of WDM sensors is discussed in more detail in Chapter 8. After the fabrication of an initial FBG the MMmPOF device was permanently spliced to a multimode (50/125 μ m) silica pigtail using Loctite 3525 optical adhesive using the technique described in Chapter 5. This enabled the monitoring of the growth of the reflected Bragg response as was done previously; however now the coupling conditions between the silica and polymer fibres was permanent. This importantly prevented the coupling conditions from deteriorating possibly due to vibrations creeping across the translation stage from the UV laser and also the movement of index matching oil away from the butt coupling joint particularly when the oil flows along the holes of the mPOF, similar to that observed with splice adhesives preventing index guiding within the core of the mPOF.

Therefore shown in Figure 6-13(a) is the captured growth curve of an 861nm FBG being fabricated in the MMmPOF using the 580nm period phase mask. The inscription setup was

exactly the same as the previous experiment with the phase mask rested directly on top of the POF. As can be seen in Figure 6-13(a), the MMmPOF is exposed to the UV interference pattern for 45 minutes, where a saturation level of the peak reflected signal was reached at around 9dBm above the noise. The resultant reflected Bragg response after fabrication can be seen in Figure 6-13(b), here the reflected signal has a Bragg wavelength of 861nm and a bandwidth (FWHM) of 0.5nm, the reflection spectrum was captured on an OSA with a bandwidth resolution of 0.5nm and had a signal-to-noise ratio of 20dBm. Interestingly the signal-to-noise ratio of the reflected Bragg response varies between the two measurements shown in Figure 6-13(a) and (b), it is suspected this is because during fabrication the POF is curved over the translation stage to enable fabrication of additional FBGs in the WDM sensors which are positioned in the centre of a 20cm length of MMmPOF, resulting in bending losses. Whereas the reflected spectra after fabrication is taken when the MMmPOF is supported along its entire length.

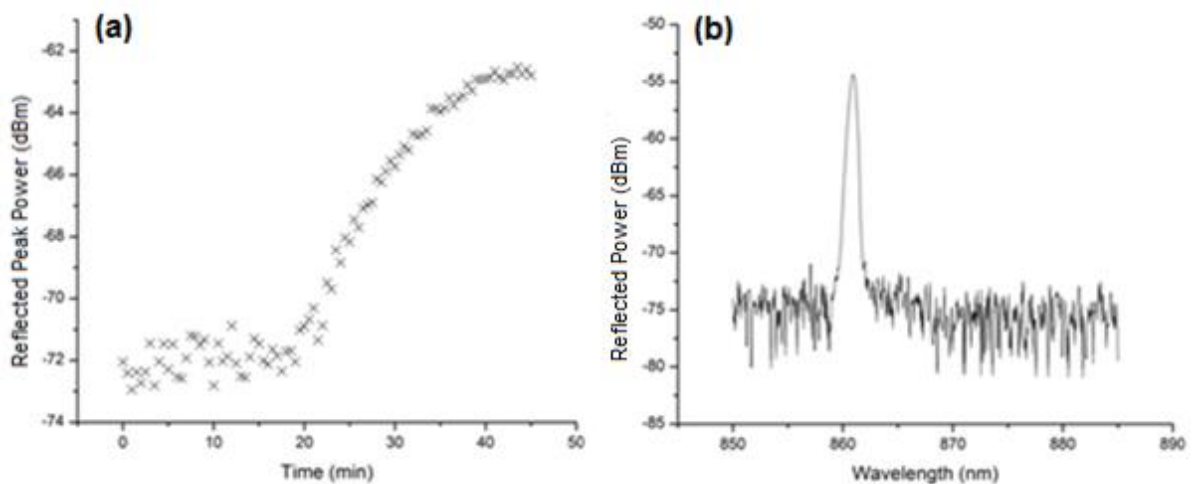


Figure 6-13(a) growth curve of FBG fabricated in MMmPOF at 861nm (b) reflected Bragg response of fabricated FBG at 861nm

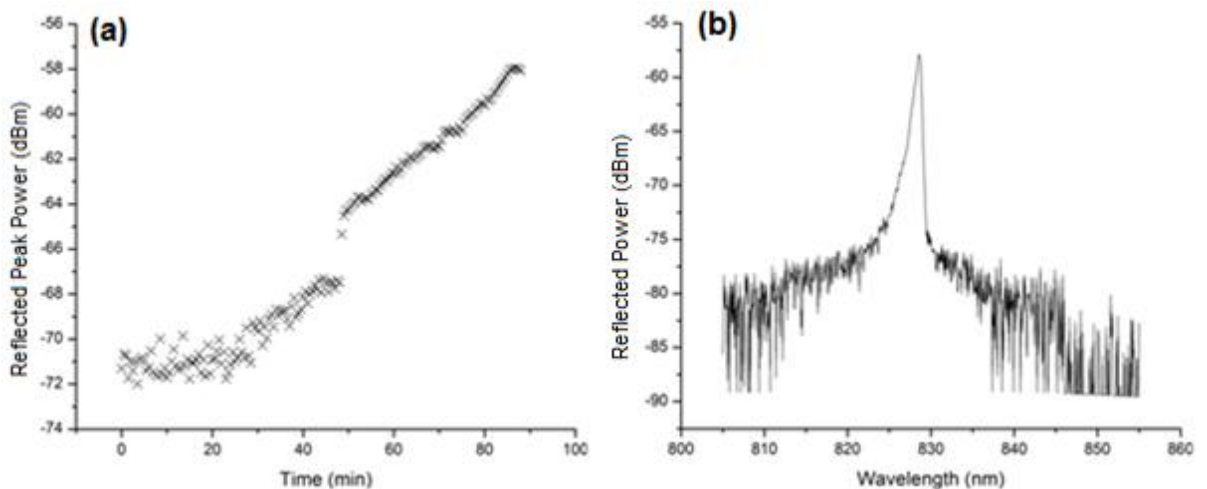


Figure 6-14(a) growth curve of peak reflected Bragg signal of a FBG fabricated in MMmPOF at 828nm (b) reflected Bragg response of a fabricated FBG, with a Bragg wavelength of 828nm

Furthermore, Figure 6-14 also demonstrates a much improved reflected Bragg response at 828nm, which has been fabricated within 50 minutes. Figure 6-14(a) illustrates a saturation level of a 12dBm signal above the noise is achieved after exposing the MMmPOF to the UV interference pattern generated from the 557.50nm period phase mask for 50 minutes. The captured Bragg response after fabrication is shown in Figure 6-14(b), here the reflected signal has a Bragg wavelength of 828nm and a bandwidth (FWHM) of 0.5nm. Incidentally the Bragg response in Figure 6-14(b) has a signal-to-noise ratio of 20dBm, which again is an increase compared to that measured from the growth curve of the same FBG, once more it is believed the increase in the reflected signal was seen once the POF device was supported along its entire length and there was no bending of the MMmPOF resulting in reduced bending losses of the Bragg signal.

Figure 6-13 and Figure 6-14 demonstrate the fabrication of FBGs with reflected Bragg responses with around a 20dBm signal-to-noise ratio within the 800nm spectral range in less than one hour. Both the Bragg responses at 861nm and 828nm had bandwidths (FWHM) of less than 0.5nm. When compared to the larger 1nm bandwidths of the Bragg responses at the same wavelengths in the two previous sections of 6.2.1 and 6.2.2, which were exposed for 90 minutes, it would suggest that the later were over exposed.

6.3 Attempted FBG Fabrication in Perfluorinated POF

In 2001 Liu *et al* [80] first demonstrated UV photosensitivity of CYTOP perfluorinated polymer. The phase mask technique was used to inscribe a Bragg grating into a thin slab of CYTOP material using a frequency tripled yttrium aluminium garnet (YAG) laser with an inscription beam pulse energy of up to 350mJ at a wavelength of 355nm. A He-Ne laser beam was passed through the CYTOP slab and a diffraction pattern from the inscribed structure was directly measured. Using an output of 280mJ at a wavelength of 355nm it became apparent that as the inscription time increased the efficiency of the inscribed Bragg grating within the slabs of CYTOP material varied. Maximum diffraction efficiency was obtained in approximately 20 minutes and thereafter the efficiency decreased. This would suggest that the CYTOP material is photosensitive and also shares inscription characteristics with PMMA.

Later in 2002 Liu *et al* [81] declared for unknown reasons Bragg gratings were limited to being inscribed in the squashed slabs of the CYTOP material, as gratings could not be inscribed in the fibre form of the CYTOP material.

6.3.1 FBG Fabrication Attempts in CYTOP PF GI POF

Attempts were also made to fabricate FBGs in CYTOP POF; however no attempts were made in slabs of the perfluorinated (PF) material. The same fabrication technique as that described in Chapter 4, which has been used to fabricate FBGs in PMMA based POF was

used. The 30mW 325nm HeCd laser was used and the phase mask technique was employed; the mask was suspended 200 μ m above the surface of the POF and had a period of 1057.2nm in an attempt to UV inscribe a Bragg grating within the CYTOP fibre. However no Bragg response was detected optically using a supercontinuum light source at a predicted wavelength of 1417nm or across a searched wide wavelength range. Additionally no index fringes were observed visually using a microscope. Further attempts were made including reducing the distance between the phase mask and fibre to 67 μ m with no success. Additionally, the CYTOP POF was UV exposed through the mask for 3 hours, in an attempt to over expose the polymer which would result in damage but would suggest some kind of photosensitivity, however this also proved unsuccessful.

Further attempts were made to replicate the work by Liu *et al*[80-81], by thermally annealing the CYTOP fibre at 100 $^{\circ}$ C for 24 hours. However this also proved unsuccessful both optically and visually when attempts were made to fabricate FBGs as previously described.

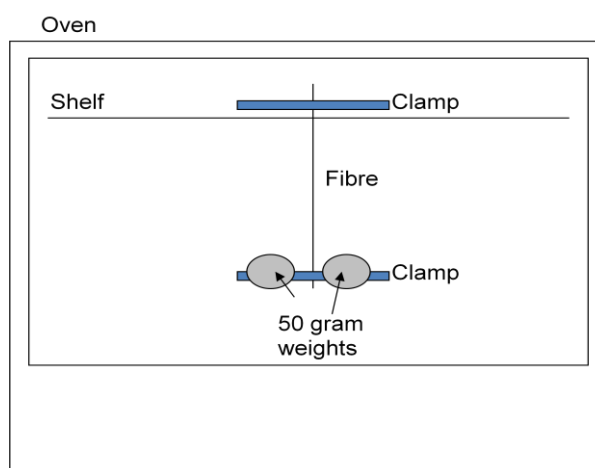


Figure 6-15 Stretching and thermally annealing CYTOP POF at 100 $^{\circ}$ C

A further endeavour was to try to stretch the CYTOP POF with 100g during a 24 hour 100 $^{\circ}$ C thermal anneal in an attempt to change the chemical structure of the material and hence induce photosensitivity at 325nm, something which may have happened as a result of heating and compressing the fibre seen by Liu *et al*[80-81]. Again after a 1 hour inscription with the phase mask suspended 66 μ m above the surface of the fibre no Bragg grating was seen either optically using an OSA or visually using a microscope.

6.3.2 FBG Fabrication Attempts in Chromis PF GI POF

Attempts were also made to fabricate FBGs in the perfluorinated (PF) Chromis POF [43]. Using the fabrication technique described in Chapter 4, the UV 325nm HeCd laser (Kimmon Koha Co, Ltd IK3301R-G) was used to expose the Chromis POF via a phase mask with a period (Λ_{pm}) of 1057.2nm, which was suspended 200 μ m above the surface of the POF using three layers of polyimide tape. The PF POF was exposed to the UV interference pattern for 60 minutes and was subsequently inspected visually using a microscope. Typical visual

results of a number of attempts are shown in Figure 6-16 and Figure 6-17 taken with a 40x objective lens microscope. Initially, Figure 6-16 suggested promising results with a Bragg grating structure visible albeit with significant damage to the material, likely to be a product of exposing the PF POF to the UV interference pattern for too long. This is endorsed by Figure 6-17, where scorching is evident as a result of the UV exposure. However the image is captured at the surface of the POF which was nearest to the phase mask, suggesting there is high absorption of the cladding of the PF Chromis POF. With additional investigation, it was apparent that the UV interference pattern was being totally absorbed by the highly photosensitive cladding. It should also be made aware that the horizontal lines seen in Figure 6-16 and Figure 6-17 is not the core of fibre, but instead the melting of the fibre where the UV beam has been focussed. Shown in Figure 6-18 and Figure 6-19 is the side view of the PF fibre with respect to the UV inscription direction, which is directed from the top down. As can be seen, Figure 6-18 illustrates the grating structure at the top surface of the fibre, nearest to the UV exposure and Figure 6-19 shows the high level of scorching on the surface of the PF Chromis POF due to the high absorption levels of the cladding material.

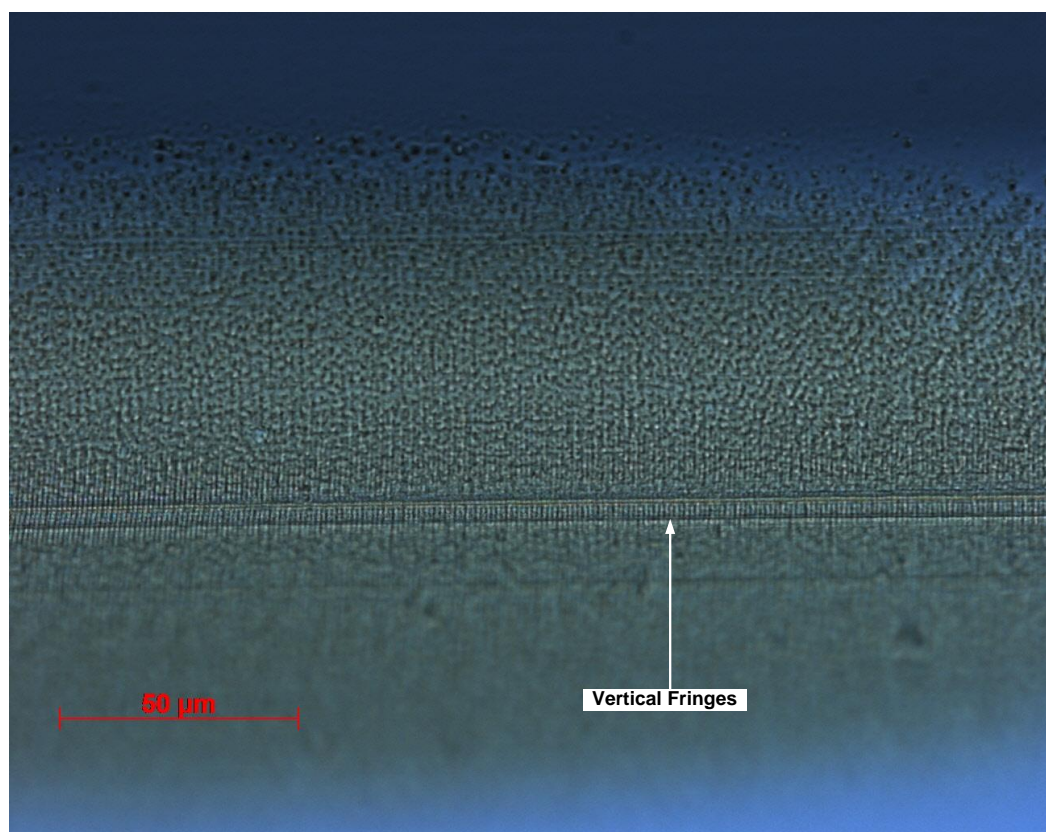


Figure 6-16 Visual inspection of attempted fabrication of FBG in PF Chromis POF focussed on fibre surface

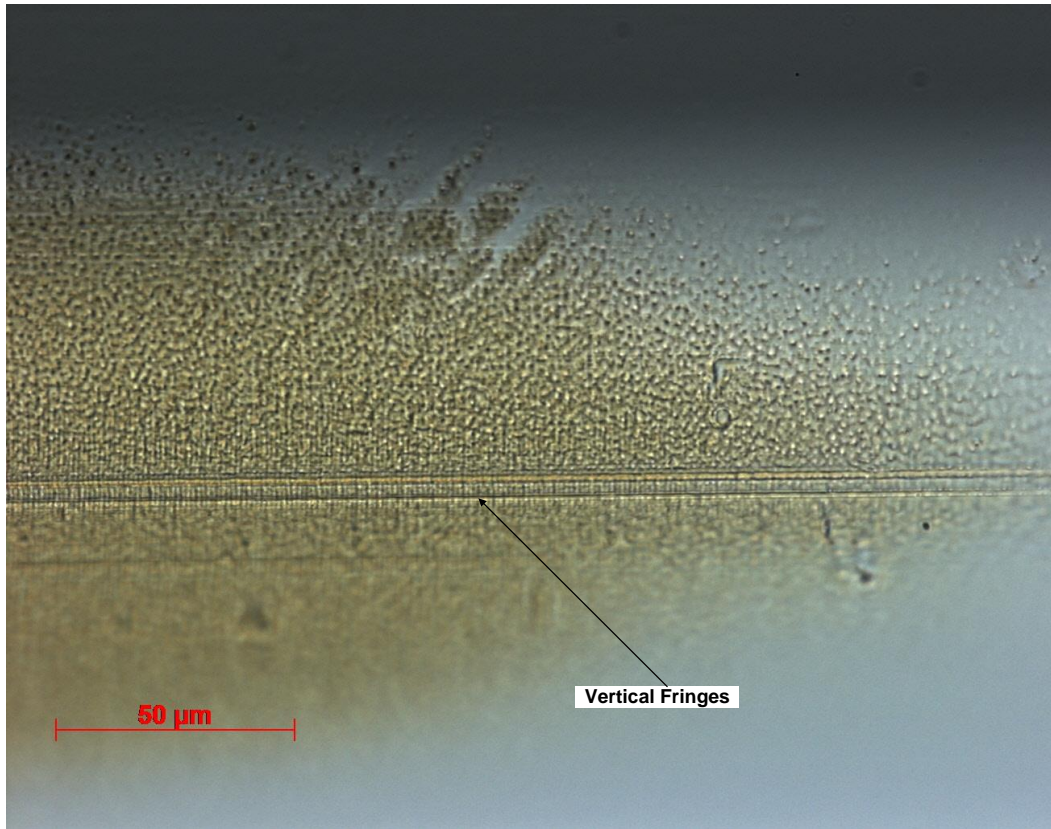


Figure 6-17 Evidence of scorching of the PF Chromis POF during FBG fabrication, focussed on fibre surface

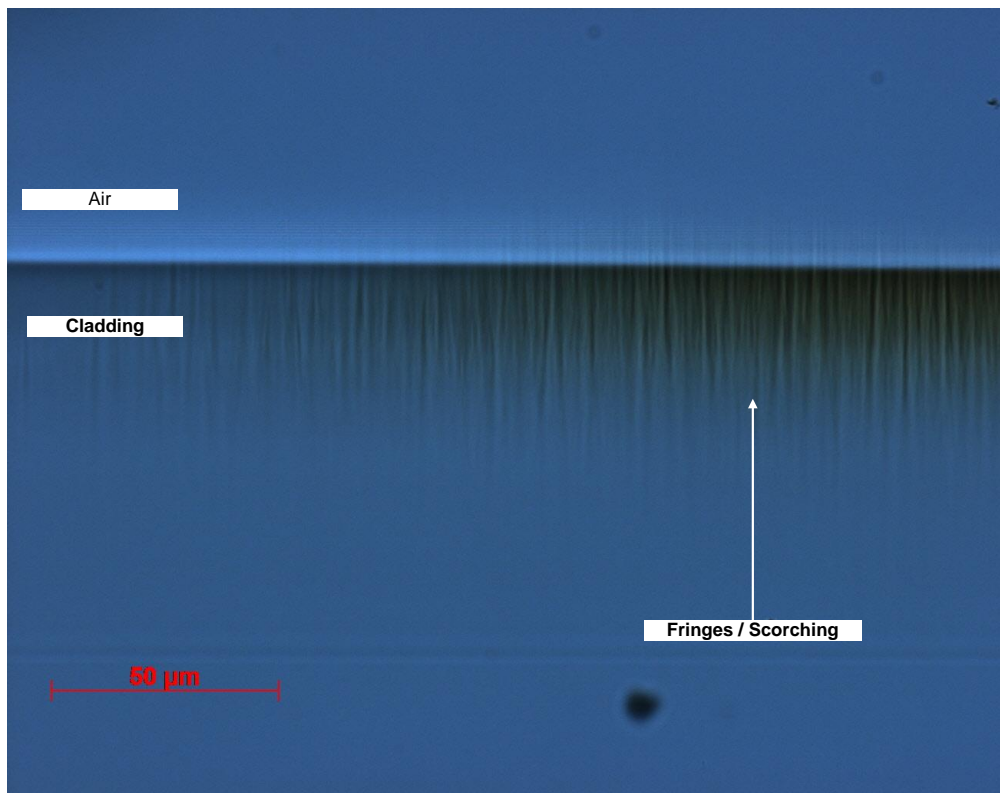


Figure 6-18 40x Microscope image of the air(top)/cladding(bottom) interface of PF Chromis POF after FBG fabrication

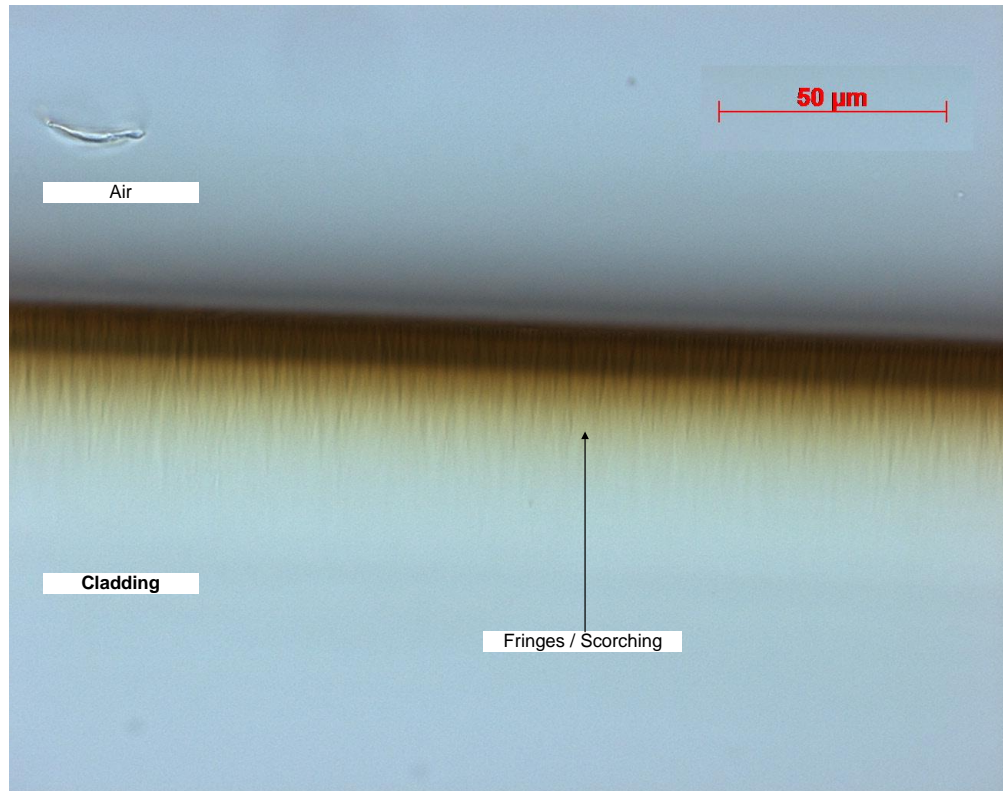


Figure 6-19 40x Microscope image of the air(top)/cladding(bottom) interface of PF Chromis POF after FBG fabrication demonstrating scorching at the surface of the POF

The PF Chromis POF was also interrogated in reflection for a Bragg response, however no response was observed using an OSA and supercontinuum interrogating light source.

After discussions with Chromis Fiber[43] representatives it was discovered there is an additional polycarbonate outer cladding layer of the PF Chromis POF and therefore explains the high absorption seen at the cladding air interface.

Attempts were made to remove this outer polycarbonate cladding by submerging the POF into

dichloromethane (DCM). As shown in Figure 6-20, a suitable outer surface was achievable after 10 minutes, where the graded index (GI) PF Chromis POF had been reduced to a diameter of 82.86μm.

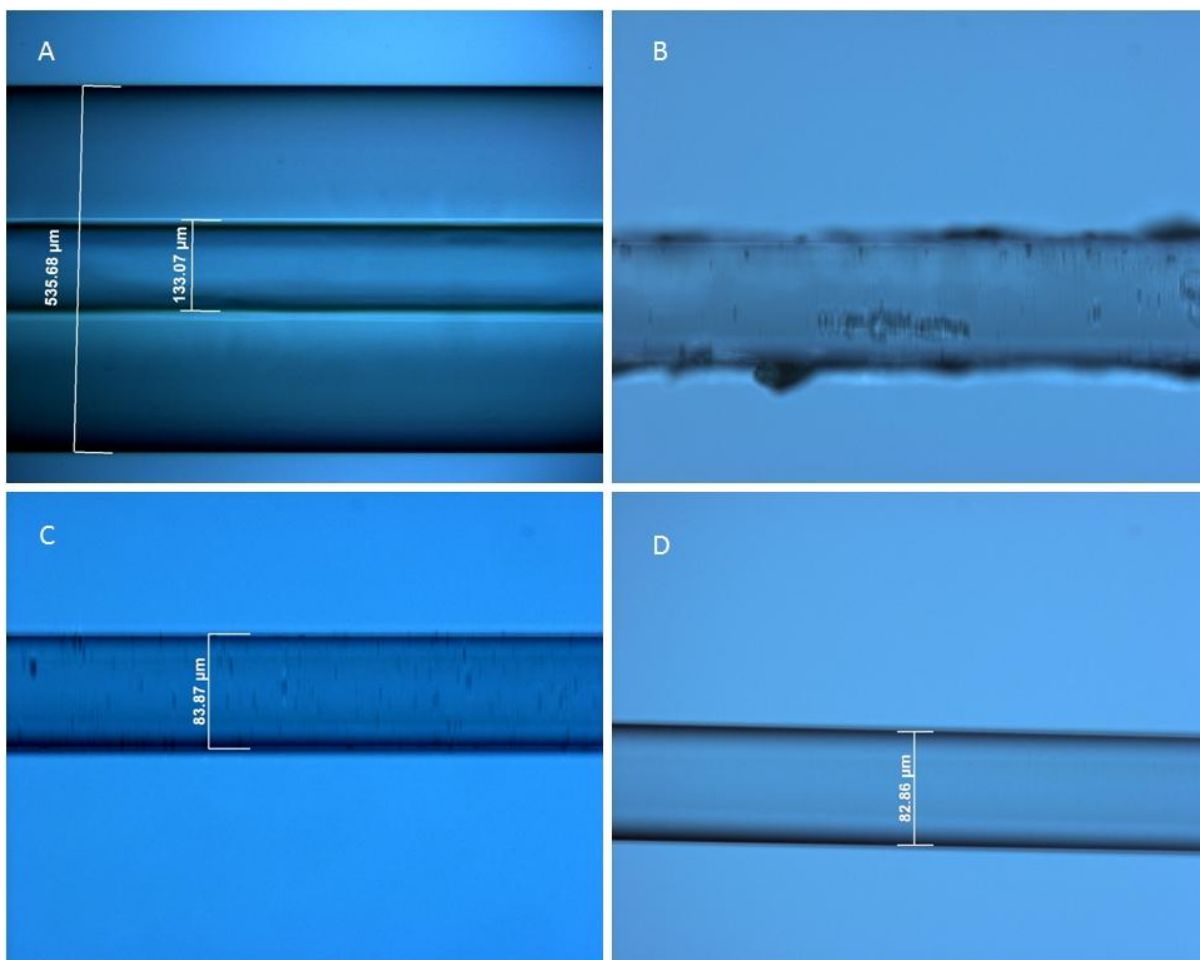


Figure 6-20 40x microscope images, comparing PF Chromis POF surface quality, when submerged in DCM for: (a) 0 minutes (b)1 minute (c) 5 minutes (d) 10 minutes

However, very much like the PF CYTOP POF, a series of fabrication attempts were made which included: UV inscription times of up to 2 hours and varying the distance of phase mask from the top surface of the fibre between 200 μm (3 layers of polyimide tape), 133 μm (2 layers of polyimide tape) and 67 μm (1 layer of polyimide tape) all of which resulted in no Bragg response. Attempts were made to observe a Bragg response both visually using a microscope and also optically by interrogating the potential device in reflection with the use of a supercontinuum interrogating light source and an OSA to monitor any reflected signal.

6.4 Summary

This chapter details the first demonstration of FBGs which have been fabricated in POF with a Bragg response within the 800-900nm wavelength range, and thus takes advantage of the lower attenuation of PMMA at these lower wavelengths of 2dB/m[59] compared to the attenuation losses of 1dB/cm at 1500nm[59]. This work resulted in a publication in 2010[71], which detailed the successful fabrication where previous attempts had failed. It is felt that the successful fabrication of 800nm FBGs in the PMMA based MMmPOF was a result in part of reducing the height of the phase masks so they were resting upon the surface of the POF, whereas previous attempts were made whilst the phase mask was suspended 200 μm above the fibre's top surface.

Optimised FBG fabrications of 45-50 minutes in the PMMA based MMmPOF resulted in reflected Bragg responses of at least 11dBm above the noise floor with Bragg wavelengths at 861nm and 828nm both of which had a measured bandwidth of less than 0.5nm. Also demonstrated was the detection of a reflected Bragg response of 15dBm above the noise floor at 828.50nm whilst being interrogated through a 23cm length of MMmPOF. This demonstrated the possibility of extending the length POFBG devices enough to allow for application specific characterisation of the FBG sensor, whilst keeping a safe distance from the fragile and bulky adhesive splice. Examples of such applications are thermal annealing (Chapter 8) and axial strain sensitivity (Chapter 7) and contributed to the publications in 2010 and 2011[71, 74].

As part of this work, FBG fabrication was also reported with a Bragg response at 1292nm with at least a 15dBm reflected signal above the noise floor. Furthermore thermal sensitivity to a 60W light bulb was demonstrated with a negative 1.5nm wavelength shift. Finally attenuation measurements of the PMMA based MMmPOF were completed using the cut back method, which gave attenuation losses of 95dB/m at 1550nm and 8dB/m at 830nm.

In conclusion the development of FBGs with responses within the 800nm spectral region significantly enhances the range of applications of polymer optical fibre Bragg gratings sensors, allowing them to be used in a wavelength range where the losses are low enough to allow practical devices, furthermore utilising suitable broadband interrogation light source which are readily available.

6.5 Future Work

To progress this work further, the FBGs which can now be reliably fabricated in the PMMA based MMmPOF should be interrogated in transmission. With the low attenuation losses it should be possible to observe a transmission dip whilst coupling both ends of the POF to silica multimode pigtails. This will allow for an impression of the true FBG strength, furthermore included in this should be the characterisation of the bandwidth of the Bragg signal using an increased bandwidth resolution on an OSA.

To really move this work forward the ambition needs to be to fabricate FBGs with a Bragg response within the 500nm – 600nm spectral range, where optimum attenuation losses of 100dB/km are experienced[59]. To achieve this periodic index changes are required with a resolution of up to 168nm, assuming a refractive index of 1.49 for PMMA. Already in this thesis line resolutions of 272.5nm have been demonstrated in a planar sample of PMMA. A reasonable step forward before 600nm FBG fabrication in POF would be to develop this work and demonstrate the 168nm index change resolution required for FBG responses around 500nm. This should be possible as Kaminow *et al* has previously documented line resolutions better than 200nm[7]. This could possibly be achieved with the purchase of

additional phase masks with periods around 745nm, however it is felt further work should be sustained using the Lloyds mirror interferometer fabrication technique. It is felt that previous attempted work using this technique was not completed as effectively as it could have been and successful FBG fabrication would be possible if the POF was UV exposed for an increased amount of time.

In an attempt to strengthen this work the fabrication of FBGs with a Bragg response within the 800-900nm wavelength range should be attempted in wider range of POF. The technique described in this thesis has been exercised to fabricate FBGs at 826nm in step index single mode POF. Furthermore FBGs with a reflected Bragg response at 849nm in the Topas Cyclic Olefin Copolymer and is documented in the following Chapter 9.

Finally the work completed investigating perfluorinated (PF) grade index (GI) POF should not be dismissed. Both the Chromis and CYTOP PF POF boost desirable attenuation losses as shown in Figure 6-21[43]. With attenuation losses less than 60dB/Km at both 850nm and 1300nm the motivation should be present to continue this work.

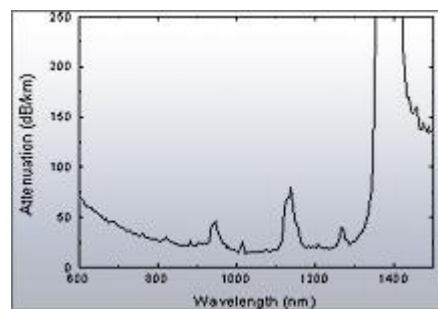


Figure 6-21 Spectral attenuation of PF GI POF

However, it is felt that the work completed Liu *et al* [80-81] demonstrating the photosensitivity of CYTOP at 355nm may have been a result of heating and compressing the CYTOP in fibre form into a thin slab by adjusting the chemical structure and thus increasing photosensitivity at the UV wavelength. One possible technique for the fabrication of FBGs in PF POF is point-by-point inscription using a femtosecond laser, something which has been achieved in silica commercial optical fibre[35]. Furthermore periodic refractive index modification in POF has been demonstrated using focussed femtosecond pulses[82]. The technique of direct write using focussed femtosecond pulses should also be investigated as a solution to fabricating low wavelength FBGs in PMMA based POF.

7

APPLICATIONS

Armed with the ability to permanently splice polymer and silica optical fibres together using optical adhesive (discussed in Chapter 5), application specific characterisation is possible. By using Loctite 3525 optical adhesive[70], POFBGs have been able to be moved away from the optical table and into or onto specific test equipment whilst retaining their reflected Bragg response without the need of butt coupling on a bulky inappropriate translation stage. Two examples of application specific characterisation of POFBG Bragg responses are axial strain and hydrostatic pressure both of which are demonstrated in this chapter.

7.1 Axial Strain Sensitivity

In this section axial strain sensitivity is investigated in the PMMA based MMmPOF, FBGs with Bragg responses in both the 1500nm and 800nm spectral regions were investigated.

7.1.1 Axial Strain Sensitivity of 1500nm POFBGs

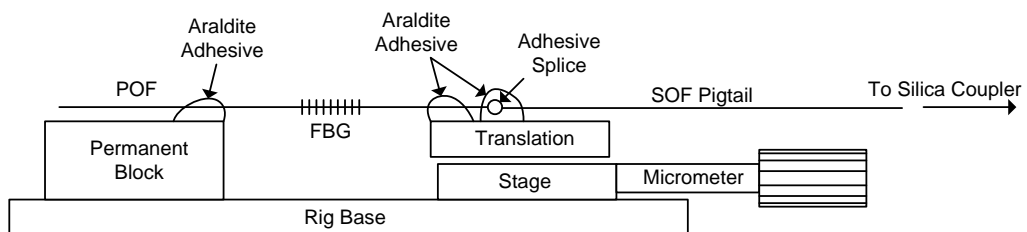


Figure 7-1 Experimental setup for axial strain characterisation

Liu, Peng *et al*[17, 23, 83] have characterised strain sensing in PMMA based single-mode (SM), step index (SI) POF (SM SI POF), therefore in this work similar characterisation of FBGs fabricated in MMmPOF was completed.

A POFBG sensing device was glued to the translation stage of the setup shown in Figure 7-1 using an Araldite® adhesive. Araldite® was also applied around the adhesive splice in an attempt to further support the splice by preventing any movement of the joint of either of the polymer or silica fibres within close proximity to the splice.

The reflected Bragg response of the POFBG used in these experiments is shown in Figure 7-2. The POFBG sensor was fabricated in the MMmPOF using a phase mask which was optimised for operation with the UV 325nm HeCd laser (Kimmon Koha Co, Ltd. IK3301R-G). The fabrication setup was the same as that discussed in Chapter 3 where the phase mask was rested directly upon the surface of the mPOF. The period of the surface relief pattern of

the phase mask was 1034.20nm, which resulted in the reflected response having a Bragg wavelength of 1529nm and a bandwidth (FWHM) of 2.5nm. The reflected Bragg response had a Bragg signal-to-noise ratio of 14dBm after a 60 minute exposure to the UV interference pattern. This POFBG sensor was permanently spliced to a multimode (50/125 μ m) silica pigtail using Loctite 3525 optical adhesive as described in Chapter 5.

The Bragg response shown in Figure 7-2, was captured in reflection using a 2x1 multimode (50/125 μ m) silica coupler with a 50:50 coupling ratio at 1550nm. The FBG was interrogated using a broadband ASE light source (Thorlabs ASE-FL7002-C4) and the reflection was captured on an OSA (HP 70951B) with a bandwidth resolution of 0.5nm, this setup remained for the entire strain experiment at 1550nm.

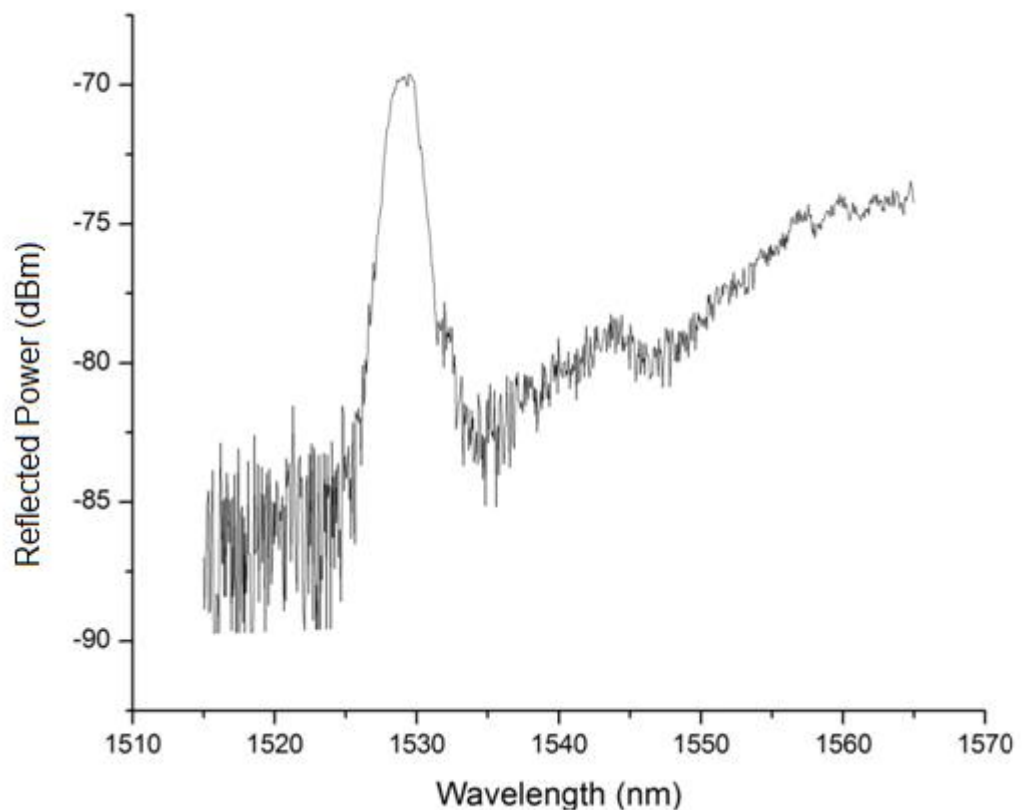


Figure 7-2 Bragg response of a FBG fabricated in MMmPOF before axial strain sensing.

The MMmPOF was glued up to the edge of either stage of the experiment rig shown in Figure 7-1; the measured distance between the two stages was 42mm, which is referred to as the gauge distance. The FBG was located at the centre of this distance between the two stages. The distance between the two stages was either increased or decreased by adjusting the micrometer of the right-hand translation stage by hand.

The strain was first increased by 2% of the gauge distance, which is equal to 20 milli-strain ($m\epsilon$). The strain was increased gradually in steps of 0.06mm; each step was increased by hand adjustment of the micrometer over an approximate time lapse of 5 seconds. After each step increase 1 minute was allowed before capturing the reflected Bragg response, this was

to allow the POF to settle after the strain was applied and also to incorporate a repeatable time delay as both the application of strain the spectra captures were operated manually. There were a total of 14 steps accumulating to a total increase in the gauge length of 0.84mm. After the capture of the Bragg response of the 14th step the strain was decreased, by reducing the gauge length in the same 0.06mm steps. Again a total of 14 steps were taken and hence returning to the original gauge length of 42mm. Once more the decrease in the gauge length was achieved by adjusting the micrometer of the translation stage which was completed by hand and took around 5 seconds to complete each step. After each decrease in length 1 minute was allowed before the reflected Bragg response was captured. The applied strains and gauge lengths are summarised in Table 6. The resulting change in Bragg wavelength of the POFBG due to the increase and following decrease of 20mε along the MMmPOF axis is presented in Figure 7-3(a). Each Bragg wavelength was determined for each reflected Bragg response after each increase or decrease in strain using the technique described in Chapter 4, where the centroid data point is calculated from all recorded data points within 3dBm of the peak, which was captured on an OSA (HP 70951B) with a bandwidth resolution of 0.5nm.

Table 6 Summary of applied axial strain to 1529nm FBG fabricated in MMmPOF

% Distance Increase	Milli- Strain (mε)	Number of Steps	Step Distance	Total Distance
2%	20	14	0.06mm	0.84mm
5%	50	30	0.07mm	2.1mm

Subsequently after 1 hour, the axial strain was increased to 50mε on the same FBG fabricated in the MMmPOF which was still fixed to the experiment rig. Applying 50mε equates to increasing the gauge length of 42mm by 5% up to 44.1mm. This was achieved in 30 individual steps of 0.07mm. Again each 0.07mm increase was completed by hand adjustment of the micrometer and took around 5 seconds to do so. A one minute time period was allowed between completing the strain increase and capturing the reflected Bragg response of the FBG. After the 30th capture of the incrementing steps, the axial strain was reduced, in the same 0.07mm steps. Once more this was completed by hand and took approximately 5 seconds to implement each step. Yet again 1 minute was allowed between completing the decrease of the gauge length to capturing the Bragg response. The applied strains and gauge distances are again summarised in Table 6. Furthermore the resulting change in Bragg wavelength as a result of increasing and decreasing the axial strain by 48mε are illustrated in Figure 7-3(b).

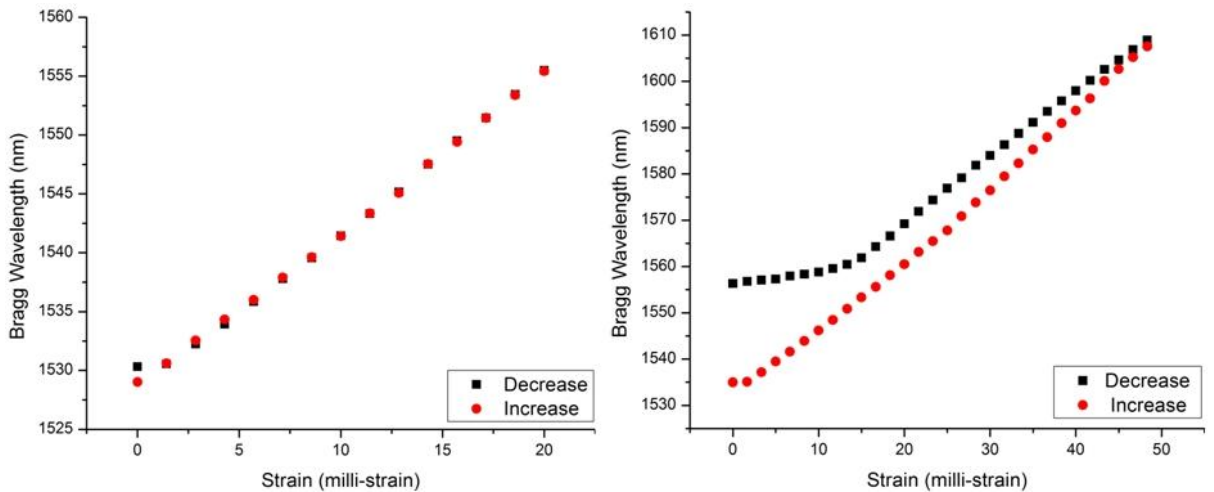


Figure 7-3 Strain response of a FBG fabricated at 1529nm in MMmPOF (a) up to 20 mε (b) up to 48 mε

As can be seen in Figure 7-3(a), applying an axial strain of 20mε under the conditions described above induced a positive Bragg wavelength shift of 26.5nm. The captured Bragg wavelengths during the increase in axial strain indicated a linear response of 1.32nm/mε. When the axial strain was reduced and the gauge distance decreased a negative Bragg wavelength shift occurred which totalled 25nm and therefore demonstrated an amount of hysteresis. The linear response when decreasing the strain from 20mε to 1.43mε was 1.35nm/mε and hence comparable to the linear response when increasing the axial strain. However a small amount of hysteresis is seen when decreasing from 1.43mε to 0mε, which resulted in a difference of the Bragg wavelength of 1.5nm.

After an additional 5 minutes of the MMmPOF relaxing with no applied strain, a further capture of the reflected Bragg response was taken. This resulted in the Bragg wavelength returning to its original position of 1529nm.

When inspecting the second application of 48mε of axial strain to the same POFBG shown in Figure 7-3(b), an approximate linear response of 1.58nm/mε was seen when increasing the gauge distance. However this was only measured after 1.67mε once the slack of the MMmPOF had been pulled taut, something which was an adverse effect of a previous experiment of increasing the strain up to a similar 4.5% axial strain whilst inspecting the wavelength range of the change of Bragg wavelength. A total positive Bragg wavelength shift of 72.5nm was observed when applying a strain of up to 48mε. When decreasing the axial strain a linear response was seen between 48mε to 16.67mε of 1.42nm/mε. However after this an increased amount of hysteresis can be seen when compared to the previous experiment where 20mε was applied. A decrease in the Bragg wavelength can be seen after this point as the MMmPOF continues to return to its original axial length, though it would be expected to take a number of days before the Bragg wavelength would return fully to the original position.

7.1.2 Axial Strain Sensitivity of 800nm POFBGs

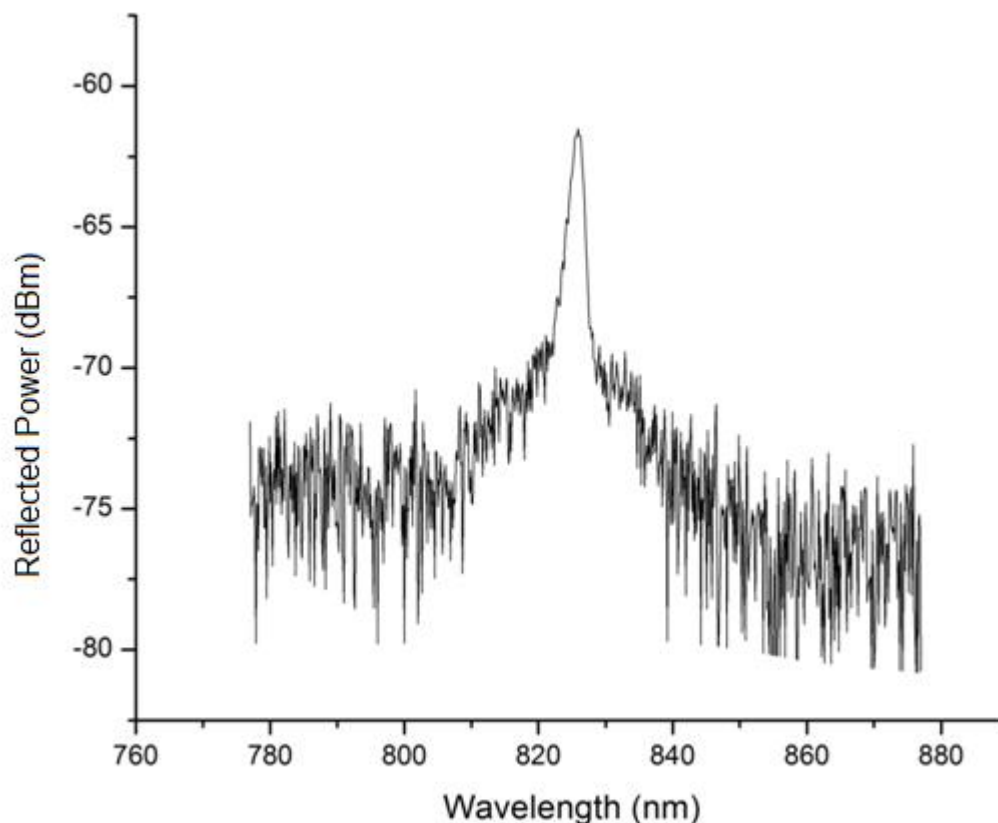


Figure 7-4 Bragg response at 825.5nm of a FBG fabricated in MMmPOF prior to strain characterisation

The successful fabrication of FBGs in the MMmPOF with a Bragg response within the 800nm spectral region is documented in Chapter 6 and ref[71], at these wavelengths the POFBGs took advantage of the lower attenuation losses of the PMMA base material[59]. In the same ref[71] an attempt to demonstrate the usability of the POFBGs as an axial strain sensor was also completed.

The reflected Bragg response of a fabricated FBG in MMmPOF prior to the axial strain characterisation experiment is shown in Figure 7-4, the reflected signal had a Bragg wavelength of 825.5nm and a bandwidth (FWHM) of 2.5nm. The MMmPOF was exposed to the UV interference pattern for 2 hours, resulting in a reflected Bragg signal-to-noise ratio of 9dBm. The FBG was fabricated using a phase mask which was optimised for operation with the HeCd UV 325nm laser (Kimmon Koha Co, Ltd, IK3301R-G) and had a surface relief pattern with a period of 557.5nm. The inscription detail is as described in Chapters 4 and 6. The 825.5nm POFBG sensor was permanently spliced to a multimode (50/125 μ m) silica 2x1 coupler with a 50:50 splitting ratio at 800nm. The reflected Bragg response shown in Figure 7-4 was interrogated using a superwide band short wavelength source (Amonics ASLD-CWDM-3-B-FA) and was captured on an OSA (HP 70951B) with a bandwidth resolution of 0.5nm, this interrogation setup was used for the entirety of the strain characterisation.

For the strain characterisation of the 800nm POFBG the same experimental setup was used as that shown in Figure 7-1. Once more, Araldite® adhesive was used to permanently fix the MMmPOF to the translation stage and stationary block of the strain rig. Furthermore the Araldite® adhesive was applied around the adhesive optical splice in an attempt to provide extra protection to the joint. A gauge length of 39.6mm was measured between the two Araldite adhesive points and the FBG was position in the centre of these two points along the fibre length.

As is summarised in Table 7, the axial strain was increased to 10mε in 40 steps by increasing the gauge length 0.01mm each step up to a total distance of 0.4mm. Each step was increased by hand adjustment lasting approximately 5 seconds. After the increase in strain 1 minute was allowed for the fibre to settle and also to gain a reproducible time delay as both strain adjustment and Bragg response captures were controlled manually. No change in Bragg wavelength due to the decrease in axial strain was taken.

Table 7 Summary of applied axial strain to FBG fabricated in MMmPOF with a Bragg response at 825.5nm

% Distance Increase	Milli- Strain (mε)	Number of Steps	Step Distance	Total Distance
1%	10	40	0.01mm	0.4mm

The resultant axial strain sensitivity of the 825.5nm FBG fabricated in the PMMA based mPOF can be seen in Figure 7-5. Here a linear axial strain sensitivity of 0.71nm/mε is calculated. And a total positive Bragg wavelength shift of 8nm is seen when increasing the axial strain up to 10mε.

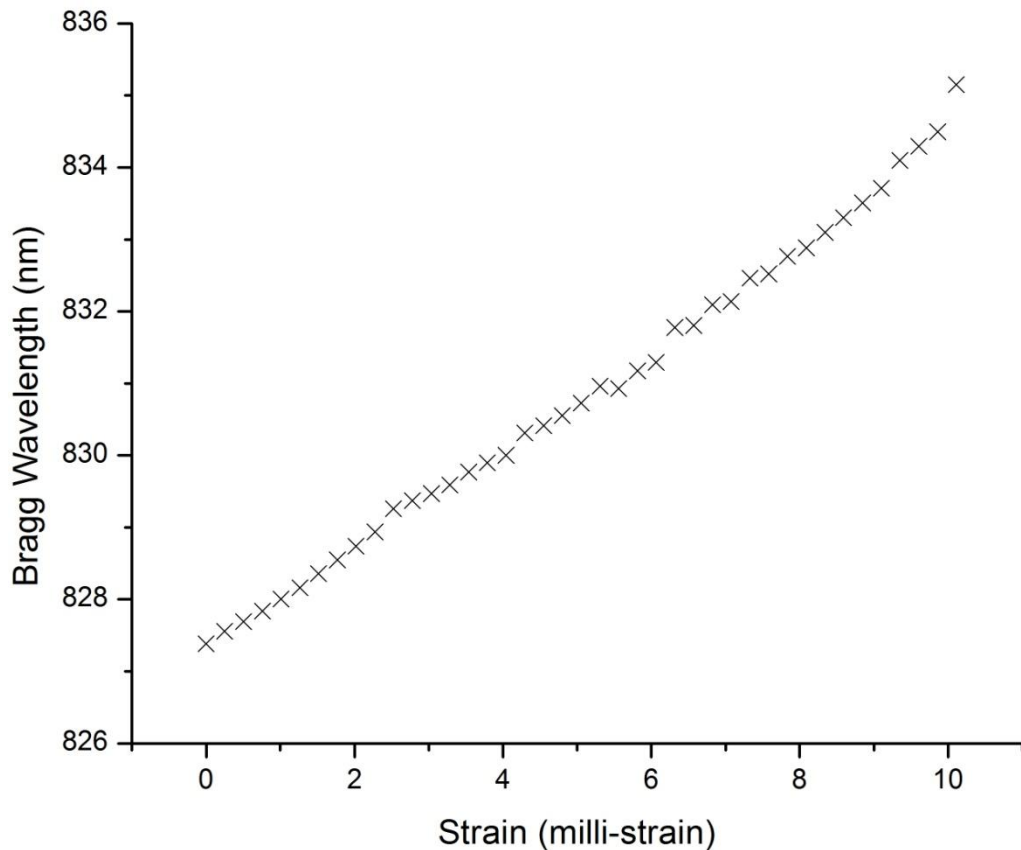


Figure 7-5 Strain response of a FBG fabricated at 825.5nm in MMmPOF up to 10mε

7.2 Summary

Axial strain sensitivities have been measured in multi mode mPOF. Axial strain sensitivities of these FBGs were calculated to be 1.32nm/mε when increasing the length of the FBG by 2% and a 1.58nm/mε when the fibre length was increased by 5%. Both of these axial strain sensitivities were published in 2010[72]. Also published in 2010[71] was the report of FBGs fabricated in MMmPOF with a Bragg response at 825.5nm, included in this report and also documented in this chapter was the axial strain sensitivity of 0.71nm/mε of the 825.5nm FBG.

7.3 Future Work

A potential future application for FBGs fabricated in POF is sensitivity to hydrostatic pressure; the next sections detail some of the current results and ongoing work.

7.3.1.1 Pressure Sensitivity

Polymer optical fibre (POF) Bragg gratings (POFBG) have been reported as sensory devices for the measurement of both temperature and strain[17, 21, 23-24]. However, reported here is on-going work into the sensitivity of POFBGs to hydrostatic pressure.

Increasing the hydrostatic pressure on a POFBG is in will have two possible effects on the Bragg wavelength. Firstly, the increase in pressure causes the fibre to compressed, this in turn reduces the period of the grating planes and a negative Bragg wavelength would be

seen. The second possibility is the refractive index of fibre increases as the pressure is increased and thus induces a positive Bragg wavelength shift. The sensitivity of the POFBG is given by²:

Equation 21

$$\frac{1}{\lambda} \frac{d\lambda}{dP} = -\frac{1}{E} \left[(1 - 2\nu) - \frac{n^2}{2} (1 - 2\nu)(p_{11} + 2p_{12}) \right]$$

Where ν is the Poisson's ratio and p_{11} p_{12} are the components of the relevant strain-optic tensor for an isotropic solid. The change in grating period due to the compression is given in the first term in the brackets, whereas the second term describes the index change as a result of the strain optic effect.

Equation 21 provides an ideal model of the effect of pressure on gratings fabricated in silica optical fibre which is an isotropic solid. However POF is not isotropic due to the alignment of the polymer molecular chains during the drawing manufacturing of the fibre. POF is actually a transverse isotropic material which means the properties of the fibre perpendicular to the fibre axis are not the same as those which are along the POF axis. The hydrostatic pressure sensitivity can be given by²:

Equation 22

$$\frac{1}{\lambda} \frac{d\lambda}{dP} = - \left[\frac{1}{E_T} (1 - 2\nu_T) - \frac{n^2}{2} \left(\left(\frac{1}{E_p} - \frac{\nu_p}{E_p} - \frac{\nu_T}{E_T} \right) (p_{11} + p_{12}) + \frac{p_{13}}{E_T} (1 - 2\nu_T) \right) \right]$$

Where E_p and E_T are the elastic moduli parallel and perpendicular to the fibre axis, ν_p and ν_t are the relevant Poisson's ratios and p_{11} , p_{12} and p_{13} are the components of the strain-optic tensor.

7.3.1.2 Pressure Chamber

A pressure chamber has been constructed and tested to hold 100bar 10MPa for 8 hours, this should provide enough time for all experimental work. The pressure chamber is shown in Figure 7-6. Compressed air was released into the chamber via an inlet valve the pressure was built up inside the chamber. The pressure inside the chamber was increased in 1MPa increments and two minutes were allowed for any temperature dependent fluctuations so subside.

² Derived from first principles by Dr David Webb at Aston University

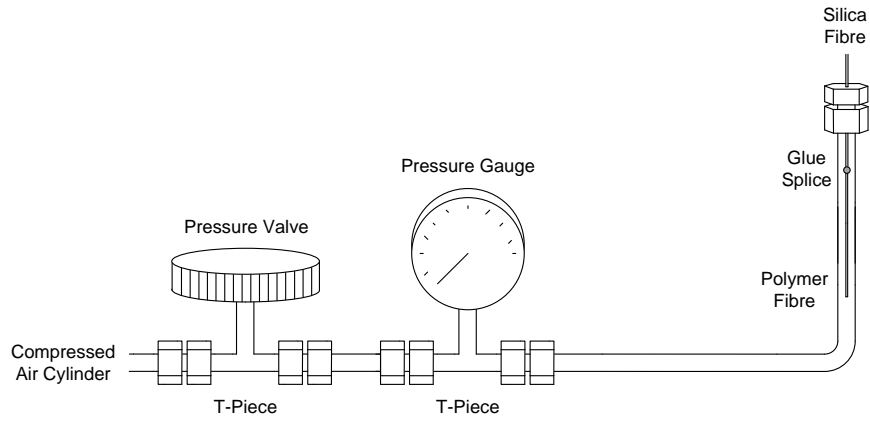


Figure 7-6 Experimental setup for pressure sensing

7.3.1.3 Hydrostatic Response of a FBG fabricated in SM silica optical fibre

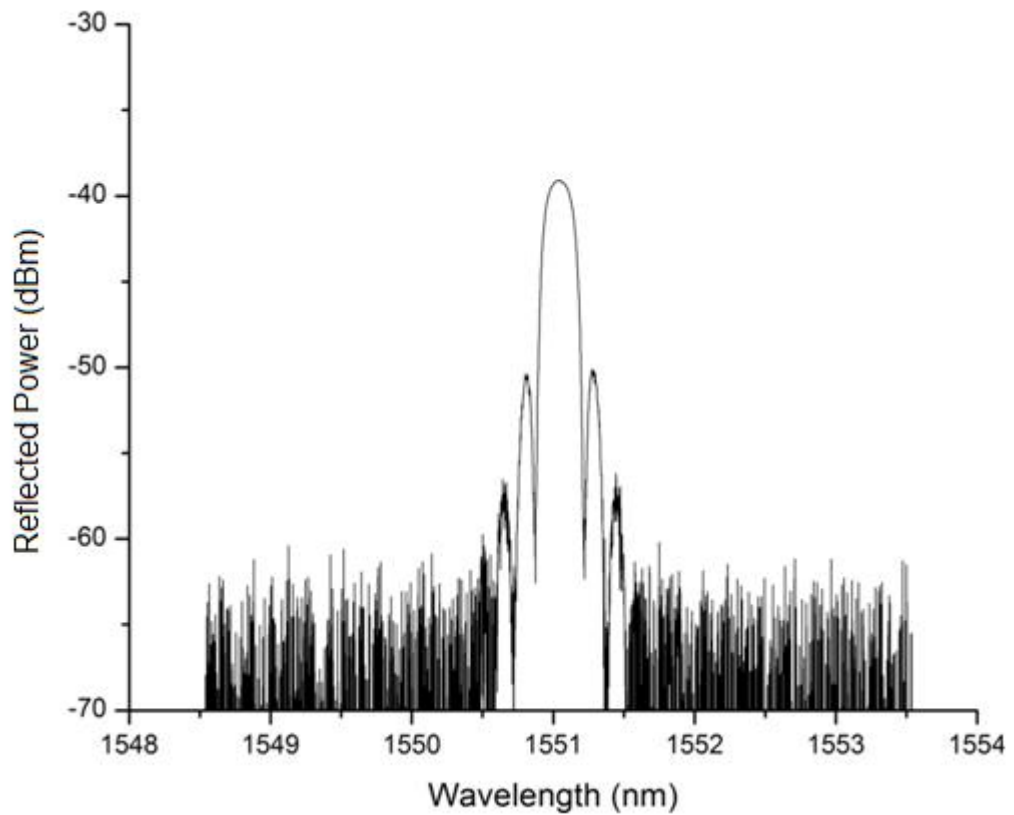


Figure 7-7 Reflected Bragg response of a FBG fabricated in singlemode silica optical fibre

First a Bragg grating fabricated in SM silica optical fibre was tested. It was chosen to first investigate a silica FBG to test the pressure chamber test setup and compare previous results reported by Xu et al[84].

The reflected Bragg response is shown in Figure 7-7, the reflected Bragg wavelength is was 1551.04nm and had a bandwidth (FWHM) of 0.22nm, captured on an OSA with a bandwidth resolution of 0.01nm, the Bragg signal-to-noise ratio was 25dBm.

The pressure sensitivity of the silica FBG was tested twice, the results of both experiments are shown in Figure 7-8. In the first experiment a linear response of 4pm/MPa was

calculated with a total Bragg wavelength shift of 3pm observed. The second experiment gave a linear pressure sensitivity of 3.9pm/MPa with a total wavelength shift of 30pm witnessed. In both experiments the pressure was increased 1MPa steps. After each increment of pressure the Bragg response was allowed to settle for 1 minute before the reflected Bragg response was measured so to allow for any change in temperature following the increase of the pressure.

These linear hydrostatic pressure sensitivities of silica FBGs are similar to those reported by Xu *et al*[84].

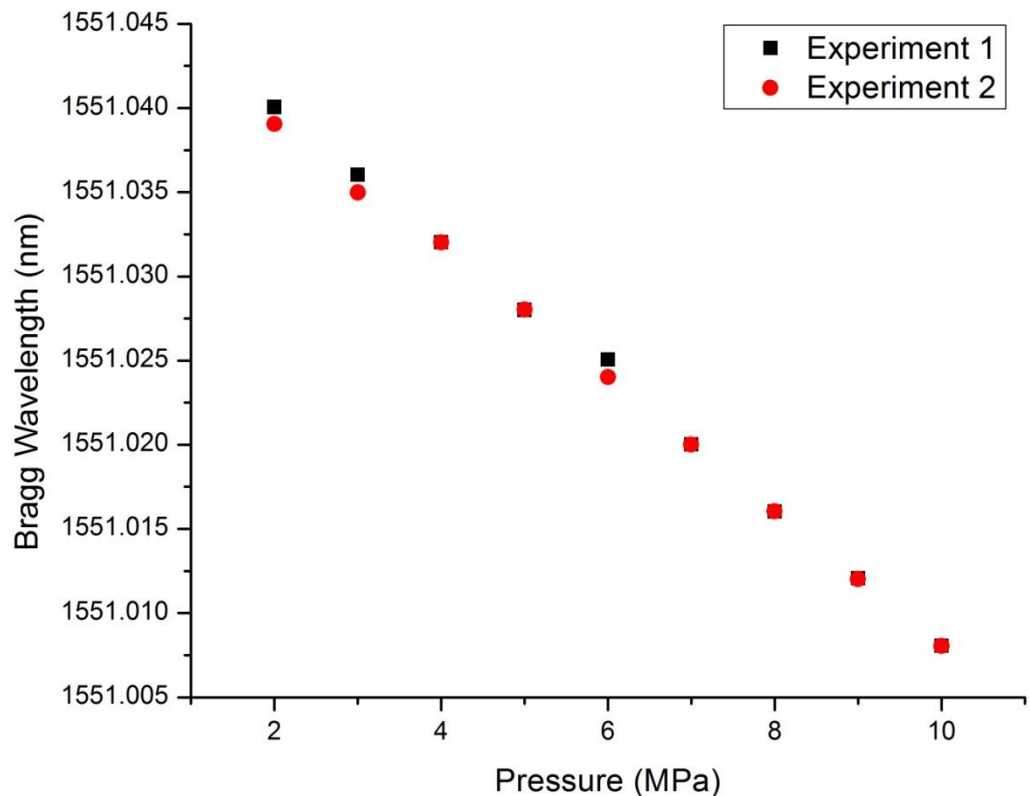


Figure 7-8 Pressure response of SOF FBG

7.3.1.4 Hydrostatic Pressure Sensitivity of a FBG fabricated in MMmPOF

Shown in Figure 7-9, is the reflected Bragg response of the FBG fabricated in MMmPOF. The FBG had a grating length of 1.8mm and was positioned 2cm from the tip of the POFBG sensor. The reflected Bragg response had a Bragg wavelength of 1562nm and a bandwidth (FWHM) of 1.5nm when using an OSA with a bandwidth resolution of 0.5nm

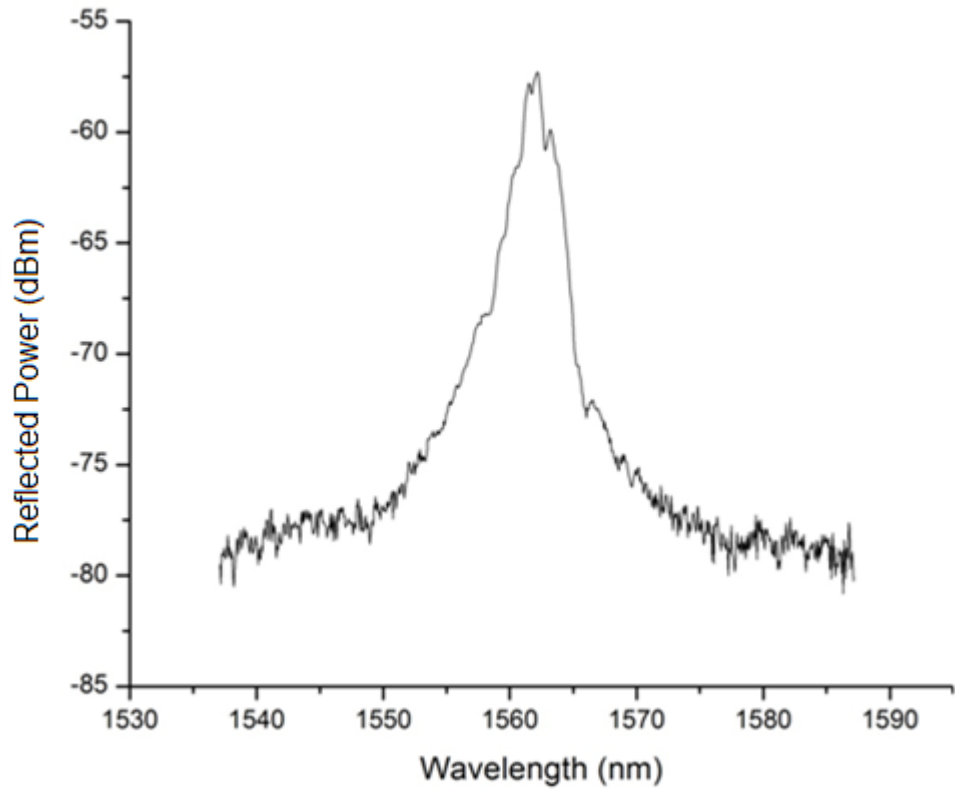


Figure 7-9 Bragg response of FBG fabricated in MMmPOF prior to pressure sensing

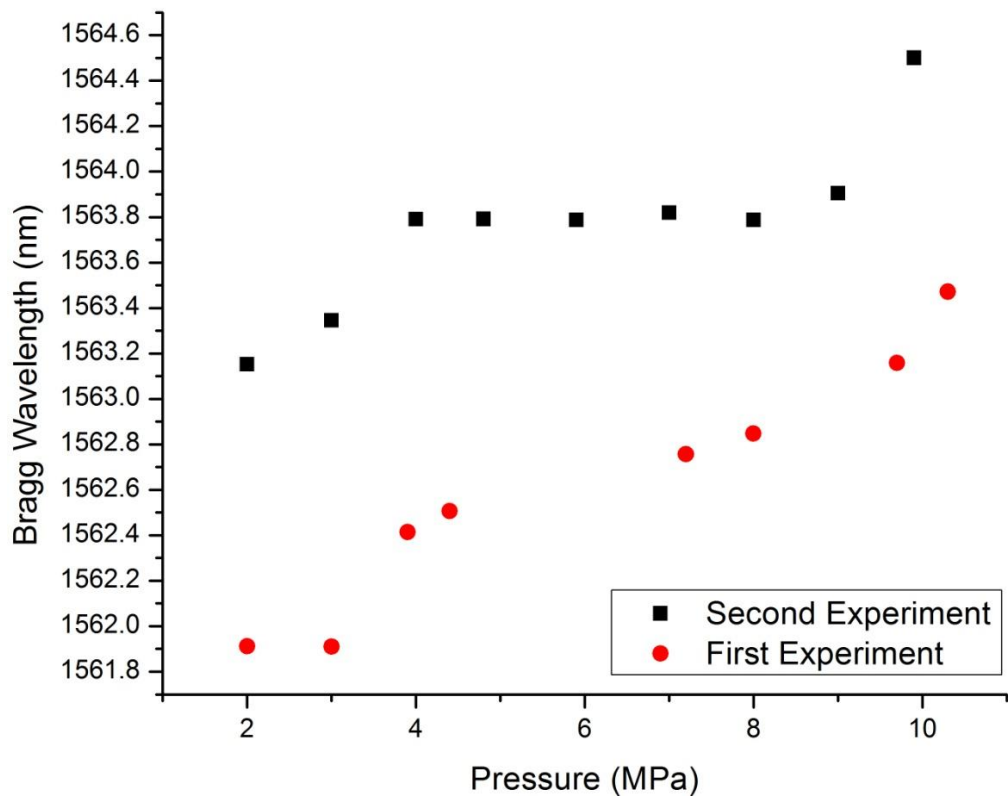


Figure 7-10 Pressure response of a multimode microstructured POFBG

Both Figure 7-10 and Figure 7-11 show positive Bragg wavelength shifts in response to the increase in hydrostatic pressure. The hydrostatic pressure was increased in 1MPa steps. Each Bragg response measurement was taken 60 seconds after the increase of pressure so to allow the temperature to stabilise. In Figure 7-10 the holes of the MMmPOF at the end of the fibre are open, it was first felt that this may cause the positive Bragg wavelength shifts. However shown in Figure 7-11 are the positive linear changes in Bragg wavelength due to the increase in hydrostatic pressure, however this time the tip of the MMmPOF has been sealed with adhesive thus sealing the holes of the microstructured fibre. Therefore it would suggest that either having the holes open or closed does not make any significant difference to the Bragg wavelength shift direction.

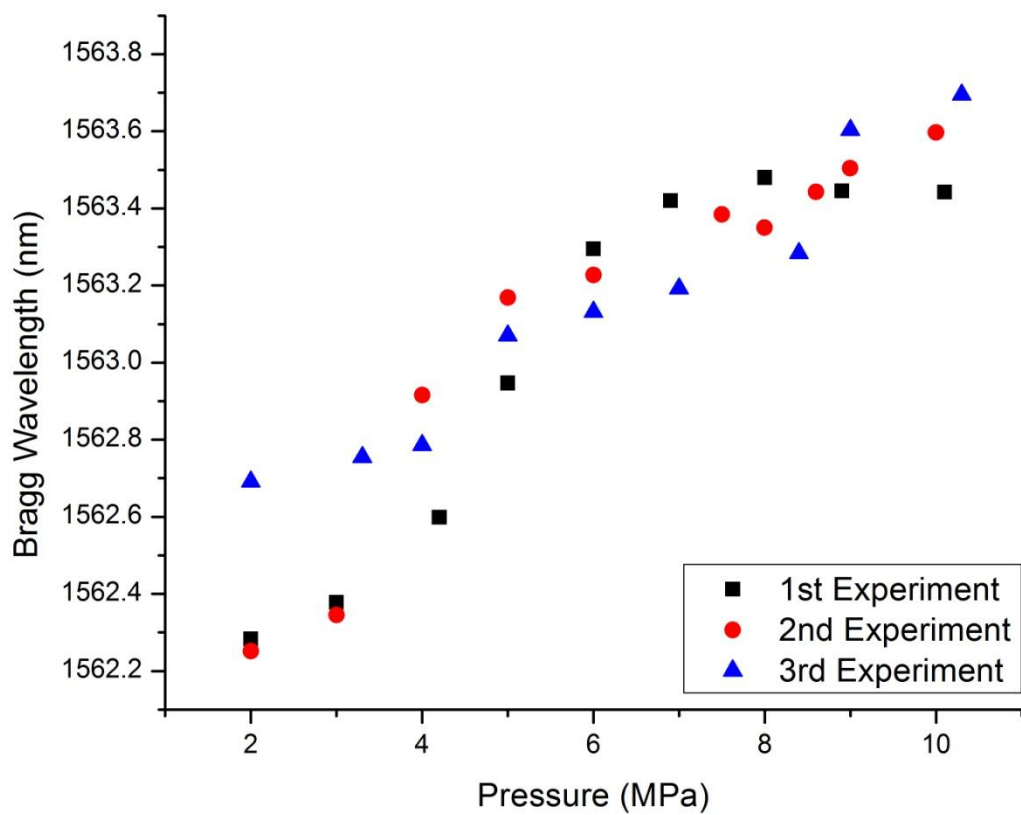


Figure 7-11 Pressure response of a FBG fabricated in MMmPOF, with the free end sealed with adhesive

7.3.1.5 Pressure Sensitivity of a FBG fabricated in SM SI POF

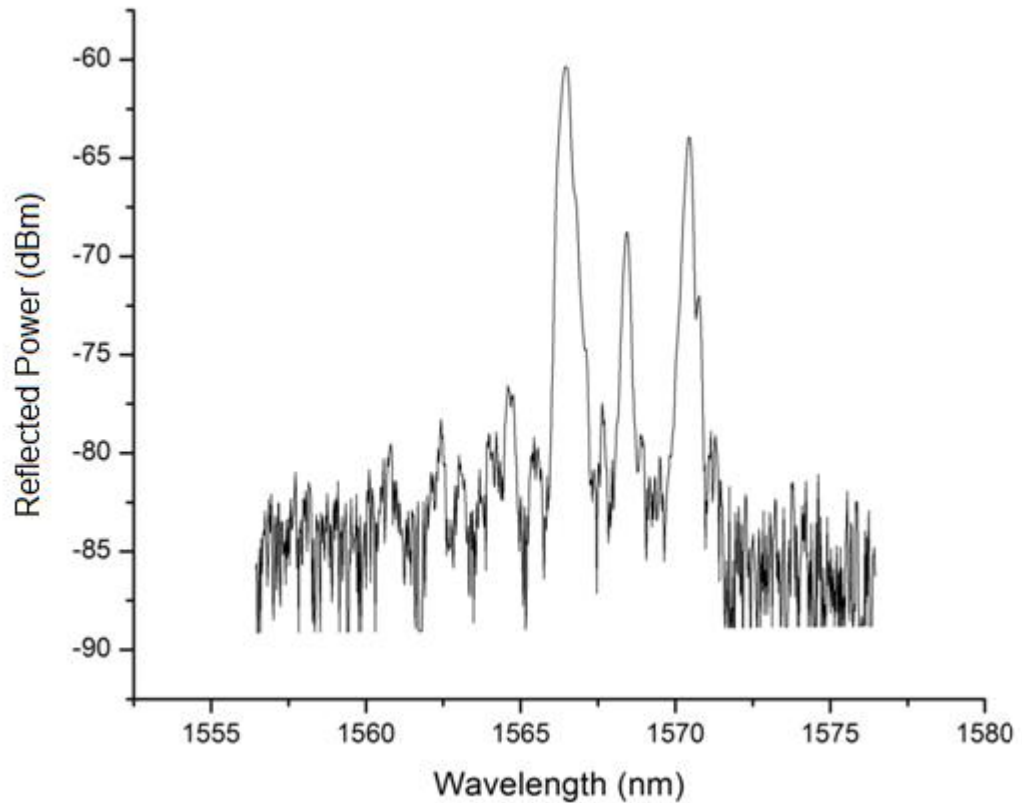


Figure 7-12 Bragg response of FBG fabricated in few mode step index POF prior to pressure sensing

Due to the possibility of the microstructured design of the POF having an adverse effect on the hydrostatic pressure sensitivity in POF, single mode (SM) step index (SI) POF was also investigated. The reflected Bragg response of the POFBG prior to the hydrostatic pressure characterisation is displayed in Figure 7-12, the POF is likely to be few mode, hence the three peaks. The reflected Bragg response was captured on an OSA with a bandwidth resolution of 0.1nm. The first peak had a Bragg wavelength of 1566.4nm, and bandwidth (FWHM) of 0.4nm and a signal-to-noise ratio of 25dBm. The second peak had a Bragg wavelength of 1568.4nm; a bandwidth (FWHM) of 0.3nm and a 17dBm signal-to-noise ratio and finally the 3rd peak had a Bragg wavelength of 1570.4nm, a bandwidth (FWHM) of 0.3nm and a signal-to-noise ratio of 22dBm. The FBG fabricated in the solid step index POF had a grating length of 1.8mm and was positioned 2cm from the tip of the fibre.

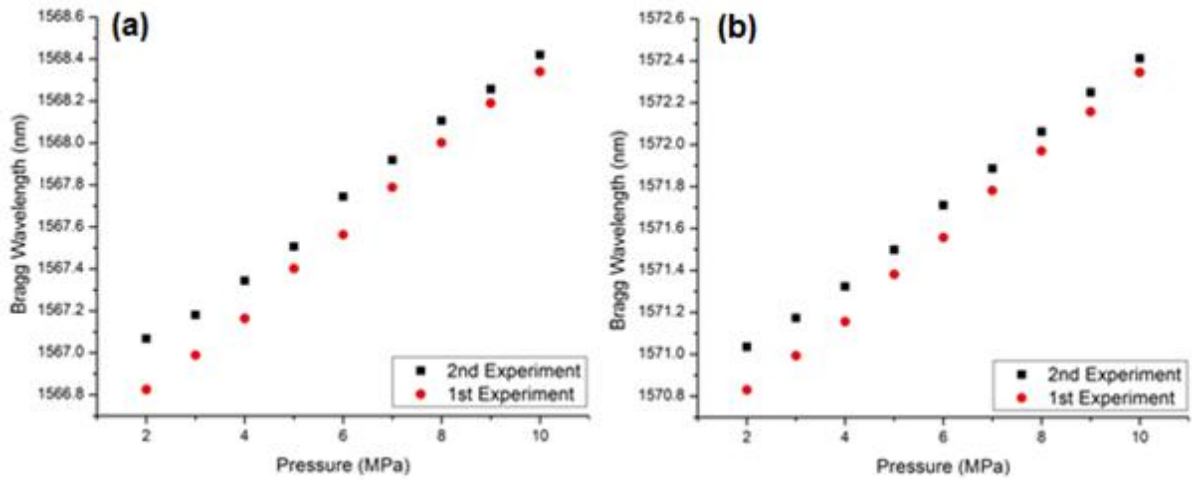


Figure 7-13 Pressure response of a FBG fabricated in few-mode step index POF; (a) tracking 1st peak, (b) tracking 3rd peak

When using the three peaked FBG sensor which was fabricated in the SM SI POF a positive Bragg wavelength change was also observed when hydrostatic pressure was increased up to 10MPa as is shown in Figure 7-13. When tracking both the 1st peak and the 3rd peak a linear Bragg response of 0.2nm/MPa was measured, when taking captures of the reflected Bragg responses with an OSA with a resolution bandwidth of 0.1nm. Also demonstrated in Figure 7-13 are the results of repeating the experiment 1 hour later, the red data points show the Bragg response during the first increase of pressure whereas the black data points shown the Bragg response during the second increase in pressure. As can be seen, there is likely hysteresis from the first experiment, it is expected this would reduce if the time delay between the experiments was increased, however this would need to be fully characterised in future work.

This work is still ongoing, the reason why a positive Bragg wavelength shift is seen due to an increase in hydrostatic pressure as opposed to a negative wavelength shift in response to increasing hydrostatic pressure when using silica FBG sensing is unknown.

This initial work has reiterated that positive Bragg wavelength shifts are reliably observed across two different POF types. The next step forward in this work would be to complete simulation modelling of the predicted hydrostatic sensitivities.

8

THERMAL ANNEALING & WDM SENSOR FABRICATION

This chapter describes a study of the effect that thermally annealing multimode mPOF has on the Bragg response of a pre-fabricated FBG. The Bragg wavelength shift has been characterised both in the 1550nm and 800nm spectral regions. In addition the Bragg wavelength shift was characterised against time when annealing the POF at either 71°C or 80°C. This has enabled tuning of the Bragg wavelength via thermal annealing to coincide with a specific interrogating light source, which may be required as part of an optical sensor system. Furthermore, thermal annealing has been used to permanently shift the Bragg wavelength of a fabricated FBG to manufacture wavelength division multiplexed (WDM) sensors in POF using a single phase mask during fabrication.

8.1 Thermal Annealing & WDM Sensors within the 1550nm Spectral Region

To begin with, this work looks at the thermal response of FBGs fabricated in POF with a Bragg response within the 1550nm spectral region. After this, work has progressed into manipulating the Bragg responses within the 800nm spectral region after the breakthrough of lower wavelength FBGs fabricated in MMmPOF documented in Chapter 6 and published in 2010[71]. Complimenting this development is the documented manufacturing of WDM sensors within the 800nm spectral region.

8.1.1 Two FBG WDM Sensors Fabricated in MMmPOF

Initial work was carried out to fabricate a WDM sensor, consisting of two FBGs in the MMmPOF with a spectral response within the 1550nm region. Each FBG was fabricated individually using two different phase masks. Firstly, an FBG was fabricated in the MMmPOF using the same phase mask ($\Lambda_{pm} = 1057.2\text{nm}$) as in Chapter 3.5, where the fabrication technique of FBGs in MMmPOF was described. The MMmPOF was UV exposed for 60 minutes using the UV HeCd laser (Kimmon Koha Co, Ltd IK3301R-G). As in Chapter 3.5 the resultant reflected Bragg response is within the 1560nm spectral region. This particular Bragg response, which is shown in Figure 8-1, had a reflected Bragg response of 1563nm and a bandwidth (FWHM) of 2nm was measured, using an OSA (HP 70951B) with a bandwidth resolution of 0.5nm.

To fabricate the second FBG a second additional phase mask was used, this had been manufactured for specific use with the 325nm HeCd laser and had a surface relief pattern with a period (Λ_{pm}) of 1034.2nm. It is expected that any resultant Bragg response would be

around 1530nm using this mask. The growth curve of a FBG fabricated in a separate length of MMmPOF using this phase mask is first shown in Figure 8-2. A noticeable Bragg reflection can be seen after 40 minutes of exposing the MMmPOF to the UV interference pattern generated from the phase mask. The exposure was stopped after 90 minutes where the growth of the reflected signal had reached a saturation level. After 90 minutes the reflected Bragg response had a signal-to-noise ratio of around 9dBm.

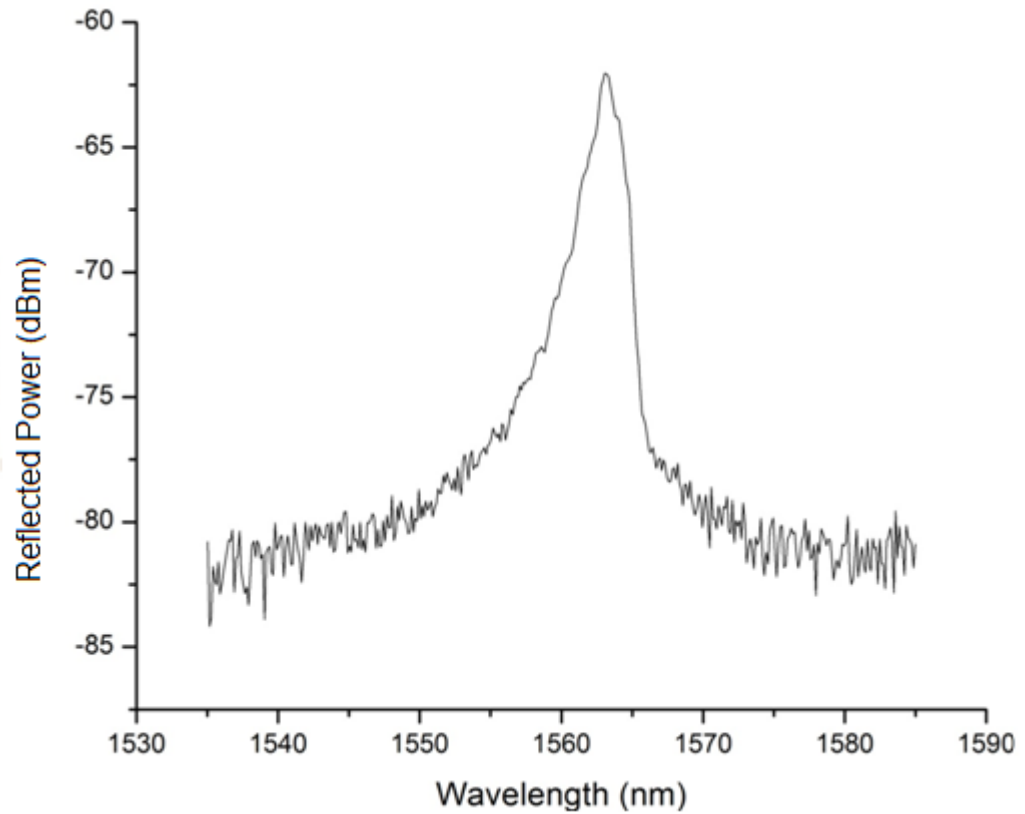


Figure 8-1 First Fabricated FBG of a two FBG WDM sensor, Bragg wavelength 1563.25nm

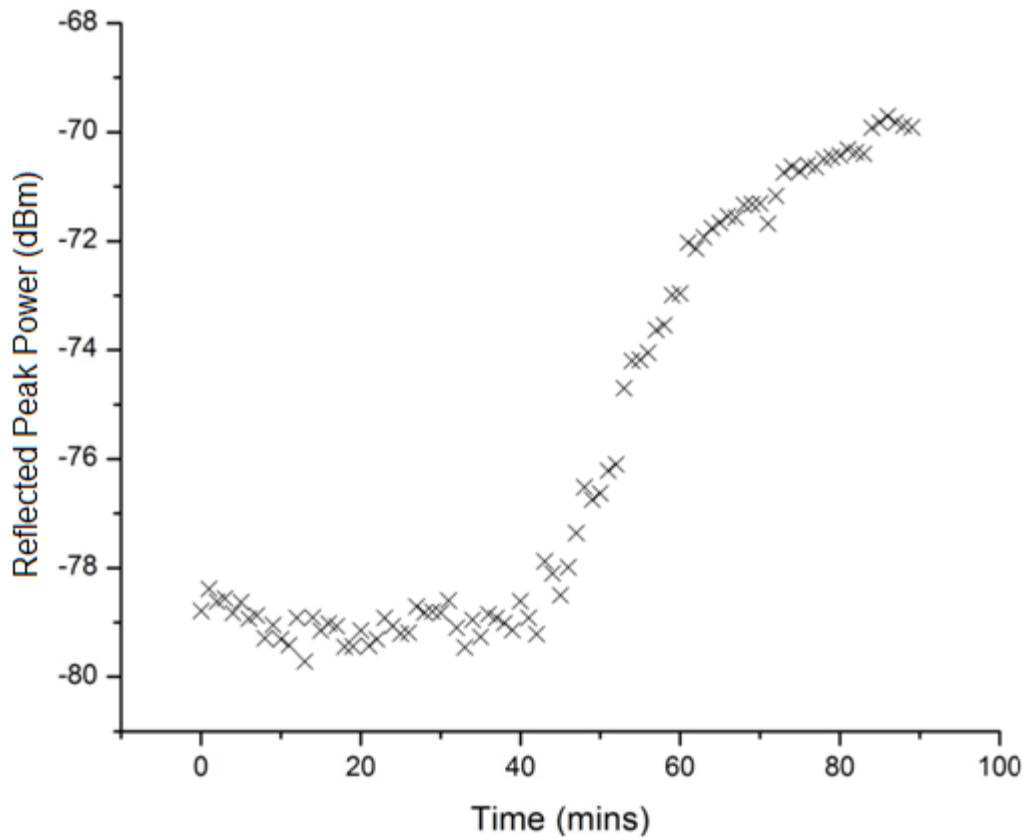


Figure 8-2 Growth Curve of a FBG Fabricated in MMmPOF, with a Bragg wavelength at 1530nm

The reflected Bragg response captured after exposing the MMmPOF to the UV interference pattern for 90 minutes can be seen in Figure 8-3. The Bragg wavelength of the response was measured to be 1529nm and the measured bandwidth (FWHM) was 2.5nm. These measurements were taken in reflection using the 50:50 (at 1550nm) silica multimode coupler and measured on an OSA (HP 70951B) with a bandwidth resolution of 0.5nm.

Further attempts were made to fabricate FBGs using this additional phase mask to produce Bragg response around 1529nm. Five more attempts were made, all of which proved successful with the typical growth curve shown in Figure 8-2 and the Bragg response shown in Figure 8-3 being typical responses of FBGs fabricated with this phase mask in MMmPOF and exposed for 90 minutes. For reasons unknown when fabricating an FBG with a Bragg wavelength of 1529nm the MMmPOF is UV exposed for 90 minutes before a saturation level is reached whereas when fabricating FBGs with a Bragg wavelength of 1562nm as demonstrated in Chapter 4 a saturation level would be reached within 1 hour.

Once confidence was built in using the new mask to fabricate FBGs with a response around 1529nm it was used to add a second FBG to the MMmPOF which was previously UV inscribed with a FBG with a response at 1563.5nm shown in Figure 8-1. The MMmPOF had a length of 8cm; the first FBG was fabricated within 2cm of the end of the fibre, which is dictated by the focus point of the UV laser beam from the cylindrical lens onto the v-groove where light is butt coupled into and out of the MMmPOF. Therefore, for the second

inscription to produce a Bragg response at the lower wavelength the MMmPOF was turned around so the opposite end is butt coupled to the silica arm of the coupler and the second FBG is fabricated 2cm away from this. Therefore there was a 4cm separation between the two fabricated FBGs along the length of the MMmPOF.

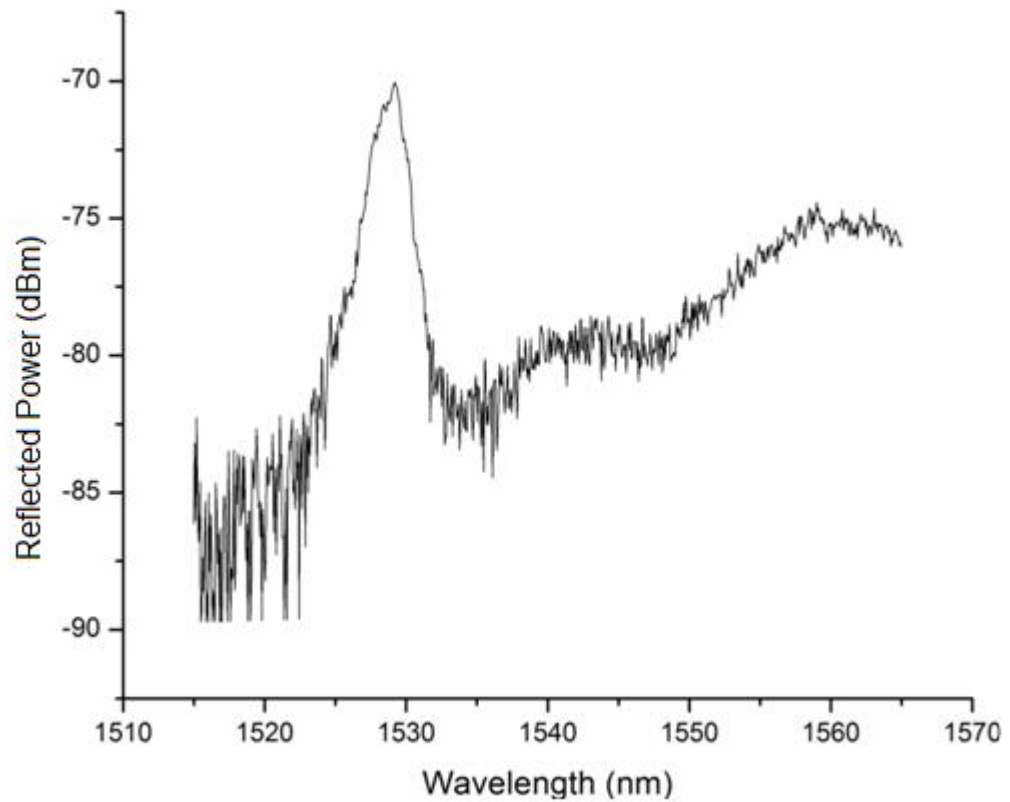


Figure 8-3 Reflected FBG response in MMmPOF with a Bragg wavelength of 1528.8nm

The second FBG was fabricated by exposing the MMmPOF to the UV interference pattern generated by the phase mask ($\Lambda_{pm} = 1034.2\text{nm}$) for 90 minutes. The resultant reflected Bragg response of both FBGs can be seen in Figure 8-4, which is the first example of a WDM sensor fabricated in MMmPOF. The reflected response was captured on the same OSA with a bandwidth resolution of 0.5nm, Bragg responses can be seen at 1530nm with a bandwidth (FWHM) of 2nm and also at 1563.5nm with a bandwidth of 2nm. There is a slight variation of the Bragg wavelengths of the two FBGs when compared to previous spectra, this is because the butt coupling between the polymer and silica fibres was adjusted to optimise the strongest reflections from both FBGs and thus optical modal power was redistributed from the previous spectra. Furthermore there is the possibility of varying amounts of axial strain applied to the POF between each capture, including the possibility of a temperature change between the captures, both of which would result in the small change of Bragg wavelength between the two Bragg responses.

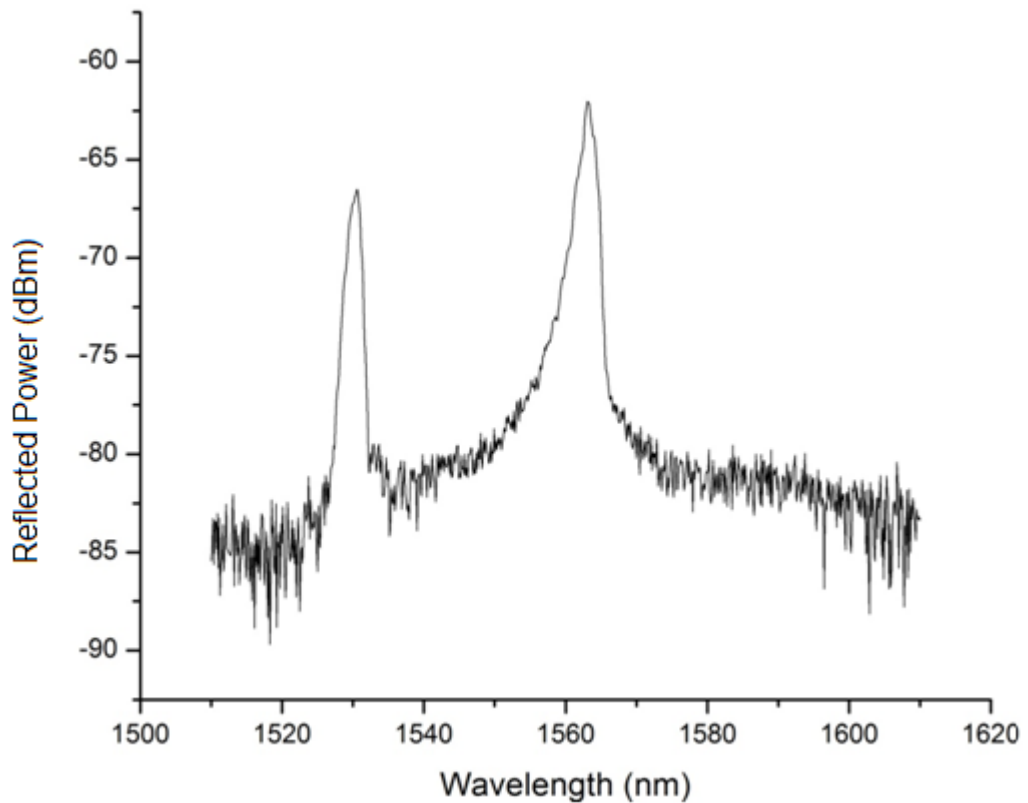


Figure 8-4 Reflected spectrum of two fabricated FBGs fabricated in MMmPOF with the use of two separate phase masks

8.1.2 Thermal Annealing of POFBGs

Building upon the previous work of fabricating a WDM sensor consisting of two FBGs it would be desirable to fabricate WDM sensors with more than 2 FBGs. However it is expensive to purchase further phase masks to fabricate additional Bragg responses within a spectral window. Therefore other options were considered to manufacture a larger number of Bragg responses within a given spectral window without the additional manufacturing or tooling costs. A solution proposed was to permanently shift a Bragg response by thermally annealing the MMmPOF, thus creating space within the spectral window for additional FBGs to be fabricated using the same phase mask as the FBG previously fabricated.

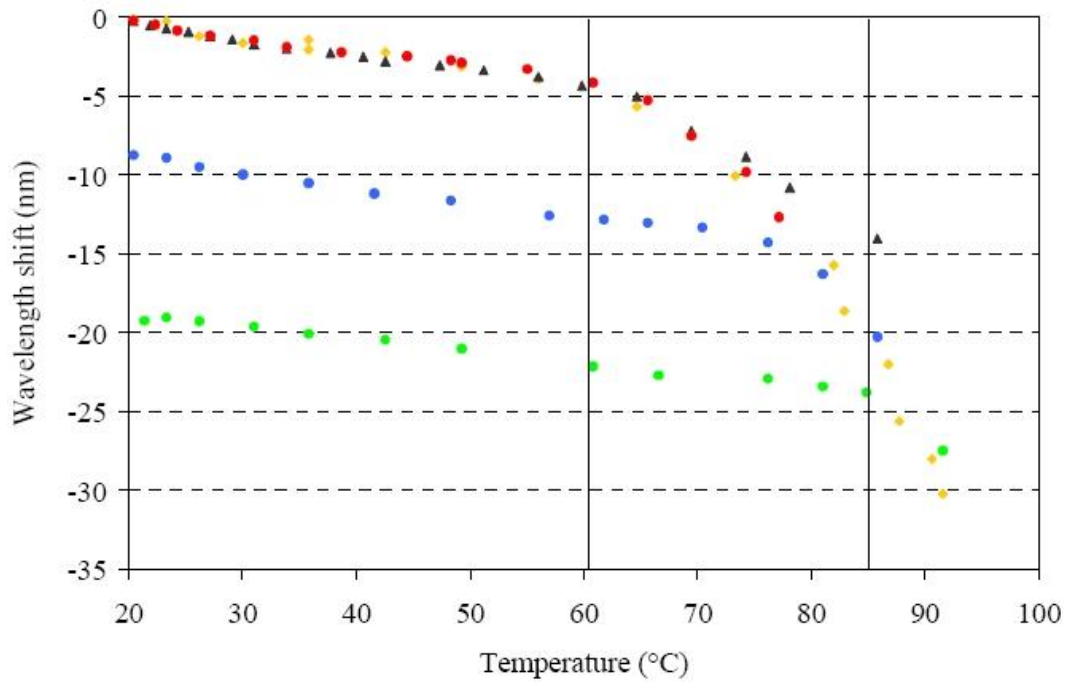


Figure 8-5 Bragg wavelength shift of three different FBGs fabricated in pure PMMA mPOF, from [24]

• first cycle - first FBG, • second cycle - first FBG, • third cycle - first FBG, ▲ second FBG, ◆ third FBG

It has been previously demonstrated that a permanent negative Bragg wavelength shift can be achieved when thermally annealing a FBG prefabricated in mPOF at 80°C for 7 hours by Carroll[24] and was discussed in Chapter 3. Furthermore, in the same publication the authors reported on the repeatability of the Bragg wavelength shift[24]. Two additional FBGs were fabricated in different lengths of the pure PMMA mPOF, albeit from the same batch. All the gratings were UV exposed for the same amount of time. As reviewed in Chapter 3, the first grating was heated in three consecutive cycles, first up to 77°C, second to 86° and finally up to 92°C, allowing the temperature to return to room temperature between each cycle. The second FBG was heated to 86°C in one cycle and the third FBG was heated to 92°C again in only one cycle. As is shown in Figure 8-5 the data collected from the Bragg wavelength shifts of the second and third FBGs agrees well with the first FBG during the first heating cycle. Furthermore, the first and third FBGs experienced the same negative Bragg wavelength shift when heated over 90°C even though the first FBG had experienced two heating cycles prior to exceeding 90°C.

The results collected by Carroll suggest good repeatability of thermal tuning of a Bragg wavelength across the three POFBGs responses. Therefore it is hypothesised the permanent induced Bragg wavelength shift can be mapped against time for a constant thermal annealing temperature. This would essentially allow for thermal tuning of a Bragg response, allowing for modification of a Bragg wavelength to coincide with an interrogating light source at a specific wavelength for example. Overlapping the Bragg response of a fabricated FBG with the spectral region of an interrogating light source is an essential requirement when monitoring a Bragg response. However, occasionally the spectral range of

a specific light source needed as part of the optical sensor setup may not cover the Bragg wavelength of a fabricated FBG in POF; therefore tuning the Bragg wavelength is needed. A technique used to induce a small tuning range in silica optical fibre is to apply axial strain to the fibre during the fabrication of FBGs. This technique may prove troublesome with POFBGs considering fabrication times of at least 45minutes needed to fabricate FBGs in pure PMMA POF and the fabrication setup where the POF is simply taped to a v-groove. Therefore, purchasing a relatively expensive new phase mask with the appropriate period (Λ_{pm}) to fabricate FBGs with a suitable Bragg response may be the only possible solution if thermal tuning is not possible. However, it should be noted that thermal annealing, although it has the potential of providing a relatively cheaper solution, the Bragg wavelength of a fabricated POFBG prior to thermal annealing would need to be within a positive 20nm spectral region of the desired wavelength. Nevertheless it is still considered to have the potential of being a versatile tool, when designing an optical interrogation system using POF. Therefore documented in the following section is the work carried out to characterise thermal annealing of FBG sensors fabricated in pure PMMA multimode mPOF (MMmPOF). Furthermore WDM sensors have been developed, taking advantage of thermal annealing and the permanently induced negative Bragg wavelength shifts.

8.1.3 Thermal Annealing of Multimode mPOF

The thermally annealed induced Bragg wavelength shift of FBGs fabricated in pure PMMA MMmPOF has been characterised, the MMmPOF used in this work was provided by The University of Sydney and was introduced in Chapter 4. Firstly, an FBG was fabricated into the MMmPOF using the same UV inscription technique as described in Chapter 3.5, the HeCd laser (HeCd Kimmon Koha 1K3301R-G) exposed the MMmPOF through a phase mask ($\Lambda_{pm} = 1057.2\text{nm}$) for 60 minutes, where the reflected peak signal reached a saturation level. The captured reflected Bragg response is shown in Figure 8-6, which was captured using an OSA (HP 70951B) with a bandwidth resolution of 0.5nm. The Bragg wavelength of the response was 1564nm, a bandwidth (FWHM) of 2nm was also measured. The reflected Bragg signal had a signal-to-noise ratio of 25dBm, when butt coupling a FC/APC connector from a silica multimode (50/125 μm) 50:50 (@1550nm) 2x2 coupler to the MMmPOF.

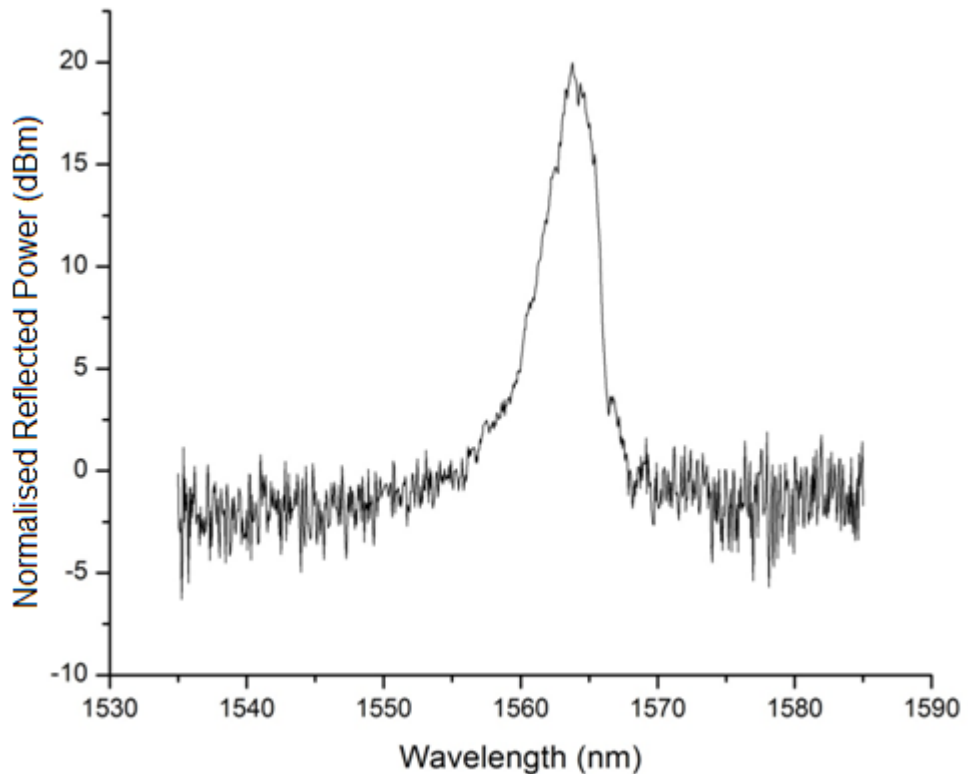


Figure 8-6 Reflected Bragg response of a FBG fabricated in MMmPOF, prior to thermal annealing

After the FBG fabrication, the MMmPOF was removed from the v-groove plates of the translation stage used for all FBG fabrication and interrogation and placed freely onto a baking tray. The baking tray was then placed onto the middle shelf of a 71°C pre-heated oven for 8 hours. After this, the fibre was then removed and re-mounted onto the v-groove plate and translation stage to enable re-alignment to the silica coupler using the same butt coupling used previously. The Bragg response of the annealed FBG is shown in **Figure 8-7**, using the same OSA and bandwidth resolution of 0.5nm. The Bragg wavelength was calculated to be 1545nm and a bandwidth (FWHM) after the thermal anneal of 3nm and the signal-to-noise ratio is now 15dBm.

Table 8 reviews the reflected Bragg responses of the FBG fabricated in the MMmPOF before and after the 8 hour thermal anneal at 71°C, both the before and after captures were taken at room temperature. It can be seen when comparing the Bragg wavelengths the thermal anneal induced a permanent Bragg wavelength shift of -19nm, confirming that the thermal tuning documented by Carroll[24] in the single mode mPOF is also possible in the MMmPOF. After the thermal anneal the signal-to-noise ratio would appear to have decreased in the region of 6dBm, this however would need to be investigated further due to the instability of the optical power reflection introduced by the varying coupling conditions for each capture, including a new cleave to the POF end face for each capture.

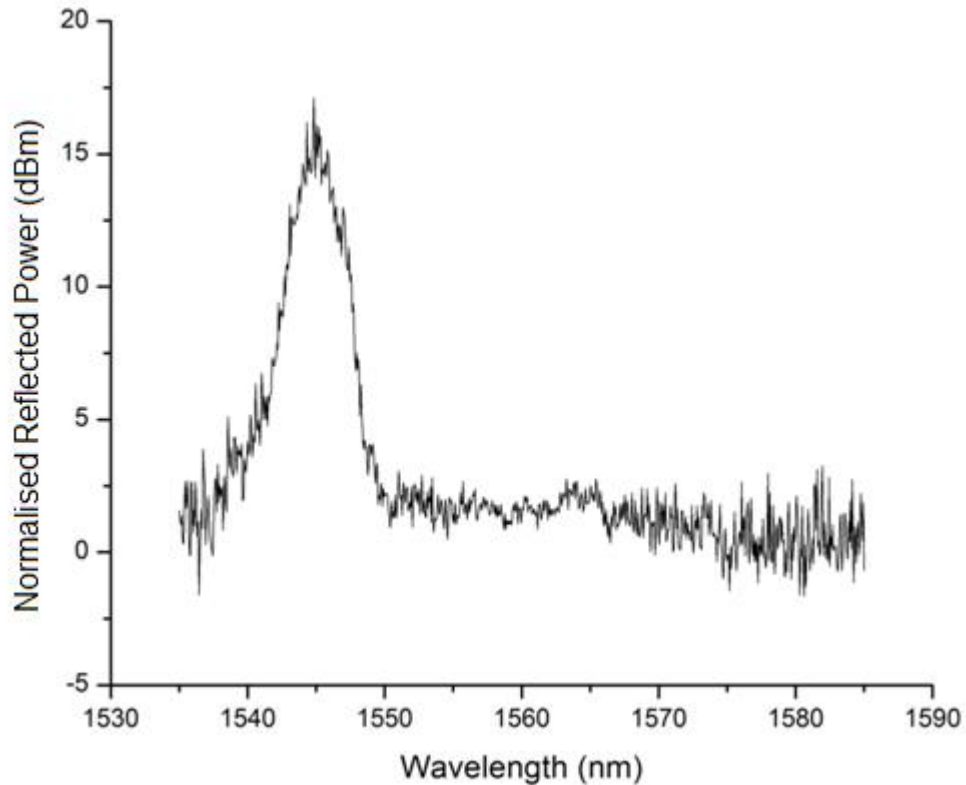


Figure 8-7 Reflected Bragg response after thermally annealing the MMmPOF at 71°C for 8 hours

Table 8 Comparison of reflected Bragg response of a FBG fabricated in MMmPOF before and after thermal annealing at 71°C for 8 hours.

	Bragg Wavelength	Bandwidth FWHM	Signal-to-noise ratio
Before Annealing	1564nm	2nm	25dBm
After Annealing	1545nm	3nm	15dBm

Once the Bragg response had been permanently shifted a second FBG was fabricated into the same fibre using the same phase mask ($\Lambda_{pm} = 1057.2\text{nm}$). The fabrication setup was exactly the same, using the UV HeCd laser and laying the MMmPOF on the v-groove, the POF was UV exposed for 60 minutes. The total length of the MMmPOF used was 8cm, the first FBG was fabricated 2cm from one end of the POF, which is governed by the focus point of the UV laser beam and the position of the v-groove plate. For the second FBG the MMmPOF was turned around so the fabrication of the second FBG was 2cm from the opposite of the MMmPOF, resulting in an approximate 4cm separation between the two FBGs along the fibre axis.

The reflected Bragg responses of the two FBGs shown in Figure 8-8 was captured using the silica multimode 50:50 coupler and an OSA with a bandwidth resolution of 0.5nm. The reflected spectrum now has two Bragg responses, the first from the thermally annealed FBG with a Bragg wavelength of 1542.5nm and a bandwidth (FWHM) of 2nm. And second from

the newly fabricated FBG with a Bragg wavelength of 1563nm and a bandwidth (FWHM) of 3nm. This demonstrates the first instance of fabricating a WDM sensor in POF using a single phase mask to produce each FBG individually and was published in 2010[72].

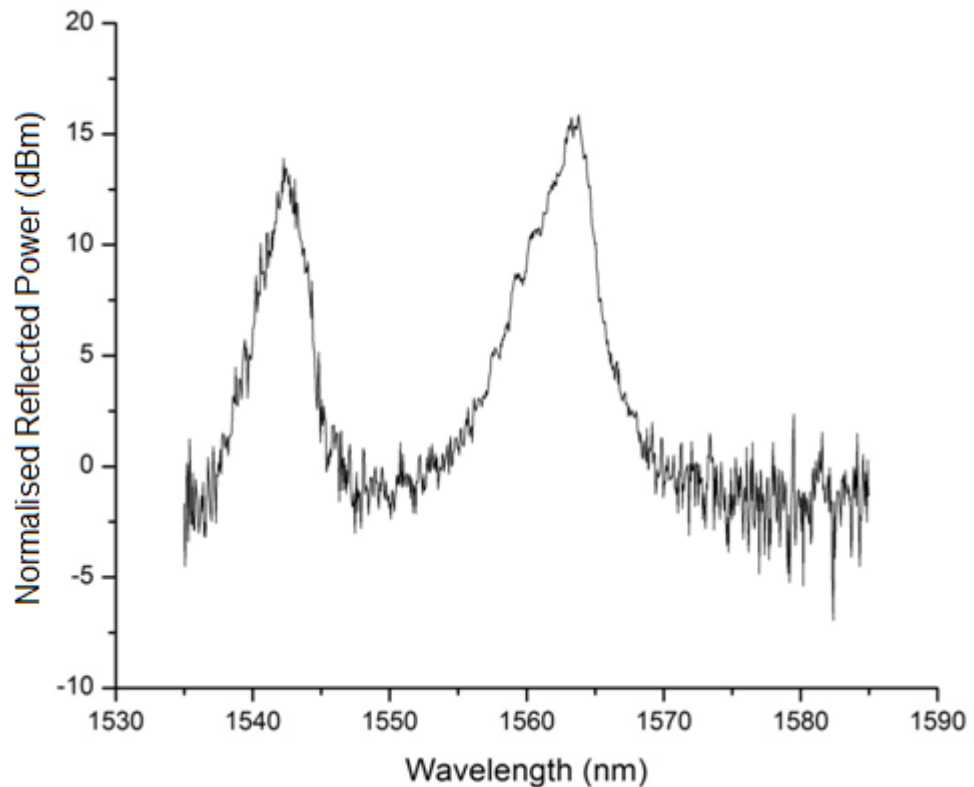


Figure 8-8 Two FBG WDM sensor fabricated in MMmPOF using a single phase mask and thermal annealing

Finally a third FBG was fabricated in the same length of MMmPOF. This third FBG was fabricated using the additional phase mask ($\Lambda_{pm} = 1034.2\text{nm}$), which was used to demonstrate a two FBG previously in this chapter. The final FBG was located in the middle of the two previously fabricated FBGs, therefore there was a 2cm separation between each of the three FBGs. Monitoring of the growth of the third Bragg response was enabled by cleaving approximately 2cm off the end of the MMmPOF used when monitoring the growth of the second FBG. Once more the MMmPOF was UV exposed for 60 minutes when a saturation level was reached of the peak reflected power of the third FBG. The captured reflected response of the three FBG WDM sensor can be seen in Figure 8-9. Again the reflection was captured with the use of a multimode 50:50 silica coupler and an OSA with a bandwidth resolution of 0.5nm. Examining the reflected Bragg responses, the first fabricated Bragg response which was thermally annealed for 8 hours at 71°C had a Bragg wavelength of 1541nm and a bandwidth (FWHM) of 4nm. The second fabricated Bragg response had a Bragg wavelength of 1561.5nm and a bandwidth (FWHM) of 4.5nm. And finally the third fabricated Bragg response had a Bragg wavelength of 1530nm and a bandwidth (FWHM) of

2.5nm. This is the first demonstration of WDM of three FBGs within the C-Band spectral region which was fabricated in pure PMMA MMmPOF and was published in 2010[72].

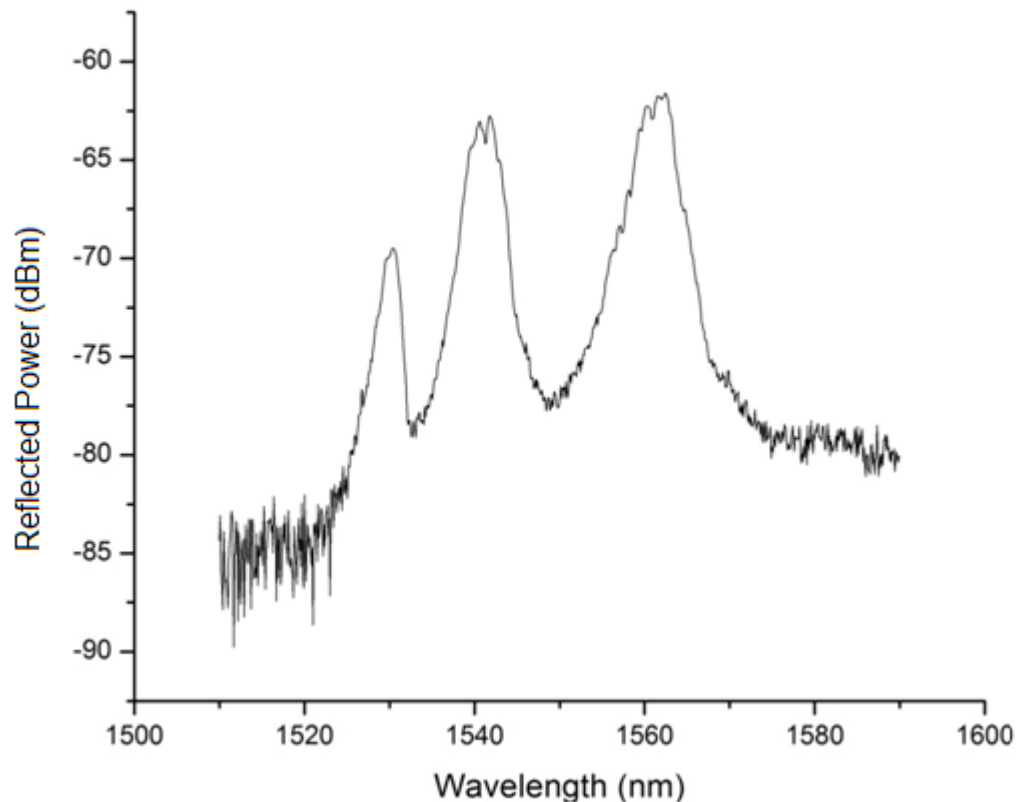


Figure 8-9 Three FBG WDM sensor fabricated in MMmPOF. OSA Bandwidth resolution of 0.5nm

8.1.4 Characterisation of Thermal Annealing Against Time

Thus far, when POF has been placed in the oven for a single thermal annealing cycle it has been between 7-8 hours, inducing a permanent negative Bragg wavelength shift of around 20nm[24, 72]. This next section of work investigates if the Bragg wavelength can be tuned within the -20nm range by varying the amount of time the MMmPOF is placed in the oven for. Firstly three FBGs were fabricated in individual lengths of the MMmPOF, each FBG was fabricated by exposing a length of MMmPOF with a UV laser beam (HeCd Kimmon Koha 1K3301R-G) which was focussed into the core of the mPOF via a phase mask ($\Lambda_{pm} = 1057.2nm$) for 1 hour. The inscription technique is described in more detail in Chapter 3.5. The three resultant reflected Bragg responses of the fabricated FBGs are shown in Figure 8-10. Each Bragg response was captured in reflection on an OSA (HP 70951B) via a multimode silica (50/125 μ M) 2x1 coupler with a coupling ratio of 50:50 at 1550nm. The Bragg response of each FBG is summarised in Table 9, where the Bragg wavelength and bandwidth (FWHM) were also documented.

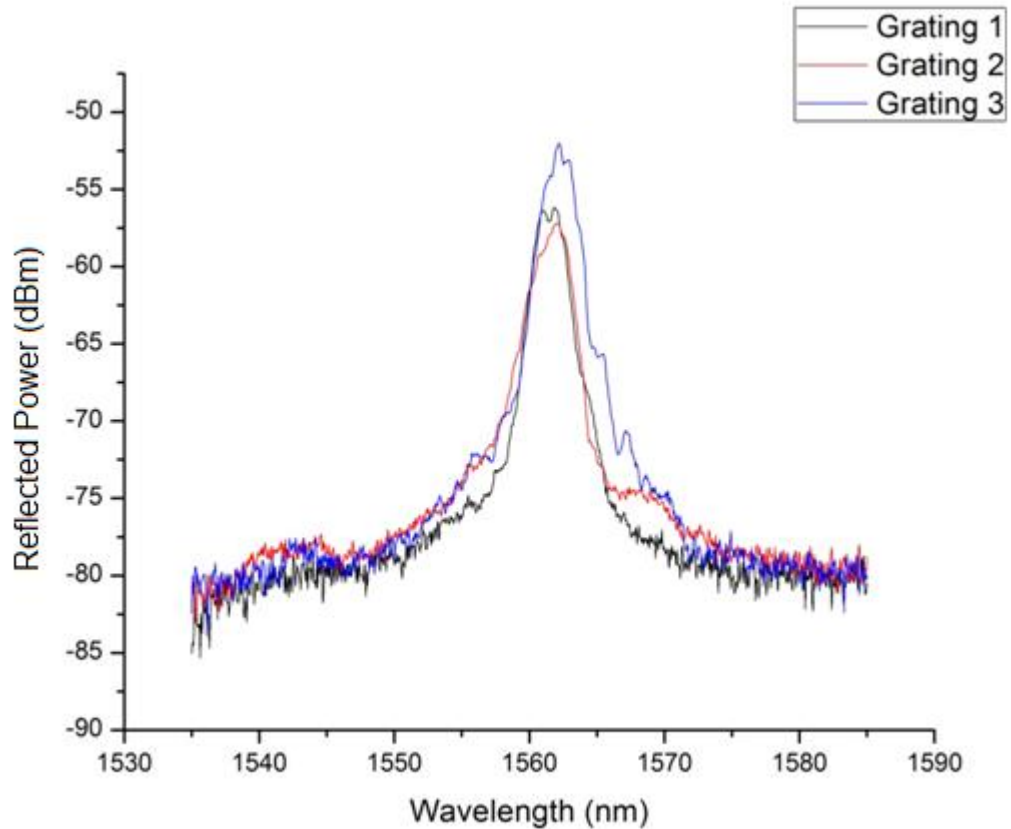


Figure 8-10 Three FBG responses fabricated in separate lengths of MMmPOF prior to thermal annealing characterisation

Table 9 Summary of the three Bragg responses shown in Figure 8-10

	Bragg Wavelength	Bandwidth (FWHM)	Signal-to-Noise ratio
FBG 1	1561.5nm	2.5nm	18dBm
FBG 2	1562nm	2.5nm	17dBm
FBG 3	1562nm	2nm	22dBm

Reviewing Table 9, reasonably small variances of the Bragg wavelength and bandwidth can be seen between the three FBGs. It is felt that this may be due to the high number of possible populated reflected modes within the multimode fibre, something which can vary if the UV interference patterns do not cover the entire cross section of the MMmPOF core. Furthermore, because of the short lengths of POF used alignment between the MMmPOF and the silica arm of the coupler dictates populated modes within the POF and hence will result in varying reflected Bragg responses. The increased value of the reflected signal-to-noise ratio of FBG 3 over FBGs 1 and 2 may possibly be because of a better cleave of the POF end face resulting in a smaller loss in the butt coupling between the polymer and silica fibres. Additionally the composition of POF is prone to change along a few centimetres of

fibre[41]; this may result in a higher UV induced refractive index change along the interference pattern within the core, therefore reflecting a stronger signal back from the FBG. These slight variations would need to be considered when thermally tuning a Bragg response to a specific wavelength. However the change in Bragg wavelength is to be characterised therefore provided the required wavelength shift is calculated then tuning to a specific wavelength would be possible, provided it is within the -20nm range.

To characterise the permanent Bragg wavelength shift with time each of the FBGs was placed in the oven repeatedly for different time periods and the reflected Bragg response captured between each heating cycle at room temperature using the same butt coupling interrogation technique previously described in this section and in more detail in Chapter 4. The oven was again pre-heated to 71°C and each time one of the FBGs was thermally annealed the POF was placed onto a baking tray which was at room temperature, and this was then placed onto the middle shelf of the oven.

FBG 1 was placed in the oven in 10 minute cycles on 6 different occasions totalling 60 minutes; FBG 2 was placed in the oven for 20 minute cycles on 8 different occasions totalling 160 minutes and finally FBG 3 is placed in the oven for 30 minute cycles on 6 different instances totally 180 minutes. The resultant Bragg wavelength of each FBG is shown in Figure 8-11, the Bragg wavelengths captured at 0 minutes show the original wavelengths prior to thermal annealing. Looking at Figure 8-11, it can be seen that the permanent Bragg wavelength of each of the three FBGs are in broad agreement with each other at a given length of time of thermal annealing and as a result define a thermal annealing curve. The annealing curve can also be seen in Figure 8-12 where the Bragg wavelength shift against time can be seen. As was discussed in reference[74], it would appear a level is reached where the blue Bragg wavelength shift will not increase further at around 140 minutes. Suggesting there is no significant shrinking of the fibre length beyond this point at the chosen annealing temperature.

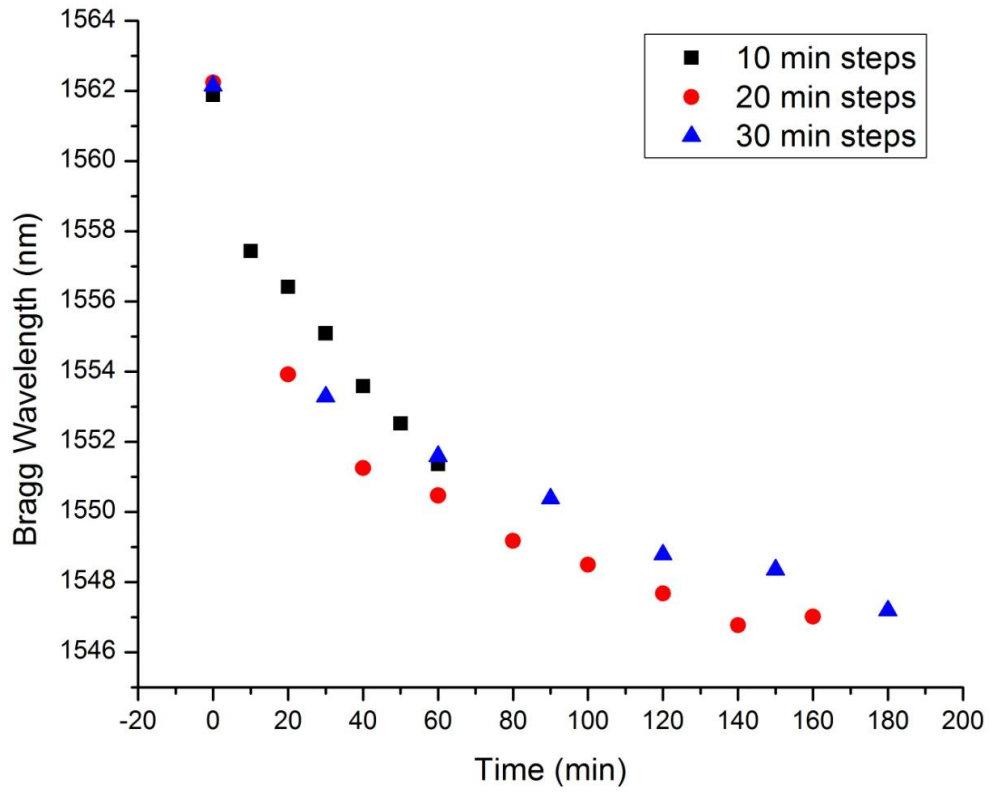


Figure 8-11 Reflected Bragg wavelength observed during thermal annealing cycles. ■ FBG1 thermally annealed in 10 minute cycles • FBG2 thermally annealed in 20 minute cycles ▲ FBG3 thermally annealed in 30 minute cycles

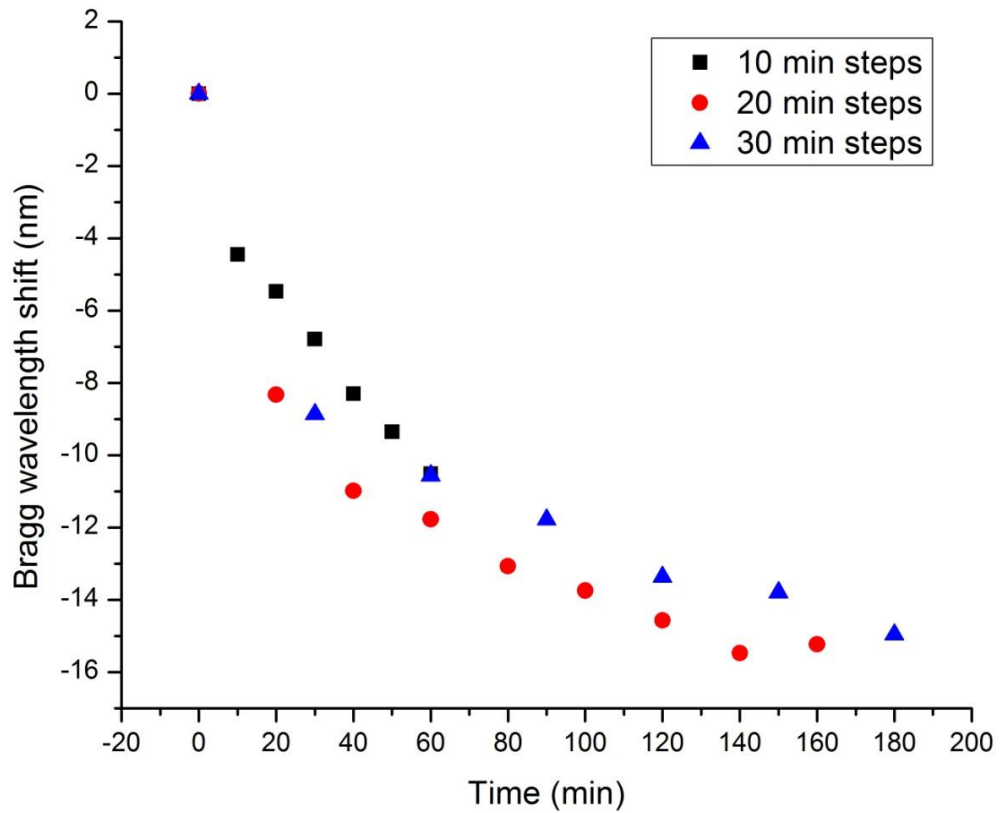


Figure 8-12 Thermally induced permanent blue Bragg wavelength shifts depending on length of time of anneal

It is felt the thermal annealing curves seen in both Figure 8-11 and Figure 8-12 could be in better agreement with each other for each FBG if heat from the oven was not lost when placing the POF inside the oven. Additionally, because the fibre was rested on a baking tray which was at room temperature before being placed in the oven a lapse of time would have occurred before the POF was annealed at 71°C as the tray also would need heating to 71°C. However this could also be characterised and included in any designed thermal annealing cycle to achieve a specific Bragg wavelength. Ideally continuous monitoring of the Bragg wavelength during the thermal annealing in the oven would be taken which would allow the continuous capture of the thermal annealing curve and would also eliminate any lapse time of the oven losing heat and heating of a baking tray between each timed heating cycle. However as fibre lengths are limited to 8cm within the 1550nm spectral region due to the attenuation losses the reflected Bragg spectrum could not be monitored continuously without having the entire length of POF within oven. This would require the adhesive splice between the polymer and silica fibres to also be in the oven and the splice would therefore be heated up to 71°C. However the glass transition temperature of the cured adhesive is 43°C, therefore it was found exceeding this temperature prevented any optical signal either being coupled into or out of the POF.

8.1.5 WDM of Three FBGs Fabricated From a Single Phase Mask

As previously documented in this chapter, WDM sensors have been manufactured in the MMmPOF using two different phase masks and exploiting the thermal properties of PMMA based POF[72]. To expand on this and exploit the thermal annealing curve obtained in Figure 8-11 and Figure 8-12 it was investigated if a WDM sensor consisting of three FBGs could be fabricated using a single phase mask. The phase mask which was used had a surface relief pattern with a period of 1057.2nm resulting in a Bragg response at around 1562nm in the pure PMMA MMmPOF, as was seen in Chapter 3.5. Each of the three FBGs was fabricated using the UV HeCd laser and the same fabrication technique also described in Chapter 4. Furthermore, the interrogation of all fabricated Bragg responses were captured in reflection with the aid of a multimode (50/125µm) 2x1 50:50 silica coupler on an OSA (HP 70951B) with a bandwidth resolution of 0.5nm, also described in Chapter 4.

Firstly an FBG was fabricated in an 8cm length of MMmPOF 2cm from the fibre end. The MMmPOF core was exposed to the UV interference pattern for 57 minutes when a saturation level was reached and a maximum signal-noise ratio was achieved of 17dBm as shown in Figure 8-13a. After 35 minutes the butt coupling between the polymer and silica fibres was adjusted to optimise the reflected Bragg signal. Shown in Figure 8-13b is the reflected Bragg response after fabrication, this has a Bragg response of 1563.5nm and a bandwidth (FWHM) of 3nm.

The MMmPOF was then thermally annealed in an oven which was pre-heated to 71°C. The fibre was first rested on a baking tray which was at room temperature and then placed on the middle shelf of the oven, where it was thermally annealed for 30 minutes and was then removed. Figure 8-14 illustrates a permanent negative Bragg wavelength shift of 7.5nm due to the thermal anneal. The response now has a Bragg wavelength of 1556nm and a bandwidth (FWHM) of 2nm. The signal-to-noise ratio of Bragg response would appear to have increased by 3dBm to around 20dBm after the thermal anneal. It is felt this is likely to be the result of an improved cleave of the MMmPOF end face the second time round rather than the thermal anneal increasing the reflected optical power of the FBG.

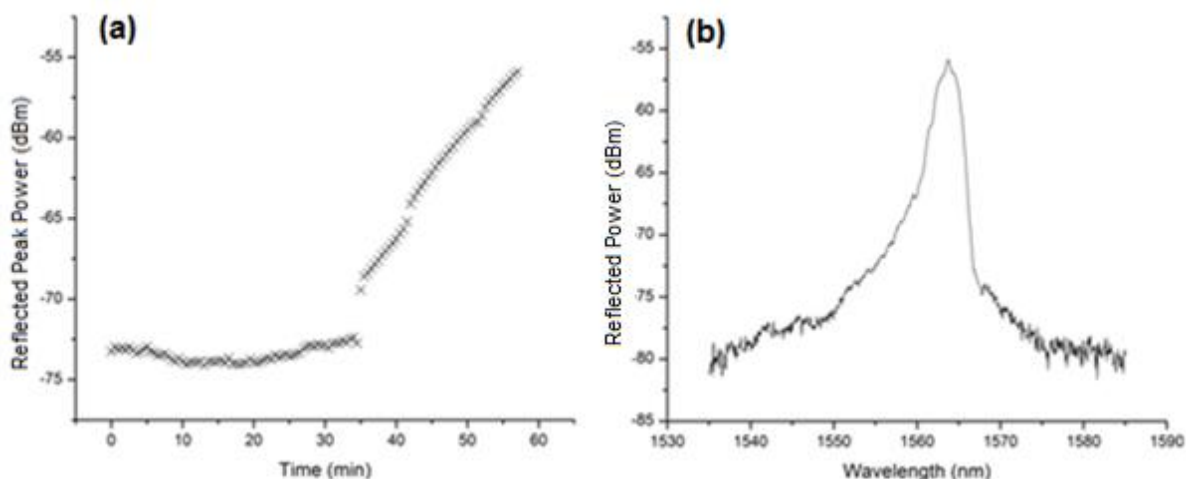


Figure 8-13 a: Growth of first FBG of a WDM sensor. b: Bragg response of first FBG of WDM sensor in the 1550nm spectral region

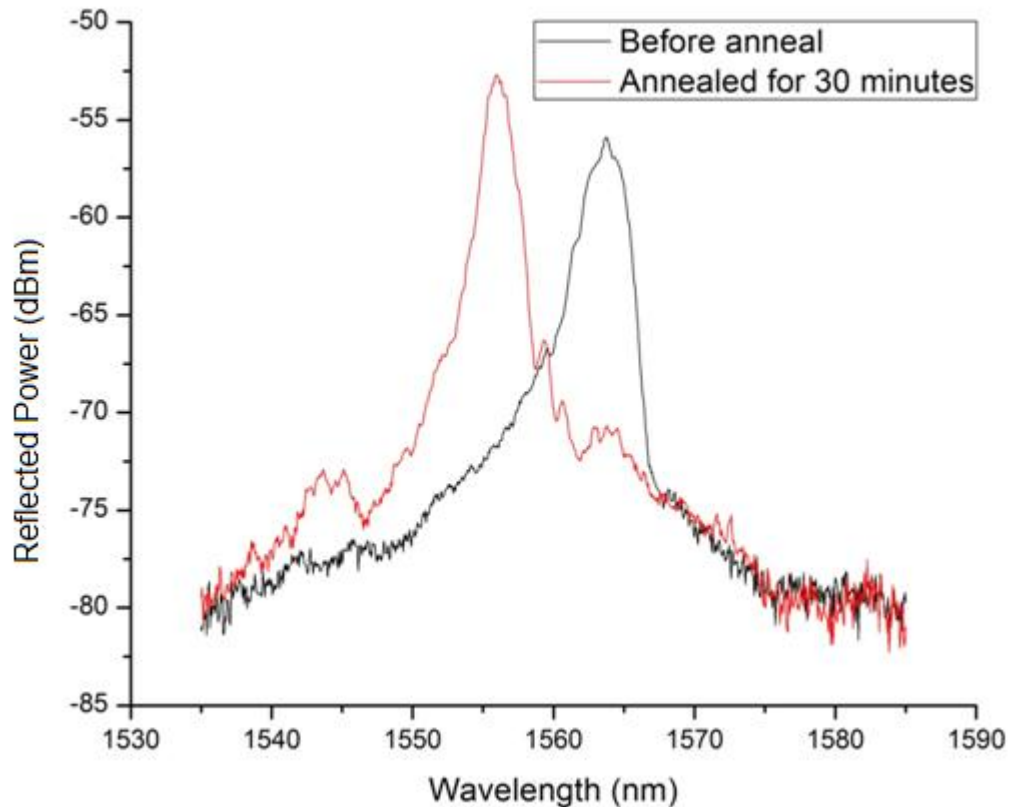


Figure 8-14 Permanent wavelength shift of the first FBG of a WDM sensor fabricated in MMmPOF due to a thermal anneal of 30 minutes at 71°C

A second FBG was then fabricated in the same length of MMmPOF using the same phase mask and fabrication technique. For this fabrication the MMmPOF was turned around on the v-groove plate so the reflected signal was interrogated from the opposite end of the fibre to the previous inscription. The FBG was fabricated 2cm from this end of the fibre, resulting in the two FBGs fabricated so far being separated by 4cm along the fibre length. The MMmPOF core was exposed to the UV interference pattern for 63 minutes when a saturation level of the growth of the peak reflected Bragg signal was achieved with a signal-to-noise ratio of 17dBm, as is shown in Figure 8-15(a). Also seen in Figure 8-15(a) is an initial higher reflected signal, this was due to an increase in the Fresnel reflection at the interface of the butt coupling between the polymer and silica fibres. This was reduced within the first 15 minutes by optimising the coupling between the two fibres. Shown in Figure 8-15(b) is the reflected Bragg responses of the two manufactured FBGs after the fabrication of the second FBG. The Bragg wavelength of the second inscribed FBG2 is 1563.5nm and the bandwidth (FWHM) of the reflected Bragg response is 2nm. Incidentally the Bragg wavelength of the first fabricated FGB1 was 1555nm and the bandwidth (FWHM) of the reflected signal was 2.5nm. This would suggest that the fabrication of the second FBG resulted in the Bragg response of the first to decrease in Bragg wavelength by 1nm and increase in bandwidth by 1nm. However it is felt since the resolution bandwidth of the OSA is 0.5nm and the coupling conditions between the polymer and silica fibres were changed

during optical interrogation this is insignificant. Nevertheless this should be investigated further in future work.

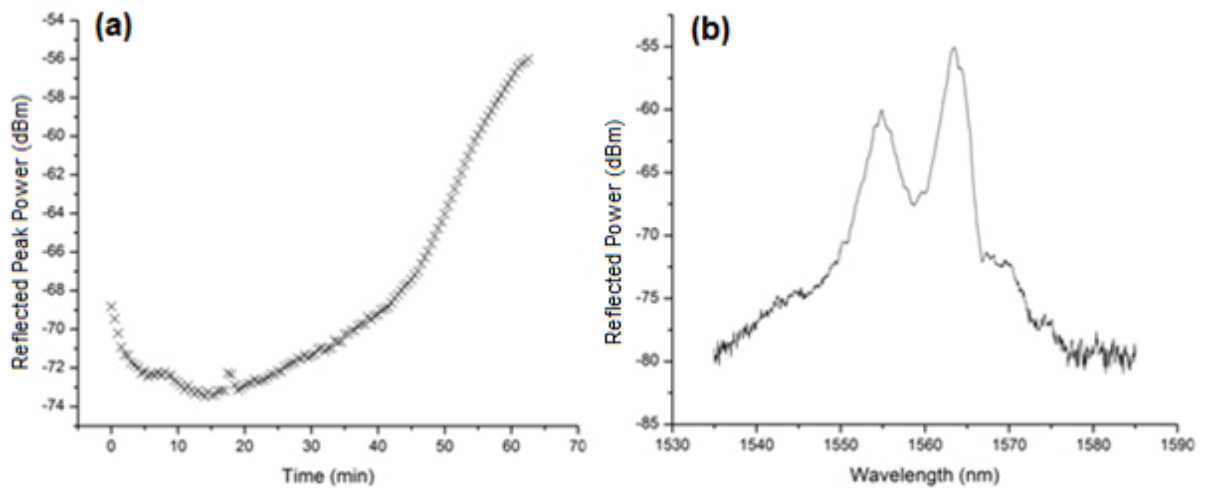


Figure 8-15 (a) the growth curve of FBG2 fabricated for 63 minutes in the MMmPOF (b) the resultant 2 FBG response fabricated in MMmPOF with a spectral response in the 1500nm wavelength range

As the Bragg wavelength of the first fabricated FBG shifted 7.5nm during the 71°C thermal anneal for 30 minutes it suggests the fibre has not yet reached a point where the fibre has stopped shrinking. If compared to Figure 8-12 the total Bragg wavelength was around 15nm for the two FBGs which were thermally annealed in 20 and 30 minute cycles. Consequently an additional wavelength shift could be achieved by shrinking the MMmPOF further, resulting in the current two Bragg responses shown in Figure 8-15 to reduce further in Bragg wavelength.

To prove this the MMmPOF was again rested on a baking tray which was at room temperature and then placed onto the middle shelf of a pre-heated oven at 71°C. The fibre was thermally annealed for 6 hours; this was annealed for longer than previous work so to ensure the saturation level was reached where the POF would not shrink any further in length. This resulted in the permanent Bragg wavelength shifts of both FBG1 and FBG2 as is demonstrated in Figure 8-16. The former now has a Bragg wavelength of 1539.5nm with a bandwidth (FWHM) of 2nm and the later now has a Bragg wavelength of 1543.5nm and a bandwidth (FWHM) of 2.5nm. The permanent thermally annealed induced Bragg wavelength shifts of both FBG1 and FBG2 due to the second anneal is summarised in Table 10.

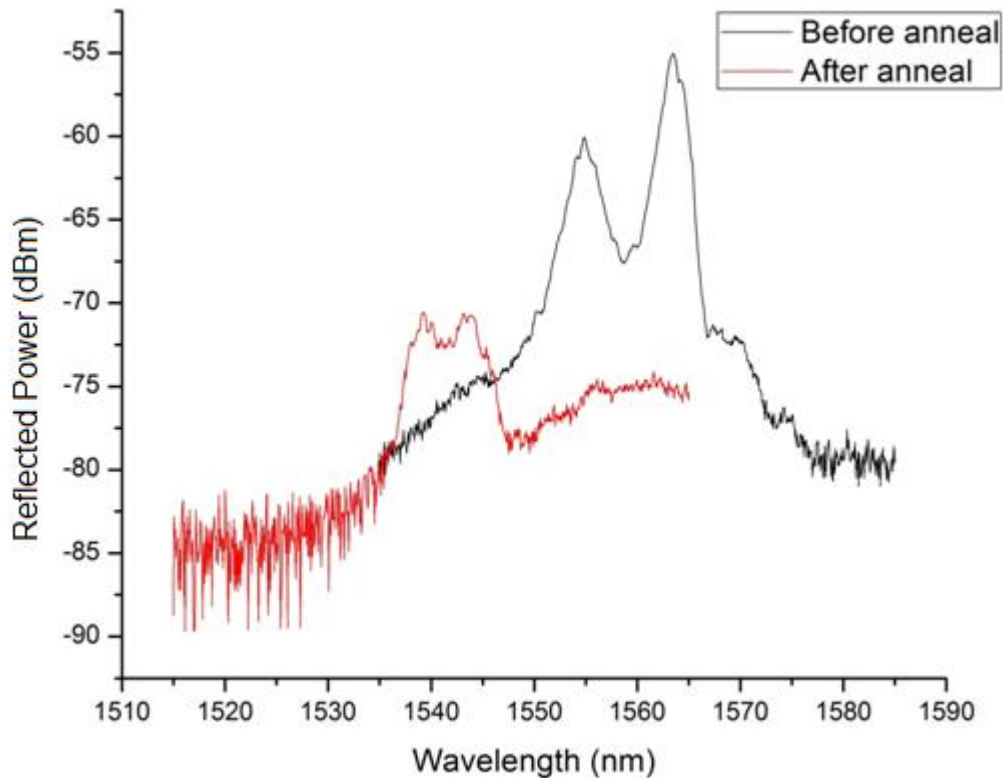


Figure 8-16 Bragg wavelength shift of 2 FBGs, due to thermally annealing the MMmPOF at 71°C for 6 hours

Table 10 Summary of Bragg responses of FBG 1 & 2 after second thermal anneal at 71°C for 6 hours, whilst manufacturing a WDM sensor

	Bragg Wavelength Before Anneal	Bragg wavelength After Anneal	Wavelength Shift
FBG1	1555nm	1539.5nm	-15.59nm
FBG2	1563.5nm	1543.5nm	-20.19nm

It can be seen in Table 10 that the induced Bragg wavelength shift of FBG2 is nearly 5nm larger than FBG1. This was not foreseen as it was expected the thermal anneal would induce a uniform rate of shrinkage resulting in the Bragg wavelength shifts of FBGs 1 and 2 to be similar if not identical. A possible reason for this is the thermal anneal releases stress which remains in the MMmPOF from FBG fabrication, thus the wavelength shift of the most recent fabricated FBG is larger. The different wavelength shifts of FBG1 and FBG2 has resulted in a non-ideal reflected response of the two FBG WDM sensor shown in Figure 8-16. The Bragg response of FBG1 has been virtually washed out by that of FBG2 and thus it would prove difficult to monitor the Bragg wavelength shift of both during any sensing application. Furthermore, the now close proximity between the Bragg wavelengths of FBG1 and FBG2 (4nm) heightens the possibility of crosstalk between the two Bragg responses during a sensing application.

Nevertheless a final third FBG was fabricated in the MMmPOF; this was located between the two previous inscribed FBGs resulting in a separation of 2cm between each FBG along the length of the POF. Monitoring of the growth of FBG3 was achieved via cleaving just under 2cm from one end of the MMmPOF to allow for interrogation previously described. The growth of FBG3 can be seen in Figure 8-17(a), as previously seen in this section the background noise is seen to drop nearly 4dBm as the butt coupling is adjusted between the polymer and silica fibres and the Fresnel reflections from the end of the fibres is reduced. The FBG3's growth was stopped after 60 minutes due to previous experience of FBGs saturating after this, here a signal-to-noise ratio of 9dB was potentially reached. At this point the decision was taken to stop the UV exposure so not to over expose the MMmPOF potentially decreasing the strength of the Bragg response of FBG3 and also affecting the responses of FBG1 and FBG2. The final response of the WDM sensor is demonstrated in Figure 8-17(b), consisting of three Bragg responses. FBG1 has a Bragg wavelength of 1539.5nm and a bandwidth (FWHM) of 2.5nm, FBG2 has a Bragg wavelength of 1543nm and a bandwidth (FWHM) of 2.5nm and finally FBG3 has a Bragg wavelength of 1563nm and a bandwidth (FWHM) of 3.5nm.

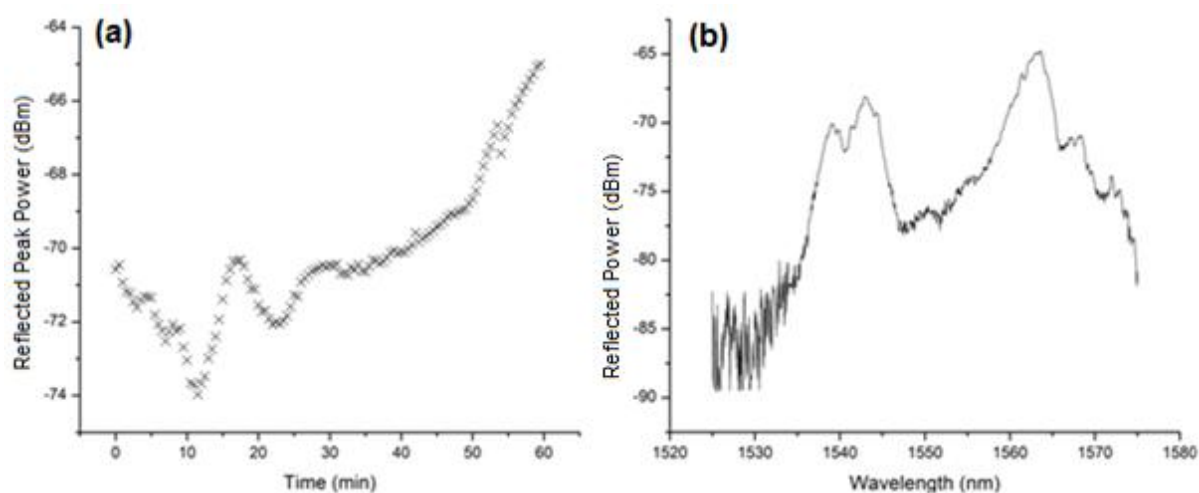


Figure 8-17 (a) The growth curve of the third fabricated FBG of the WDM sensor (b) Spectral response from the first demonstrated WDM sensor fabricated in POF using a single phase mask

Figure 8-17(b) demonstrates the first example of a WDM sensor manufactured in pure PMMA MMmPOF which has been manufactured using a single phase mask. This WDM sensor consists of three FBGs which have been fabricated with the use of thermal annealing to induce a negative Bragg wavelength shift on two of the Bragg responses. This result proves the concept of utilising thermal annealing when manufacturing WDM sensors in POF as was reported in 2011[74]. Thermal annealing allows for additional Bragg responses over a 20nm range without the need to purchase additional phase masks. Further improvement is needed to prevent FBG responses from overlapping and preventing any tracking of each Bragg wavelength during a sensing application. It is felt the second thermal anneal during this work was too long and should be reduced to improve the results, however additional

work is needed to understand the different rates of Bragg wavelength shift of FBG1 and FBG2 during the second thermal anneal.

8.2 Thermal Annealing & WDM Sensors within the 800nm Spectral Region

The work which was completed to map a thermal annealing curve of FBG responses at 1562nm was also completed for FBGs with a response in the 800nm spectral region. Any potential WDM sensors fabricated within this spectral window will take advantage of the lower attenuation of PMMA and will be able to be interrogated over larger lengths of POF of at least tens of centimetres giving rise to more possible applications[41, 59].

8.2.1 Two FBG WDM Sensor Fabricated in the 800nm Spectral Region

At the outset, it was investigated whether two individual FBGs (FBG1 and FBG2) could be fabricated within the same length of PMMA based MMmPOF and their reflected Bragg responses both monitored. As was demonstrated in Chapter 6, two phase masks are available that would generate Bragg responses at different wavelengths within the 800nm region, these were first used without the use of any thermal annealing.

Firstly FBG1 was fabricated in the MMmPOF with a Bragg wavelength of 861nm and a bandwidth (FWHM) of 0.5nm, using a phase mask with a surface relief pattern period of 580nm. Secondly FBG2 was fabricated in the same length of POF with a Bragg wavelength of 828nm and a bandwidth (FWHM) of 0.5nm using a phase mask with a surface relief pattern period of 557.50nm. The length of the MMmPOF was 8cm, FBG1 was fabricated 2cm from the end of the POF and FBG2 was fabricated 2cm from the opposite end of the POF, enabling the monitoring of the growth of each FBG, thus the two FBGs were separated by 4cm. FBG1 had a signal-to-noise ratio of 16dBm, which was achieved after a 50 minute UV exposure. FBG2 had a signal-to-noise ratio of 7dBm; the UV exposure was stopped after 60 minutes, at this point the growth had appeared to have halted and over exposure was not desired which may have resulted in either of the Bragg responses becoming messy. The reflected Bragg responses of the WDM sensor are shown in Figure 8-18, this were captured on an OSA (HP 70951B) with a bandwidth resolution of 0.5nm.

This initial result would suggest that WDM sensors are possible at lower wavelengths in the MMmPOF. Furthermore, the smaller bandwidths (FWHM) of less than 1nm have the potential to enable clearer individual Bragg responses of a WDM sensor and thus allow for easier tracking of Bragg wavelength shifts during a sensing application.

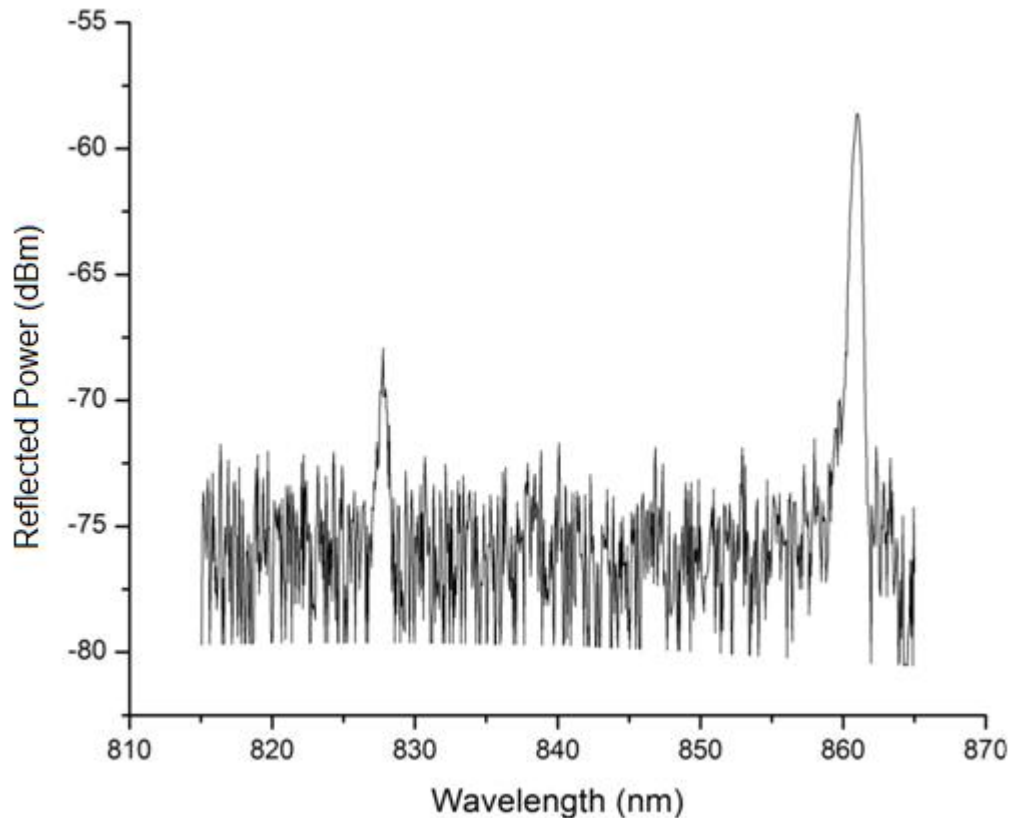


Figure 8-18 A WDM sensor made of 2 FBGs fabricated in MMmPOF using individual phase masks

8.2.2 Characterisation of Thermal Annealing of FBG Responses within the 800nm Spectral Region

The next step in this work was to monitor the thermal annealing induced Bragg wavelength shift over time. Initially this was completed the same way as was done with FBGs with a Bragg response in the 1550nm spectral region. Three FBGs were fabricated in individual 8cm long lengths of the PMMA MMmPOF, situated 2cm from one end of the POF. The 3 reflected FBG responses used in these experiments are shown in Figure 8-19, before any thermal annealing. All reflected Bragg signals were captured in reflection using a multimode (50/125 μ m) 2x1, 50:50 silica coupler at 800nm and captured on an OSA (HP 70951B) with a bandwidth resolution of 0.5nm. Each FBG was UV inscribed for 90 minutes where a maximum peak reflection was seen and a saturation level of the peak power was achieved. The inscription technique described in Chapters 4 and 6 with a HeCd laser (Kimmon Koha Co, Ltd, IK3301R-G) was used with a phase mask that had a surface relief pattern with a period (Λ_{pm}) of 580nm, the three Bragg responses are summarised in Table 11.

Each FBG was repeatedly thermally annealed at 80°C for various amounts of time; FBG1 was annealed in 10 minute steps on 9 occasions totalling 90 minutes, FBG2 was annealed in 20 minute steps on 6 occasions totalling 120 minutes and FBG3 was annealed in 30 minute steps on 4 occasions totalling 120 minutes. Between each annealing step the

reflected Bragg response of the FBG was captured at room temperature using the butt coupling technique between the polymer fibre and silica coupler on a translation stage. The thermal annealing was completed in a pre-heated 80°C oven, the MMmPOF was first rested on a baking tray which was at room temperature and this was then placed on the middle shelf of the oven.

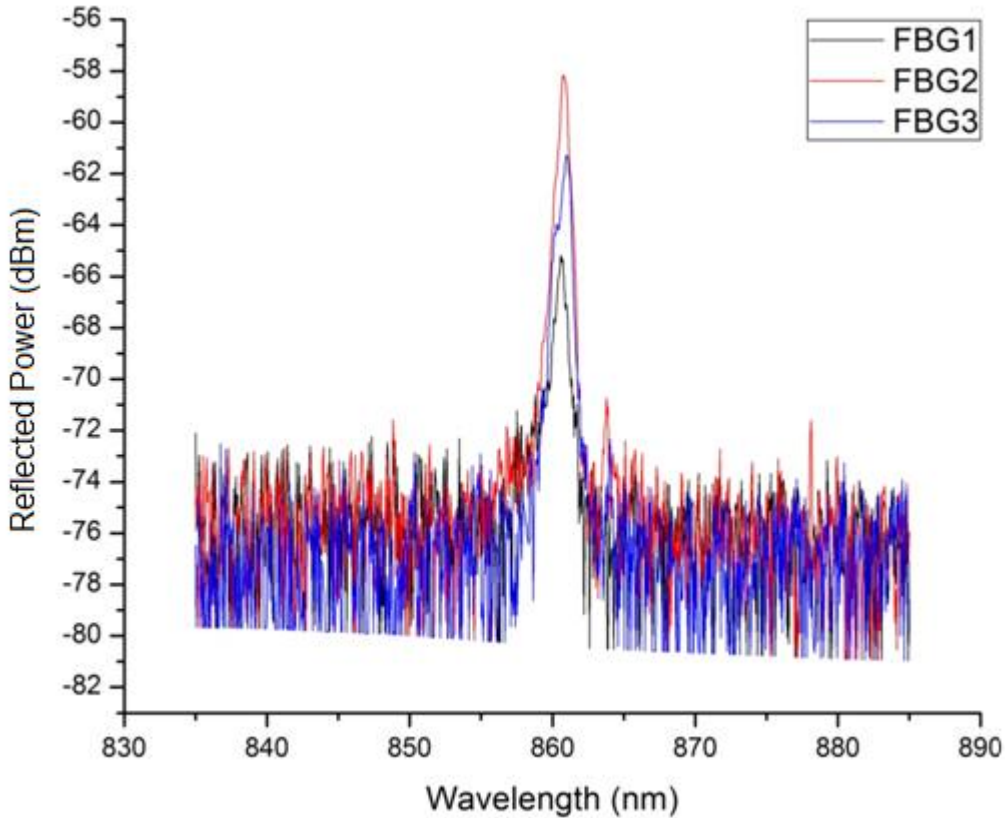


Figure 8-19 Three reflected responses within the 800nm spectral region of FBGs used in thermal annealing characterisation

Table 11 Summary of the Bragg responses of the seen in Figure 8-19

	Bragg Wavelength	Bandwidth (FWHM)
FBG1	860.5nm	1nm
FBG2	861nm	0.5nm
FBG3	861nm	1nm

The Bragg wavelength of each FBG at the different intervals of thermal annealing can be seen in Figure 8-20. It can be seen that the 80°C thermal annealing induces a permanent negative Bragg wavelength shift on all three FBGs and thus suggested the MMmPOF had decreased in length. The longer the time period of each individual step, the further the Bragg wavelength appeared to shift. This may be due to the fibre and baking tray having more time to reach the 80°C in addition to allowing the oven to return to 80°C once the oven had been opened to place in the POF. If the Bragg wavelengths of the three FBGs are compared after

90 minutes, then it can be seen that leaving the POF in the oven 10 minutes longer on each occasion results in a further 5nm Bragg wavelength shift. It would appear FBG1 is nearing a maximum Bragg wavelength shift of 12nm after 90 minutes. Whereas FBG3 has experienced a permanent shift of 18nm after 120 minutes but does not seem to have reached a constant wavelength. This needs to be considered when using thermal annealing to tune a Bragg response to a particular desired Bragg wavelength, for example placing the MMmPOF in the oven for two periods of 10 minutes will not have the same effect on the Bragg wavelength as placing it in the oven for a single 20 minute period. It is believed that this effect was also seen during the similar experiment using the FBGs with a Bragg response in the 1550nm spectral region shown in Figure 8-12. There the oven was heated to 70°C, whereas during this work the oven was heated 80°C³, hence the larger variation in the induced Bragg wavelength shift due to more time needed for the temperature to rise an additional 10°C.

Nevertheless this section has proved the permanent Bragg wavelengths within the 800nm region are achievable through thermal annealing. Additionally if this method of cycled annealing were chosen to tune a Bragg wavelength then it is felt it could be used reliably once full characterisation of the permanent Bragg wavelength shift induced by the varied amount of timed cycles were completed.

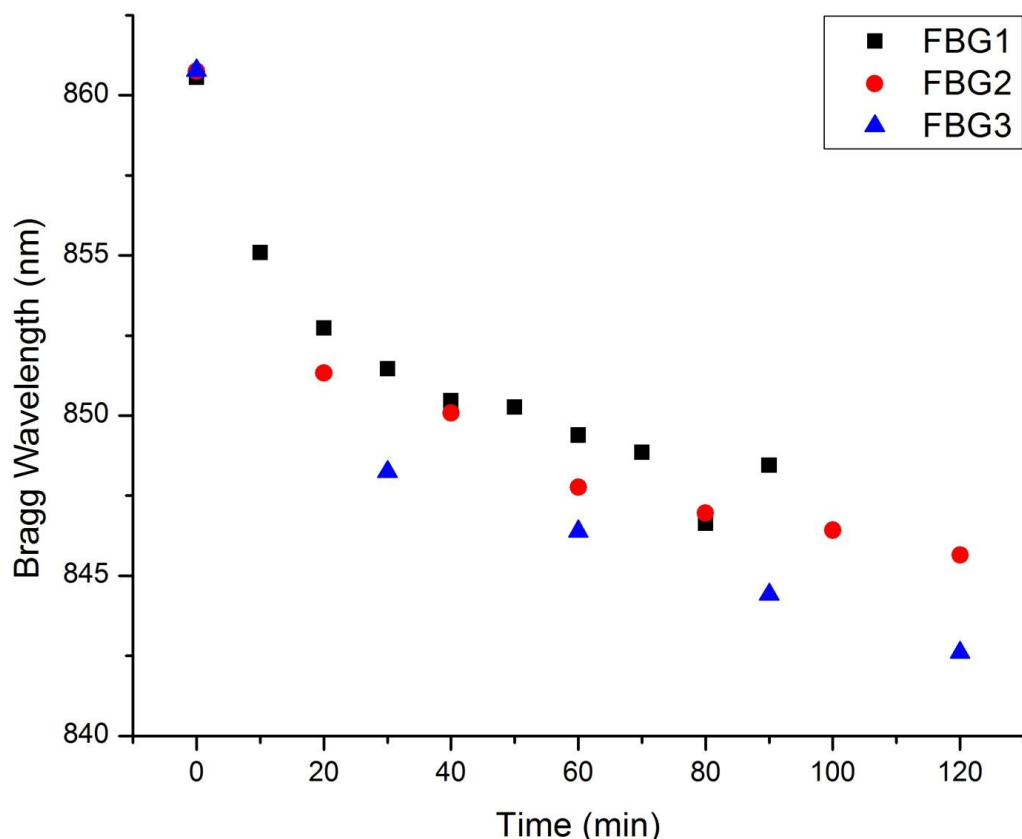


Figure 8-20 The Bragg wavelength shift of each FBG at the different intervals of thermal annealing - 10 minutes, • 20 minutes, ▲ 30 minutes

³ Found difference in oven temperature output readings resulted in the two temperatures used

8.2.3 Continuous Monitoring of the Bragg Wavelength Shift Due to Thermal Annealing

Ideally the thermal annealing curve shown in Figure 8-20 would be captured in real time rather than cycling the amount of time the MMmPOF is left in the oven. Previously when fabricating FBGs with a response in the 1550nm spectral region this was not achievable due to the short lengths required to interrogate a Bragg reflection, because of this the adhesive splice which would need to be positioned in the oven, however the glass transition temperature of the adhesive is 43°C[70]. However, the breakthrough of the fabrication of FBGs in the MMmPOF with a Bragg response within the 800nm spectral region[71] allows for reflected Bragg responses to be monitored over lengths of at least 20cm, as was demonstrated in Chapter 6. This gives the possibility to lower the MMmPOF into an oven via an access hole whilst still protecting the adhesive splice and thus permitting continuous monitoring of the Bragg wavelength shift due to thermal annealing.

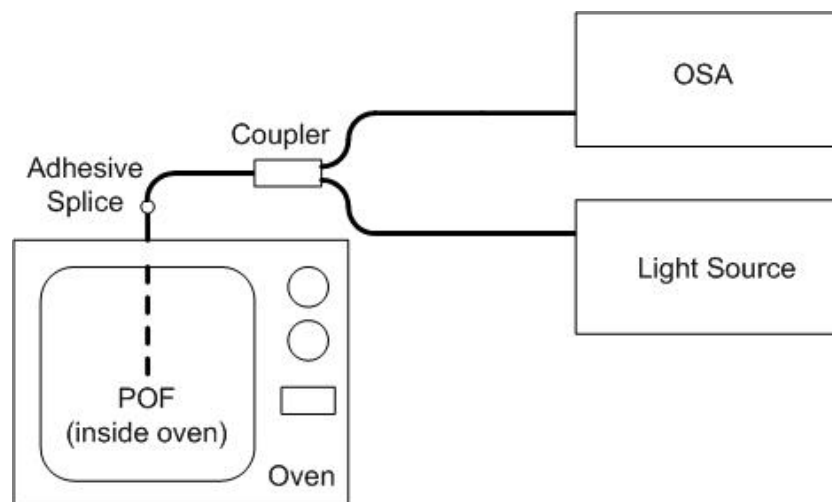


Figure 8-21 Experimental setup to monitor the real time Bragg wavelength shift due to thermal annealing

Therefore work was carried out to monitor the Bragg wavelength shift of a reflected Bragg signal fabricated in the MMmPOF. The MMmPOF was permanently spliced to a silica pigtail using the technique described in Chapter 5 and connected to a silica multimode (50/125 μm) 2 \times 1 coupler, with a coupling ratio of 50:50 at 800nm, as shown in Figure 8-21. This enabled the real time monitoring of the induced Bragg wavelength shift due to thermal annealing when the oven was pre-heated to 80°C. The FBG was fabricated in a 20cm length of the MMmPOF and was situated 2cm from the tip of the fibre suspended within the oven; a 10cm length of fibre was approximately within the oven.

The reflected FBG response once permanently spliced to a silica pigtail is shown in Figure 8-22, the grating was fabricated by exposing the core of the MMmPOF to the UV interference pattern for 90 minutes. The HeCd UV laser and a phase mask with a period (Λ_{pm}) of 557.50nm were used with the inscription technique described in Chapter 6 to fabricate the FBG. The reflected response had a Bragg wavelength of 827.5nm and a

bandwidth (FWHM) of 0.5nm. A signal-to-noise ratio of 13dBm was observed at this stage of the experiment.

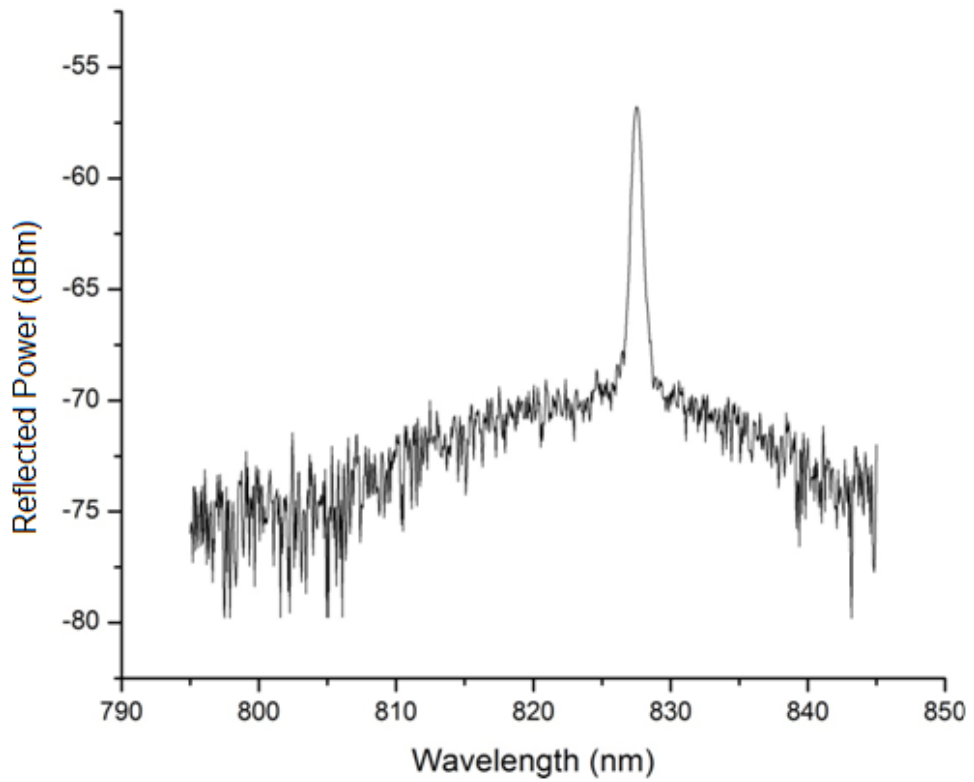


Figure 8-22 Reflected Bragg response of FBG to be used in real time monitoring of thermal annealing at 80°C

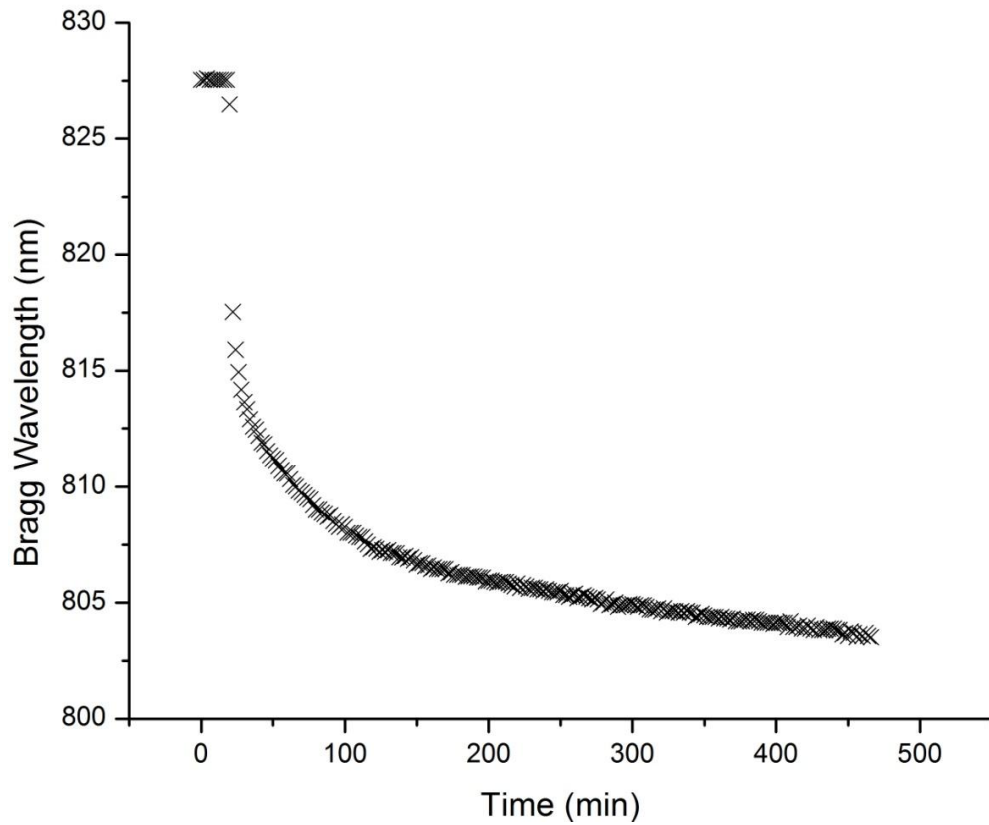


Figure 8-23 Real time monitoring of the Bragg wavelength of a FBG fabricated in MMmPOF which was thermally annealed at 80°C for 7.5 hours.

Shown in Figure 8-23 is the monitored reflected Bragg wavelength of the FBG whilst in the 80°C heated oven for 7.5 hours. For the first 20 minutes the reflected Bragg response was captured at room temperature so to gain an understanding of any possible wavelength shift due to an additional component. After this the MMmPOF was lowered into the oven and the effect on the Bragg wavelength was seen immediately with a Bragg wavelength shift of at least 10nm in the first 5 minutes. A total Bragg wavelength shift of 24nm was observed over the 7.5 hour thermal anneal at 80°C. Provided the characterisation curve is repeatable then this offers a tool to permanently shift a Bragg response to a particular wavelength to coincide with a light source for example or to allow for a Bragg response to be shifted and for an additional FBG to be fabricated with the same phase mask thus creating a WDM sensor, as was documented in [85]. Figure 8-24 suggests that the negative Bragg wavelength shift has not finished possibly due because the fibre has not finished shrinking. It is conceivable the fibre would not stop shrinking for a number of days.

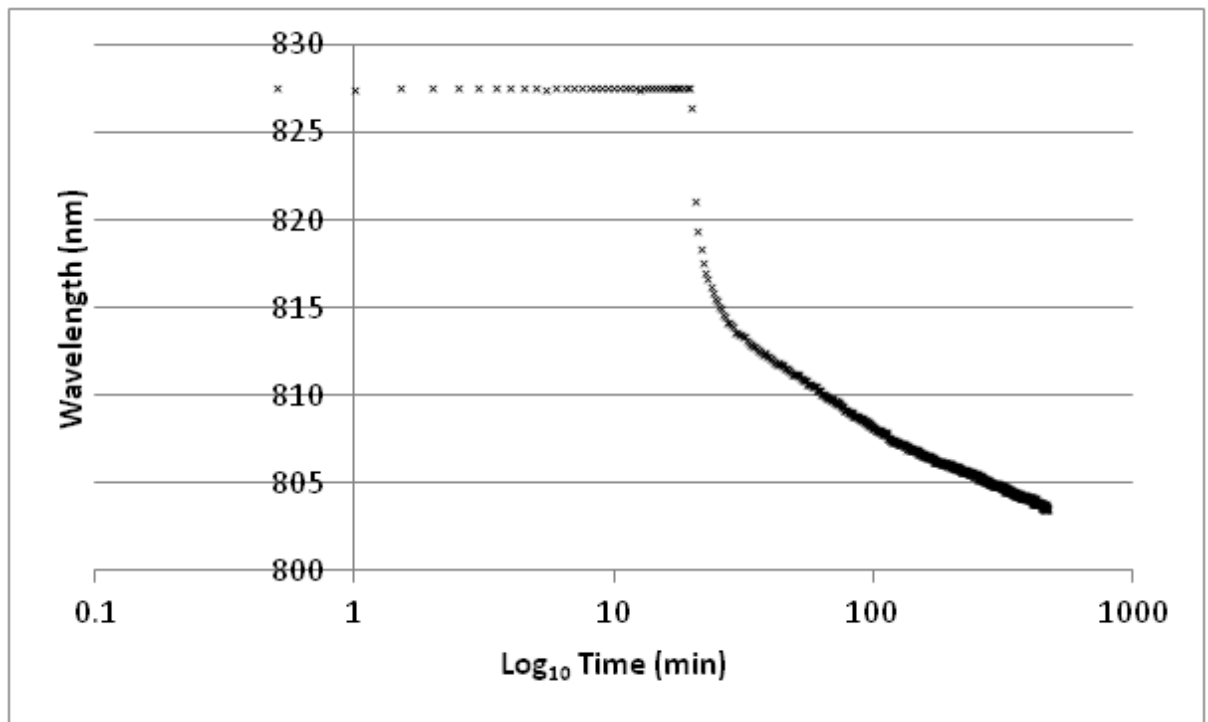


Figure 8-24 Bragg wavelength against time on a log scale monitoring of the Bragg wavelength of a FBG fabricated in MMmPOF which was thermally annealed at 80°C for 7.5 hours.

However if thermal annealing is to be used as a tool to induce a permanent negative shift of a Bragg response then the effect of returning to room temperature of the Bragg wavelength needs to be considered. Figure 8-25 shows the positive Bragg wavelength shift experienced once the oven was turned off after the 7.5 hour thermal anneal. After the oven was turned off for 1 minute the oven door was opened. The temperature inside the oven was monitored with a thermocouple sensor, which indicated that room temperature was reached after 13 minutes. During this time the Bragg wavelength increased by approximately 1nm, thus suggesting the POF relaxed once the temperature decreased but also may demonstrate the

change in relative humidity of the environment. This may indicate that stress between the molecule chains within the POF which was introduced during the drawing of the fibre was not totally dissipated. As was suggested by Carroll not all the induced stress between the aligned molecule chains would be totally dissipated until the glass transition temperature was achieved (105°C)[24, 39]. After the monitoring of the first 20 minutes, the reflected Bragg wavelength was further monitored for the next 48 hours at 10 minute intervals, as shown in Figure 8-26. Here, a further positive wavelength shift of around 1nm was seen, again suggesting stress remained between the molecular chains of the polymer. Additionally, Figure 8-26 shows no long term trend of returning Bragg wavelength; rather it appears to follow the reoccurring environmental cycle of the laboratory. This may also explain the positive Bragg wavelength, after the thermal annealing the MMmPOF will also be exposed to the relative humidity of the laboratory. Therefore, this may cause the MMmPOF to swell slightly with water absorbed into the fibre from the laboratory environment, something which is discussed in further detail in Chapters 3 and 9.

Moreover, it is clearly seen in Figure 8-23 and Figure 8-24 that the Bragg wavelength has not stopped shifting and a point had not been reached where the MMmPOF had stopped shrinking. Therefore, this work was continued in the next section where a FBG fabricated in the MMmPOF was thermally annealed for 24 hours.

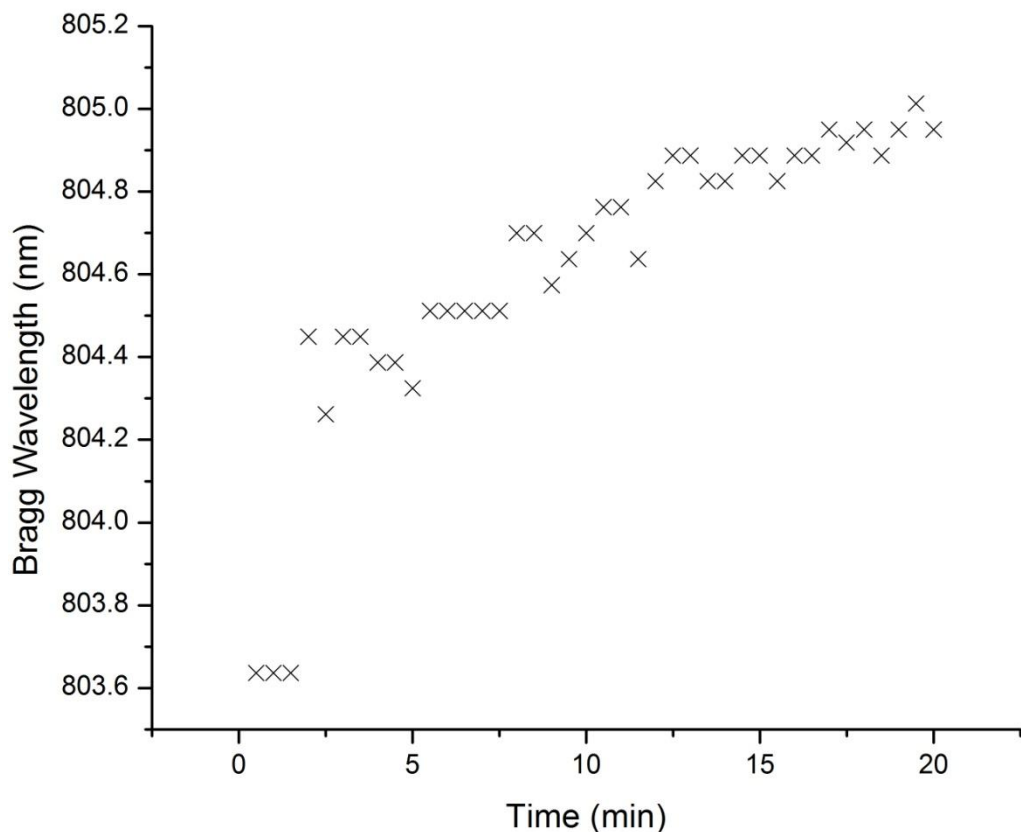


Figure 8-25 Immediate effect on Bragg wavelength after thermal annealing, whilst returning to room temperature

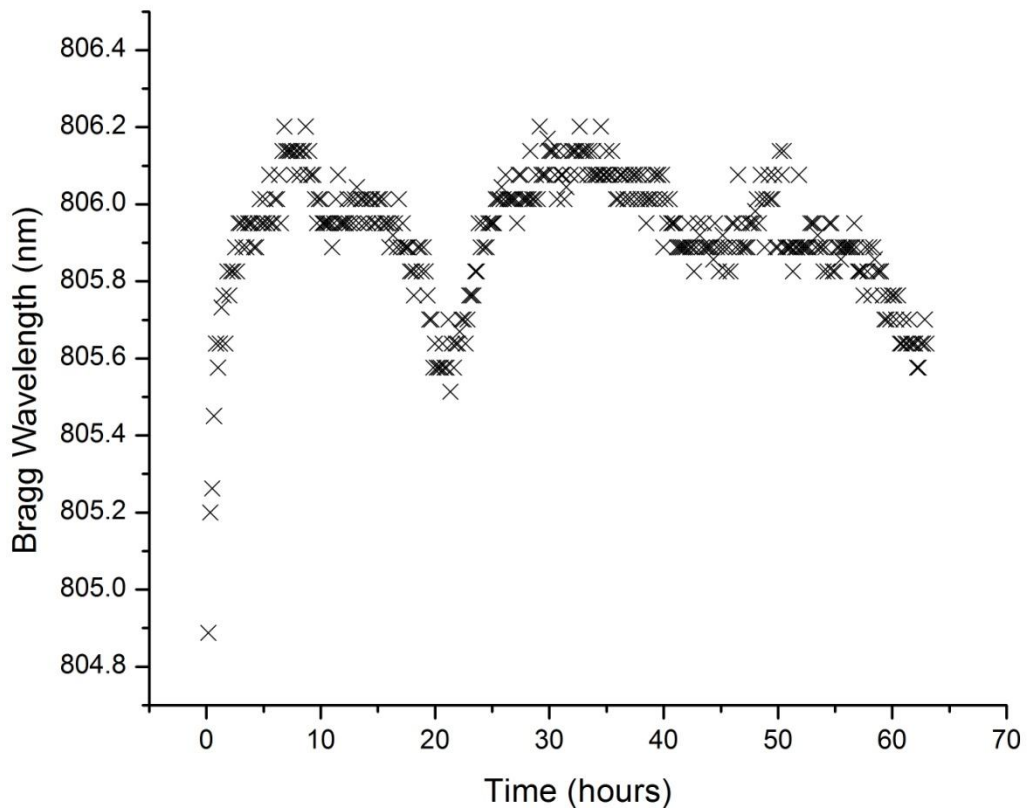


Figure 8-26 Change in Bragg wavelength following thermal annealing, once at room temperature

8.2.4 24 Hour Thermal Annealing of a FBG Fabricated in the MMmPOF

In an attempt to reach a situation where during thermal annealing the shrinking of the fibre length stops and hence the shift in Bragg wavelength ceases, the MMmPOF was thermal annealed for 24 hours. The decision was made to use a temperature of 70°C so to preserve the MMmPOF from being destroyed over a time period where there would be no manual monitoring.

For this experiment an FBG was again fabricated into a 20cm length of the MMmPOF located 2cm from the tip of the POF. The same experimental setup shown in Figure 8-21 is used to monitor the reflected Bragg response whilst in the oven. The FBG was fabricated once more by exposing the core of the fibre to a UV interference pattern for 90 minutes using the HeCd laser and a phase mask with a surface relief pattern period of 580nm. The produced Bragg response is shown in Figure 8-27, with a Bragg wavelength of 860.5nm and a bandwidth (FWHM) of 1.5nm, an OSA with a bandwidth resolution of 0.5nm was used. A Bragg signal-to-noise ratio of 11dBm was measured, which is adequate for this experiment and the monitoring of the Bragg wavelength shift.

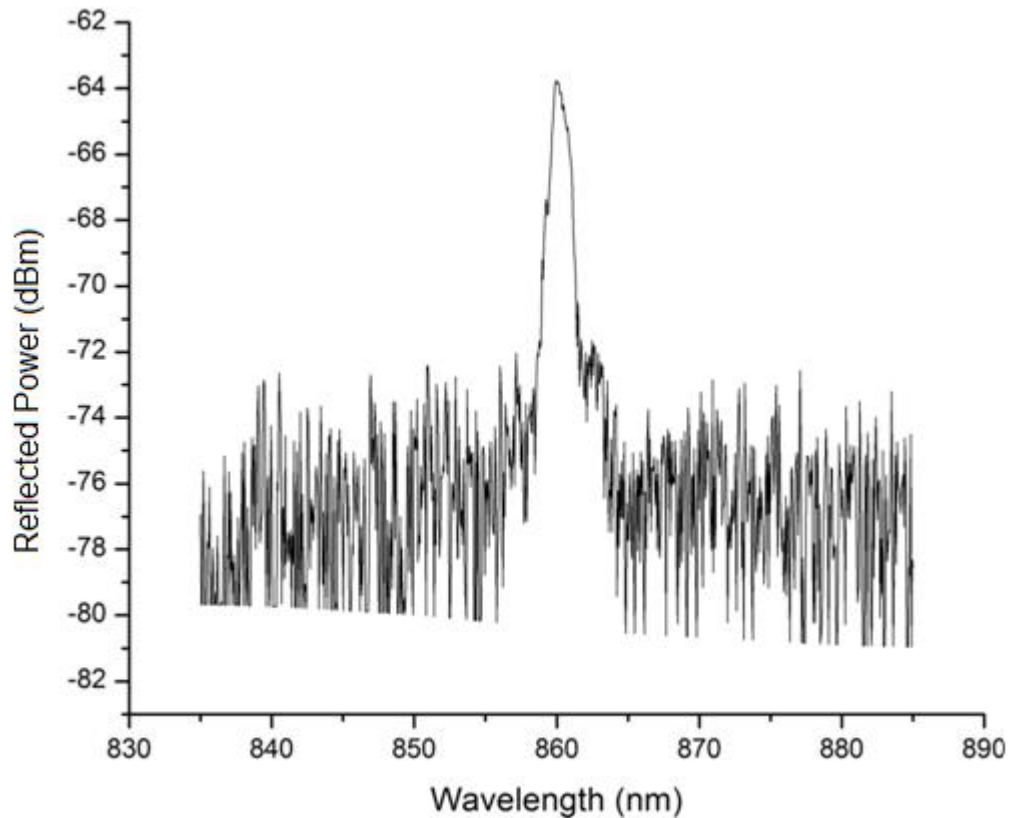


Figure 8-27 Reflected Bragg response of a FBG fabricated in MMmPOF prior to 70°C thermal annealing for 24 hours

The reflected Bragg wavelength of the FBG was captured at room temperature for the first 60 minutes, so to test the stability of the optical system. The MMmPOF was then lowered into the 70°C pre-heated oven, which generated an immediate negative Bragg wavelength shift as can be seen in Figure 8-28. The MMmPOF was then thermally annealed for 24.5 hours which resulted in a negative Bragg wavelength shift of 18nm. After this the oven was turned off and the door opened, resulting in the Bragg wavelength to increase by 1.5nm in the following 60 minutes. Again this is likely to be a result of the POF returning to the relative humidity of the laboratory.

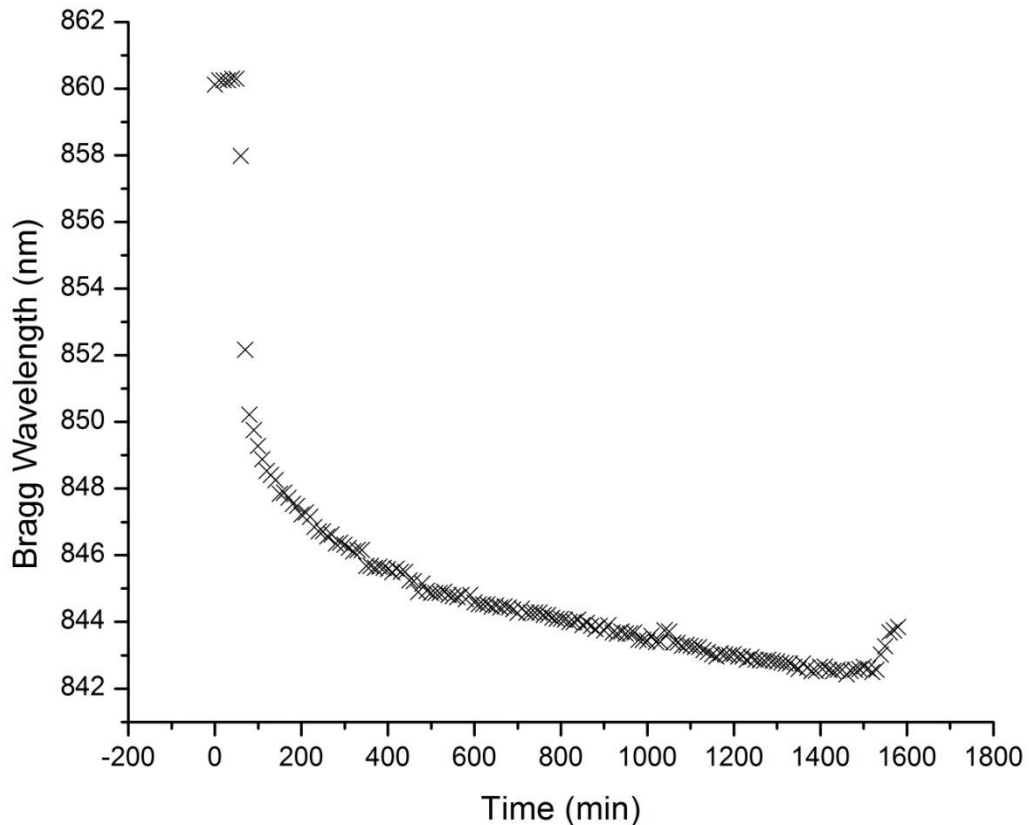


Figure 8-28 Real time monitoring of the Bragg wavelength of a FBG fabricated in MMmPOF which was thermally annealed at 70°C for 24 hours.

It is unsurprising to see that the Bragg wavelength shift does not appear to have reached a stage of stopping in Figure 8-28. The total Bragg wavelength shift was 18nm, which was 6nm short of the shift seen when thermally annealing for 7.5 hours at 80°C which suggests that it is still capable of shrinking further in length. However it is felt that the wavelength shift seen after 7.5 hours at 80°C may not be achievable if annealed for one week or more at 70°C as the increase in temperature provides the energy needed to relax the alignment of the molecule chains further. Annealing at 80°C releases more of the trapped stress between the polymer molecule chains than at 70°C, and for all the stress to be removed the fibre needs to be heated at the glass transition temperature ($T_g = 103^\circ\text{C}$ for PMMA[39]), only here will the molecular chains become free to move across each other. With the current results it is felt that if either of the MMmPOFs in the previous two experiments were left for extensive periods of time in excess of 1 week would still not result in the maximum amount of shrinkage possible of the POF length and thus the maximum Bragg wavelength shift. Additionally it is felt that thermal annealing at 70°C would not result in the same Bragg wavelength shift as that induced by thermal annealing at 80°C if both were annealed for one week or more. To fully understand this, Bragg wavelength shifts need to be monitored over long thermal annealing periods of at least one week, at various temperatures up the glass transition temperature, which for PMMA is 103°C[39]. Additionally it should be highlighted that the thermal annealing curves are a function of the drawing parameters used to

manufacture the fibre[54], therefore the results found here are likely to be different to any taken using different POF which has been manufactured under different parameters.

Nevertheless it should be highlighted that the Bragg wavelength of FBGs fabricated in the PMMA MMmPOF can be tuned in at least a -18nm spectral range by thermal annealing up to 24 hours at either 70-80°C. Thermal annealing can be used to shift a Bragg response from either FBG fabricated with a Bragg length of 828nm or 860nm to coincide with a specific light source that may be needed as part of a sensing application.

Furthermore there is the potential of manufacturing WDM sensors in the 800nm spectral region. Figure 8-18 demonstrated where a WDM sensor was manufactured from two FBG fabricated from individual phase masks. Using thermal annealing will allow for the fabrication of additional FBGs as part of the WDM sensor without the need for additional phase masks. The following sections of this chapter will explore this further.

8.3 WDM Sensors Manufactured in the 800nm Spectral Region

In this section the initial attempt to manufacture a WDM sensor consisting of 3 FBGs, by only using a single phase mask is described. To begin with a FBG (FBG1) was fabricated in a 20cm length of the MmmPOF, situated 2cm from one of the cleaved ends of the POF. FBG1 was fabricated by exposing the core of the fibre to the UV interference pattern generated from the HeCd UV laser (Kimmon Koha 1K3301R-G) and a phase mask ($\Lambda_{pm} = 557.50\text{nm}$) for 90 minutes. The reflected Bragg response of FBG1 is shown Figure 8-29(a), the response has a Bragg wavelength of 828.5nm and a bandwidth (FWHM) of 0.5nm. All reflected Bragg responses were interrogated with the Amonics 800nm Benchtop super wide band wavelength source (ASLD-CWDM-3-B-FA) and captured on an OSA (HP 70951B) with a bandwidth resolution of 0.5nm. The reflection was captured via a 2x1 silica multimode (50/125 μm) coupler with a 50:50 splitting ratio at 800nm. A signal-to-noise ratio of 15dBm was measured.

The MMmPOF was then placed onto a baking tray at room temperature and then placed onto the middle shelf of an 80°C pre-heated oven for 10 minutes. This resulted in FBG1 having a Bragg wavelength shift of 3.0nm as the Bragg wavelength of the reflected response after annealing was 825.5nm and the bandwidth (FWHM) was 1nm, as shown in Figure 8-29(b). The signal-to-noise ratio has been reduced to 8dBm but it is felt this is more likely to be because of the difference in cleaving quality of the POF end face rather than a weakening of the reflected Bragg response due to thermal annealing.

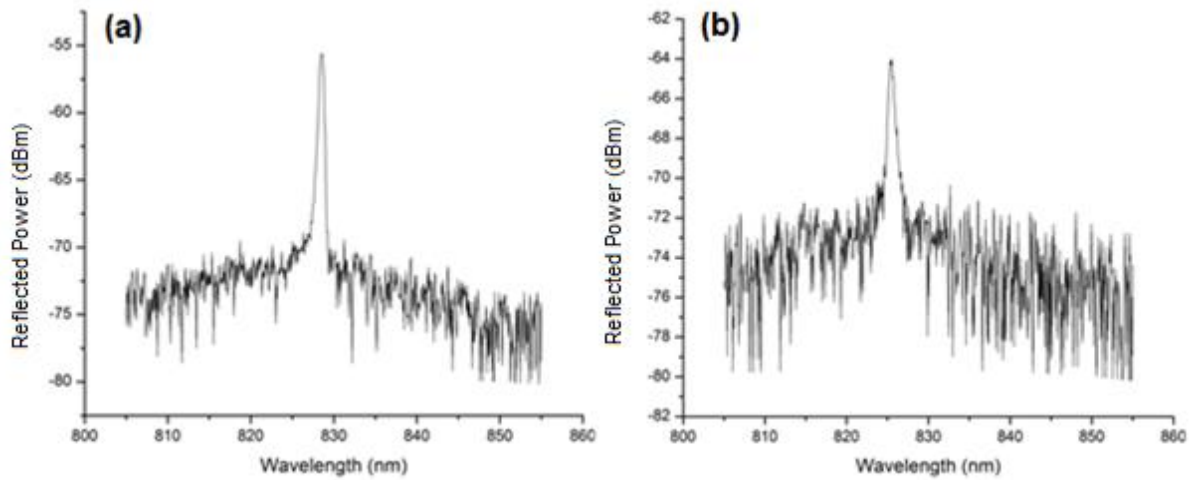


Figure 8-29 (a) Reflected Bragg response of the first fabricated FBG (FBG1) (b) Bragg response of FBG1 after thermally annealed at 80°C for 10 minutes

A second FBG (FBG2) was then fabricated in the MMmPOF again using the same UV laser and phase mask. The core of the POF was exposed for 90 minutes to the UV interference pattern. FBG2 was situated 2cm inside FBG1 along the length of the fibre. As the total length of the fibre was 20cm the fibre could not be rotated and interrogated from the opposite of the fibre whilst keeping each grating relatively close together, therefore FBG2 was fabricated without monitoring of the growth of the Bragg response. After fabrication the reflected Bragg responses were interrogated and are shown in Figure 8-30(a). FBG1 became almost undetectable for reasons unknown, the signal-to-noise ratio of FBG1 was reduced to around 2dBm and had a Bragg wavelength of 825nm. FBG2 had a Bragg wavelength of 827.5nm and a bandwidth (FWHM) of 0.5nm. FBG2 had a measured signal-to-noise ratio of 14dBm.

The MMmPOF was again thermally annealed at 80°C. The POF was rested onto a baking tray at room temperature and placed into the pre-heated oven for 30 minutes. The resultant Bragg responses of FBG1 and FBG2 can be seen in Figure 8-30(b). FBG1 now has a Bragg wavelength of 822nm and FBG2 currently has a Bragg wavelength of 824.00nm. FBG1 had shifted 3nm, whereas FBG2 had shifted 3.5nm. The difference in Bragg wavelength shifts between FBG1 and FBG2 with the most recently fabricated FBG shifting further is something that was seen when manufacturing WDM sensors in the 1550nm spectral region using a single phase mask. A possible reason for this difference is maybe because the thermal annealing is releasing stress which was gained during the FBG fabrication. Equally with a bandwidth resolution of 0.5nm used on the OSA the difference in the Bragg wavelength shifts may be insignificant.

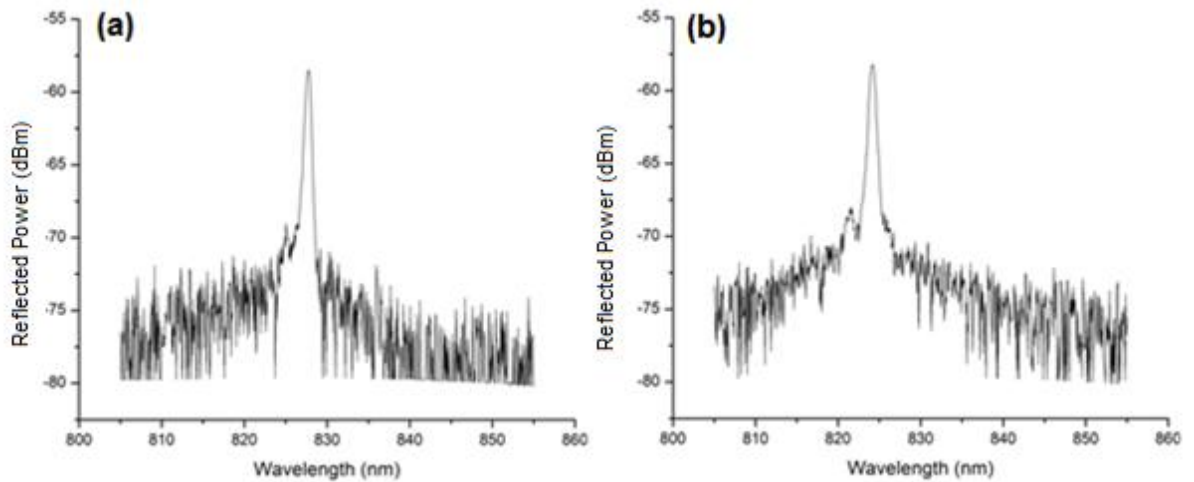


Figure 8-30(a) Bragg response of the WDM sensor after fabrication of the second FBG (FBG2) (b) Bragg response after the second thermal anneal at 80°C for 30 minutes

A third FBG (FBG3) was fabricated into the same length of the MMmPOF using the same UV HeCd laser and the same phase mask. FBG3 was located 2cm inside FBG2 and 4cm from FBG1; again FBG3 was fabricated by exposing the core of the MMmPOF to the UV interference pattern for 90 minutes. The reflected Bragg responses of the 3 FBGs is shown in Figure 8-31(a). The Bragg response of FBG1 can now not be observed. FBG2 has a Bragg wavelength of 824.0nm and a bandwidth (FWHM) of 1.0nm and FBG3 had a Bragg wavelength of 828nm and a bandwidth (FWHM) of 1.00nm. FBG2 had a measured signal-to-noise ratio of 12dBm and FBG3 had a signal-to-noise ratio of 11dBm.

The MMmPOF was thermally annealed again for one final time at 80°C; again the POF was placed on the baking tray at room temperature and placed in the preheated oven for 2 hours. The resultant Bragg responses of the FBGs after annealing is shown in Figure 8-31. FBG2 now has a Bragg wavelength of 823nm and FBG3 has a Bragg wavelength of 824.5nm. Therefore through the course of the third thermal anneal the Bragg wavelength of FBG2 shifted 1.00nm and FBG3 shifted 3.50nm. Here, there appears to be a clearer difference between the Bragg wavelength shifts of FBG2 and FBG3 due to the 2 hour thermal anneal. Again this was something that was not expected but appears to be becoming a repeatable effect.

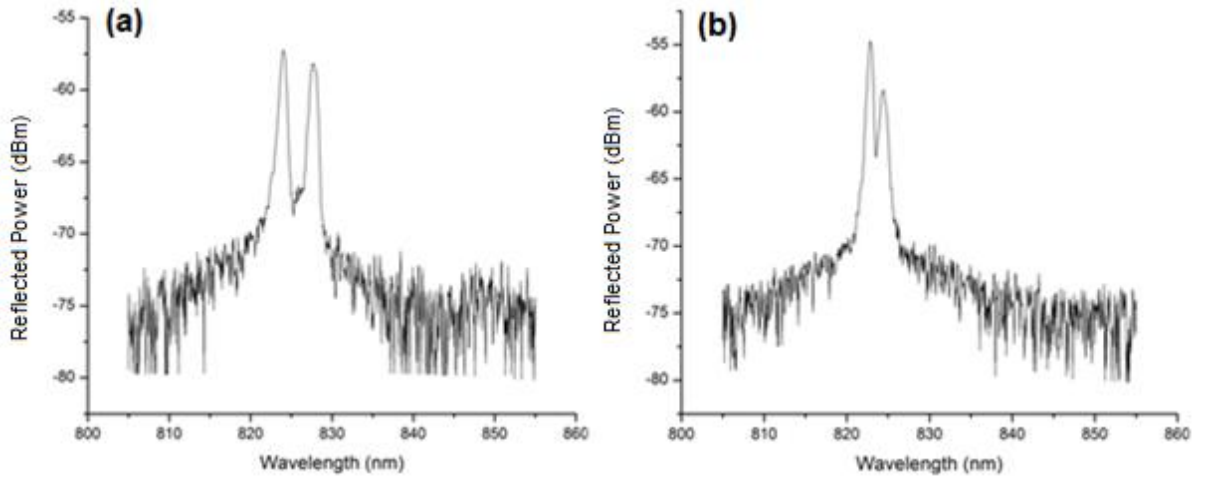


Figure 8-31(a) Reflected Bragg responses of the WDM sensor after the fabrication of the third FBG (FBG3) (b) Reflected response after the third thermal anneal at 80°C for 2 hours

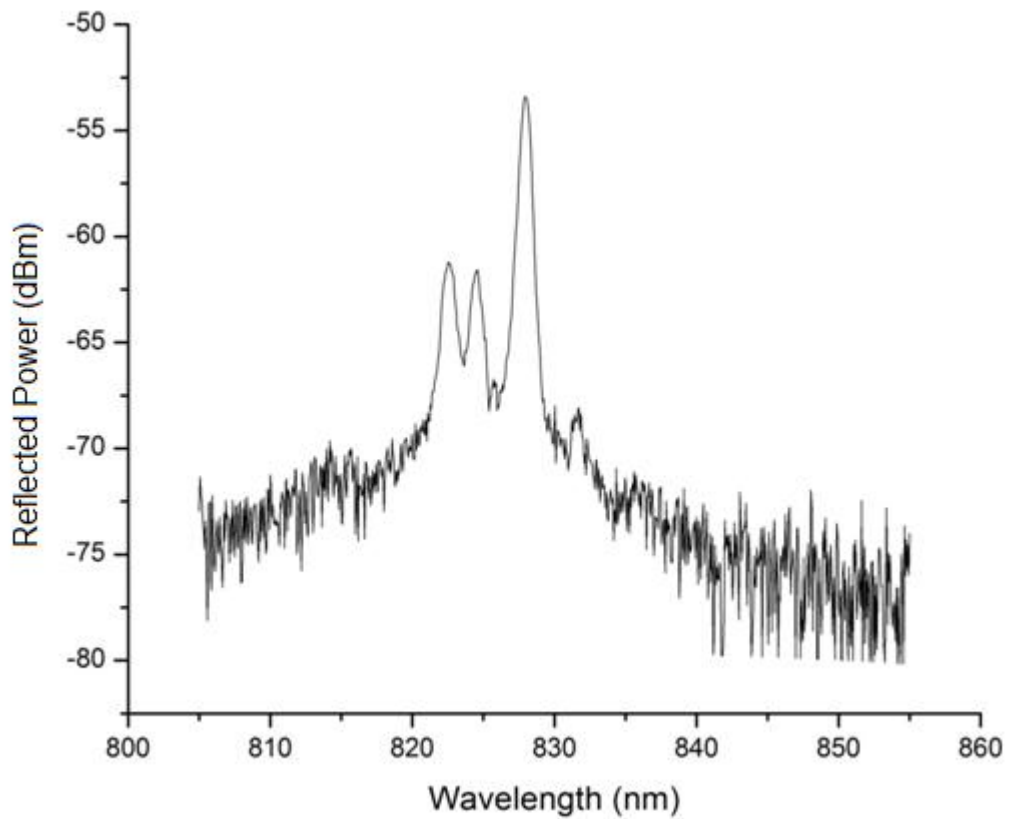


Figure 8-32 First demonstration of a MMmPOF WDM sensor manufactured in the 800nm spectral region, consisting of 3 FBGs fabricated from a single phase mask

Finally a fourth FBG (FBG4) was fabricated in the same length of MMmPOF as the previous 3 FBGs. This was fabricated 2cm from FBG3 and thus 8cm from the near POF end face. Note the growth of FBG4 was unable to be monitored due to the location of FBG4 in the MMmPOF and the fabrication setup. FBG4 was fabricated by exposing the core of the MMmPOF to the UV interference pattern for 90 minutes, again the same HeCd UV laser and the same phase mask was used for this fabrication. The final Bragg responses of the WDM

sensor are shown in Figure 8-32. Individual responses can be seen at the following wavelengths; FBG2 has a Bragg wavelength of 822.50nm with a bandwidth (FWHM) of 1.00nm, FBG3 has a Bragg wavelength of 824.50nm and a bandwidth (FWHM) of 1.0nm and FBG4 has a Bragg wavelength of 828.00nm and a bandwidth (FWHM) of 1.00nm. Additionally a possible FBG response can be seen at a wavelength of 832nm. It is unknown what this reflected response is of, or whether it is a reflected signal rather than an increase in the noise level at this particular wavelength due to the interrogation setup.

In summary, this is the first demonstration of a WDM sensor manufactured in PMMA MMmPOF consisting of 3 FBG responses which has a spectral response in the 800nm wavelength region. Each was fabricated using a single phase mask and utilising thermal annealing at 80°C, their Bragg wavelengths were adjusted to allow further fabrications without further costs of additional phase masks and was therefore documented in[85].

The reason why FBG1 disappeared during the manufacture of the WDM sensor is unknown, as it was the first to be fabricated it was also the furthest away from the end of the POF which was butt coupled to the silica arm of the coupler. One possible cause was that there was damage to the MMmPOF between FBG1 and the rest of the FBGs, this preventing interrogating light reaching the FBG1 or a returning reflected signal from FBG1 being detected.

8.3.1 Second Attempt at the Manufacture of a WDM Sensor Using a Single Phase Mask

A second attempt of manufacturing a WDM sensor was completed which consisted of three FBGs that again were fabricated using a single phase mask ($\Lambda_{pm} = 557.50\text{nm}$). Each of the 3 FBGs was fabricated by exposing the core of the fibre to the UV interference pattern generated from the HeCd laser and phase mask for 90 minutes.

Firstly the MMmPOF was thermally annealed prior to any FBG fabrication, this was completed by placing the 20cm length of fibre onto a baking tray at room temperature and then this was placed onto the middle shelf of an 80°C pre-heated oven for ten minutes. This was an attempt to avoid the initial large Bragg wavelength shift seen in Figure 8-23 and Figure 8-28 and prevent any possibility of the first Bragg response from disappearing as was seen previously. The first FBG (FBG1) was fabricated in the core of the MMmPOF, 2cm from the end of the POF. The fibre was then thermally annealed for a second time at 80°C for 30 minutes. The second FBG (FBG2) was then fabricated in the core of the MMmPOF 2cm from the first towards the centre point of the fibre length. The MMmPOF was then thermally annealed for the final time at 80°C for two hours. To finish, a third FBG (FBG3) was fabricated into the core of the MMmPOF, which was located 2cm from FBG2.

The resultant Bragg responses from the 3 FBGs of the WDM sensor are shown in Figure 8-33, which was captured on an OSA with a bandwidth resolution of 0.5nm. FBG1 had a Bragg wavelength of 822.00nm and a bandwidth (FWHM) of 1.00nm, FBG2 had a Bragg wavelength of 824.00nm and a bandwidth (FWHM) of 1.00nm and FBG3 had a Bragg wavelength of 828.00nm and a bandwidth of 1.0nm. Figure 8-34 demonstrates the normalised reflecting power of the WDM sensor. During this fabrication there was no disappearing first FBG response, all fabricated FBG responses remained throughout each fabrication and thermal annealing stage. Furthermore there is no evidence of an additional reflected response at higher wavelengths to FBG3, again something that was observed in the previous experiment.

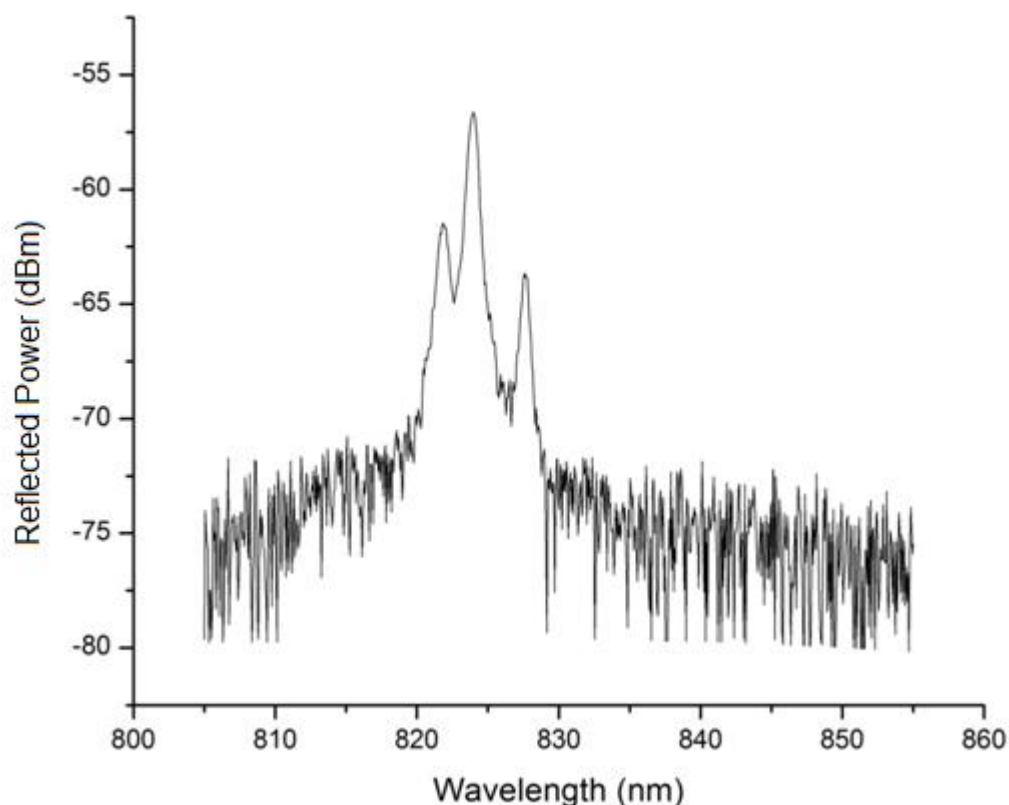


Figure 8-33 Second manufactured WDM sensor, consisting of 3 FBGs fabricated from a single phase mask

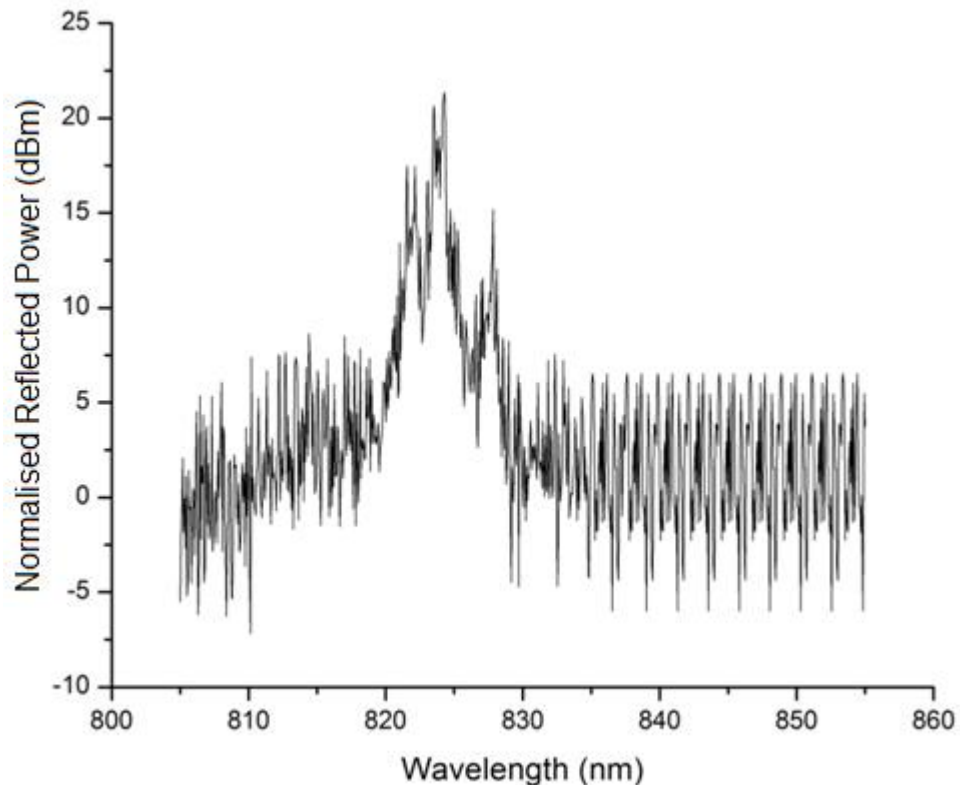


Figure 8-34 Normalised Reflected Power WDM sensor around 820nm

This second manufacture of a WDM sensor adds to the likelihood of repeatability of success using this method. With additional tuning of the amount of time needed for each thermal anneal the effect of Bragg wavelength shifts changing at different rates could also be accommodated for, something which was also seen in the second manufacture.

However the close proximity of the 3 Bragg responses would make it difficult to track any change in Bragg wavelength of each FBG. Circumstances would be made increasingly difficult in the probable chance of cross sensitivity of the reflected Bragg signals during a sensing application. Furthermore the varying reflected optical powers of each FBG is not ideal, with even optical power distribution across the FBGs ideally wanted again to aid with detection and tracking of the Bragg signals.

8.4 Fabrication of a WDM Sensor Using Two Phase Masks

In addition to the WDM sensors manufactured in the previous section a further WDM sensor was made using the two phase masks ($\Lambda_{pm} = 557.50\text{nm} \ \& \ 580\text{nm}$) which have already been used to produced Bragg responses within the 800nm spectral region in the PMMA MMmPOF. The WDM sensor consisted of two separate FBGs fabricated from the individual phase masks and also a third which was thermally annealed and thus resulted in a negative Bragg wavelength shift. The third FBG was actually fabricated first using the 580nm period phase mask which was thermally annealed prior to the next two fabrications. The motivation for this WDM sensor is to still manufacture a 3 FBG device, whilst increasing the spectral range between the 3 Bragg responses. This will allow for undemanding detection of each

FBG response and tracking of potential Bragg wavelength shifts when compared to previous WDM sensors demonstrated in the previous section. Furthermore the risk of cross talk between the Bragg responses will be reduced during any sensing application. The manufacture and response of the WDM sensor is detailed below.

This WDM was manufactured with a pressure sensing application in mind; therefore a 20cm length of the MMmPOF was used. The sensing application required all FBGs to be at least 10cm from either end of the POF, so the first FBG was located 10cm from one of the cleaved ends of the fibre. This however meant that the growth of this first FBG could not be monitored. As the core of the MMmPOF had been UV exposed for 90 minutes for the majority of FBGs fabricated in the 800nm spectral region, the first FBG (FBG1) was also fabricated for 90 minutes. FBG1 was fabricated using the 580nm period phase mask and as with all the FBGs using the HeCd laser and the inscription setup described in Chapter 6. After fabrication the reflected Bragg response was interrogated using the Amonics 800nm Benchtop superwide band wavelength source (ASLD-CWDM-3-B-FA) and captured on an OSA (HP 70951B) with a bandwidth resolution of 0.5nm. The reflection was captured via a 2x1 silica multimode (50/125 μ m) coupler with a 50:50 splitting ratio at 800nm. The reflected Bragg response is shown in Figure 8-35(a), with a Bragg wavelength of 860nm and a bandwidth (FWHM) of 1.50nm.

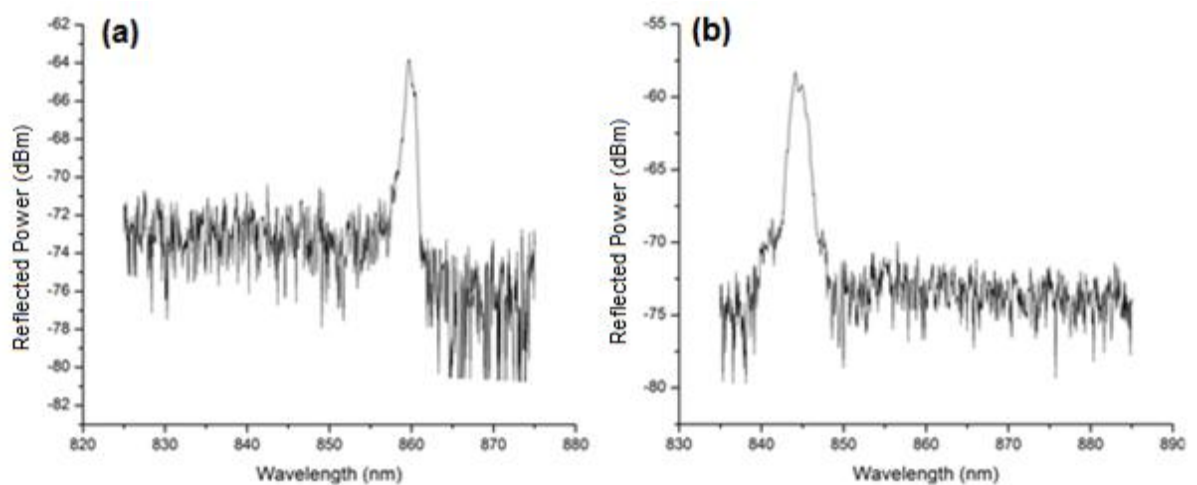


Figure 8-35 Reflected Bragg response of the first fabricated FBG of a 3 device WDM sensors prior to thermal annealing (b) Bragg response of same FBG after thermal annealing at 70°C for 24 hours

The MMmPOF was then thermally annealed at 70°C for 24 hours. Using the procedure previously exercised the MMmPOF was first rested on a baking tray at room temperature; this was then placed onto the middle shelf of the pre-heated oven for 24 hours. The reflected Bragg response of FBG1 was then captured again and is shown in Figure 8-35(b). FBG1 now has a Bragg wavelength is 844.50nm and the bandwidth (FWHM) is 2nm. Therefore the thermal anneal induced a Bragg wavelength shift of 15.50nm, which is in the region of the

wavelength shift seen in Figure 8-28. Also it would appear that due to the thermal annealing the bandwidth had increased by 0.5nm.

The MMmPOF was then permanently spliced to a silica multimode (50/125 μ m) pigtail using the technique described in Chapter 5. This allowed for monitoring of the growth of the second and third FBG fabrications, something which would not have been possible without the adhesive splice due to the location of the FBGs along the length of fibre and the current fabrication setup.

The second FBG (FBG2) was fabricated in the MMmPOF core 2cm from FBG2. The same phase mask ($\Lambda_{pm} = 580\text{nm}$) was used during this fabrication as that of FBG1. The MMmPOF was exposed to the UV interference pattern for 45 minutes; the growth of FBG2 is shown in Figure 8-36(a), where a signal-to-noise ratio of 9dBm was attained. The resultant Bragg response of FBG2 can be seen in Figure 8-36(b) together with FBG1. FBG2 had a measured Bragg wavelength of 861nm and a bandwidth (FWHM) of 0.5nm, again using an OSA (HP 70951B) with a bandwidth of 0.5nm.

Finally the third FBG (FBG3) was fabricated in the same length of MMmPOF; this was located 2cm away from the location of FBG2 and hence 4cm away from FBG1. Figure 8-37(a) demonstrates the growth curve of FBG3 which appeared to saturate after 50 minutes when a 9dBm Bragg signal-to-noise ratio was gained. As a result Figure 8-37(b) illustrates the Bragg responses of all three FBGs of the WDM sensor. The FBG3 has a Bragg wavelength of 828nm and a bandwidth (FWHM) of 0.5nm. Incidentally the signal-to-noise ratios of both FBG2 and FBG3 appear larger when interrogated after the monitoring of the growth of each FBG. It is believed this is a result of capturing the final Bragg responses whilst the MMmPOF was straight and taut along its axis whilst during fabrication the POF was curved over the edge of each end of the v-groove plate used for inscription, thus inducing bending losses.

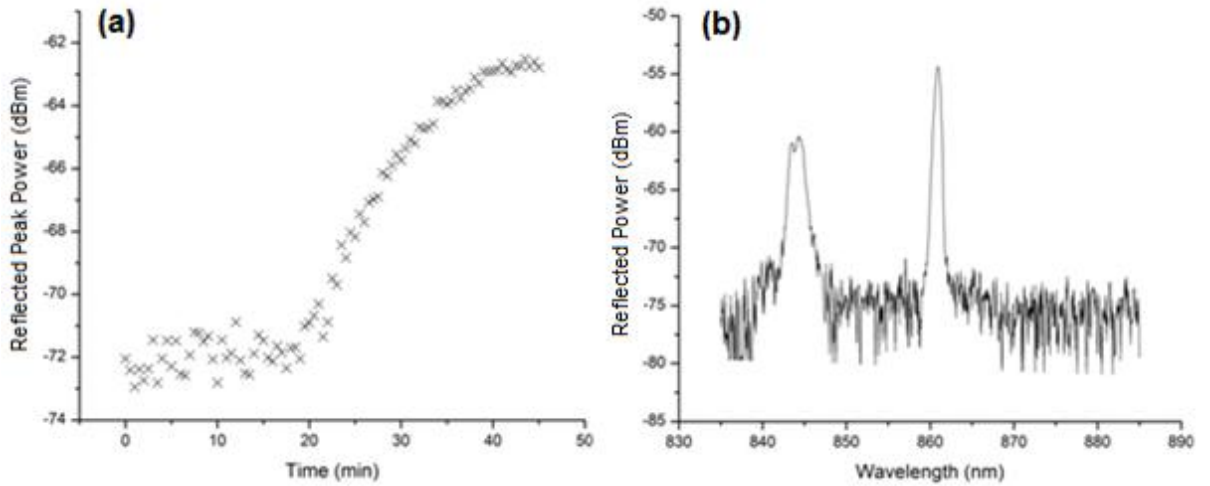


Figure 8-36 (a) growth curve of FBG2 of the WDM sensor fabricated at 861nm (b) reflected Bragg responses of FBG1 and FBG2 of the WDM sensor

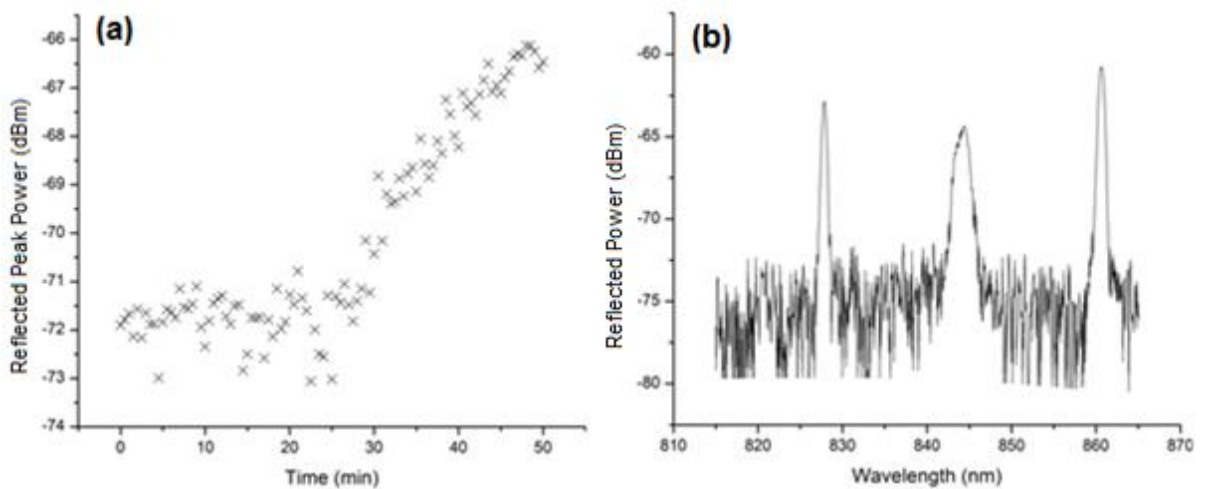


Figure 8-37 (a) growth curve of FBG3 of the WDM sensor fabricated at 828nm (b) reflected Bragg response of all three FBGs of a WDM sensor manufactured with two phase masks and the aid of thermal annealing

8.5 Summary

Thermal tuning of Bragg responses have been demonstrated in both the 1500nm and 800nm spectral regions. A total permanent negative Bragg wavelength shift of 19nm was experienced when thermally annealing a FBG fabricated in MMmPOF with a Bragg response in the 1550nm wavelength range for 7 hours at 71°C, complementing this work was the thermal annealing curve captured over a course of 180 minutes where a total Bragg wavelength shift of 16nm was observed, which contributed to the publications in 2010 and 2011[72, 74]. Furthermore, the change in Bragg responses in the 800nm was observed in the MMmPOF whilst thermally annealing the POF. Total permanent Bragg wavelength shifts of up to 24nm were seen when thermally annealing the fibre at 80°C for 7.5 hours, also total Bragg wavelength shifts of 18nm were seen when thermally annealing the MMmPOF at 70°C for 24.5hours, this later result was publish in 2011[85].

These negative Bragg wavelength shifts of at least -16nm allow for tuning to specific interrogating light sources which may be required for a specific optical interrogation system without the need to purchase additional relatively expensive phase masks. Furthermore, the thermal tuning has allowed for the possibility to fabricate WDM sensors from one of two phase masks. Demonstrated in this chapter is a 3 FBG WDM sensor which was fabricated with the use of a single phase mask. The fabrication of WDM sensors in both the 1500nm and 800nm wavelength regions have been detailed both in this chapter and in recent publications[72, 74, 85]. Currently the detailed fabrication of WDM sensors is not a repeatable process. Rather a guide of a particular process path to fabricate WDM sensors which utilises thermal annealing of POF. In excess of 50 POFBGs were fabricated in the WDM study yet only a few 3 FBG WDM sensors were able to be demonstrated. It is felt that for thermal annealing to be a variable solution for WDM fabrication the yield of FBGs fabricated in POF needs to be improved, in particular after the POF has been thermally annealed. Potentially good performing FBGs were damaged from thermally annealing the fibre. Therefore further studies need to be completed to enable thermal annealing to be used as a processing step for WDM sensor fabrication whilst still having a high yield of fabrication and hence a repeatable process.

8.6 Future Work

The detailed manufacturing of the 3 FBG WDM sensor across an 820nm - 870nm wavelength range proved the most successful production of a WDM device, this device provided a wide enough wavelength range to identify each individual FBG response and reduce the risk of cross talk when monitoring any potential Bragg wavelength shifts of each FBG in a sensing application, this was further aided by the smaller bandwidths of FBG responses at the reduced wavelengths.

The next step in this work is to characterise the WDM sensors in application specific experiments. One ongoing example of this is where the sensor shown in Figure 8-37(b) has been embedded in a PDMS tube to enable diagnostic data of the motor function of the sphincters and the oesophageal body.

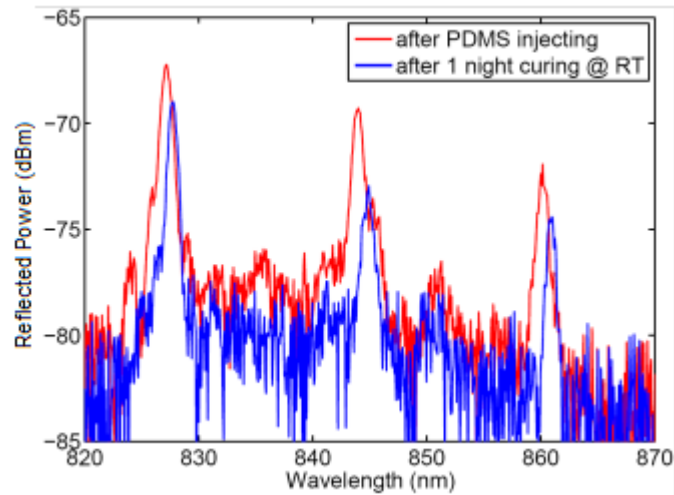


Figure 8-38 Reflected Bragg response of a 3 FBG WDM sensor fabricated in MMmPOF which has been embedded in a PDMS tube, Figure supplied by Bram Van Hoe, Ghent University.

Figure 8-38 demonstrates the Bragg responses from all 3 FBGs of the WDM sensor prior to and after the curing of PDMS which is used to fill a polymer tube.

Further work should be completed to investigate the phenomenon of observing different Bragg wavelength shifts of 2 FBGs when thermally annealed which have been fabricated in the same length of MMmPOF. As the FBG which experienced the smaller of the two wavelength shifts had already been thermally annealed it would suggest that the induced larger wavelength shift of the recently fabricated FBG is a result of releasing stress which was introduced to the MMmPOF during the FBG fabrication. One possible experiment to determine this is to thermally anneal a length of MMmPOF prior to FBG fabrication until it is believed the MMmPOF has fully shrunk. After this a FBG should be fabricated in the annealed fibre, following this fabrication the MMmPOF should then be annealed again to determine if any Bragg wavelength shift was induced as a result of the second thermal anneal.

Further characterisation of the thermal annealing should be completed by investigating the resultant Bragg responses over a much longer time period of at least 1 week, included in this work should be the characterisation of the Bragg response of thermally annealing over a larger temperature range up to the glass transition temperature of PMMA.

Finally thermally annealing and the manufacturing of WDM sensors should be investigated in other polymer optical fibres. A two FBG WDM sensor has been fabricated in the TOPAS POF which has a spectral response in the 800nm wavelength region and is documented Chapter 9. However Bragg wavelength tuning due to thermal annealing has not been investigated in this particular POF.

9

TOPAS CYCLIC OLEFIN COPOLYMER

In this chapter, previous experiments demonstrating POFBG sensitivity to relative humidity are discussed, together with the mechanisms involved which result in a positive Bragg wavelength shift as the relative humidity increases. TOPAS Cyclic Olefin Copolymer (COC) is introduced to offer a solution to eliminate cross-sensitivity to relative humidity as TOPAS POF has a much lower water affinity when compared to PMMA based POF. Documented within this chapter are FBG sensors which have been fabricated within endlessly single mode microstructured TOPAS mPOF, together with the temperature and relative humidity sensitivity characteristics. Finally fabrication of FBG sensors within the lower 800nm spectral region are investigated, here lower attenuation losses are documented which allow longer lengths of TOPAS mPOF to be used as was investigated in Chapter 6 when working with PMMA based POFs.

9.1 Cross-Sensitivity to Relative Humidity in PMMA based POF

Thus far in this thesis, all FBGs and LPGs have been fabricated in PMMA based POF. An inconvenience of employing FBG sensors fabricated in PMMA POF is the influence of water absorbing into the fibre upon the Bragg response, consequently when monitoring measurands such as temperature; cross-sensitivity to humidity is highly probable. PMMA is a porous material and is able to absorb moisture from the environment it is in; PMMA may have a water content of up to 2% at 23°C[86-87]. As with many polymers, the higher the relative humidity (RH) the PMMA is in, the higher amount of water content will be in the material which increases through a water absorption process where the water bunches together within the polymer molecular matrix[88].

A positive Bragg wavelength shift of a reflected response from a POFBG based on PMMA is observed with an increase in the relative humidity of the environment the fibre is in. The change in the Bragg wavelength can be observed in Figure 9-1[89], where a relative humidity sensitivity of 38.3pm/% was established. Additionally, as is shown in Figure 9-2[89] the diffusion of water into the PMMA based POF can take around 30 minutes before a saturation level is achieved and the Bragg wavelength becomes stationary. For these particular experiments the POF had a diameter of 200µm.



Figure 9-1 Relative humidity sensitivity of a FBG sensor fabricated in step index PMMA based POF at 22°C [89]



Figure 9-2 Time response of the diffusion of water into a 200µm diameter POF [89]

Two mechanisms that are likely to affect the wavelength of the Bragg response when the content of water within the PMMA based POF is increased are as follows; Firstly, as more water is absorbed into the fibre the fibre will swell, thus increasing the period of the fringes

(Λ) of the photo-inscribed interference pattern in the fibre core[87]. Secondly, the refractive index changes as the water content increases within the fibre; the humidity dependency of the refractive index of deuterated polyfluoromethacrylate (*d*-PFMA) has been reported to be around 0.3% between relative humidity of 20% and 98% at 20°C[53].

An example of water diffusion into a PMMA mPOF can be seen when using the LPG response of the LPG whose fabrication was documented in Chapter 4. Here, Sáez-Rodríguez demonstrated the effect of water diffusion into the fibre on a single attenuation resonance when the fibre containing the grating was immersed into a bath of distilled water[65].

Figure 9-3 illustrates an initial positive red wavelength shift as the water enters the cladding of the mPOF. This is because as the water content is absorbed into the cladding of the POF the cladding swells resulting in strain being applied to the LPG thus a positive wavelength shift is observed. For around the first hour the water content within the fibre is limited to the cladding and at first did not have an effect on the refractive index of the core. After one hour the diffused water reaches the core resulting in a dominating refractive index change within the core of the fibre, causing a negative blue wavelength shift of the attenuation resonance which reaches a saturation level with a net negative wavelength shift of 80nm after around 8 hours. When the LPG is taken out of the bath of distilled water and left to dry a large initial negative wavelength shift is observed as the water diffuses out of the fibre cladding and the fibre shrinks. There is then a secondly drying effect where the fibre has stopped shrinking but the refractive index of the core is still increases as it dries over a much longer time period, resulting in a positive LPG wavelength shift.

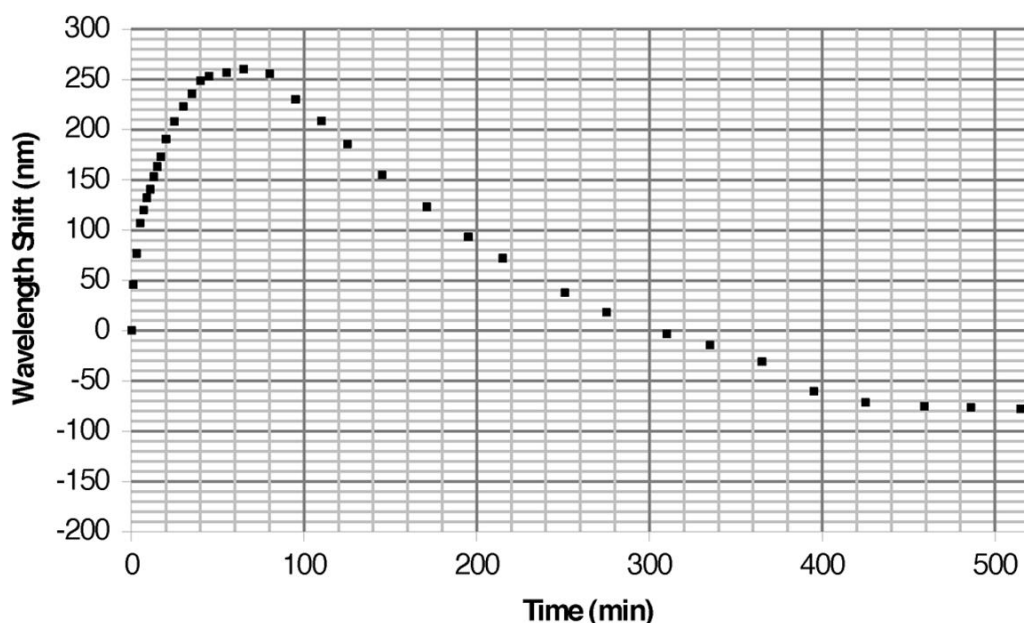


Figure 9-3 LPG attenuation resonance wavelength shift due to water diffusion into PMMA mPOF

9.2 TOPAS COC POF

TOPAS® is a trade name for a cyclic olefin copolymer (COC). The TOPAS COC family consists of amorphous, transparent copolymers which are similar to glass in its natural form, and are based upon cyclic olefins and linear olefins. COCs are a relatively new group of thermopolymer materials, and have some appealing characteristics which may help to eliminate or reduce the cross sensitivity to relative humidity, whilst either monitoring changes in temperature or strain in a given environment. TOPAS COCs have extremely low water absorption and have excellent water vapour barrier properties[57]. TOPAS is one type of COC, which is a copolymer of ethylene and norbornene and is polymerised by metallocene catalysts, thermopolymers have no vinyl monomers which are used to produce vinyl polymers such as PMMA[90-91]. TOPAS COC has a refractive index of 1.5259 at 830nm and 1.5217 at a wavelength of 1550nm, additionally optical losses of TOPAS COC are given as 0.5dB/cm at 820nm and 0.7dB/cm at 1550nm[90]. In addition TOPAS COC has a moisture absorption of less than 0.01% compared to 0.3% for PMMA[90].

A further potential advantage of TOPAS COC is its ability to be employed in novel bio-sensing applications, this is because linker molecules are required when attaching bio-sensing layers to the TOPAS COC; this therefore allows for the possibility of defining specific areas for sensing[91].

The glass transition (T_g) temperature of TOPAS COC, may however be considered a disadvantage, as the T_g of TOPAS COC 8007F-04, which was used to manufacture mPOF for the work in this thesis is 78°C, which is nearly 30°C less than the typical 103 °C T_g of PMMA[39].

9.3 Fabrication of FBG sensors in TOPAS POF

Previous attempts to fabricate FBG sensors in TOPAS POF were made by C Zhang[56], here photosensitivity to 325nm UV laser exposure was reported. However a single captured Bragg response was not reproducible, additionally the Bragg response could be seen in transmission but not in reflection which proved the fabrication of a FBG in the TOPAS POF as inconclusive. Initial experiments in the documented work monitored the temperature sensitivity of the Bragg response in transmission which suggested a large positive Bragg wavelength shift with an increase in temperature.

Reported in this thesis is the repeatable fabrication of FBG sensors in TOPAS COC mPOF, including interrogation of the Bragg response in reflection. This work was published in February 2011, and repeatedly demonstrated a negative Bragg wavelength shift in response to an increase in temperature within an environmental chamber[73].

The TOPAS COC mPOF fibre was manufactured by collaborating colleagues at The Technical University of Denmark (DTU). Here a solid cylindrical perform of TOPAS® 8007F-

04 with a diameter of 6cm was prepared by drilling two rings of holes each with a 3mm diameter. The holes will create the air holes required to enable index guiding within the core of the fibre once the plastic perform had been drawn down into mPOF fibre. The resultant pure TOPAS COC mPOF, which was used for all FBG fabrication had an overall diameter of 270 μ m. Each hole had a diameter of 3.8 μ m and a hole pitch of 8.5 μ m, and the fibre was designed to be single mode within the 1550nm spectral region. A microscope image of a cleaved end face of the TOPAS mPOF is shown Figure 9-4. It should be noted that the end face of the TOPAS mPOF is prepared by cleaving the end with a feather razor blade as is described in Chapter 3, however, neither the fibre nor the razor blade are required to be heated to 80°C and are able to remain at room temperature.

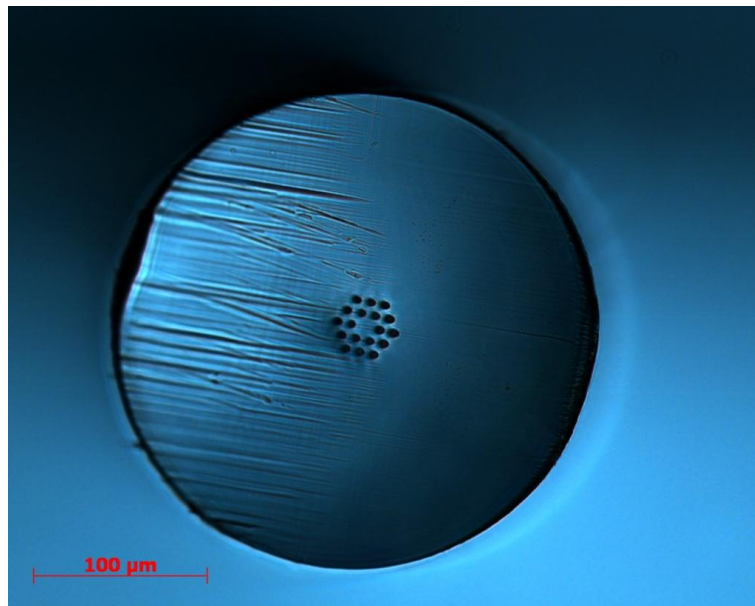


Figure 9-4 Cleaved end face of TOPAS COC mPOF

Fabrication of FBGs in the TOPAS mPOF was carried out using the same 325nm 30mW HeCd laser (Kimmon Koha Co, Ltd, IK3301R-G) and phase mask inscription setup as for FBGs fabricated in PMMA mPOF which was described in Chapter 4. The phase mask which was optimised for use with a 325nm laser had a period (Λ_{pm}) of 1034.2nm and was rested directly onto the TOPAS mPOF, which was mounted onto a v-groove plate. The fabricated FBGs in the TOPAS mPOF were interrogated in reflection using a broadband light source (Thorlabs ASE-FL7002-C4, Broadband ASE Light Source 1.53-1.61 μ m) and monitored on an OSA (HP70951B) with a resolution bandwidth of 0.5nm. Light was coupled into and out of the TOPAS mPOF via butt coupling a FC/APC arm of a 50:50 single mode silica 2x2 coupler and aligned using a translation stage, a technique previously used when interrogating FBGs fabricated in PMMA mPOF and discussed in more detail in Chapter 3.5. A typical captured reflected Bragg response is demonstrated Figure 9-5. Using a bandwidth resolution of 0.5nm a Bragg wavelength of 1568nm was measured using the centroid calculation for all data points collected within 3dBm of the peak value and a bandwidth (FWHM) of the reflected

Bragg response of 1.0nm was measured. The length of the FBGs fabricated in the TOPAS mPOF was defined by the diameter of the HeCd laser beam which in this case was 1.2mm ($1/e^2$). As shown in Figure 9-6, using a UV laser beam power of 30mW, a notable growth of the FBG started after around 10 minutes when a Bragg response could be seen in reflection during fabrication, and approximately 45 minutes were required before the peak reflected power would reach a saturation level, where a signal-to-noise ratio of 19dBm was measured in this instance.

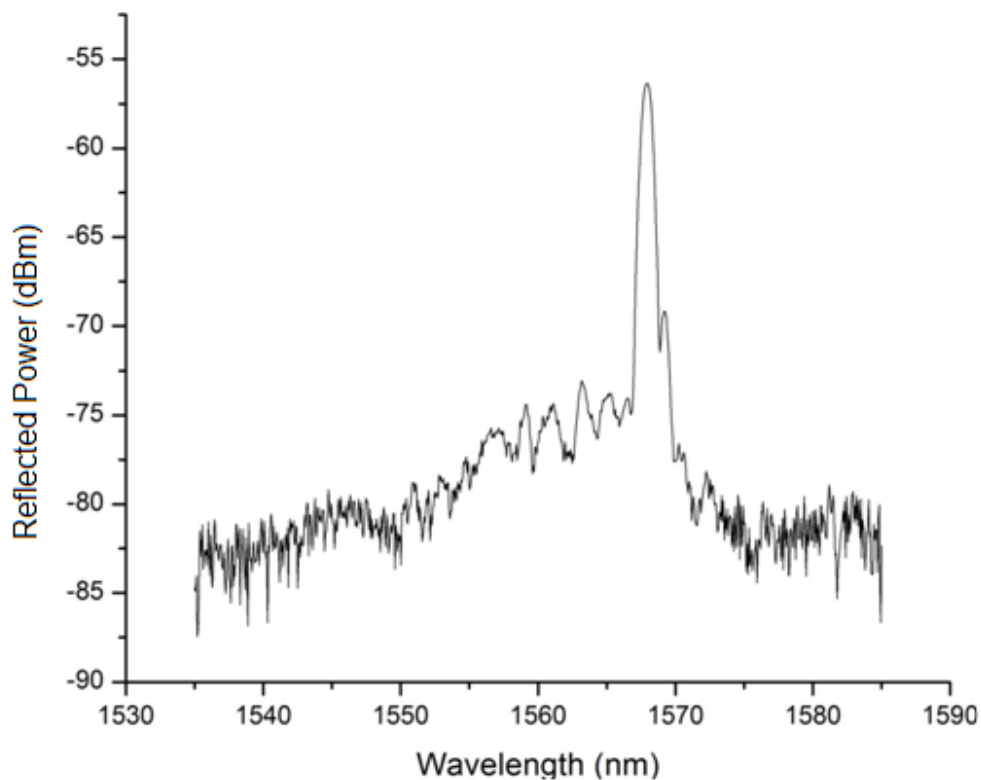


Figure 9-5 Reflection spectrum from a FBG fabricated in TOPAS mPOF, with a Bragg wavelength of 1568nm

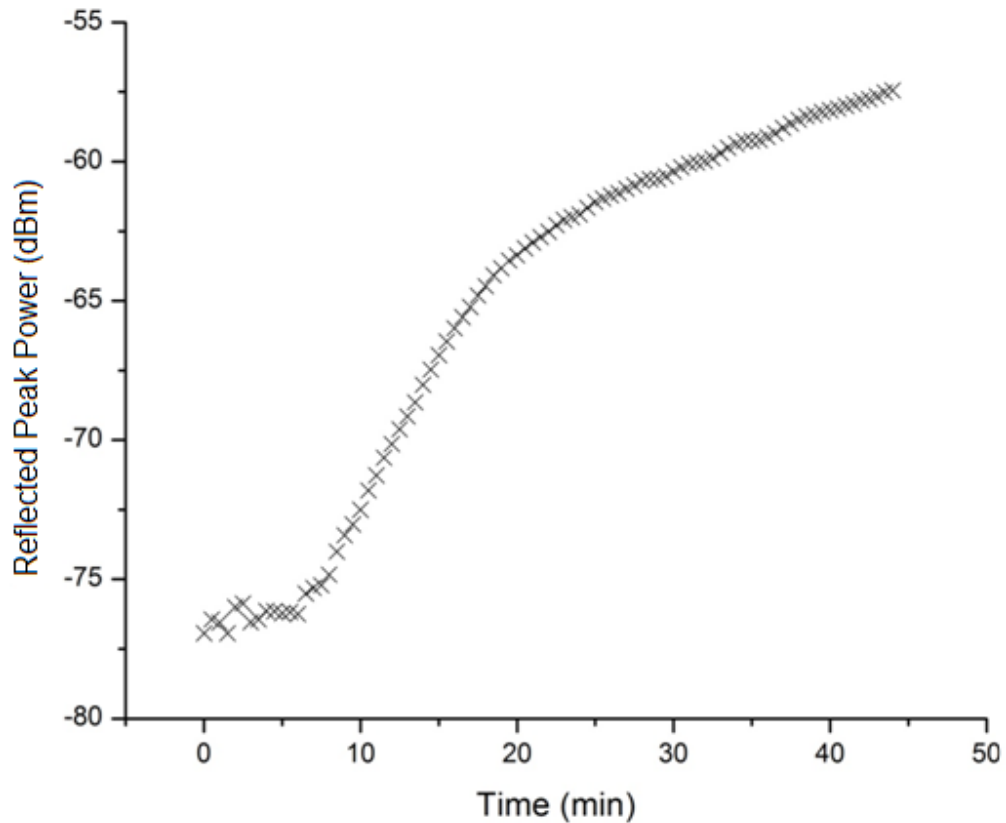


Figure 9-6 Growth of a FBG reflection against time during fabrication in TOPAS mPOF, with a Bragg wavelength of 1567.9nm

9.4 Temperature Characteristics of Fabricated FBG sensor in TOPAS mPOF

The FBG with a Bragg response shown in Figure 9-5 was fabricated in a 10cm length of TOPAS mPOF. This fibre was then spliced to a single mode (50/125 μ m) silica pigtail using UV curing optical adhesive (Loctite 3525), using the same technique which was described in detail in Chapter 5 with no significant optical loss due to the adhesive splicing process. This enabled the TOPAS mPOF to be removed from the optical work bench whilst still interrogating the Bragg response of the fabricated FBG. This created the opportunity to characterise the temperature sensitivity of the TOPAS POFBG in an environmental chamber (Sanyo Gallenkamp), whilst retaining the relative humidity at 55% so to eliminate any possibility of cross sensitivity to relative humidity whilst varying the temperature. The temperature of the environmental chamber was varied from 20 to 35°C, this upper temperature limit was not exceeded to protect the Loctite 3525 optical adhesive, which has a glass transition temperature of 43°C[70]. The temperature was increased rapidly every 2 hours, data was collected every 60 seconds once a stabilising period of 30 minutes was allowed after each increase of the temperature. The median value of the Bragg wavelength was then taken and plotted against the temperature as is shown in Figure 9-7. The temperature sensitivity data was collected by a collaborating PhD student at Aston University, Lutful Khan, and is presented in Figure 9-7. A temperature sensitivity of -

36.5±0.3pm/°C was obtained. This temperature sensitivity of TOPAS is within the same region as the measured temperature sensitivity of PMMA based POFBGs in the 1550nm spectral region (-43pm/°C)[14]. Additionally, a negative Bragg wavelength shift with increasing temperature was seen, thus contradicting the positive Bragg wavelength seen in [56]. Although the temperature characteristics were demonstrated here using a single TOPAS POFBG, it should be noted that initial work involved four separate FBGs fabricated in individual lengths of the TOPAS mPOF, each showing the similar temperature characteristics.

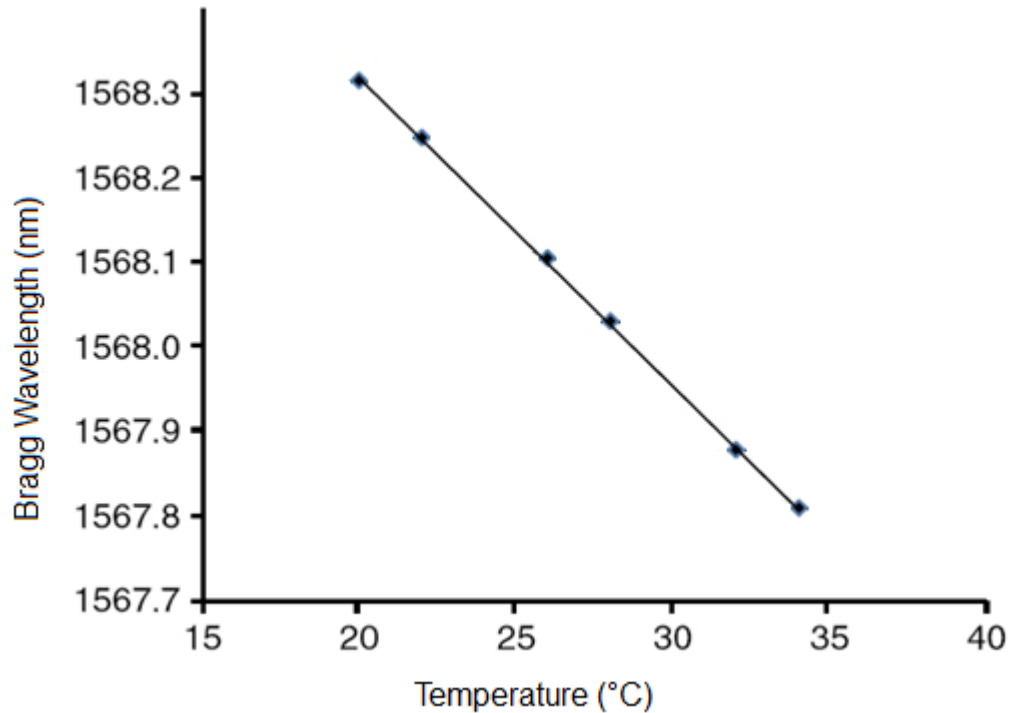


Figure 9-7 Thermal response of a FBG fabricated in TOPAS mPOF

9.5 Fabrication of TOPAS POFBGs in the 800nm Spectral Region

In an attempt to offer more functionality to FBG sensors fabricated in the TOPAS mPOF, larger lengths of fibre are required. For instance, this will give the potential to characterise the temperature sensitivity over a greater range, increasing the upper limit to near the glass transition temperature of TOPAS 8007F-04 of 78°C[57], whilst protecting the adhesive splice by removing it away from the heat source. FBG sensors within the 800nm region will experience an optical loss of 0.5dB/cm[90] and thus allowing for interrogation of reflected Bragg responses over longer lengths of the TOPAS mPOF. Additionally suitable broadband sources are readily available around 800nm.

To demonstrate the possibility of fabricating FBG sensors over larger lengths of TOPAS mPOF gratings have also been fabricated within the 800nm spectral region, using the same fabrication and interrogation techniques as previously used to fabricate TOPAS POFBGs with a Bragg wavelength of 1567.9nm, which was documented earlier. Firstly a phase mask

with a surface relief pattern period (Λ_{pm}) of 557.5nm was used, which as with the TOPAS POFBGs fabricated at 1567.9nm was optimised for inscription with the 325nm HeCd laser and rested directly on top of the TOPAS mPOF. The resultant reflected Bragg response is shown in Figure 9-8, with a Bragg wavelength of 849nm, calculated using the centroid calculation of the data points captured within 3dBm of the peak as was detailed in Chapter 4, the bandwidth (FWHM) of the reflected Bragg response was 0.5nm. A bandwidth resolution of 0.5nm was used on a HP 70951B OSA to capture the reflected spectra. The light source used to interrogate the fabrication of this FBG and further fabrications in the 800nm spectral region was an Amonics Superwide band Short Wavelength Source (ASLD-CWDm-3-B-FA, typical output power 1.5mW and a minimum spectral density -35dBm/nm), which has a spectral bandwidth range of 730-900nm. Additionally a single mode (9/125 μ m) silica 2x1 coupler was used to monitor the reflected Bragg response; the coupler had a 50:50 ratio at 800nm. The growth of this TOPAS POFBG was also interrogated in reflection; the rise in peak reflected power of the Bragg response against time is shown in Figure 9-9 as can be seen optimisation of the coupling between the silica and polymer fibres takes place after 45 minutes resulting in the break in the growth curve. The noise floor of the reflected Bragg response was continuously changing which, together with the small signal-to-noise ratio of the Bragg response resulted in a noisy growth curve. However, it can be seen that significant growth starts within 30 minutes and a saturation level was reached by 80 minutes. The fabrication of this particular TOPAS POFBG was left for 90 minutes to ensure the saturation of the growth of the FBG was reached. Further attempts were made to fabricate stronger FBGs using this phase mask ($\Lambda_{pm} = 557.5$ nm), however for reasons unknown this was not possible with further fabrications producing similar FBG strengths.

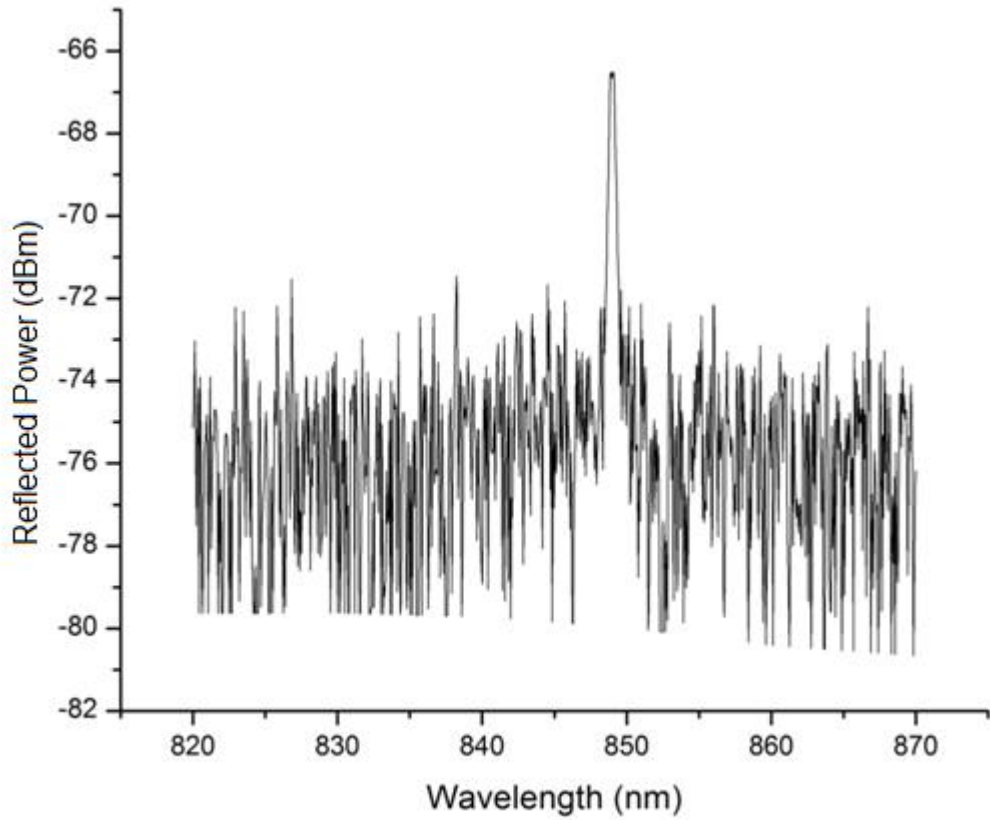


Figure 9-8 Reflection spectrum from a FBG fabricated in TOPAS mPOF, with a Bragg wavelength of 849nm

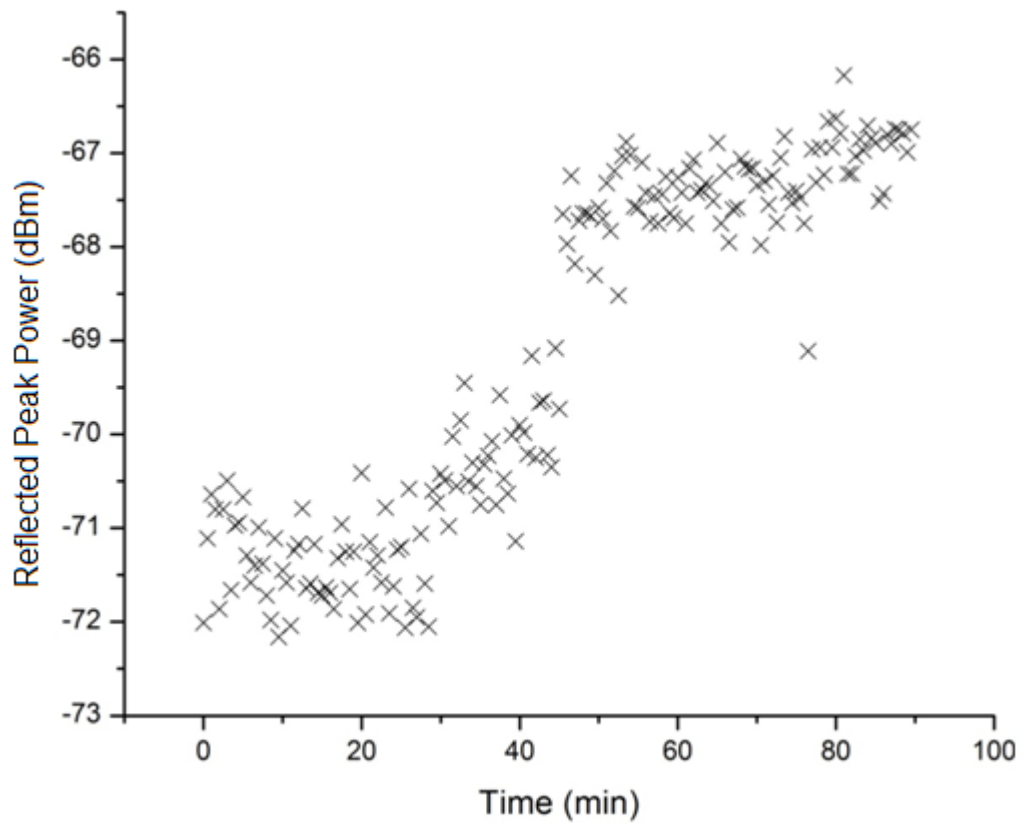


Figure 9-9 Growth of the reflected power against time during fabrication of a TOPAS POFBG, with a Bragg wavelength of 849nm

Additional attempts were made to fabricate TOPAS POFBGs within the 800nm spectral region. Bragg gratings were also fabricated using a different phase mask with a period (Λ_{pm}) of 580nm; again the phase mask was optimised for fabrication with the HeCd UV laser and was rested directly upon the TOPAS mPOF which was mounted upon the v-groove plate as detailed in Chapter 4, also detailed in Chapter 4 is the remainder of the fabrication setup used for this FBG fabrication. The fabricated TOPAS POFBG shown in Figure 9-10, has a Bragg length of 882.39nm and a bandwidth (FWHM) of 0.5nm. The reflected Bragg response was captured on an OSA (HP 70951B) with a bandwidth resolution of 0.5nm and was interrogated with an Amonics Superwide Band Short Wavelength Source (ASLD-CWDm-3-B-FA). A signal-to-noise ratio of 15dBm was measured after 40 minutes at which point a saturation level of the Bragg response growth was reached. Optimisation of the coupling between the polymer and silica fibres took place after 35 minutes which resulted in the observed break in the growth curve of Figure 9-11.

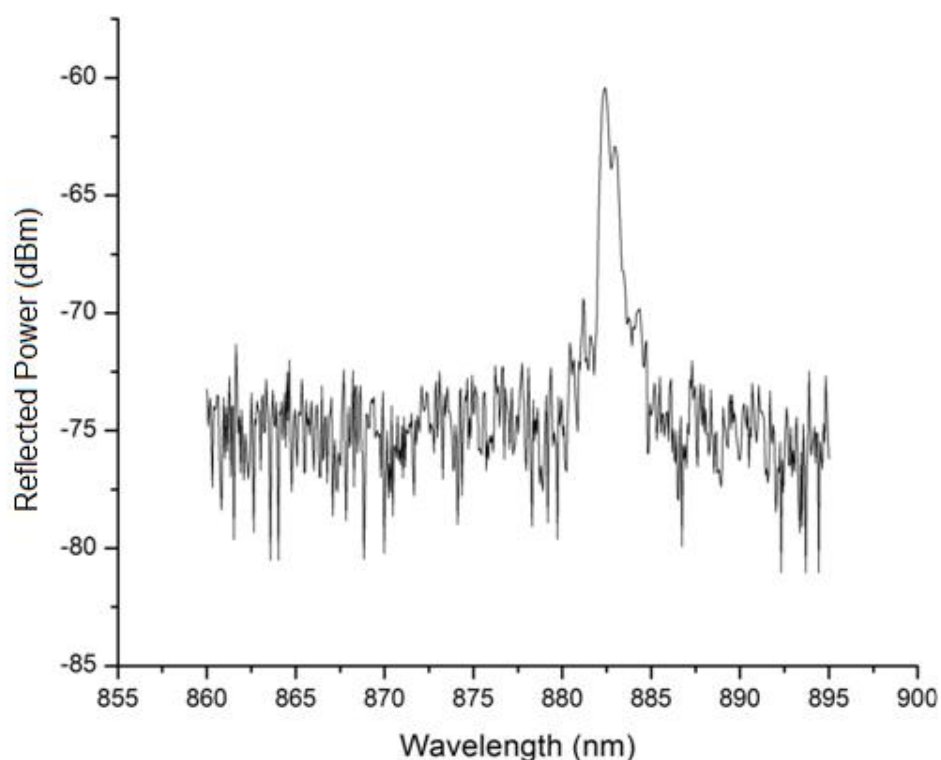


Figure 9-10 Reflection spectrum from a FBG fabricated in TOPAS mPOF, with a Bragg wavelength of 882nm

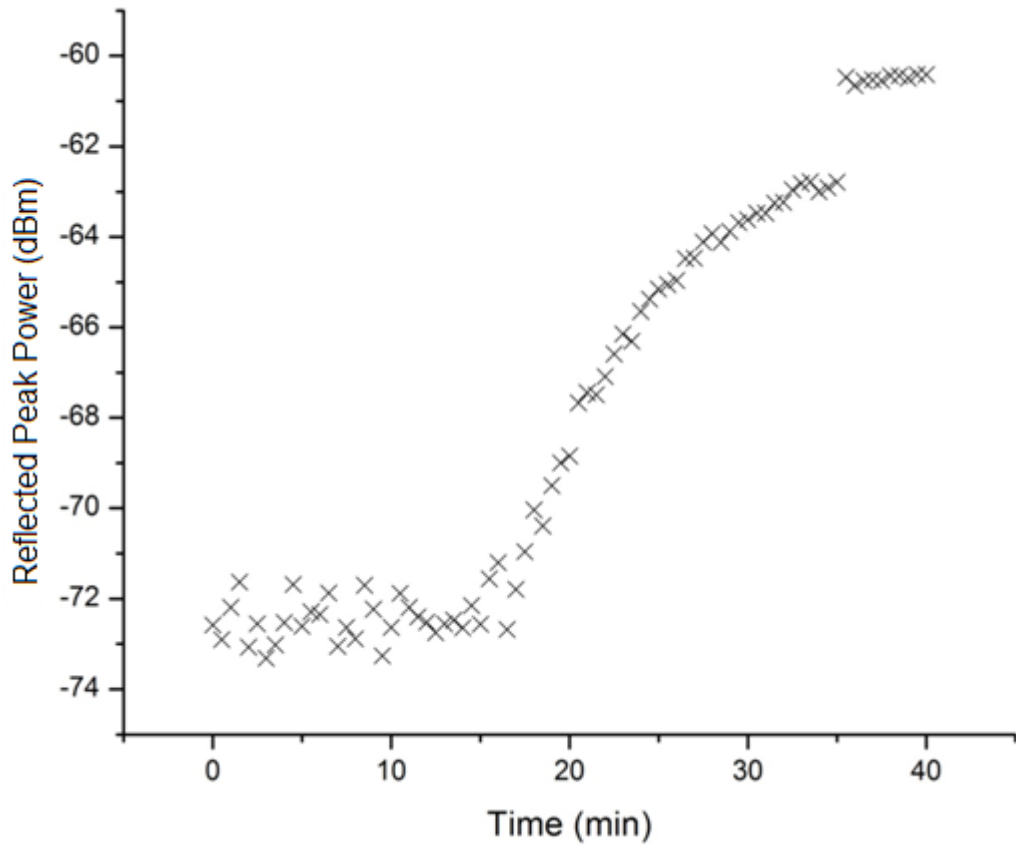


Figure 9-11 Growth of the reflected power against time during fabrication of a TOPAS POFBG, with a Bragg wavelength of 882nm

9.5.1 Fabrication of a WDM Sensor in TOPAS POF

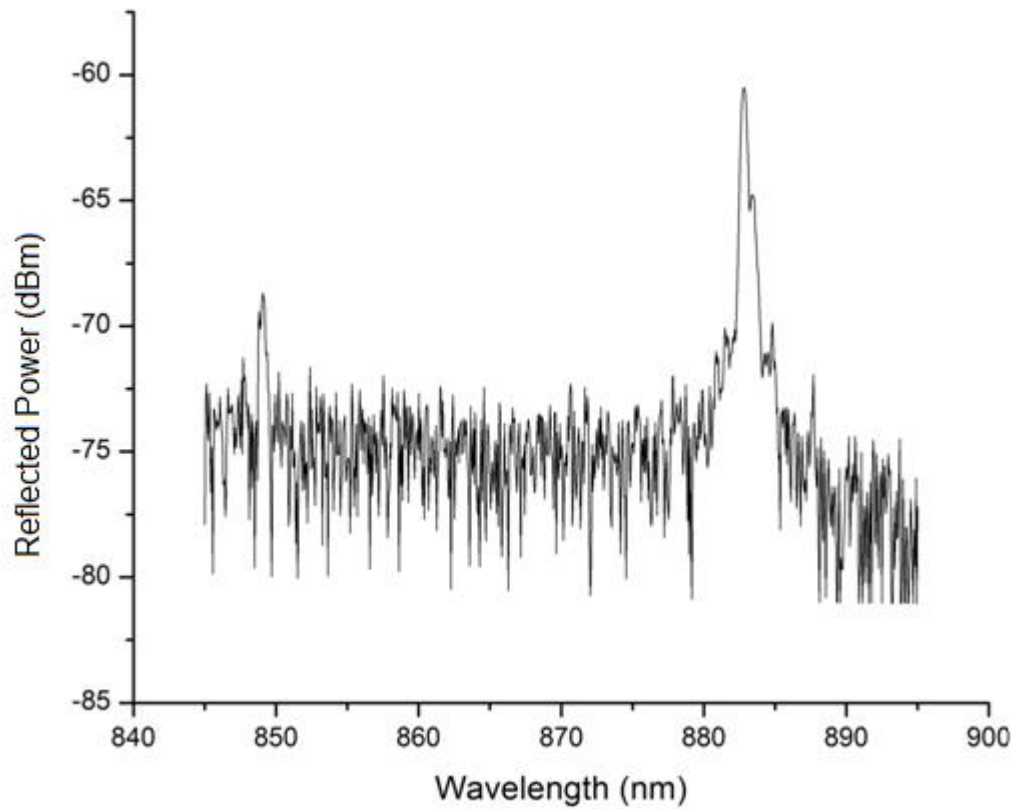


Figure 9-12 WDM sensor response within the 800nm spectral region, fabricated in TOPAS mPOF

Figure 9-12 demonstrates the first example of a WDM sensor manufactured in the TOPAS mPOF captured in reflection on an OSA (HP 70951B) with a bandwidth resolution of 0.5nm. The sensor consists of two FBGs each fabricated with individual phase masks, which have previously been used in this chapter. First a FBG was fabricated with a Bragg response at 849nm and a bandwidth (FWHM) of 0.5nm using a phase mask with a period of 557.50nm. And secondly a FBG was fabricated with a Bragg response at 883nm with a bandwidth (FWHM) of 0.5nm using a phase mask with a period of 580nm. Both FBGs were fabricated using the same technique previously described in this chapter when fabricating FBGs in the TOPAS mPOF, both FBGs were fabricated for 45 minutes.

9.6 Humidity Sensitivity

In collaboration with Lutful Khan⁴ at Aston University, the humidity sensitivity of the fabricated FBG in TOPAS mPOF with a Bragg response at 1568nm similar to Figure 9-5 was tested. The FBG sensor was permanently spliced to a single mode (9/125 μ m) silica pigtail using the adhesive splice technique which is described in Chapter 5, and the Bragg response was monitored in reflection using a 2x1 silica single mode (9/125 μ m) coupler with a 50:50 splitting ratio at 800nm. The reflected Bragg response was captured on a OSA with a bandwidth resolution of 0.1nm. The FBG sensor was placed in an environmental chamber (Sanyo Gallenkamp) which was set to 25°C. For this experiment the relative humidity (RH) was increased in steps of 10% RH from 30-90%. Each programmed RH condition was left for 2 hours, during which time the Bragg response was monitored every 30 seconds. At each RH setting the first 30 minutes of data was neglected to allow the system to acclimatise. All other Bragg wavelength data for each RH was averaged and the error was calculated for each RH as shown in Figure 9-13.

⁴ The FBG in the TOPAS mPOF was fabricated by I. Johnson, all humidity sensing was completed by Lutful Khan

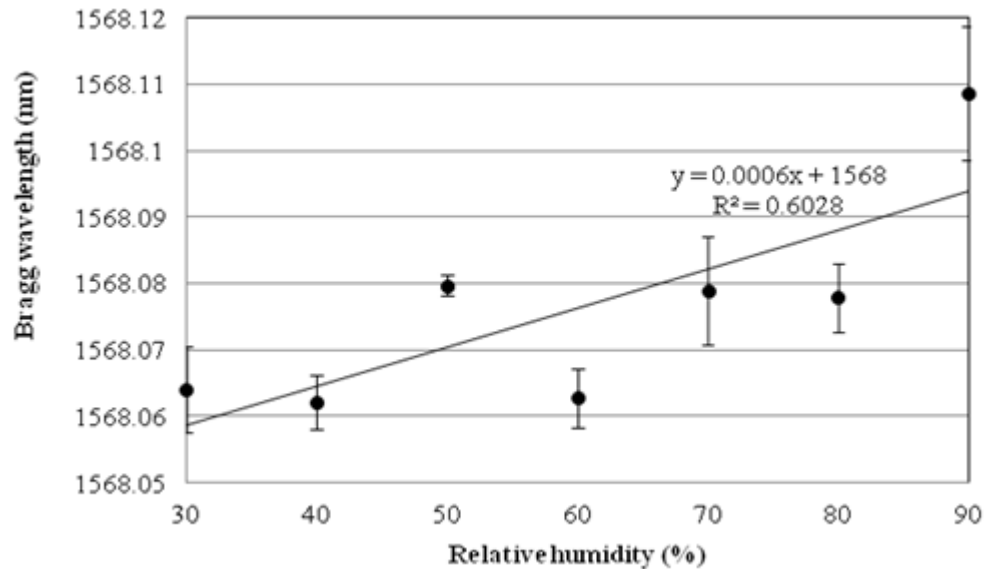


Figure 9-13 Relative humidity sensitivity of a FBG fabricated in TOPAS mPOF with a Bragg wavelength of 1568nm

From Figure 9-13, the linear RH sensitivity of the TOPAS POFBG was calculated to be -0.6pm/% RH with a linear regression of 0.6. A total Bragg wavelength shift of 36pm was seen across the 30-90% RH range, however the environmental chamber has a stated thermal stability of 0.3pm/°C, therefore this also could induce a Bragg wavelength shift of 33pm. In summary a FBG fabricated in PMMA based SI SM POF displayed a RH sensitivity of 38.4 ± 0.4 pm/% RH, thus demonstrating that the TOPAS POFBG has a RH sensitivity which is 65 times smaller than that of PMMA based FBGs.

9.7 Summary

Demonstrated in this chapter is the repeatable fabrication of FBGs in TOPAS POF with Bragg responses in both the 1500nm and 800nm wavelength ranges. Using a FBG which was fabricated at 1568nm, the temperature sensitivity was calculated to be -36.5 ± 0.3 pm/°C and together with the successful FBG fabrication was documented in 2011[73].

Furthermore also using a FBG with a Bragg response at 1568nm the relative humidity sensitivity was calculated to be 65 times smaller than that of FBGs fabricated in PMMA based POF. This has therefore significantly reducing the potential of cross sensitivity to relative humidity when employing TOPAS POFBGs to monitor measurands such as temperature and strain.

9.7.1 Future Work

Firstly the repeatability of the practically immunity to relative humidity should be demonstrated. After which, to complement this work the temperature and axial strain sensitivities should be taken to demonstrate their usability as a sensor whilst eliminating cross sensitivity to relative humidity. After the demonstration of Bragg responses within the 800nm work should continue in this wavelength region so to take advantage of the lower

attenuation losses of the TOPAS POF and also the wide availability of broadband interrogating light sources.

Furthermore, since the demonstration of FBG fabrication in TOPAS POF, a range of applications devices can be explored, such as the WDM sensor demonstrated in this chapter, all of which have the potential to be practically immune to relative humidity.

10

DISCUSSION

This chapter discusses the scientific and technological advances made to the polymer optical fibre Bragg gratings (POFBG) technology during the research of this thesis. Contributions to POFBG research activities included technological advances such as: the permanent adhesive splicing of POF to silica optical fibre, POFBGs with a Bragg response within the lower attenuation 800nm spectral region, multiplexed POFBGs in both the 1550nm and 800nm spectral regions, demonstrations of utilising thermal annealing to tune the Bragg wavelength of a POFBG, multimode POFBGs, demonstrations of monitoring hydrostatic pressure using POFBGs and fabrication of FBGs in TOPAS cyclic olefin copolymer where the cross sensitivity to relative humidity is minimised whilst monitoring changes in temperature. Many of these developments have been combined to provide working demonstrations of POFBG sensors embedded in flexible Polydimethylsiloxane (PDMS) tubing.

Throughout these discussions recommendations have been given to how the technology can be taken forward and possible areas of future work are considered.

10.1 Fabrication of Polymer Optical Fibre Bragg Gratings

Fibre Bragg gratings have been fabricated in an array of POFs using the phase mask technique detailed in Chapter 4. Based on literature reviews and previous research completed at Aston University a 325nm HeCd continuous wave laser was used to inscribe the FBGs. Work was completed investigating the inscription setup where the distance of the phase mask above the POF and the duration of the UV irradiation were optimised. With a success rate of around 80%, in excess of 30 FBGs were fabricated in the SM SI POF with a Bragg response within the 1550nm spectral region. These gratings went on to aid various studies in this thesis including the development of adhesive splicing, hydrostatic pressure sensitivity studies and comparative work whilst investigating FBGs fabricated in TOPAS POF. A similar amount of FBGs were fabricated in FMmPOF, again with a success rate of around 80%. As with SM SI POF, although results are limited for Bragg gratings fabricated in FMmPOF many were used in the development of other studies. In particular the adhesive splicing study proved challenging due to the adhesive flowing along the hole cladding structure of the mPOF, resulting in many FBGs being destroyed.

Table 12 Review of POF which were used for FBGs fabrication using the Phase Mask Inscription Technique

Fibre Type	Acronym	Source	Comments	Discussed
Few moded, microstructured	FMmPOF	A	Pure PMMA	Chapter 4
Multimode, microstructured	MMmPOF	A	Pure PMMA	Chapters 3.5, 5, 6, 7, 8
Single Mode, microstructured	TOPAS	B	TOPAS cyclic olefin copolymer	Chapter 9
Single Mode, Step index	SM SI POF	C	Doped fibre, fabrication time decreased to 7.5 minutes with 30mW HeCd laser power	Chapters 5 & 7

A = Institute of Photonics and Optical Science, University of Sydney

B = Department of Photonics Engineering, Technical University of Denmark

C = University of New South Wales

After continued investigative work a solution was established to also fabricate FBGs in MMmPOF using the phase mask technique. This involved a process of elimination where the height of the phase mask above the MMmPOF was adjusted until a successful fabrication rate of at least 90% was established. Using a technique where the phase mask was rested directly on top of the fibre resulted in advance of 100 FBGs being fabricated in the MMmPOF. Once more, although results may suggest fabrication of gratings were limited many sensors were sacrificed in the development of studies such as adhesive splicing, thermal annealing of POFBGs and the fabrication of WDM sensors in POF. Furthermore many FBG sensors fabricated in the MMmPOF were shared with other groups around the world, contributing to other POF Bragg sensing research activities. Fibre Bragg gratings fabricated in the MMmPOF also contributed heavily to the Photonic Skins For Optical Sensing (PHOSFOS) research and technology development project, where sensors were embedded in flexible skins and tubing, which is discussed later in this chapter. It should be noted that the research presented in this thesis produced the first results of FBGs fabricated in multimode POF and was presented in 2010[72]. Advantages such as greater tolerances in alignment to silica fibre are possible when using the multimode POF, as well as potentially using cheaper broad emitting light sources in a multimode interrogation system were discussed in the presentation.

It is felt that resting the POF upon a v-groove plate as part of the phase mask inscription technique works well and gives a relative high fabrication success rate for the FBG inscription times of around 40-60 minutes needed when using POF. However it is felt that the inscription technique could be improved in a number of ways, these include: translating the UV laser beam along the phase mask thus creating longer POFBGs, this in-turn would produce stronger Bragg gratings with a narrower bandwidth. A second recommendation

would be to develop a technique of suspending the phase mask above the POF whilst being able to control the separation between the two in a controllable manner. Ideally this could be accomplished with a micrometer translation stage; where the height of the phase mask could be adjusted depending upon the POF being used. Finally, it is believed an optical inspection setup would aid with the alignment of the UV laser beam to the POF core. Currently alignment is achieved by observing the back scattering off the POF surface. However a potentially more efficient method would be to observe the core of the POF during the alignment setup using a microscope setup, hence ensuring the UV inscription beam is focussed within the core of the POF. An additional attempt of improving the alignment would be to monitor the guidance of the UV along the core of the POF during the alignment process. During the work in this thesis guidance of the UV within the core was often seen when the irradiation beam was focussed within the core of the POF.

Along with the suggested improvement to the inscription setup it is also believed there is scope to improve the POF itself. In particular the geometry of the SI SM POF proved varied along lengths as short as 10cm. This resulted in situations where optical alignment of silica fibre to the core of the POF would be optimised for one length of POF but would not be for the next length of POF and therefore required re-alignment for each new length of POF. It was also suspected the composition of the POF used in this thesis varied along the fibre length. This possibly led to areas along the POF which were more UV photosensitive than others and in some cases not photosensitive at all.

A suggestion for future studies would be a detailed investigation of the optimum laser power and irradiation time required for the greatest change in refractive index. For the work completed in this thesis the laser power was constant at 30mW and the irradiation time was varied depending on when a saturation level in the growth of the Bragg grating was considered to have been reached. It is considered that gratings fabricated in this thesis were over exposed beyond a 60 minute UV irradiation as the bandwidth of the Bragg response often increased after this stage of the fabrication, and hence an optimum change in refractive index may not have been achieved. It should be noted that it is expected the optimum laser power and irradiation time is likely to be different for each type of POF and also the conditions may have to be tweaked for different lengths of the same POF.

Using the phase mask technique limits the variation of the Bragg wavelength due to the fixed period of the phase masks used in the fabrication of POFBGs. Unless a large array of relatively expensive phase masks were purchased it is believed future work in POF may be limited. A suggestion of future work would be to investigate point-by-point femtosecond inscription, something which is discussed in more detail later in this chapter. By using a point-by-point inscription technique the possible Bragg wavelengths are more widely achievable without any additional costs once the inscription setup was established.

Furthermore using this technique it would be possible to fabricate a range of longer FBGs, LPGs and also more complex grating designs such as chirped and superstructure FBGs in POF.

10.1.1 Interrogation of Polymer Optical Fibre Bragg Gratings

The responses of the POFBGs fabricated throughout this thesis have been monitored in reflection. Predominantly a Bragg response was captured on an OSA (HP 70951B) with a bandwidth resolution of 0.5nm. It is felt a future study should investigate the Bragg response with an increased bandwidth resolution to allow for greater characterisation. Furthermore, using a greater sensitivity would enable a better understanding of the growth of a Bragg grating in POF during fabrication. Figure 10-1, shows the growth of a FBG fabricated in FMmPOF with a Bragg wavelength of 1562nm. The growth curve would suggest that a UV induced refractive index change does not occur until at least 12minutes into the inscription. However this growth curve may be limited by the sensitivity of the interrogation setup. Therefore future work should investigate the limiting factors of the interrogation setup to establish when a Bragg response is actually first seen once the UV irradiation has started. Potentially this work could lead onto understanding the UV photosensitivity of POF and the induced refractive index changes.

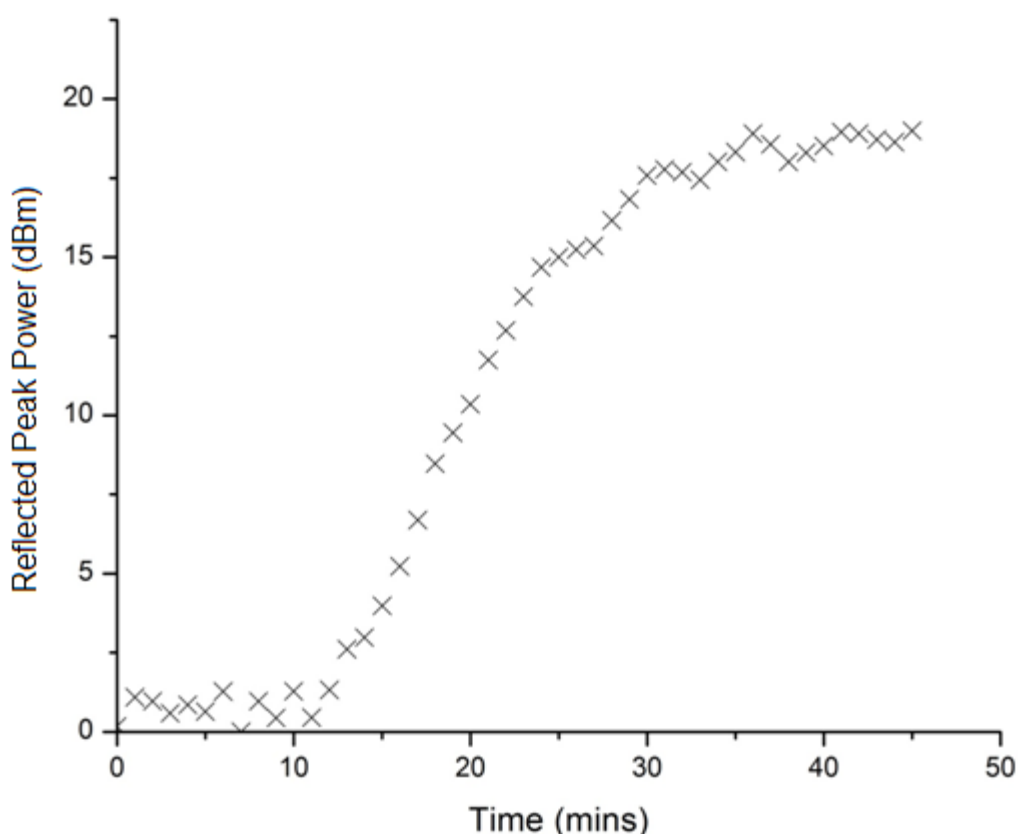


Figure 10-1 The growth characteristics of a FBG fabricated in FMmPOF with a Bragg length of 1562nm

A more accurate method of measuring the strength or reflectivity of a fabricated POFBG would be to interrogate a POFBG in transmission. Previously attempts prior to this thesis to

interrogate POFBGs in transmission were unsuccessful. The high attenuation losses of 1dB/cm of PMMA[41] are likely to be the most probable reason for the lack of a FBG response detection in transmission.

Part of the completed work in this thesis included the first fabrications of POFBGs with Bragg responses within the 800nm spectral region. Attenuation losses of 8dB/m were measured in MMmPOF at a wavelength of 830nm. Therefore it was anticipated it would be possible to detect a Bragg response of a FBG fabricated in the fibre using a transmission interrogation setup at this lower interrogation wavelength. However after numerous attempts no transmission spectrum of a POFBG was observed from a POFBG with a Bragg response within the 800nm spectral range. Interestingly the POFBG could be interrogated successfully in reflection from either end of the POF and transmission was deemed viable when inspecting visually the transmission of a HeNe red laser along the core of the fibre. Needless to say future work should focus on obtaining a true characterisation of POFBGs in available POF via transmission interrogation.

10.2 Adhesive Splicing

A large proportion of the results obtained in this thesis were made possible from the development of an optical adhesive splice between polymer and silica optical fibres. As is shown in Figure 10-2, POFBGs can now be moved away from the optical bench they were fabricated on and into measurand specific environments. This is something which was not possible prior to this thesis and after the time spent experimenting with various adhesive application methods it is now possible to splice both step index and microstructured POF to silica optical fibre.

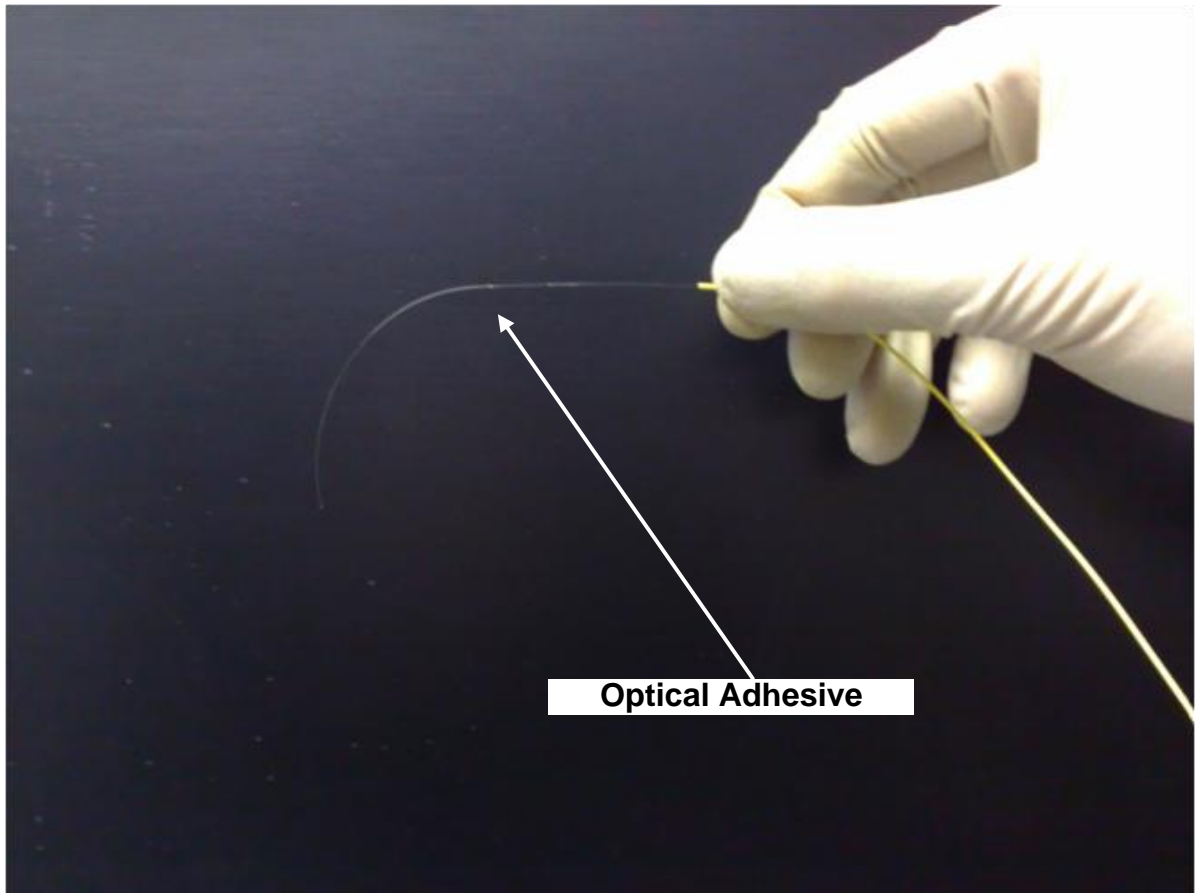


Figure 10-2 Demonstration of POF spliced to silica optical fibre using optical adhesive

It is felt further work is needed to connect polymer and silica optical fibre together in a more user friendly manner whilst maintaining sufficient optical coupling. Although the optical adhesive splice is a functional method to employ POFBGs in specific environments it is time consuming to construct and remains relatively fragile. With this in mind, future work should contain a full characterisation of the adhesive splices, in particular the mechanical strength of the splice and the impact this has on the transmitting optical signals that pass through it. Additionally using the Loctite 3525 adhesive is limited by a glass transition temperature of 43°C, which would clearly limit the working temperature of a POFBG sensor.

Possible avenues of investigation to connect polymer and silica optical fibre together could involve embedding the POF into a ferrule connector and then polishing the end face to connect to a silica pigtail, as was first investigated by Lwin[60]. This method would be best suited to FBGs fabricated in the MMmPOF where the alignment requirements between polymer and silica fibre would be more relaxed than they would be for single mode POF.

10.3 POFBGs with Bragg Responses in Lower Attenuation Wavelengths

The fabrication of POFBGs with a Bragg response within the 800nm spectral region was a key result for POFBG research. Using the phase mask inscription technique, POFBGs were fabricated with Bragg response within the 800-900nm spectral range. Bragg responses such as that seen in Figure 10-3 were not achieved prior to this thesis, however it has now been

demonstrated it is possible to fabricate FBGs where the measured attenuation losses are much lower at 8dB/m allowing for longer length POFBG sensors.

As with fabricating POFBGs with responses in the 1550nm spectral region, the phase mask was again required to rest directly upon the POF. The success rate of fabricating POFBGs within the 800-900nm spectral region was much lower at around 50%. The phase masks were regularly cleaned and different parts of the masks were used in an attempt to improve yield of the lower wavelength FBGs, however neither appeared to improve the FBG yield. One possible reason for this may be the reduced feature sizes required and the composition of the fibre. It is possible depending on the structure of the polymer backbone, their sidechain location and repeatability of the sidechain along the backbone, that the feature size of the refractive index changes are not always possible along the entire length of POF when fabricating FBGs with lower Bragg wavelengths around 800nm.

Ideally future work should aim for POFBGs with Bragg responses within the red wavelength regime. Within this red spectral region attenuation losses of 100dB/km are expected around 670nm[41]. One possible avenue to explore whilst attempting to lower the Bragg wavelength of POFBGs would be to investigate whether the feature size of refractive index changes would be possible with femtosecond point-by-point inscription.

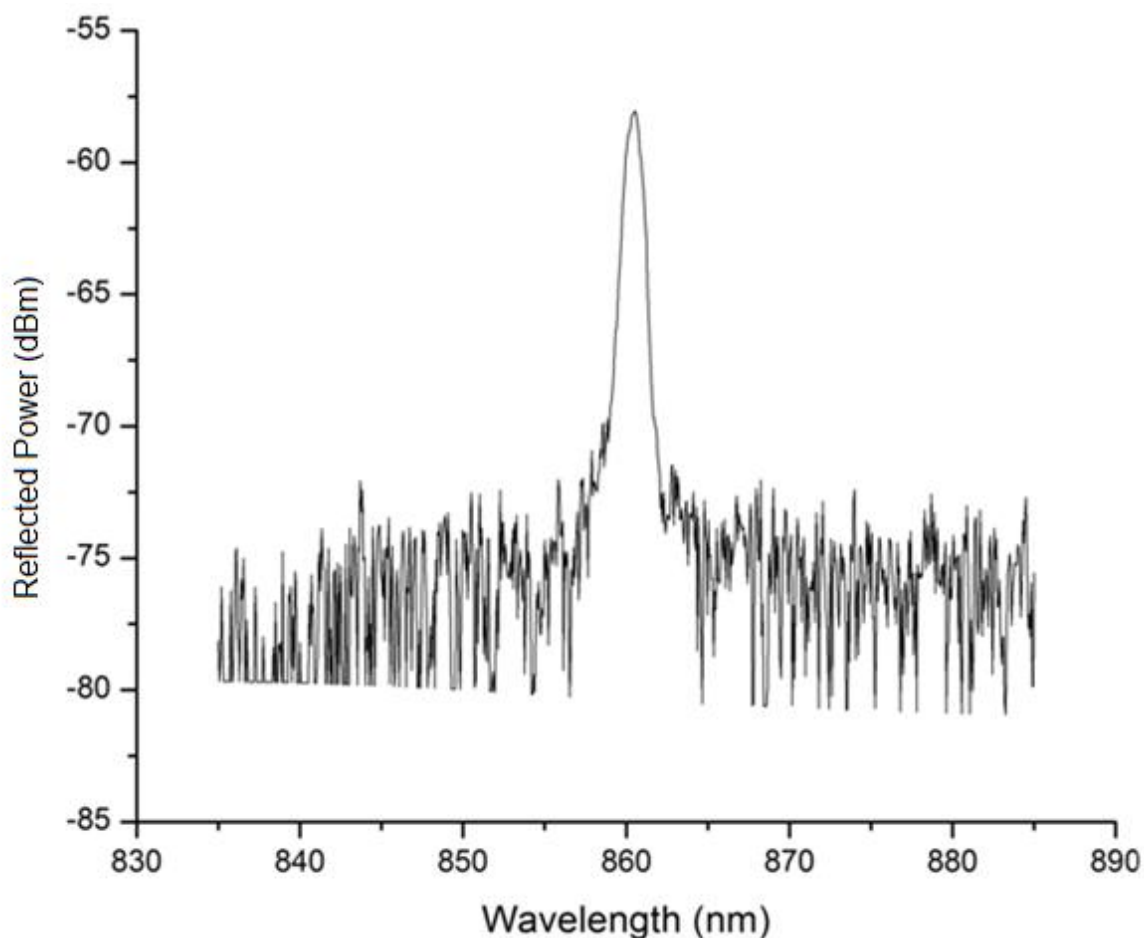


Figure 10-3 POFBG fabricated in MMmPOF with a Bragg wavelength of 860.5nm

10.4 Applications and WDM sensors

Work in this thesis has provided the first demonstration of WDM sensors in POF. WDM sensors have been demonstrated in both PMMA based MMmPOF and TOPAS POF. The fabrication of WDM sensors consisting of 3 FBGs in the MMmPOF utilised the ability to permanently blue shift a Bragg response via thermal annealing of the POF, which was a technique first reported in this thesis. Real time monitoring of the change in Bragg wavelength was also monitored for the first time during thermal annealing, something which was made possible via the breakthroughs of adhesive splicing and FBGs within the 800-900nm spectral region.

It is felt a more detailed evaluation of the thermal annealing characteristics is needed in forthcoming studies. It was clear that the induced wavelength shifts were not stable after 24 hours. Therefore monitoring over much longer time periods needs to be investigated. Nevertheless thermal annealing has been demonstrated as a tool to tune Bragg responses to a particular wavelength within a given range. This induced change in Bragg wavelength enables the tuning to a particular interrogating light source as one potential application. With further studies and a greater depth of understanding thermal annealing could be a repeatable process and used as a manufacturing process. However, it is felt that currently it is felt it is not repeatable process with wavelength shifts apparently dependent on whether the fibre has been previously annealed and the amount of FBGs already fabricated in the POF. Additionally on occasions thermally annealing a POFBG resulted in the total loss of Bragg responses for reasons unknown. Therefore whilst this still occurs thermal annealing cannot be total solution for manufacturing but rather is limited to research applications. Finally it is felt that a future solution to fabricating WDM sensors with an increased amount of FBGs could be possible via femtosecond point-by-point inscription. This would enable a wide range of Bragg responses to be chosen without the need to purchase separate phase masks for each FBG.

Additional work carried out in this thesis has demonstrated the first results of sensitivity to hydrostatic pressure up to 10MPa. Figure 10-4 demonstrates the results from the initial studies of hydrostatic pressure sensitivity where a linear sensitivity is observed whilst increasing the pressure by 1MPa every 2 minutes. Evidently these are very early results and extensive research needs to be completed to understand the mechanism behind this sensitivity and any advantages POF may have over other sensing equipment. It is felt the time dependence of the Bragg response to pressure sensitivity should be investigated together with monitoring the characteristics whilst the hydrostatic pressure is decreased as well as increased. Once more it is felt it should be highlighted that this initial characterisation would not have been possible without the developments of adhesive splicing and FBGs at lower wavelengths made in this thesis.

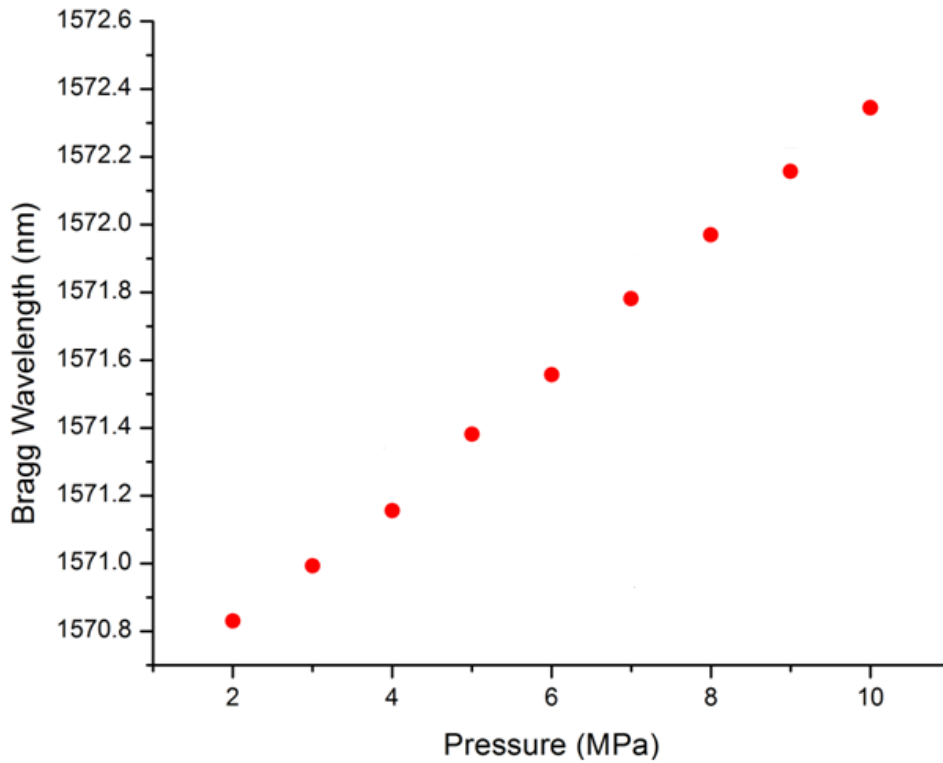


Figure 10-4 Bragg wavelength shift of a FBG fabricated in step index POF whilst monitoring an increase in hydrostatic pressure

An additional development made to the POFBGs technology is the fabrication of FBGs in TOPAS POF. A limited amount of FBGs were made in this fibre using the same phase mask technique as used for the PMMA POF types, however with limited fabrication it is difficult to comment on the fabrication success. Nevertheless it was possible to demonstrate the potential that TOPAS POF provides. Whilst varying the relative humidity between 30-90% a FBG fabricated in the TOPAS demonstrated a potential sensitivity of 0.6pm/% whereas a PMMA based SI POF had a much higher sensitivity of 38pm/%. Therefore potentially, FBGs fabricated TOPAS POF can significantly reduce the cross sensitivity to relative humidity which has been experienced when using PMMA based POFBG sensors whilst monitoring measurands such as changes in temperature[24].



Figure 10-5 Oesophageal Sensor [92]

Finally it should be highlighted that a number of the breakthroughs made during this thesis have been combined to manufacture an oesophageal sensor (Figure 10-5[92]) for the

PHOFOS framework 7 research and technology development project. Here a WDM sensor consisting of three FBGs with wavelengths within the 800-900nm region were fabricated, one of which had a blue shifted Bragg response by thermal annealing. The sensor was then embedded in a PDMS tube and was permanently spliced to a silica pigtail using optical adhesive to allow for interrogation of the sensor.

10.5 Future Work with Femtosecond Point-by-Point Inscription

It is believed an alternative method of writing periodic refractive index perturbations in POF is to use a point-by-point inscription technique. This is where each refractive index perturbation is inscribed individually one step at a time via a pulsed laser source. One possible way of achieving this is using a femtosecond (fs) laser as was used by Martinez *et al* in 2004 to fabricate FBGs of the first and higher orders using fs inscription[35]. Additionally an fs laser has also been used to inscribe an LPG using a point-by-point technique by Konda *et al* in 1999[38].

In 2007 Baum *et al* first observed the physical structure of fs irradiation in single mode POF[93], within this report fs index modification of clinical grade PMMA was discussed as providing the potential for optical sensors for bio medical applications which removes the need for photosensitivity dopants within the core of the POF. Furthermore Scully *et al* in 2003 demonstrated that commercially available un-doped bulk PMMA can be photo-modified by fs irradiation[94]. Baum *et al* suggested from the results of fs photo-modification experiments that the cleavage of the polymer backbone under formation of monomers lead to a refractive index change which could be used to fabricate a POFBG[95].

By using an fs point-by-point inscription technique it would potentially be possible to fabricate FBGs at specific wavelengths without the need to purchase additional phase masks. Furthermore the length of the grating can be controlled by the amount of irradiation points chosen and the period pattern could be varied to enable gratings structures such as chirped and superstructure FBGs. The limiting factor of this type of fabrication technique would be the resolution of the translation stage the POF would be mounted upon. Furthermore it would be possible to fabricate WDM sensors with an increased amount of FBGs whilst not purchasing additional expensive phase mask for each FBGs. In addition, fs inscription also provides opportunities to explore FBG fabrication in perfluorinated POF, which has significantly lower attenuation losses which are less than 20dB/km in the 1300nm communications spectral region[57]. Work in this thesis demonstrated the non-photosensitivity to UV irradiation in this type of perfluorinated POF however fs inscription offers a new avenue of exploration in an attempt to realise the low attenuation of perfluorinated POF.

11

AUTHORS PUBLICATIONS

1. D. Sáez-Rodríguez, J. L. Cruz, **I. Johnson**, D. J. Webb, M. C. J. Large, A. Argyros, "Water Diffusion Into UV Inscripted Long Period Grating in Microstructured Polymer Fiber" IEEE Sensors Journal, 10(7), 1169-1173 (2010).
2. David Sáez-Rodríguez, Jose L. Crus, **I. Johnson**, David J. Webb, Maryanne C. J. Large, Alexander Argyros, Marij A. Van Eijkelenborg, "Long period fibre gratings photoinscribed in a microstructured polymer optical fibre by UV radiation", SPIE Europe Optics and Optoelectronics, Prague (2009)
3. **I. P. Johnson**, David J. Webb, Kyriacos Kalli, Maryanne C. J. Large, Alexander Argyros, "Multiplexed FBG sensor recorded in multimode microstructured polymer optical fibre", SPIE Europe, Brussels (2010).
4. **I. P. Johnson**, K. Kalli, D. J. Webb, "827nm Bragg grating sensor in multimode microstructured polymer optical fibre", Electronics Letter, 46(17), 1217-U74 (2010)
5. **I. P. Johnson**, W. Yuan, A. Stefani, K. Nielsen, H. K. Rasmussen, L. Khan, D. J. Webb, K. Kalli, O. Bang, "Optical fibre Bragg grating recorded in TOPAS cyclic olefin copolymer", Electronics Letters, 47(4), 271 (2011)
6. **Ian P. Johnson**, David J. Webb, Kyriacos Kalli, Wu Yuan, Alessio Stefani, Kristian Nielsen, Henrik K. Rasmussen, Ole Bang, "Polymer PCF Bragg grating sensors based on poly(methyl methacrylate) and TOPAS cyclic olefin copolymer", SPIE Europe Optics and Optoelectronics, Prague (2011)
7. **Ian P. Johnson**, David J. Webb, Kyriacos Kalli, "Utilisation of thermal annealing to record multiplexed FBG sensors in multimode microstructured polymer optical fibre", Proceedings of SPIE 7753, 77536T, Ottawa (2011)

-
- [1] K. O. Hill, *et al.*, "PHOTOSENSITIVITY IN OPTICAL FIBER WAVEGUIDES - APPLICATION TO REFLECTION FILTER FABRICATION," *Applied Physics Letters*, vol. 32, pp. 647-649, 1978.
- [2] B. S. Kawasaki, *et al.*, "NARROW-BAND BRAGG REFLECTORS IN OPTICAL FIBERS," *Optics Letters*, vol. 3, pp. 66-68, 1978.
- [3] D. K. W. Lam and B. K. Garside, "CHARACTERIZATION OF SINGLE-MODE OPTICAL FIBER FILTERS," *Applied Optics*, vol. 20, pp. 440-445, 1981 1981.
- [4] G. Meltz, *et al.*, "FORMATION OF BRAGG GRATINGS IN OPTICAL FIBERS BY A TRANSVERSE HOLOGRAPHIC METHOD," *Optics Letters*, vol. 14, pp. 823-825, Aug 1989.
- [5] K. O. Hill and G. Meltz, "Fiber Bragg grating technology fundamentals and overview," *Journal of Lightwave Technology*, vol. 15, pp. 1263-1276, 1997.
- [6] Tomlinso.Wj, *et al.*, "PHOTOINDUCED REFRACTIVE INDEX INCREASE IN POLY(METHYLMETHACRYLATE) AND ITS APPLICATIONS," *Applied Physics Letters*, vol. 16, pp. 486-&, 1970.
- [7] I. P. Kaminow, *et al.*, "POLY(METHYL METHACRYLATE) DYE LASER WITH INTERNAL DIFFRACTION GRATING RESONATOR," *Applied Physics Letters*, vol. 18, pp. 497-&, 1971.
- [8] M. J. Bowden, *et al.*, "MECHANISM OF PHOTOINDUCED REFRACTIVE-INDEX INCREASE IN POLYMETHYL METHACRYLATE," *Applied Optics*, vol. 13, pp. 112-117, 1974.
- [9] G. Barton, *et al.*, "Fabrication of microstructured polymer optical fibres," *Optical Fiber Technology*, vol. 10, pp. 325-335, Oct 2004.
- [10] Z. Xiong, *et al.*, "Highly tunable Bragg gratings in single-mode polymer optical fibers," *Ieee Photonics Technology Letters*, vol. 11, pp. 352-354, Mar 1999.
- [11] H. Y. Liu, *et al.*, "Observation of type I and type II gratings behavior in polymer optical fiber," *Optics Communications*, vol. 220, pp. 337-343, May 15 2003.
- [12] H. Y. Liu, *et al.*, "Polymer fiber Bragg gratings with 28-dB transmission rejection," *Ieee Photonics Technology Letters*, vol. 14, pp. 935-937, Jul 2002.
- [13] H. B. Liu, *et al.*, "Novel growth behaviors of fiber Bragg gratings in polymer optical fiber under UV irradiation with low power," *Ieee Photonics Technology Letters*, vol. 16, pp. 159-161, Jan 2004.
- [14] N. G. Harbach, "Fiber Bragg Gratings in Polymer Optical Fibers," *PhD Thesis, École Polytechnique Fédérale De Lausanne*, 2008.
- [15] H. Dobb, *et al.*, "Continuous wave ultraviolet light-induced fiber Bragg gratings in few- and single-mode microstructured polymer optical fibers," *Optics Letters*, vol. 30, pp. 3296-3298, 2005.
- [16] F. Baldini and A. G. Mignani, "Optical-fiber medical sensors," *Mrs Bulletin*, vol. 27, pp. 383-387, May 2002.
- [17] H. B. Liu, *et al.*, "Strain and temperature sensor using a combination of polymer and silica fibre Bragg gratings," *Optics Communications*, vol. 219, pp. 139-142, Apr 2003.
- [18] M. Silva-Lopez, *et al.*, "Strain and temperature sensitivity of a single-mode polymer optical fiber," *Optics Letters*, vol. 30, pp. 3129-3131, Dec 2005.
- [19] D. J. Webb, "Optical-fiber sensors: An overview," *Mrs Bulletin*, vol. 27, pp. 365-369, May 2002.
- [20] G. F. Fernando, *et al.*, "Optical-fiber sensors," *Mrs Bulletin*, vol. 27, pp. 359-364, May 2002.
- [21] H. Y. Liu, *et al.*, "Thermal tuning of polymer optical fiber Bragg gratings," *Ieee Photonics Technology Letters*, vol. 13, pp. 824-826, 2001.

- [22] H. Y. Liu, *et al.*, "Polymer optical fibre Bragg gratings based fibre laser," *Optics Communications*, vol. 266, pp. 132-135, Oct 1 2006.
- [23] H. Y. Liu, *et al.*, "Strain sensing characterization of polymer optical fibre Bragg gratings," in *17th International Conference on Optical Fibre Sensors*, Brugge, BELGIUM, 2005, pp. 663-666.
- [24] K. E. Carroll, *et al.*, "Thermal response of Bragg gratings in PMMA microstructured optical fibers," *Optics Express*, vol. 15, pp. 8844-8850, Jul 2007.
- [25] J. Wilson and J. F. B. Hawkes, *Optoelectronics An Introduction Second Edition*. UK: Prentice Hall International, 1989.
- [26] A. Othonos and K. Kalli, "Fiber Bragg Gratings Fundamentals and Applications in telecommunications and Sensing," *Boston: Artech House*, 1999.
- [27] S. W. James and R. P. Tatam, "Optical fibre long-period grating sensors: Characteristics and application," *Measurement Science & Technology*, vol. 14, pp. R49-R61, May 2003.
- [28] T. Erdogan, "Cladding-mode resonances in short- and long-period fiber grating filters," *Journal of the Optical Society of America a-Optics Image Science and Vision*, vol. 14, pp. 1760-1773, Aug 1997.
- [29] A. D. Kersey, *et al.*, "Fiber grating sensors," *Journal of Lightwave Technology*, vol. 15, pp. 1442-1463, 1997.
- [30] K. O. Hill, *et al.*, "BRAGG GRATINGS FABRICATED IN MONOMODE PHOTSENSITIVE OPTICAL FIBER BY UV EXPOSURE THROUGH A PHASE MASK," *Applied Physics Letters*, vol. 62, pp. 1035-1037, 1993.
- [31] D. Z. Anderson, *et al.*, "PRODUCTION OF IN-FIBER GRATINGS USING A DIFFRACTIVE OPTICAL-ELEMENT," *Electronics Letters*, vol. 29, pp. 566-568, 1993.
- [32] Z. Xiong, *et al.*, "Effects of the zeroth-order diffraction of a phase mask on Bragg gratings," *Journal of Lightwave Technology*, vol. 17, pp. 2361-2365, Nov 1999.
- [33] Q. Zhang, *et al.*, "TUNING BRAGG WAVELENGTH BY WRITING GRATINGS ON PRESTRAINED FIBERS," *Ieee Photonics Technology Letters*, vol. 6, pp. 839-841, 1994.
- [34] B. Malo, *et al.*, "POINT-BY-POINT FABRICATION OF MICRO-BRAGG GRATINGS IN PHOTSENSITIVE FIBER USING SINGLE EXCIMER PULSE REFRACTIVE-INDEX MODIFICATION TECHNIQUES," *Electronics Letters*, vol. 29, pp. 1668-1669, Sep 2 1993.
- [35] A. Martinez, *et al.*, "Direct writing of fibre Bragg gratings by femtosecond laser," *Electronics Letters*, vol. 40, pp. 1170-1172, Sep 16 2004.
- [36] L. Zhang, *et al.*, "Design and realization of long-period grating devices in conventional and high birefringence fibers and their novel applications as fiber-optic load sensors," *Ieee Journal of Selected Topics in Quantum Electronics*, vol. 5, pp. 1373-1378, Sep-Oct 1999.
- [37] A. M. Vengsarkar, *et al.*, "Long-period fiber gratings as band-rejection filters," *Journal of Lightwave Technology*, vol. 14, pp. 58-65, Jan 1996.
- [38] Y. Kondo, *et al.*, "Fabrication of long-period fiber gratings by focused irradiation of infrared femtosecond laser pulses," *Optics Letters*, vol. 24, pp. 646-648, May 15 1999.
- [39] J. Brandrup, *et al.*, "Polymer Handbook (4th Edition)."
- [40] R. P. Kusy and A. R. Greenberg, "INFLUENCE OF MOLECULAR-WEIGHT ON THE DYNAMIC MECHANICAL-PROPERTIES OF POLY(METHYL-METHACRYLATE)," *Journal of Thermal Analysis*, vol. 18, pp. 117-126, 1980 1980.
- [41] D. Webb and K. Kalli. (2011). *Polymer fiber Bragg gratings*
- [42] J. Ballato, *et al.*, "Theoretical performance of polymer optical fibers, planar waveguides, and amplifiers," in *Conference on Design and Fabrication of Planar Optical Waveguide Devices and Materials*, Seattle, Wa, 2002, pp. 1-8.
- [43] <http://www.chromisfiber.com>
- [44] http://www.lucina.jp/eg_lucina/indexeng.htm
- [45] W. Daum, *et al.*, *POF - Polymer Optical Fibers For Data Communication*. Berlin London: Springer, 2002.

- [46] J. M. Moran and I. P. Kaminow, "PROPERTIES OF HOLOGRAPHIC GRATINGS PHOTOINDUCED IN POLYMETHYL METHACRYLATE," *Applied Optics*, vol. 12, pp. 1964-1970, 1973 1973.
- [47] C. Wochnowski, *et al.*, "UV-laser-assisted modification of the optical properties of polymethylmethacrylate," *Applied Surface Science*, vol. 154, pp. 706-711, Feb 2000.
- [48] R. Srinivasan, *et al.*, "ULTRAVIOLET-LASER ABLATION AND DECOMPOSITION OF ORGANIC MATERIALS," *Pure and Applied Chemistry*, vol. 62, pp. 1581-1584, Aug 1990.
- [49] F. P. Laming, "HOLOGRAPHIC GRATING FORMATION IN PHOTOPOLYMERS - POLYMETHYLMETHACRYLATE," *Polymer Engineering and Science*, vol. 11, pp. 421-&, 1971 1971.
- [50] G. D. Peng, *et al.*, "Photosensitivity and gratings in dye-doped polymer optical fibers," *Optical Fiber Technology*, vol. 5, pp. 242-251, Apr 1999.
- [51] J. M. Yu, *et al.*, "Trans-4-stilbenemethanol-doped photosensitive polymer fibers and gratings," *Optics Letters*, vol. 29, pp. 156-158, Jan 15 2004.
- [52] Z. Y. Zhang, *et al.*, "Thermo-optic coefficients of polymers for optical waveguide applications," *Polymer*, vol. 47, pp. 4893-4896, 2006.
- [53] T. Watanabe, *et al.*, "Polymeric optical waveguide circuits formed using silicone resin," *Journal of Lightwave Technology*, vol. 16, pp. 1049-1055, 1998.
- [54] T. Ishigure, *et al.*, "Graded-index plastic optical fiber with high mechanical properties enabling easy network installations. I," *Journal of Applied Polymer Science*, vol. 91, pp. 404-409, Jan 2004.
- [55] E. E. Shafee, "Effect of photodegradation on the [beta]-relaxation in poly(methylmethacrylate)," *Polymer Degradation and Stability*, vol. 53, pp. 57-61, 1996.
- [56] C. Zhang, *et al.*, "Bragg grating inscription in TOPAS microstructured polymer optical fibre," *Proceedings of XVI International Conference on Polymer Optical Fibres Paper SEN-I-1*, 2007.
- [57] <http://www.topas.com>
- [58] H. L. Dobb, "Fibre Gratings In Novel Optical Fibres For Applications In Sensing," *PhD Thesis, Aston University*, 2007.
- [59] H. P. A. van den Boom, *et al.*, "High-capacity transmission over polymer optical fiber," *Ieee Journal of Selected Topics in Quantum Electronics*, vol. 7, pp. 461-470, May-Jun 2001.
- [60] R. Lwin, "Connecting microstructured polymer optical fibres to the world," presented at the The 18th international conference on plastic optical fibers, Sydney, 2009.
- [61] Z. C. Li, *et al.*, "Fabrication of long-period gratings in poly(methyl methacrylate-co-methyl vinyl ketone-cobenzyl methacrylate)-core polymer optical fiber by use of a mercury lamp," *Optics Letters*, vol. 30, pp. 1117-1119, 2005.
- [62] M. A. van Eijkelenborg, *et al.*, "Mechanically induced long-period gratings in microstructured polymer fibre," *Optics Communications*, vol. 236, pp. 75-78, 2004.
- [63] M. P. Hiscocks, *et al.*, "Stable imprinting of long-period gratings in microstructured polymer optical fibre," *Optics Express*, vol. 14, pp. 4644-4649, 2006.
- [64] <http://www.corning.com>.
- [65] D. Saez-Rodriguez, *et al.*, "Water Diffusion Into UV Inscripted Long Period Grating in Microstructured Polymer Fiber," *Ieee Sensors Journal*, vol. 10, pp. 1169-1173, 2010.
- [66] H. Dobb, *et al.*, "Grating based devices in polymer optical fibre - art. no. 618901," *Optical Sensing II*, vol. 6189, pp. 18901-18901, 2006.
- [67] R. Kashyap, *et al.*, "UV WRITTEN REFLECTION GRATING STRUCTURES IN PHOTSENSITIVE OPTICAL FIBERS USING PHASE-SHIFTED PHASE MASKS," *Electronics Letters*, vol. 30, pp. 1977-1978, 1994.
- [68] J. Canning and M. G. Sceats, "PI-PHASE-SHIFTED PERIODIC DISTRIBUTED STRUCTURES IN OPTICAL FIBERS BY UV POST-PROCESSING," *Electronics Letters*, vol. 30, pp. 1344-1345, 1994.
- [69] D. Uttamchandani and A. Othonos, "Phase shifted Bragg gratings formed in optical fibres by post-fabrication thermal processing," *Optics Communications*, vol. 127, pp. 200-204, 1996.
- [70] <http://www.loctite.co.uk>.

- [71] I. P. Johnson, *et al.*, "827 nm Bragg grating sensor in multimode microstructured polymer optical fibre," *Electronics Letters*, vol. 46, pp. 1217-U74, Aug 2010.
- [72] I. P. Johnson, *et al.*, "Multiplexed FBG sensor recorded in multimode microstructured polymer optical fibre," 2010, p. 77140D.
- [73] I. P. Johnson, *et al.*, "Optical fibre Bragg grating recorded in TOPAS cyclic olefin copolymer," *Electronics Letters*, vol. 47, pp. 271-+, 2011.
- [74] I. P. Johnson, *et al.*, "Utilisation of thermal annealing to record multiplexed FBG sensors in multimode microstructured polymer optical fibre," *Proc. SPIE 7753*, 2011.
- [75] C. C. Ye, *et al.*, "Applications of polymer optical fibre grating sensors to condition monitoring of textiles - art. no. 012020," in *Sensors & Their Applications Xv*. vol. 178, A. T. Augousti and G. McConnell, Eds., ed Bristol: Iop Publishing Ltd, 2009, pp. 12020-12020.
- [76] L. Richard, "Connecting microstructured polymer optical fibres to the world," presented at the The 18th international conference on plastic optical fibers, Sydney, 2009.
- [77] T. Kaino, *Polymer Optical Fibre*. New York: M Dekker, 1992.
- [78] S. H. Law, *et al.*, "Cleaving of microstructured polymer optical fibres," *Optics Communications*, vol. 258, pp. 193-202, 2006.
- [79] S. D. Terblanche J, "Fibre Bragg gratings in polymer optical fibres at 980 nm," 2009.
- [80] H. Y. Liu, *et al.*, "Photosensitivity in low-loss perfluoropolymer (CYTOP) fibre material," *Electronics Letters*, vol. 37, pp. 347-348, Mar 15 2001.
- [81] H. Y. Liu, *et al.*, "Thermal stability of gratings in PMMA and CYTOP polymer fibers," *Optics Communications*, vol. 204, pp. 151-156, Apr 1 2002.
- [82] N. Stecher, *et al.*, "Periodic refractive index modifications inscribed in polymer optical fibre by focussed femtosecond pulses," presented at the 18th International Conference on Plastic Optical Fibers, Sydney, 2009.
- [83] G. D. Peng and P. L. Chu, "Polymer optical fiber photosensitivities and highly tunable fiber gratings," *Fiber and Integrated Optics*, vol. 19, pp. 277-293, 2000 2000.
- [84] M. G. Xu, *et al.*, "OPTICAL IN-FIBER GRATING HIGH-PRESSURE SENSOR," *Electronics Letters*, vol. 29, pp. 398-399, Feb 18 1993.
- [85] I. P. Johnson, *et al.*, "Polymer PCF Bragg grating sensors based on poly(methyl methacrylate) and TOPAS cyclic olefin copolymer," presented at the SPIE Optics and Optoelectronics, Prague, 2011.
- [86] O. V. Startsev, *et al.*, "REVERSIBLE MOISTURE EFFECTS IN THE CLIMATIC AGING OF ORGANIC GLASS," *Polymer Degradation and Stability*, vol. 39, pp. 373-379, 1993 1993.
- [87] S. H. Goods, *et al.*, "Thermal Expansion and Hydration Behavior of PMMA Molding Materials for LIGA Applications," *Technical Report, Sandia National Laboratories SAND Report, SAND2003-8000*, 2003.
- [88] J. A. Barrie and B. Platt, "The diffusion and clustering of water vapour in polymers," *Polymers*, vol. 4, pp. 303-313, 1963.
- [89] C. Zhang, *et al.*, "Water detection in jet fuel using a polymer optical fibre Bragg grating," in *Proc. SPIE 7503, 7500380*, Edinburgh, 2009.
- [90] G. Khanarian and H. Celanese, "Optical properties of cyclic olefin copolymers," *Optical Engineering*, vol. 40, pp. 1024-1029, 2001.
- [91] G. Emilianov, *et al.*, "Localized biosensing with Topas microstructured polymer optical fiber," *Optics Letters*, vol. 32, pp. 460-462, Mar 2007.
- [92] www.phosfos.eu.
- [93] A. Baum, *et al.*, "Optical characterization of PMMA phase gratings written by a 387 nm femtosecond laser," *Optics Communications*, vol. 284, pp. 2771-2774, Jun 1 2011.
- [94] P. J. Scully, *et al.*, "Femtosecond laser irradiation of polymethylmethacrylate for refractive index gratings," *Journal of Optics a-Pure and Applied Optics*, vol. 5, pp. S92-S96, Jul 2003.
- [95] A. Baum, *et al.*, "Photochemistry of refractive index structures in poly(methyl methacrylate) by femtosecond laser irradiation," *Optics Letters*, vol. 32, pp. 190-192, Jan 15 2007.